# Assessing drug-induced oxidative stress and its interactions with other stressors using a novel transgenic zebrafish model


Submitted by Rebekah Boreham

to the University of Exeter as a thesis/dissertation for the degree of

*Doctor of Philosophy* in Biological Sciences

February 2022.

UNIVERSITY OF EXETER



I certify that all material in this thesis which is not my own work has been identified and that any material that has previously been submitted and approved for the award of a degree by this or any other University has been acknowledged.

Signature R.L.J. Boreham

# Abstract

Pharmaceuticals discharged into the environment are potentially harmful to wildlife as many drug targets are conserved across divergent phyla. Oxidative stress (OS) is a major mechanism by which many pharmaceutical contaminants can induce toxicity. However, this mechanism is relatively poorly understood, particularly regarding multiple stressor interactions.

Transgenic zebrafish are an increasingly popular, highly integrated tool for elucidating chemical mixture effects, and in recent years there have been developments in the semi-automation of bioimaging tools to increase throughput using them. However, transgenic models are currently underutilised for studies into physical-chemical interactions and mixture effects of chemicals with different modes of toxicity. In this thesis, the application of the novel OS transgenic zebrafish model EpRE:mCherry (visualising activation of the electrophile response element; EpRE) is developed, together with the Acquifer semi-automated imaging platform. This system is used to screen environmental pharmaceuticals for pro-oxidative action, and assess their interaction with an oestrogenic chemical (EE2) and a physical stressor (temperature).

EpRE:mCherry embryo-larvae were exposed to one of a range of pharmaceuticals from 0 – 4 dpf (aqueous exposure) and tissue-specific fluorescence intensity was assessed as a measure of OS. Paracetamol, diclofenac and doxorubicin consistently induced strong OS responses in the TG model, while cisplatin and cyclophosphamide induced responses only during specific exposure windows. The pronephros was generally the most responsive to pharmaceutical-induced OS, followed closely by the liver, except for in response to doxorubicin which had the strongest effect in the gastrointestinal tract. Analytical chemistry techniques confirmed that atenolol, ibuprofen, clarithromycin and clozapine were taken up by exposed larvae, but induced no response in the TG model and so are assumed not to act via the EpRE.

Previous studies have investigated the contraceptive hormone ethinyl estradiol (EE2) as part of oestrogenic chemical mixture effects, but there is limited data on its interactive effects with other chemical classes of compounds. *In vitro* data suggests that oestrogens may have antioxidative properties by upregulating antioxidant enzymes via intracellular signalling pathways, but this has not yet been shown in a whole organism. This was investigated in zebrafish embryo-

larvae exposing them to a combination of paracetamol and EE2. However, no effect of EE2 was found on paracetamol- induced OS in the EpRE:mCherry model. Nevertheless, an oestrogen receptor inhibitor ICI 182,780 exhibited potential to exacerbate drug-induced OS, indicating endogenous oestrogen may play an antioxidative role.

There is growing evidence that climate change may exacerbate the toxic effect of pollutants and, as poikilotherms, fish are particularly vulnerable to rising temperatures. Incubation of zebrafish at temperatures 2-5°C above standard husbandry temperatures were found to exacerbate drug-induced OS and this was demonstrated for 3 pharmaceuticals from a range of therapeutic classes and potencies (namely, paracetamol, diclofenac and doxorubicin). LC-MS/MS data indicated this interaction is at least partly due to increased uptake of the drug. This indicates the need for future environmental risk assessments to more fully consider the influence of temperature (and other abiotic factors) on chemical toxicity. This is of particular interest as climate change is predicted to result in increased global temperatures and more frequent extreme weather events, potentially increasing the risk of chemicals detected in waterways at concentrations currently considered to be safe. The data presented here also demonstrates the utility of the EpRE:mCherry model and Acquifer as a new screening system for chemical effects analyses and to facilitate more targeted environmental risk assessments.

# Acknowledgments

This PhD studentship was funded by the BBSRC, AstraZeneca, and University of Exeter. Thank you to my supervisors, Charles Tyler, Malcolm Hetheridge, Jon Ball, and Stewart Owen for the opportunity to undertake this project. Particular thanks to Jon for always being willing to answer my stupid questions (often with minimal sarcasm!) and to Stewart who was my constant cheerleader. Thanks also to Matt Winter for reading my imaging work and helping me talk through my dilemmas. I also owe a huge thanks to Anna Tochwin for everything she taught me in the first year of my PhD, I truly would have sunk without her help!

Thank you to Greg Paull, Hannah Littler and all the ARC staff for their support and excellent care of my zebrafish. I also need to thank Hannah for all the wonderful advice and pep talks. Thanks to Aya Takesono for teaching me how to use and manage transgenic fish, and for all the advice on my literature review.

There are countless more people I need to thank for their technical support and training: Jeremy Metz for image analysis; Maciej Trznadel for chemical analysis; Jochen Gehrig and others at Acquifer for the training and continued technical support; John Swales, Gregory Hamm and James Blades at AstraZeneca for all their work on the MSI.

I count myself very lucky to have been part of such a wonderful, tight-knit post-grad community at Exeter. They say PhDs can be very lonely affairs but thanks to everyone in 201 I never felt alone. Thank you, Fishspotters, for all the coffee breaks and fancy-dress parties. Thank you, Michelle, for being an excellent emotional support cat. Thank you Sophie and Charlie, the original Team Tyler, who never hesitated to help with the most tedious tasks or annoying questions and created a lab camaraderie I will deeply miss.

I absolutely must thank Lauren for being the best housemate and most caring and considerate friend. I don't think anyone could ever rival her late-night pep talks and capacity for trashy tv.

I also need to thank Ashley for being insanely patient and supportive during a ridiculously stressful period of my life. Also thank you for reading my work, even when I wasn't so keen on your honest feedback!

Finally, thanks to Mum and Dad for listening to countless teary phone calls, sending me booze and biscuits in the post, and for reading practically every piece of written work to come out of the last four years- even if they didn't understand a word of it.

# Table of Contents

# List of Figures

# List of Tables

## Author's Declaration

I carried out all the larval chemical exposures, compound preparation, image acquisition and analysis. LC-MS/MS analysis was performed by Maciej Trznadel (MT; research assistant), the sample preparation for which was conducted both by me and MT. MT drafted the analytical chemistry methods (Chapter 2, section 2.8). DESI imaging (Chapter 4) was conducted and analysed by James Blades (undergraduate placement student) at AstraZeneca, supervised by Dr Greg Hamm. For that work, I embedded and sectioned the samples. I carried out all statistical analyses, data interpretation, and wrote the thesis with discussion on the data interpretations and editing from my supervisors.

## Covid Impact Statement

The mass spectrometry imaging (MSI) work (presented in Chapter 4) was originally intended to form a larger part of the thesis work, but this was prevented due to covid. A series of experiments was planned for using MSI to visualise the distribution of pharmaceuticals, their metabolites, as well as biomarkers such as lipids and antioxidants within the body of zebrafish larvae with idea to colocalise this with the fluorescence responses (OS induction) observed in the transgenic model. Due to the pandemic, AstraZeneca closed their laboratories and had restricted access to visitors after the lockdowns, so the experiment never progressed beyond the pilot stage.

Generation of data for chapter 6 was also impeded by the lockdown and for some time afterwards. After the laboratories re-opened, access was still limited and had to be requested separately for the aquarium and the lab. This required coordination between the two facilities as well as with other researchers and so work could not resume unimpeded for around 4 months.

# List of Abbreviations

| Abbreviation | Definition |
|---|---|
| 4-octyl phenol | OP |
| ABC | ATP-binding cassette |
| ADME | Absorption, distribution, metabolism and excretion |
| AMPK | Adenosine monophosphate-activated protein kinase |
| ANOVA | Analysis of Variance |
| APAP | Paracetamol |
| API | Active pharmaceutical ingredient |
| ARC | Aquatic Resource Centre |
| ATL | Atenolol |
| ATP | Adenosine triphosphate |
| BCF | Bioconcentration factor |
| BioMEMS | Biological micro-electromechanical systems |
| BPA | Bisphenol A |
| CAM | Clarithromycin |
| CAT | Catalase |
| Cis | Cisplatin |
| Cloz | Clozapine |
| CP | Cyclophosphamide |
| CW | Clean water |
| CYP450 | Cytochrome P450 |
| DASPEI | 2-(4-(dimethylamino)styryl) -N-Ethylpyridinium Iodide |
| DCF | Diclofenac |
| DESI | desorption electrospray ionisation |
| DMC | Desmethyl clozapine |
| DMSO | Dimethyl sulfoxide |
| DNA | Deoxyribonucleic acid |
| Dox | Doxorubicin |
| dpf | Days post fertilisation |
| E1 | Oestrone |
| E2 | Estradiol |
| EC | Environmental concentration |
| EE2 | Ethinyl estradiol |
| EpRE | Electrophile response element |
| ER | Effect ratio |
| ER | Oestrogen receptor |
| ERA | Environmental risk assessment |
| ERE | Oestrogen response element |
| ESR | Oestrogen receptor subtype |
| FET | Fish embryo toxicity |
| FPM | Fish plasma model |

| | |
|---|---|
| FssPC | Fish steady state plasma concentration |
| GFP | Green fluorescent protein |
| GI | Gastrointestinal tract |
| GPx | Glutahione peroxidase |
| GR | Glutathione reductase |
| gRNA | guide RNA |
| GSH | Glutathione |
| GSSG | Glutathione disulphide |
| GST | Glutathione-S-transferase |
| hpf | Hours post fertilisation |
| HTPC | Human therapeutic plasma concentration |
| HTS | High throughput screening |
| IBF | Ibuprofen |
| ICI | ICI 182, 780 (fulvestrant) |
| Keap1 | Kelch-like ECH-associated protein 1 |
| LC-MS/MS | Liquid chromatography tandem mass spectrometry |
| LGR | L-glutahione reduced |
| LLSM | Lattice light sheet microscopy |
| LOEC | Lowest observable effect concentration |
| Log D | distribution coefficient |
| Log Kow | logarithm of the octanol/water partition coefficient |
| LOQ | Limit of quantification |
| LSM | Light sheet microscopy |
| m/z | mass-to-charge ratio |
| MAPK | Mitogen-activated protein kinase |
| MBP | 4-Methyl-2,4-bis(4-hydroxyphenyl)pent-1-ene |
| MDA | Malondialdehyde |
| mER | Membrane bound oestrogen receptor |
| Min | Minute |
| MNLC | Maximum non lethal concentration |
| mRNA | Messenger RNA |
| MS-222 | Tricaine mesylate |
| MSI | Mass spectrometry imaging |
| NAC | N-acetyl-L-cysteine |
| NACA | N-acetyl-L-cysteine amide |
| NADPH | Reduced nicotinamide adenine dinucleotide phosphate |
| NAPQI | N-acetyl-p-benzoquinone imine |
| NO | Nitric oxide |
| Nrf2 | Nuclear factor-erythroid factor 2-related factor 2 |
| OS | OS |
| PCB | Polychlorinated biphenyls |
| PCR | Polymerase chain reaction |
| PCT | Pronephric convoluted tubule |

| | |
|---|---|
| PD | Pronephric duct |
| pKa | Acid strength |
| $P_{Plasma:Water}$ | Partitioning coefficient of a compound in fish plasma compared to water |
| PT | Pronephric tubule |
| qPCR | real-time quantitative reverse transcription PCR |
| RFP | Red fluorescence protein |
| RNA | Ribonucleic acid |
| ROI | Region of interest |
| ROS | Reactive oxygen species |
| SC | Solvent control |
| SEM | Standard error of the mean |
| SERM | Selective oestrogen receptor modulator |
| SOD | Superoxide dismutase |
| SRO | Salt reverse osmosis |
| TCDD | 2,3,7,8-Tetrachlorodibenzo-p-dioxin |
| TG | Transgenic |
| UAS | Upstream amplification system |
| VAST | Vertebrate automated screening technology |
| VTG | Vitellogenin |
| WIK | Wild Indian Karyotype |
| WT | Wild type |
| WWTW | Waste water treatment works |

# Chapter 1- General Introduction

## 1.1 Introduction

Pollution presents a major threat to the environment; contamination by organic chemicals have contributed to declines in freshwater ecosystem services and biodiversity (Malaj *et al.*, 2014). Aquatic wildlife is susceptible to chemical pollution because freshwater and marine environments act as sinks for most discharge chemicals. Waterways around the world are polluted with a range of contaminants, the primary sources of which include wastewater treatment work (WWTW) effluent and wastewater from industrial plants or agriculture, mining effluents, and diffuse land run off (Bound & Voulvoulis, 2005; Jain & Das, 2017; Pal et al., 2010; Williams & Cook, 2007). These contaminants extend to a wide range of diverse chemicals including heavy metals such as cadmium and mercury, chemicals found in fossil fuels such as polycyclic aromatic hydrocarbons (PAHs), pesticides and surfactants (Gasperi et al., 2008; Pal et al., 2010). Pharmaceuticals and their metabolites derived from agricultural and patient use are increasingly detected in the aquatic environment as global sales increase (Corcoran et al., 2010). Of the 350,000 chemicals and mixtures that are registered globally (Wang et al., 2020b), only a fraction have been thoroughly assessed for environmental risk. There is therefore a need to better understand how these chemicals may affect wildlife to assess their risk for environmental and human health protection.

Chemical effects assessments have traditionally relied on the endpoints of mortality, growth, development and/or reproduction to identify hazards, which are then used to extrapolate to population risk. More subtle effects however can lead to harm for the individual or populations as illustrated for various endocrine disrupting chemicals (EDCs). For example, EDCs have been shown to impair the ability of a fish to respond to stress by interfering with production of the stress hormone, cortisol. The mechanism of this effect is unclear but numerous studies have shown proximity to an upstream WWTW can result in impaired cortisol production in response to a stimulus (reviewed in (Matthiessen et al., 2018)).

There is an increasing emphasis on the use of molecular mechanism of toxicity in order to better understand the pathways by which compounds can induce

deleterious effects and this has led to the development of Adverse Outcome Pathways (AOPs). An AOP identifies and links the series of molecular and cellular events that ultimately result in a toxic effect in an organism (Ankley *et al.*, 2010). A key aim of the AOP framework is for more targeted assessment methods, in particular with regard to testing the most appropriate species and endpoint for maximising environmental protection (Ankley *et al.*, 2010). The AOP framework seeks to provide a more efficient approach to environmental risk assessments (ERAs) through the integration of *in vitro, in vivo,* and *in silico* data (Villeneuve *et al.*, 2014). As well as potentially providing more accurate predictions of toxicity and encouraging the economical use of time and resources, the AOP framework encourages alignment to the 3Rs (Replacement, Reduction, Refinement) of animal research by seeking to reduce the number of animals needed in chemical effects analyses. Interest is now growing around quantitative AOPs (qAOPs) which go a step further, defining the thresholds along a pathway needed for a molecular initiating event to lead to an adverse outcome, and the likelihood that these thresholds will be exceeded, aiding in the prioritisation of compounds for more thorough ERAs and regulation. These qAOPs, however, will require standardisation before they can proceed to any possible regulatory application (Spinu et al., 2020).

Transgenic (TG) fish can provide a valuable *in vivo* tool in the development of specific AOPs. TG fish contain exogenous DNA deliberately introduced into the genome to enhance a desired trait and have been applied in a range of fields for decades. These include aquaculture to increase growth rate (reviewed in (Zbikowska, 2003)); the development of pharmaceuticals (for example, in screening cardiovascular drugs (Kithcart & MacRae, 2017)); as models for human disease (including neurodegenerative diseases, reviewed in (Sager et al., 2010)); and in developmental biology for gene function analysis (reviewed in (Gong et al., 2004)). TG models are increasingly being applied in (eco)toxicology for identifying specific receptors or pathways involved with a chemical response. They offer highly integrated models which can provide meaningful mechanistic data by linking a molecular interaction between a stressor and a receptor (as indicated by the induction of fluorescence) to an adverse outcome. A criticism of the AOP framework can be the tendency to oversimplify biological pathways and lack consideration of feedback loops or cross-talk between pathways. The use of

different receptor- and cell-specific TG models can link multiple key events, even facilitating the construction of an AOP network (Villeneuve *et al.*, 2014). In addition to their role in the construction of predictive models for AOPs, TG fish can be used to confirm their predictions, improving faith in their robustness.

Through the visualisation of responses at the cell-specific level, TGs can also provide detailed mechanistic data without the need for more severe endpoints or time-consuming laboratory techniques. For example, a target organ can be quickly identified in a TG model by a tissue-specific fluorescence response and avoid the need to wait for a change in tissue function or morphology, which may take longer to manifest, require more of the test compound, and has greater welfare implications for the animal. As well as providing a highly efficient means for generating mechanistic data, TG models can also provide sensitive and convenient biosensors for aquatic contaminants (Kusik et al., 2008; Liu et al., 2016).

TG models also potentially allow for the response to a chemical to be measured (through changes in fluorescence intensity) in order to rapidly indicate the up- or down-regulation of genes of interest in real time. This contrasts with non-transgenic zebrafish, which for gene expression requires dissection of tissue, cell lysis, RNA extraction and qPCR/RNA seq to measure changes in gene regulation and which often requires animal destruction. The more integrated information provided through the use of TG fish can also facilitate an overall reduction in the number of animals used in an experiment, improving adherence to the 3Rs and enhancing the robustness of the data.

However, the insertion of a transgene into the genome of an animal can potentially interfere with normal genetic function and may result in unpredictable consequences (Ormandy et al., 2011) in the rest of the genome and therefore the phenotype. There is a lack of data comparing the chemical responses of a TG model with those of a WT zebrafish (Lee et al., 2015) and so for most models it is unclear the extent to which the TG model is truly representative of a wild fish. Also, the severity of impact on animal welfare associated with genetic manipulation isn't yet fully understood and has considerations with regard to the 3Rs.

Additionally, although the use of a TG fish can reduce the number of animals needed for an experiment, the process of generating and establishing a breeding stock of stable TG fish can require a large number of individuals. Some methods of transgene insertion can carry high mortality rates (such as microinjection, which can have variable results (Hayat *et al.*, 1991)), and many embryos can be lost at the screening stage as individuals of the F0 generation that do not carry the transgene or exhibit insufficient integration are terminated. Although some TG lines can be screened before the point of protection (age of independent feeding, or 96 hpf for zebrafish) if the fluorescence is clearly expressed early enough. Furthermore, transgenic methods that result in fish with varying integration sites may lead to the researchers requiring to raise several different lines with the only difference being the integration sites- further increasing the number of animals used (Ormandy *et al.*, 2011). Additionally, a TG model requires extensive validation before the embryos can be used as a replacement for adults because certain chemical effects may only manifest in later life-stages (Lee et al., 2015), this again requires more time and animals. While experiments using TG rodents are beginning to decline, the popularity of TG zebrafish, and therefore the numbers of fish used, is rapidly increasing (Great Britain & Home Office, 2019).

Zebrafish (*Danio rerio)* and medaka (*Oryzias latipes)* are the most popular TG fish models. This is due to several features they share: a short generation time of 2-3 months (Matsui et al., 2012) allowing rapid generation of new lines; transparent eggs and rapid organogenesis facilitating direct observation of egg/embryo development; high fecundity; and being relatively cheap and easy to maintain in a laboratory. Importantly, both species also have fully sequenced genomes (Lee et al., 2015), facilitating DNA editing and providing a rich library of genetic resources. Additionally, there are many useful established mutant lines relevant for biomedical research. Zebrafish and medaka have been adopted for studies in developmental biology and genetics, including their roles in human disease (Matsui *et al.*, 2012). The choice of either the medaka or zebrafish depends on the aim of the study, which transgenics are available, and laboratory preference. The zebrafish is more widely used in Europe, contrasting with Japan where the medaka is favoured. Medaka spawn every day (compared to once/twice a week for female zebrafish), but an individual medaka only produces 20-40 eggs per spawning event, compared with up to a hundred or more for

zebrafish (Furutani-Seiki & Wittbrodt, 2004). Both are freshwater species but, medaka can live at a wider range of temperatures compared to zebrafish (Furutani-Seiki & Wittbrodt, 2004) and tolerate saline conditions (Miyanishi et al., 2016), expanding the potential applications of this species for developmental and toxicological assessments in wider environmental conditions. However, medaka can be more challenging to image for several reasons, including highly mobile embryos in early life stages; the chorion are covered in hairs; and eggs contain oil droplets. Harder chorions also complicate microinjection.

There are very limited data on direct comparisons of the sensitivity and efficacy of a TG medaka lines with zebrafish lines. One study showed that the zebrafish Cyp1a:GFP model (a biosensor for hypoxia or organic xenobiotic exposure) was more sensitive to specific dioxin-like compounds than its medaka counterparts. However, this did not apply to all compounds in this class (Xu et al., 2018), indicating a more complex story. A search on PubMed for the terms 'transgenic', 'chemical' and 'zebrafish' yields 491 publications in the last 20 years, compared with 56 for 'transgenic', 'chemical' and 'medaka' (accessed on 5/6/21), illustrating the wider uptake of zebrafish (vs medaka) in ecotoxicology.

## 1.2 Transgenic generation and reporter genes

There are several approaches to generate a TG line. These include meganucleases, bacterial artificial chromosomes (BACs) or transposons for construction of the vector, or Zinc finger nucleases (ZFNs). All involve the same basic stages of: a) construction of a recombinant DNA plasmid containing a promotor and a gene of interest (such as a reporter gene, or fluorophore); b) insertion of this plasmid, or vector, into the embryo at the 1-2 cell stage; and c) cross-breeding of the TG fish (F0) with wild type fish, the offspring of which are then screened for homozygosity. The result is an animal model in which, when the promotor of interest is activated, the reporter gene/fluorophore is also upregulated to produce a fluorescent signal. More recent advances in TG model generation use CRISPR/Cas9 for genome editing (reviewed in (Lee et al., 2015)) due to its improved efficiency and simplicity. The co-injection of a donor plasmid along with a short guide RNA (sgRNA) for genome digestion, a sgRNA for donor plasmid digestion, and CAs9 mRNA allows the highly targeted insertion (or 'knock-in') of a fluorophore into the promoter region of a gene of interest (Abdelmoneim et al., 2020; Kimura et al., 2014).

A wide range of fluorophores are used in TG fish, and the choice of fluorophore depends heavily on the purpose of the TG model. Green fluorescent protein (GFP) is one of the more popular fluorophores due to its brightness and photostability. However, there is a high noise:signal ratio due to the wavelength needed to excite the GFP which also produces strong autofluorescence, potentially masking weaker signals of low-level expression. For genes with very low expression levels, red fluorescent proteins (RFPs) can be preferable as they have a lower noise:signal ratio due to the longer wavelength required for excitation of the protein (Heppert *et al.*, 2016). Dynamic reporters are also becoming more popular, such as the photoconvertable fluorophore kaede, used for sequential tracking of labelled cells (Sato et al., 2006). There are also DNA-encoded calcium indicators (DECI) like GCaMP which can visualise calcium dynamics of brain activity in zebrafish *in vivo* for developmental biology (Chen et al., 2017), to detect chemicals that may affect motor function (Shahid *et al.*, 2016), and to profile the effects of chemoconvulsants (Winter *et al.*, 2017).

## 1.3 Application of TG lines in ecotoxicology

Hundreds of TG fish models have been developed for chemical effects studies. Those TG lines which have, arguably, advanced the field more have done so due to their versatility and/or the priority of the contaminant class they detect, including for studies on specific cell types, oestrogens and cellular stress. The range of models available are illustrated below (see Fig. 1.1); how these lines operate, where they have been applied and the new discoveries made using them are described. In particular, the ERE:GFP model for the oestrogen response element (ERE) and EpRE:hsp70:mCherry model for the electrophile response element (EpRE), both of which are used in this project, are introduced.

Although exposure conditions can vary between studies, typically TG zebrafish are exposed to the contaminant aqueously (mimicking conditions in the environment). In most cases also TG zebrafish were most often used at 0-4 dpf, when they are still transparent to allow visualisation of internal tissues, and prior to independent feeding and are hence not classed as protected species by European legislation (EC, 2010).

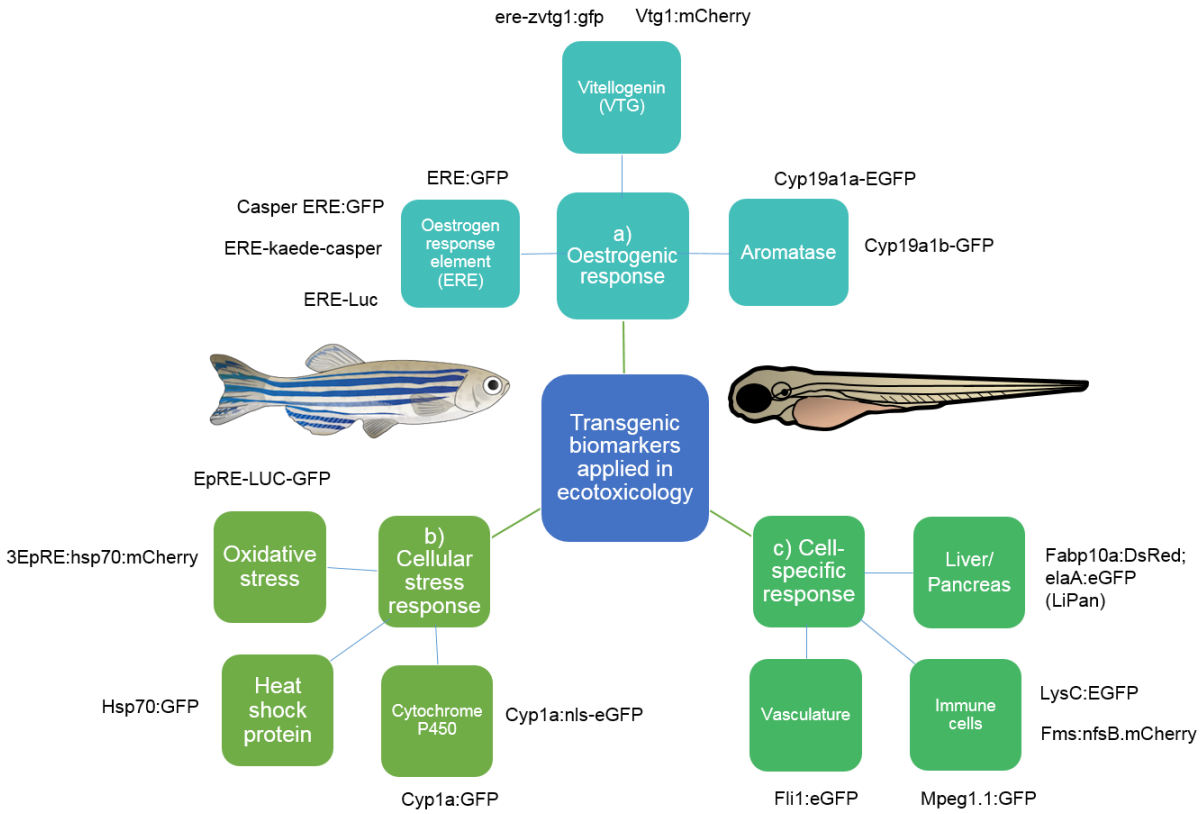


*Figure 1.1* ***The range of models to be discussed in this review and how they relate to one another***

### 1.4.1 Specific cell-type response

A series of TG zebrafish systems have been generated that consist of reporter genes with cell-specific expression that facilitate the study of specific tissues. This can be useful for identification of the organ (e.g. to aid in its extraction/sectioning), to assess changes in its morphology, or to analyse changes in its function (which can often be inferred from changes in expression of the fluorophore). These models cover a broad range, including for the kidney(Zhou et al., 2010) and for neuromasts/hair cells(Choi et al., 2013). Here I have chosen to focus on LiPan (for the liver and pancreas), Fli1 (vasculature), and LysC and mpx/mpo (immune cells) models as they represent common targets for pollutants and are among the most popular for ecotoxicology studies. These models can be used to screen contaminants for organ-specific toxicity, or to help build a mechanism of toxicity for that organ.

#### *1.4.1.1 Liver/ pancreas*

The fabp10a:DsRed;elaA:eGFP TG model (abbreviated to LiPan), expresses red fluorescence in the liver under the control of the hepatic fatty acid promoter *fabp10a*, and green fluorescence in the exocrine pancreas under the control of the pancreas *elaA* promoter (Korzh *et al.*, 2008), and has been used to develop

an *in vivo* hepatotoxin screening assay (Zhang et al., 2014). Liver fatty acid binding protein is commonly used as a biomarker for acute kidney damage, and the red fluorescence and *fabp10a* mRNA (confirmed using RT-PCR) has been shown to faithfully reflect liver toxicity. The limitations of this model relate to those in common with other TG models: changes in mRNA levels are often greater than changes in the fluorescent protein, thus mRNA quantification may be a more sensitive measurement than fluorescence intensity (Maier et al., 2009).

The model can be used to further understanding on the mechanism behind chemical-induced hepatotoxicity; as reflected in reduction of fluorescence intensity (suggesting perturbation of fatty acids metabolism pathway) or in changes in liver size (suggesting a secondary effect of severe liver damage). The LiPan model has been applied successfully to test for mixture effects of known hepatotoxins ( a combination of paracetamol, aspirin, isoniazid and phenylbutazone) (Zhang et al., 2014) and to test the combined toxicity of common mycotoxins found in grains and animals feeds (Zhou et al., 2017). Here, high content screening was used to examine for liver abnormalities using an automated epifluorescence microscope (Zhou et al., 2017). Paired with a suitable imaging platform (such as VAST (Pardo-Martin *et al.*, 2010), Acquifer (Westhoff *et al.*, 2020), or ArrayScan (Green *et al.*, 2016)), the model has potential as a HTS system for human pharmaceuticals for hepatotoxicity- helping to streamline drug development.

#### *1.4.1.2 Vasculature*

The *fli1* promoter is crucial to vasculogenesis and is a popular endothelial biomarker. A zebrafish Fli1:eGFP model was originally developed for visualisation of embryonic vascular development (Lawson & Weinstein, 2002) and subsequently applied in toxicology studies (Jergensen et al., 2019; Jin et al., 2019; Moon et al., 2020; Park et al., 2020). *Fli1*- driven fluorescence is expressed in blood vessels and can be used to visualise the blood vessel structure and, more importantly, development of the vasculature, allowing chemical-induced perturbations to be rapidly identified. Early uses of the model facilitated the characterisation of a possible mechanism behind the 'string-like' heart phenotype induced by 2,3,7,8-tetrachlorodibenzo-p-dioxin (TCDD), as the pattern of fluorescence showed reduced common cardinal vein growth (Bello et al., 2004). Similar to other TG models, the fli1:eGFP zebrafish is at least as sensitive as

traditional endpoints and can detect contaminants more quickly in the response cycle (Bello et al., 2004; Delov et al., 2014). Use of this model in a fish embryo toxicity (FET) assay has been validated as it can provide more refined, quantifiable measurements at sub-lethal concentrations of environmental contaminants in comparison to traditional FET assays which use mortality as an endpoint. Additionally, in contrast with bright-field based morphology assessments, measurement of the fluorescent pattern is more sensitive (Delov *et al.*, 2014). More recently, Moon, Atiqu and An (2020) used this model as part of a wide array of biological measurements in an ecological risk assessment of a polluted urban stream, where they showed exposure caused the development of an abnormal heart (Moon *et al.*, 2020).

#### *1.4.1.3 Immune cells*

Immune cell TG models have not been used widely in ecotoxicology studies, particularly when compared with biomedical research where they have been applied to further understanding of immune function and the inflammatory response. Indeed, a search on Pubmed using the terms ‘transgenic’, ‘zebrafish’ and ‘immune function’ yields 125 results compared with 16 when ‘function’ is replaced with ‘toxicity’ (date searched 13/7/21). This reflects the use of the zebrafish immune TG models in human health studies and the fact that there is a high level of homology between teleost and mammalian immune cells (Ellett & Lieschke, 2010). Immune cell models however are now starting to be applied in drug mechanism studies, and to assess for toxic interactions between pollutants and the inflammatory response, and notably for nanomaterials (Chakraborty et al., 2016; Pensado-López et al., 2021). Unlike in the case of the LiPan model, where a whole organ is labelled, in immune cell TGs individual immune cells are labelled enabling the visualisation of the dynamic responses, often studied as they migrate towards an injury site. These models include lysC:DsRed, in which a subset of neutrophils and macrophages are labelled, that allow investigations into the mechanism by which pollutants can cause hepatic injury and the role of the immune response in mediating this reaction (Chen et al., 2018). However, some LysC labelled cells have also been found to contain transcripts for myeloperoxidase, potentially calling into question the specificity of this model (Hall et al., 2007).

More specific lines are available, such as mpx or mpo-labelled models which identify neutrophils only by labelling the promoter for the enzyme myeloperoxidase (Renshaw *et al.*, 2006). Macrophage-labelled reporter lines are also available, including mpeg1.1:GFP and mpeg1.1:mCherry, which use the promoter for macrophage-expressed gene encoding *perforin-2* and have been used in over 100 publications on macrophage function and lineage (Ferrero *et al.*, 2020). In the zebrafish model fms:nfsB.mCherry, wherein fluorescence is controlled by the *fms* promoter for the macrophage-specific CSF2R protein, it is possible that not all macrophages express the transgene (Gray *et al.*, 2011). Here therefore, a trade-off is made between specificity and comprehensively labelling all target cells. For assays where specificity is less of a priority, broader-based models such as LysC are the most suitable.

### 1.4.2 Oestrogen response

Chemicals with oestrogenic activity have been linked to adverse outcomes in individual fish (Lange & Paull, 2009; Xu et al., 2008) and fish populations (Hamilton et al., 2015; Jobling et al., 2002; Kidd et al., 2007; Tyler & Jobling, 2008). Many compounds are now known to act as oestrogen receptor (ER) agonists, although their molecular structures vary, making it difficult to reliably predict which chemicals will present the greatest risk based on the chemical structure activity relationship (SAR) alone (Bakos et al., 2019; Saliner et al., 2006; Schmieder et al., 2003). Adding to this concern on chemicals with oestrogen activity, the contraceptive oestrogen (ethinyl estradiol, EE2) (Tyler et al., 1998) has been identified as amongst those active pharmaceutical ingredients (APIs) posing the greatest risk to the environment (Gunnarsson *et al.*, 2019). This concern has fuelled the development of TG models for oestrogens and these have been applied to screening for oestrogenic activity (Brion *et al.*, 2012; Legler *et al.*, 2000; Moreman *et al.*, 2017), detecting xenoestrogens in environmental samples (Bakos et al., 2019; Chen et al., 2010), and identifying target organs for oestrogenic effects (Gorelick & Halpern, 2011; Green et al., 2016, 2018; Moreman et al., 2018).

#### 1.4.2.1 Oestrogen response element

Various TG lines have been developed to study environmental oestrogens. The first TG zebrafish line developed as an oestrogen biosensor used an oestrogen binding sequence linked to a TATA box (a type of promoter sequence) and a

luciferase reporter gene (Legler *et al.*, 2000). A limitation of this model was luciferase was not directly visible in live fish and further labour intensive steps were required to measure the level of luciferase induction. A major advancement in oestrogen TG zebrafish was in the generation of a stable ERE (oestrogen response element) TG model that allowed real-time *in vivo* visualisation of the oestrogenic response using 5 consecutive EREs, a mouse c-*fos* promoter, and GFP. This model identified target organs that had not previously been identified as responsive to oestrogens in fish, including the heart (Gorelick & Halpern, 2011). The model has since been combined with other molecular techniques to provide more detail on the oestrogenicity of environmental samples. RNA *in situ* hybridisation confirmed that different water effluent samples could induce tissue-dependent fluorescence in the TG model due to differing expression of the different ER subtypes (*esr1* was expressed in heart valves but not the liver, and *vice versa* for esr2b) (Gorelick et al., 2014).

One of the most sensitive oestrogen response models, and the one which is used in the first data chapter of this thesis, is the ERE:GFP model (see Table 1.2). This TG zebrafish is responsive to environmentally relevant concentrations of EE2 (as low as 1ng/L), with responses seen in a range of tissues including liver, heart, skeletal muscle, and brain. The tissue response profiles across time and tissue type varied with the different environmental oestrogens tested, including bisphenol A (BPA) and nonylphenol (NP), demonstrating the application of this model for screening the potential health effects of different oestrogenic chemicals (Lee et al., 2012a). The TG model can also be used to refine subsequent studies to elucidate the mechanism behind these chemical responses. In work comparing the oestrogenic potencies and targets of BPA and other plasticisers (Moreman *et al.*, 2017), the ERE:GFP model was combined with immunostaining to show BPA targets the heart valves affecting their development and subsequent functioning (Moreman *et al.*, 2018).

Further, the ERE:GFP model has also been combined with other genetic manipulation methods to refine our understanding of these molecular mechanisms. In the ERE:GFP model the ERE ligand can bind with any of the 3 ER subtypes found in fish, which means the fluorescence signal does not distinguish through which of these ER subtypes the response is mediated. The use of morpholinos to systematically knock down expression of each of the ER

subtypes was used to identify that esr1 mediates the developmental response of heart valves to BPA and 4-Methyl-2,4-bis(4-hydroxyphenyl)pent-1-ene (MBP; a metabolite of BPA) (Moreman *et al.*, 2018).

The combination of ERE:GFP line with a pigment-free 'casper' phenotype has further expanded the use of the ERE:GFP model as the lack of pigment allows the fluorescent signal to be detected in later life stages than would otherwise be possible (Brown et al., 2019). By combining this model with an ArrayScan, this model has also been developed for high-throughput and high-content analysis (Green *et al.*, 2016).

These ERE:GFP lines have also recently been applied successfully to the study of complex mixtures of oestrogenic chemicals contained in WWTW effluent, illustrating their utility for studies on environmental samples (Cooper et al., 2021a, 2021b). It should be emphasised that in addition to the nuclear ERs in fish (and in mammals too) there are other variants of ER including the orphan receptor oestrogen related receptor (ERR) and membrane bound oestrogen receptors (mER), the roles of which are not well established and could potentially be involved in the ERE mediated fluorescent response in a TG model (Green *et al.*, 2016). This, of course complicates interpretation on the precise mechanism of action for exposure to environmental oestrogens.

To enhance the utility of the ERE- casper TG zebrafish model for studies into the dynamics of the oestrogenic response, a revised model with kaede, a photoconvertable fluorophore has been developed (Green *et al.*, 2018). Kaede turns from green to red under UV light exposure (Ando et al., 2002). Kaede is a fluorophore reporter that has most notably been used for tracking cell fate and cell dynamics (Hatta et al., 2006; Sato et al., 2006). Green *et al.* applied the casper ERE-Kaede TG model to show early life exposure to EE2 altered (sensitised) responsiveness to a variety of different oestrogens for subsequent exposures. This emphasised the importance of the history of exposure to oestrogens when considering the potential health consequences for exposure and with implications for ERAs (Green *et al.*, 2018). However, use of this casper ERE-TG line is still largely limited to early life stages as the increasing opacity of the organs and tissue thickness as they grow (i.e., even in the absence of skin pigmentation) reduces the ability to detect a fluorescent signal as the larvae develops.

#### 1.4.2.2 Other models for oestrogenic responses

*Cyp19a1b* encodes for brain aromatase, is responsible for production of oestrogen, and is expressed only in radial glial progenitors in the brain. Brion *et al.* (2012) developed a TG *cyp19a1b*-GFP zebrafish to show that radial glial cells are a target of endocrine disrupting chemicals (EDCs) and that brain aromatase responds in a dose-dependent manner to a wide range of oestrogenic chemicals, as well as androgens and synthetic progestogens (Brion *et al.*, 2012). Prior to this study, little attention had been paid to the effect of oestrogens on the brain development of fish or indeed the role of aromatase in vertebrate brain development. This study was one of the first to highlight the brain as a target organ for oestrogenic chemicals in fish (Brion *et al.*, 2012), and was one of the first models to be included in OECD testing guidelines (*Test No. 250: EASZY Assay - Detection of Endocrine Active Substances, Acting through Estrogen Receptors, Using Transgenic Tg(Cyp19a1b:GFP) Zebrafish EmbrYos*, 2021).

A TG model for gonadal aromatase, *Cyp19a1a*-EGFP (enhanced GFP), has subsequently been developed which can be applied to provide complementary mechanistic data in the OECD Fish Short Term Reproduction Assay (test no. 229). The GFP expression in the gonads of this model can provide additional information on the time and concentration dependent effects of the compound of interest without compromising the reproductive output of the fish, therefore still providing the standard information required by this test (De Oliveira et al., 2020; *Test No. 229: Fish Short Term Reproduction Assay*, 2012)

Vitellogenin has been used extensively as a biomarker for detecting oestrogen activity and has traditionally been measured using biochemical assays (protein ELISA, gene PCRs etc.) (reviewed in (Wheeler et al., 2005)). Vitellogenin is a yolk protein precursor under the control of ERE (Wahli et al., 1981) and can be induced by oestrogenic exposure (Flouriot *et al.*, 1993). Some highly sensitive TG models have been generated based on the *vtg1* gene that are able to detect a variety of oestrogens, and for some, at environmentally relevant concentrations, including EE2 down to 1ng/L (Bakos et al., 2019; Chen et al., 2010). Recently, Abdelmoneim, Clark and Mukai used CRISPR/Cas9 to generate a vtg1:EGFP model, albeit it was less sensitive than some of the other lines (e.g Bakos *et al* 2019). This may relate to the fact that Bakos *et al.* used homozygous F4

generation zebrafish in their exposure studies, where Abdelmoneim, Clark and Mukai used a heterozygous F1 generation (Abdelmoneim *et al.*, 2020).

Vitellogenin is only produced in the liver, and as such these models act as biosensors for oestrogen exposure only rather than provide any information on possible functional consequences for oestrogen exposure. Additionally, although both sexes possess the *vtg1* gene, levels of endogenous vitellogenin in maturing and adult females limit the application of this model as a biosensor in adults to males only.

In summary, the different TG zebrafish models described above for detecting oestrogen exposure exhibit a range of different sensitivities (see also Table 1.2), and they have also been designed for different purposes in mind. Models incorporating ERE enables the visualisation of oestrogenic responses throughout the body and facilitates identification of target organs (Gorelick & Halpern, 2011; Green et al., 2016; Lee et al., 2012a; Moreman et al., 2018), the *Cyp19a1b* model facilitates detailed analysis on how oestrogenic compounds interfere with brain development specifically (Brion *et al.*, 2012), and the *vtg1* models provide sensitive systems for detecting exposure and hepatic responses to oestrogens (Bakos et al., 2019; Chen et al., 2010).

### 1.4.3 Cellular stress response

There are many mechanisms by which a pollutant can cause cellular stress, and as such this is one of the broadest categories of TG models. Oxidative stress (OS) is the mechanism by which countless toxic effects are mediated, and here the common causes, consequences, and measurements of OS are discussed. TG models for the study of OS are introduced, including the novel TG(EpRE:mCherry) which forms the backbone of this thesis work. TG models comprised of the heat shock protein (hsp70) or cytochrome P450 (cyp1a) are also briefly discussed and compared as they are popular models for understanding toxic effects through these mechanisms.

#### 1.4.3.1 Oxidative Stress

OS occurs as a result of an imbalance between reactive oxygen species (ROS) production and anti-oxidative defence systems (see Fig. 1.2). ROS include oxygen ions and free radicals, which are oxygen molecules with one or more unpaired electrons, rendering it extremely reactive, and are produced naturally

by normal cellular metabolism and can play a key role in cellular signalling. ROS are primarily produced as byproducts of the mitochondrial respiratory chain, but also by NADPH and lipoxygenase activity (Deavall et al., 2012). Cellular antioxidative defence consists of a combination of low-weight antioxidants, such as ascorbic acid and glutathione (GSH), and enzymes such as glutathione peroxidase (GPx) and superoxide dismutase (SOD) (Deavall *et al.*, 2012) (see Fig. 1.3). In fish, most of these antioxidants are obtained from food, but GSH is synthesised and regulated based on environmental or physiological conditions. GSH is maintained in its reduced form by glutathione reductase, which uses NADPH to reduce oxidised glutathione (GSSG) to GSH (Lushchak, 2016). Hence, the ratio of GSH:GSSG can be used as a measure of cellular redox state. ROS play a key role in cellular signalling but, when ROS production exceeds the capacity of cellular anti-oxidative defence mechanisms, ROS can go on to cause oxidative damage such as via lipid peroxidation, protein damage, DNA damage or triggering signalling cascades (Deavall *et al.*, 2012).

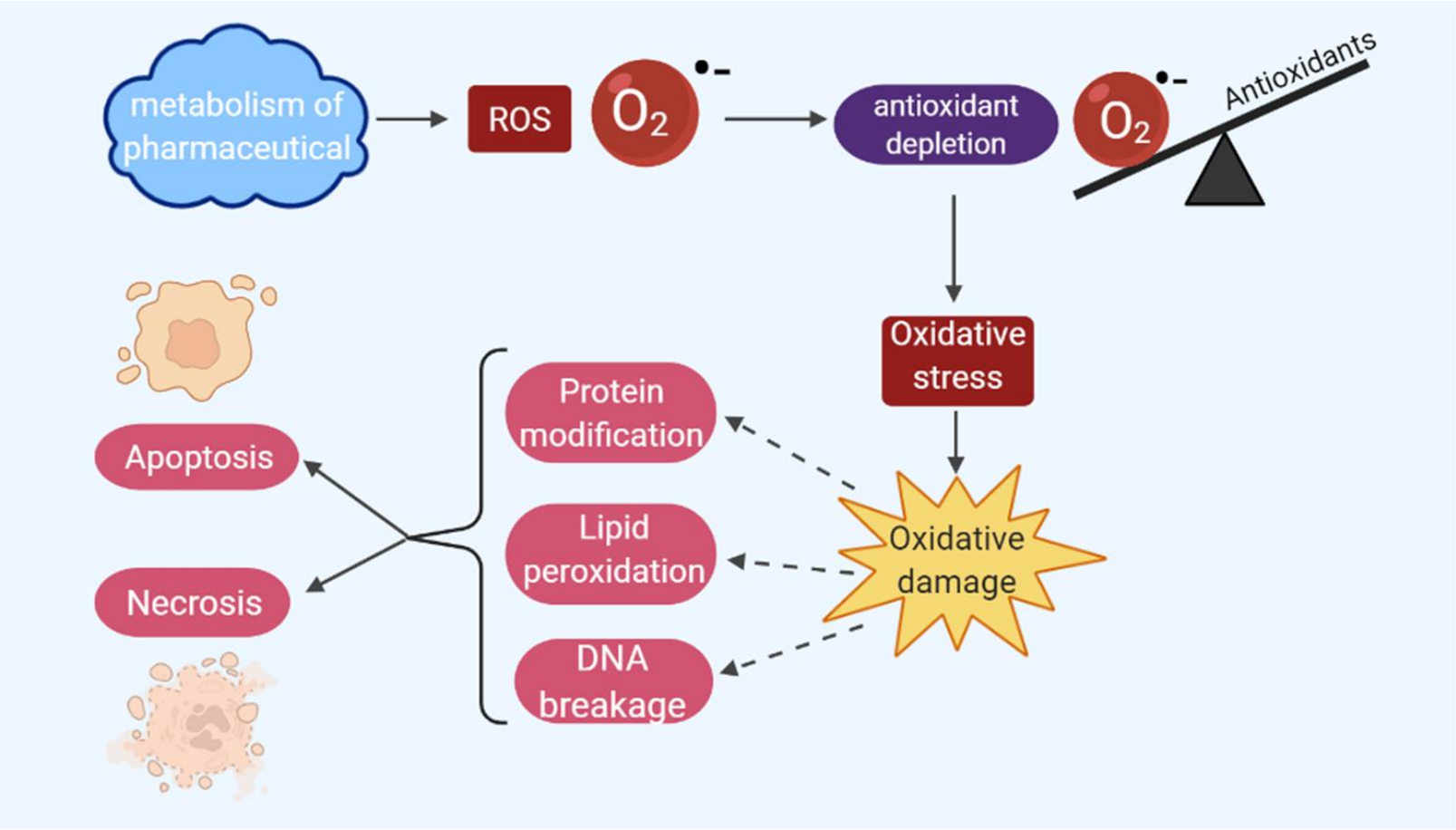


*Figure 1.2* ***OS occurs when there is an imbalance between reactive oxygen species (ROS) generation and the cellular antioxidants****. This can result in oxidative damage including via protein modification, lipid peroxidation, and DNA breakage, and can sometimes lead to cell apoptosis or necrosis.*

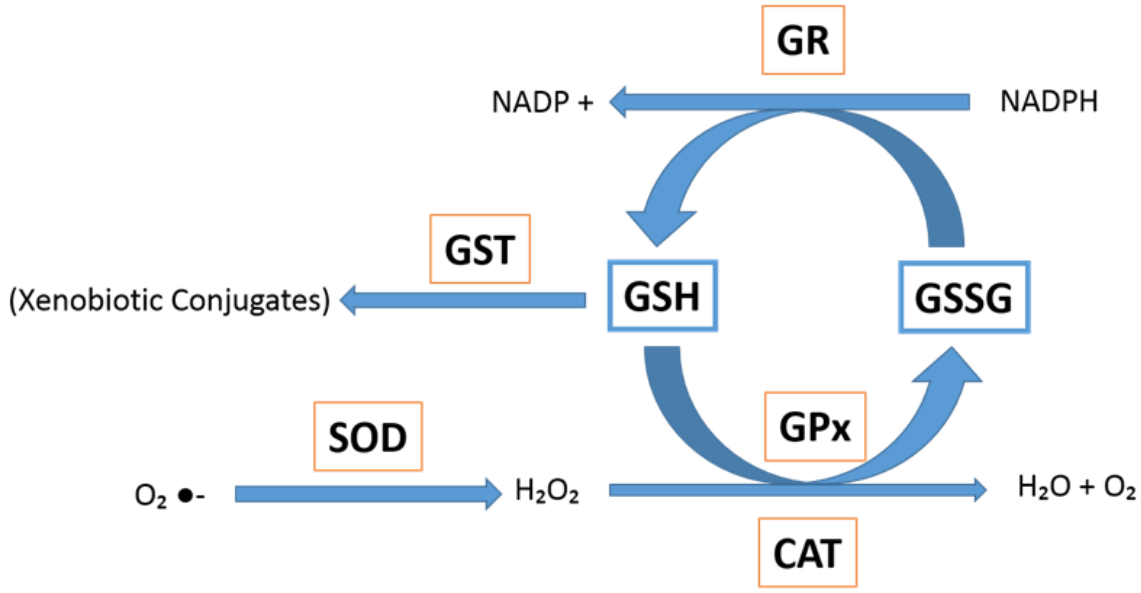


*Figure 1.3* ***Schematic of the enzymatic antioxidant system****.*

***GR: Glutathione reductase*** *- Encoded by the GSR gene, catalyses the reduction of GSSG (glutathione disulphide) to GSH (glutathione) to maintain the GSSG:GSH balance.* ***GPx: Glutathione peroxidase*** *- Family of enzymes with peroxidase activity. Reduces $H_2O_2$ (hydrogen peroxide) using GSH and reduces lipid peroxidases, prevents oxygen from forming radicals.* ***GST: Glutathione-S-Transferase*** *- Family of Phase II metabolic enzymes. Catalyses conjugation of GSH to xenobiotics to make them more water soluble and aid excretion. Also detoxifies peroxidised lipids.* ***SOD: Superoxide dismutase*** *- Catalyses the dismutation of the superoxide radical ($O_2$ ●-) into molecular oxygen and $H_2O_2$.* ***CAT: Catalase*** *- Catalyses decomposition of $H_2O_2$ to water and oxygen.*

OS is a major mechanism of damage which can mediate many pathogenic or toxic effects and can also be triggered by a range of factors, including via an immune response or chemical exposure. OS induced damage to DNA is implicated in health conditions including cardiovascular disease, cancer, and neurodegenerative diseases such as Alzheimer's (Russo *et al.*, 2012). In the effect cascade, metabolism of toxic compounds can generate ROS through production of a reactive intermediate which can directly reduce molecular oxygen or the reaction with metal ions. ROS then exert their toxic effect through a range of pathways, including via mitochondrial dysfunction (including cytochrome C release which can trigger apoptosis) (Jin et al., 2011) or modification of signalling cascades (e.g., mitogen-activated protein kinases; MAPKs) (Son *et al.*, 2011). ROS can also be produced by endogenous sources such as the mitochondria via the electron transport chain, peroxisomes or endoplasmic reticulum (Phaniendra

et al., 2015). OS can be induced by a range of pathways and cause damage through a number of molecular and cellular events, but they are not fully understood. Pharmaceutical-induced OS (reviewed in (Deavall *et al.*, 2012) is often implicated in drug toxicity even if the mechanisms of ROS generation have not been fully characterised (Deavall *et al.*, 2012)

Due to the instability of ROS, it is virtually impossible to measure their levels *in vivo* (Lushchak, 2011), but there are multiple methods for measuring the levels of products modified by ROS, such as lipid peroxidation, or levels of anti-oxidants, such as SOD activity (see Table 1.1). While these do not measure OS directly, they can measure proxies and indicate consequences of OS; no single method is necessarily preferable as it can depend on the study aims, tissue type and sampling method (Birnie-Gauvin et al., 2017). However, none of these methods can provide real-time measurements, and can be difficult to indicate localisation of responses, unlike TG models which can visualise tissue-specific responses in real time and without destructive methods.

*Table 1.1* ***Some of the more popular traditional measures of OS in fish biology****. Adapted from Birnie-Gauvin et al. 2017*

| OS biomarker | Method | Application | Reference |
|---|---|---|---|
| **Protein carbonyls** | Protein carbonyl formation | Protein damage, fragmentation; insight into overall oxidative stress levels | Levine *et al.*, 1990; Stadman and Berlett, 1997 |
| **DNA damage** | 8-hydroxy-2'deoxyguanosine assay | DNA damage; insight into overall OS levels | Kasai, 1997 |
| **Lipid peroxidation** | Thiobarbituric acid reactive substance test | Lipid damage; insight into overall OS levels | Draper *et al.*, 1972 |
| **Catalase (CAT)** | CAT enzymatic activity assay | Insight into antioxidant defences; higher activities may be associated with higher levels of H2O2 | Sinha, 1972 |
| **Superoxide dismutase (SOD)** | SOD activity assay | Insight into antioxidant defences; higher activities may be associated with higher levels of O2•− | Beauchamp & Fridovich, 1971; Ōyanagui, 1984 |
| **Glutathione peroxidase (GPX)** | GPX activity assay | Insight into antioxidant defences; higher activities may be associated with higher levels of ROS | Flohé & Günzler, 1984; Paglia & Valentine, 1967 |
| **Glutathione reductase (GR)** | GR activity assay | Insight into antioxidant defences; GR reduces GSSG back to GSH; higher activities of GR may be associated with higher levels of GSSG | Carlberg and Mannervik 1975; Wheeler, Salzman, Elsayed, Omaye, & Korte, 1990 |

| | | | |
|---|---|---|---|
| **Glutathione (GSH); total glutathione (TGSH); glutathione disulphide (GSSG)** | Glutathione assay | Provides insight into oxidative damage (GSH to GSSG ratio or vice versa) and antioxidant defences (GSH) | Akerboom & Sies, 1981; Smith, Vierheller, & Thorne, 1988 |
| **Vitamin C (ascorbic acid)** | Ascorbic acid assay | Insight into antioxidant defences (provides an electron to quench ROS) | Deutsch & Weeks, 1965; Roe & Kuether, 1943 |
| **Vitamin E (α-tocopherol)** | Vitamin E assay | Insight into antioxidant defences (peroxyl radical scavenger) | Prieto, Pineda, & Aguilar, 1999 |
| **Low molecular weight antioxidants** | Oxygen radical absorbance capacity (ORAC) assay | Insight into total low molecular weight antioxidant defences. | Cao, Alessio, & Culter, 1993 |

The main promoter used to generate TG models for detection of OS is for the EpRE. This can be used alone or in combination with hsp70 (a type of heat shock protein, which can also be used as an indicator of OS). The EpRE is a region of DNA responsible for coding for many cytoprotective proteins (Hayes et al., 2005) including phase II detoxifying enzymes (Nakajima *et al.*, 2011). The EpRE forms part of one of the major OS-response pathway, mediated by the Nrf2/Keap1 (Nuclear factor-erythroid factor 2-related factor 2/ Kelch-like ECH-associated protein 1) modulatory system, which acts on the EpRE in response to a change in RedOx homeostasis (discussed in more detail in chapter 3). This balance can be disrupted by a range of environmental stressors including environmental contaminants. TG fish exploiting this biomarker can be used as biosensors to detect pollutants (Kusik *et al.*, 2008) or to differentiate tissue responses to such stressors (Mourabit *et al.*, 2019).

### *OS TG models*

In the first EpRE TG line generated, the plasmid consisted of EpRE from the glutathione-S-transferase (GST) enhancer region fused to the minimal mouse metallothionein1 promotor (Kusik *et al.*, 2008). The model was considerably more sensitive than in the zebrafish cell lines transfected with the same reporter, and morphology- or mortality-based assays; responses were detected at ten-fold lower exposure concentrations of mercury than in the cell lines reported (Carvan *et al.*, 2001), and at concentrations lower than those required to cause any obvious deformities. In this model, luciferase, used for quantification of the response, was detectable in both the transient and stable lines, however GFP (used for localisation of the response) was only induced in the transient line (Kusik *et al.*, 2008).

More recently, an EpRE:mCherry (3EpRE:hsp70:mCherry) line allows for responses to be visualised and measured across tissues in real-time and non-destructively (via imaging). This model is sensitive to a range of pro-oxidative contaminants, with different response profiles for different contaminants that align closely with their known toxicological mechanisms in mammals. For instance, paracetamol and cisplatin both induce OS in the pronephric proximal tubules, but only cisplatin in the neuromasts and only acetaminophen in the liver (Mourabit *et al.*, 2019).

Reporter genes in this model are fused to EpRE, which is ubiquitously expressed throughout the body, meaning the OS response can be visualised across all tissues in these models. This allows for detection of a wide array of biological processes perturbed by OS and a clear advancement on many more traditional approaches such as biochemical assays quantifying levels of specific antioxidants, or molecular methods, which most often are limited to assessing the OS in a pre-defined tissue (Mourabit *et al.*, 2019; Nakajima *et al.*, 2011).

The EpRE:mCherry model is introduced in more detail in chapter 4, but a limitation of this model is that OS may not be detected if it is buffered by a mechanism not involved in the Keap1/Nrf2 pathway. Indeed, EpRE is not the only transcriptional regulator that responds to OS; AP-1 (Activator protein 1) is activated by JNK (c-Jun N-terminal kinases) and can affect cell proliferation, and NF-kB (nuclear factor kappa B) regulates pro-inflammation proteins. Both of these other mechanisms have been shown to mediate redox-responsive gene expression (Dunaway et al., 2018; Zhou et al., 2001). Additionally, some environmental pollutants can inhibit antioxidant enzymes (Fonseca et al., 2018; Zhang et al., 2021a). Antioxidant inhibition could occur upstream or downstream of the EpRE and it is unknown if/how this could feedback to the promoter, but it has the potential to downregulate mCherry fluorescence and so complicate interpretation of the redox state of the animal.

#### 1.4.3.2 Other cellular stress models

Heat shock proteins (HSPs) are a family of highly conserved proteins produced in response to a variety of stressors including temperature, wound healing, and toxins. They are molecular chaperones which aid in the folding, transport, and degradation of cellular proteins (Blechinger et al., 2002). Hsp70 encodes for a highly responsive isoform and is amongst the best characterised family of HSPs. Numerous studies have shown hsps can be upregulated by a variety of environmental contaminants and therefore are a popular biomarker for toxicity screening (Aït-Aïssa et al., 2000; Braeckman et al., 1999; Salminen et al., 1996; Tully et al., 2000).

One of the first TG zebrafish models to incorporate the hsp70 promoter was developed by Halloran *et al.* in 2000 (Halloran *et al.*, 2000). The hsp70 promoter has since been applied in TG zebrafish for assessing the developmental toxicity of cadmium exposure (Blechinger *et al.*, 2002), understanding wound healing

(Richardson *et al.*, 2016), and has been combined with the EpRE promoter to investigate environmentally-induced OS (Mourabit *et al.*, 2019), demonstrating the wide versatility of this model. It has been shown to be more sensitive than the traditional cultured cells assay; exhibiting observable fluorescence at 0.2uM cadmium compared to 0.5-50uM reported in various cultured cells assays, including insect and human HeLa cells (Aït-Aïssa *et al.*, 2000; Blechinger *et al.*, 2002; Braeckman *et al.*, 1999). A drawback of this model is the lag time between induction of hsp70 transcription (as measured by *in situ* hybridisation) and the detection of the fluorescent signal, which is likely due to differences in the translational rates of hsp70 compared with eGFP, and/or in the levels of mRNA stability (Blechinger *et al.*, 2002). This delay can present a challenge with regard to interpreting temporal responses to chemical exposures, i.e. the molecular response to a stressor may occur more rapidly than indicated by the onset of the fluorescent signal. Hsp70 can also be regulated by the Nrf2 pathway, and so can also be used to study OS more generally during vertebrate development (Hahn *et al.*, 2014).

Cyp1a encodes for cytochrome P450 1A, an enzyme with crucial roles in phase I metabolism, important in drug and xenobiotic detoxification. Its transcriptional activation is mediated via the aryl hydrocarbon receptor (AhR) (Kim et al., 2013b) and it is thus a popular biomarker for a range of pollutants and AhR agonist exposure. Cyp1a is also a highly conserved gene, albeit humans have two isoforms while fish have one (Kim et al., 2013a). This provides a tool for the study of potential human health effects as well as for detecting a range of pollutants (including dioxins, dioxin-like compounds, and polycyclic aromatic hydrocarbons (PAHs)) in the aquatic environment (Kim et al., 2013a; Mattingly et al., 2001; Xu et al., 2015, 2018). cyp1a:GFP models are equally or more sensitive than the EROD assay, particularly for analysing AhR activity in adult livers (Xu et al., 2015), as well as more rapid and convenient. These models furthermore have potential for development as a HTS system for the identification of AhR agonists (Xu et al., 2015).

However, a comparison of TG zebrafish models comprised of the zebrafish Cyp1a promoter versus the medaka Cyp1a promoter shows that, while the relative potencies of different contaminants appeared to translate well between species (TCDD having similar affinities for both promoters), tissue-specific

expression of this gene is not preserved between species (Kim et al., 2013a; Xu et al., 2015). Therefore, these TG lines are more limited for making inferences for effects across species than the TG EpRE zebrafish line, where the ubiquity of the EpRE gene and its conservation between species mean patterns of expression can be used to infer potential health impacts for different wildlife or humans.

*Table 1.2 Comparison of the sensitivities of the TG models discussed, including exposure regimens and imaging method used, in order of decreasing sensitivity. Unless stated otherwise, TG embryos were exposed via culturing medium (water) from 0 dpf.*

| TG model | Biomarker | Sensitivity (nM) | Test Compound | Exposure time | Imaging method | Reference |
|---|---|---|---|---|---|---|
| cyp1a:GFP (zebrafish model, medaka promoter) | Cytochrome P450 | 0.001 | TCDD | 1 day (from 4 dpf) | Fluorescent stereomicroscope | Xu *et al.* 2015 |
| ERE:GFP | Oestrogen | 0.00337 | EE2 | 4 days | Inverted confocal microscope | Lee *et al.* 2012a |
| casper ERE:GFP | Oestrogen | 0.00337 | EE2 | 5 days | ArrayScan | Green *et al.* 2016 |
| ERE-kaede-casper | Oestrogen | 0.00337 | EE2 | 5 days | Inverted compound microscope | Green *et al.* 2018 |
| ere-zvtg1: gfp | Oestrogen (via vitellogenin) | 0.00337 | EE2 | 5 days | Fluorescence microscope | Chen *et al.* 2010 |
| vtg1:mCherry | Oestrogen (via vitellogenin) | 0.00337 | EE2 | 5 days | Fluorescent stereomicroscope | Bakos *et al.* 2019 |
| cyp1a:GFP (medaka model) | Cytochrome P450 | 0.005 | TCDD | 1day | Inverted fluorescence microscope | Ng and Gong 2013 |
| cyp1a:nls-eGFP (zebrafish model, zebrafish promotor) | Cytochrome P450 | 0.01 | TCDD | 3 days | Fluorescent stereomicroscope and confocal (for fixed embryos) | Kim *et al.* 2013 |

| | | | | | | |
|---|---|---|---|---|---|---|
| Cyp19a1b-GFP | Oestrogen (via Brain aromatase) | 0.05 | EE2 | 5 days | Fluorescent microscope and confocal (for fixed embryos) | Brion *et al.* 2012 |
| ERE-Luc (not in vivo visualisation) | Oestrogen | 0.1 | EE2 | 4 days | Luciferase activity assayed using a luminometer following homogenisation | Legler *et al.* 2000 |
| 5xERE:GFP | Oestrogen | 1.6869 | EE2 | 3 days | Fluorescent stereomicroscope | Gorelick and Halpern 2011 |
| Vtg1:EGFP | Oestrogen (via vitellogenin) | 5 | E2 | 3 days | Fluorescent stereomicroscope | Abdelmoneim, Clark and Mukai 2020 |
| 3EpRE:hsp70:mCherry | Oxidative stress | 17.31 | copper | 2 days (from 2dpf) | Fluorescence microscope and Confocal microscope | Mourabit *et al.* 2019 |
| cyp19a1a-EGFP | Oestrogen (via Gondal aromatase) | 45.66 | EE2 | 21 days (adults) | IVIS Lumina II fluorescence imaging system | De Oliveira *et al.* 2020 |
| EPRE-LUC-GFP | Oxidative stress | 200 | HgCl2 | 1 day | Inverted fluorescence microscope (visualisation of GFP) and luciferase assay (quantification) | Kusik, Carvan and Udvadia 2008 |
| hsp70:GFP | Heat shock proteins | 200 | cadmium | 3 hours (from 3dpf) | Epifluorecent microscope | Blechinger *et al.* 2002 |

| | | | | | | |
|---|---|---|---|---|---|---|
| fabp10a:DsRed;elaA:eGFP | Liver and Pancreas (LiPan) | 810.714 | phenylbutazone | 5 days | Fluorescent microscope | Zhang, Li, Gong 2014 |
| fli1:eGFP | Vasculature | N/A | N/A | N/A | Inverted fluorescence microscope | Delov *et al.* 2014 |
| LysC:EGFP and LysC::DsRED2 | Myelomonocytic cells | N/A | N/A | N/A | Fluorescent stereomicroscope | Hall *et al.* 2007 |
| Fms:nfsB.mCherry | Macrophage | N/A | N/A | N/A | | |
| Mpeg1.1:eGFP | Neutrophils | N/A | N/A | N/A | | |
| mpeg1.1:mCherry | Neutrophils | N/A | N/A | N/A | | |

## 1.3 Image acquisition and analysis

New methods of image acquisition and analysis will inevitably open up new opportunities for the use of TG models in ecotoxicology. A single model can have multiple applications depending on the imaging platform, the choice of which depends on the aim of the assay or the type of response being assessed Table 1.3). For example, microscopes equipped with an appropriate filter for epifluorescence are popular as they allow rapid and convenient observation of a fluorescence signal to indicate the presence/absence of a response to the toxicant of interest. From images captured, software such as ImageJ can be used to quantify the intensity or changes in expression pattern of the fluorescence signal and therefore the level of the response to the stressor (Chen et al., 2010; Zhang et al., 2014).

For studies requiring more detailed analyses at cellular and tissue levels, higher content imaging methods are applied (Table 1.3). Confocal microscopy achieves spatial localisation by preventing light from outside the small field of focus reaching the detector (Jemielita et al., 2013), providing high resolution images and allowing detailed visualisation of tissue response to chemical exposure. By blocking light emitted from points outside of the field of focus, confocal microscopy gives a high signal:noise ratio (Jemielita *et al.*, 2013). This allows the distinction of weaker signals from background fluorescence and thereby facilitating visualisation of more subtle responses.

Other high-content imaging platforms include light sheet microscopy (LSM) which achieves good optical sectioning and high signal:noise ratio by only illuminating one plane at a time, using a detector perpendicular to the plane of light (Jemielita et al., 2013; Keller et al., 2008). The wide field, camera-based image acquisition also enables higher capture speeds compared to confocal, facilitating the imaging of rapid dynamic responses (Icha *et al.*, 2016) such as calcium signalling in the brain of zebrafish (Winter *et al.*, 2017). However, confocal microscopy is more widely used due to its superior resolution (<micron compared to micron) (Icha *et al.*, 2016).

There have been recent developments made in LSM to further improve the resolution, notably lattice light sheet microscopy (LLSM). In contrast with

conventional LSM, in which the plane of light is too thick for submicron imaging, LLSM uses ultra-thin light sheets from optical lattices to achieve high speed subcellular imaging with reduced phototoxicity (Chen et al., 2014). Manley *et al.* in 2020 applied this system to reveal previously unknown dynamics and characteristics of leucocytes in zebrafish *in vivo.* The superior resolution of LLSM elucidated behaviour of neutrophils, but their rapidly changing morphology also necessitated the use of the faster single-plane LLSM, in which z-depth was sacrificed for temporal resolution (Manley *et al.*, 2020).

The throughput of LLSM is limited because each embryo must be embedded in agarose before imaging. Recently, Logan *et al.* sought to develop a system using the 3D imaging of LSM but without the time-consuming sample preparation, albeit the resolution of this system is inferior to conventional low-throughput LSM (Logan *et al.*, 2018).

In recent years various systems have been developed to (semi-) automate image acquisition in order to facilitate high throughput screening (HTS). These include the Arrayscan (Green *et al.*, 2016) and the Acquifer (Wittbrodt et al., 2014), or microfluidic systems known as 'Fish-on-a-chip' (Yang et al., 2016). The ArrayScan was used by Green *et al.* in 2016 in combination with a skin pigment-free TG model to develop a highly integrated system for HTS (Green *et al.*, 2016). The Acquifer, the platform primarily used in this thesis, uses a 3D printed agarose mould to ensure all embryo are uniformly orientated for imaging by an automated fluorescence microscope (Wittbrodt *et al.*, 2014). Multi-plate systems such as the Acquifer, while rapid and convenient, do not allow for 3D imaging, unlike microfluidic systems (Table 1.3).

Microfluidics will inevitably play a future role in optimising HTS. Currently, biological micro-electromechanical systems (bioMEMS; or 'fish-on-a-chip') (Yang *et al.*, 2016) appear to use microfluidics to either; a) automatically load and orient embryos for imaging, such as the VAST (vertebrate automated screening technology) system (Pardo-Martin *et al.*, 2010), or b) to create dynamic culturing systems and allow constant microperfusion, such as Akagi *et al.*'s microarray (Akagi *et al.*, 2012). This chip allows embryos to be cultured for up to 72 hours and imaged at multiple time points. No manual handling is required between steps or developmental stages, thereby reducing stress caused to the animal, and movement is not restricted which may otherwise impair development (Yang

*et al.*, 2016). In this system however, hatching is delayed by hydrodynamic forces (Akagi *et al.*, 2012). These bioMEMS, however, image the embryos as they happen to be positioned in the well and there is the risk of using sub-optimal angles for visualising specific organs. Guo *et al.* (2017) proposed some improvements to the VAST system by using profile-based 3D reconstruction based on axial views to generate volume and surface area data on the embryo. This would improve quantification of the fluorescent signal by normalising the data based on animal volume, and allow relative comparison between experiments (Guo et al., 2017).

Combining these systems could minimise stress caused to the animal by manual handling and maximise the automation potential for imaging, including for time-lapse imaging to facilitate real-time assessment of developmental toxicity.

HTS imaging systems can yield large amounts of data and so analysis can also present a bottleneck. Workflows and algorithms can go some way to streamlining this process, such as automation of embryo phenotyping (Pardo-Martin *et al.*, 2013) or fluorescence intensity measurement in TG embryos, minimising user interaction and increasing throughput (Jarque *et al.*, 2018). However, workflows still require some manual input, such as Jarque *et al.*'s 'KNIME' workflow in which area of interest (in this case, the thyroid gland) still needs to be manually selected to minimise interference from nearby autofluorescent pigment cells. Additionally, throughput was still limited by the imaging system as loading, positioning, focusing and image acquisition took about 2 minutes per embryo, despite the automation of the VAST system used (Jarque *et al.*, 2018).

Winter *et al.* developed a custom Python pipeline which allowed a labelled 3D map of a brain to be automatically superimposed over the images of TG(elavl3:GCaMP6S) zebrafish larvae, acquired using LSM, which can visualise neural activity. This facilitated the quantification of specific spatiotemporal responses for individual brain regions, allowing the comparison of changes in neural function between regions of interest caused by neuroactive drugs (Winter *et al.*, 2017). This pipeline was later applied in a study to validate the use of TG zebrafish in high throughput assessments of the efficacy and safety of seizurogenic pharmaceuticals across a range of classes and mechanisms (Winter *et al.*, 2021). This study shows how advances in image analysis can improve the throughput and content of functional neuroimaging and these

approaches are likely to lead to further improvements in spatiotemporal resolution of signal detection.

*Table 1.3* ***Advantages and disadvantages of a selection of popular imaging platforms***

| Imaging Platform | Reference | Advantages | Disadvantages |
|---|---|---|---|
| **Confocal microscopy** | Jemielita et al. 2013 | High resolution<br>High signal:noise ratio | Time consuming sample preparation |
| **Light sheet microscopy** | Jemielita et al. 2013; Philipp et al. 2008; Icha et al. 2016 | Good optical sectioning<br>High signal:noise ratio<br>Higher speeds compared to confocal | Time consuming sample preparation<br>Inferior resolution compared to confocal |
| **Lattice light sheet Microscopy** | Chen et al. 2014; Logan et al. 2018 | High speed for dynamic processes<br>Subcellular imaging<br>Reduced phototoxicity<br>Higher throughput | Time consuming sample preparation<br>Reduced resolution |
| **Arrayscan** | Green et al. 2016 | High throughput | Cannot achieve 3D imaging |
| **Acquifer** | Wittbrodt, Liebel, Gehrig 2014 | High throughput<br>Rapid, uniform sample preparation | Cannot achieve 3D imaging |
| **VAST (example of bioMEMS)** | Yang et al. 2016; Chang et al. 2012 | Can be used for 3D imaging<br>High throughput<br>Automated positioning and orientation | Large quantity of data produced require further processing<br>Cannot be used for long term culturing/immobilisation |
| **Miniaturised Array (example of bioMEMS)** | Akagi et al. 2012 | High throughput<br>long-term culturing<br>Reduced stress to animals due to no manual handling required | Delayed hatching due to hydrodynamic forces<br>Cannot be used for embryos >72 hpf<br>Does not allow for orientation of sample |

## 1.5 Issues relating to interpreting responses measured using TG zebrafish models

TG zebrafish have many advantages for applications in chemical assessment, but there are issues also regarding interpretations on the data they provide. The first is that induction of a fluorescent signal indicates upregulation of a promotor for that gene only, and it is not necessarily the case that a deleterious effect will follow (just as the upregulation of gene transcription as measured by qPCR does not necessarily indicate an adverse effect). Further, there can be a delay between upregulation of the gene of interest and detection of the corresponding fluorescent signal (as seen with Blechinger ***et al's*** hsp70 model (Blechinger *et al.*, 2002) ), which has implications for assessing responses in 'real-time' for these TG models. The sensitivity and consistency of the model can be reduced over generations as gene silencing can result in reduction of expression of the transgene. This can occur via epigenetic mechanisms including histone modification or methylation (Thummel et al., 2006) or post-transcriptionally through mRNA degradation or repression (Filipowicz & Paszkowski, 2013). Silencing is a particular risk for models which include Gal4/UAS: a 2-stage amplification system consisting of GAL4, a yeast transcription activator protein under the control of a promoter, and an upstream activated sequence (UAS) fused to the reporter gene (Duffy, 2002; Hartley et al., 2002). This system is often paired with a transgene to amplify the signal, but the UAS sequence is prone to CpG methylation and hence silencing, particularly in complexes with high UAS copy number (Goll et al., 2009; Subedi et al., 2014). There have been developments to ameliorate this problem, including the use of bipartite reporter systems such as Q transcriptional regulatory system, similar to GAL4/UAS but which has no CpG sequence in the QF binding site (Subedi et al., 2014; Suli et al., 2014). With regards to the breeding and maintenance of a TG line, it is therefore important to balance maintaining levels of fluorescence expression whilst avoiding inbreeding depression. To ensure reliability and robustness of the data generated over different generations, each new generation should be thoroughly assessed against the preceding one. This can be achieved by comparing the fluorescence intensity of each generation in response to a reference compound at a given concentration, or comparing the lowest

observable effect concentration (LOEC) of the reference compound for each generation.

In creating a TG animal, this genetic manipulation can potentially result in off-target alterations that may in turn affect how the organism responds to stressors and even its fitness more generally. There are little data on how genome editing of a zebrafish may influence its response to chemical exposure, however. In one case, that for the casper mutant zebrafish, this genetic manipulation been shown to be associated with mitochondrial dysfunction (D'Agati *et al.*, 2017).

## 1.6 Future prospects

The above sections illustrate some of the lines of TG models available for studies in ecotoxicology, including those that were developed specifically for studies on environmental toxicants and those that were originally designed for studies in developmental biology or human health studies and are now finding their way into ecotoxicology research (Chaturantabut *et al.*, 2020; Korzh *et al.*, 2008; Lawson & Weinstein, 2002). In the ZFIN database there are more than 25,000 results for transgenic insertions (Ruzicka *et al.*, 2019) indicating that a model may be available for almost every potential target of environmental toxicants.

More complex models are needed to facilitate understanding on both mixture effects and the effects of chemicals across multiple molecular and physiological pathways. There are numerous examples where multiple transgenes have been incorporated into zebrafish to effectively study the mechanisms controlling developmental processes. Examples include the crossing of the LiPan line, originally developed to track liver development, with a fli:eGFP line to track vasculogenesis in the developing liver (Korzh *et al.*, 2008). There is also the hepatocyte TG model, fabp10a:DsRed, which was crossed with an ERE:GFP model in order to better establish the role of ER signalling in hepatocyte differentiation (Chaturantabut *et al.*, 2020).

The fms:nfsB.mCherry line, wherein fluorescence is controlled by the *fms* promoter for the macrophage-specific CSF2R protein, has been crossed with a range of other TG lines to visualise different interactions. Crossing this line with the mpx:GFP line for neutrophils facilitated visualisation of the response dynamics of these two different types of immune cells simultaneously, or crossing the macrophage line with fli1:GFP line for vasculature elucidated the role of

macrophages in vasculogenesis (Gray *et al.*, 2011). The latter multiple TG model was recently used in conjunction with high resolution lattice light sheet microscopy to reveal new characteristics of neutrophil dynamics and their interaction with the endothelium (Manley *et al.*, 2020).

To date there have not been any published studies on multiple target TG zebrafish developed specifically for ecotoxicology studies, but the field is now moving towards this. A model which combines visualisation of OS with that of immune cells has been developed in order to better understand how environmental compounds can impact immune function via OS, and an ERE/aromatase model has been developed for understanding the role of oestrogen in brain development (Takesono et al., 2022). Multiple target TG zebrafish could be invaluable for elucidating cross-talk between different chemical pathways and therefore advancing our understanding of multiple stressor effects.

### 1.6.1 Mixture effects

Mixtures and multiple stressors are a rapidly growing area of study within ecotoxicology and there is increasing concern on how chemicals may interact with other environmental stressors (Holmstrup *et al.*, 2010; Saaristo *et al.*, 2019). There has been a series of studies using fish and other species to investigate the effects of chemical mixtures, but TG models are still underutilised in this regard and the field could benefit from the mechanistic understanding that TG models can provide.

Better understanding of mixture effects in the environment is a major research focus in ecotoxicology. This has been identified as a major challenge for designing appropriate management strategies for mixture effects by government, industry and academic stakeholders as early as 2006 (Doerr-MacEwen & Haight, 2006). Additionally, ERAs of mixtures are further complicated by the fact that chemical mixtures can be highly dynamic and variable, even between similar types of emission sources. The chemicals (including pharmaceuticals) themselves are also susceptible to a wide range of chemical, physical and biological degradation or transformation processes, producing an even more complex mixture of compounds (Backhaus, 2014).

The two key aspects of pharmaceutical mixtures which makes them a particular environmental concern are a) a mixture is usually more toxic than any one compound individually, and therefore b) a mixture can be highly toxic, even if each individual compound is present in low, so called 'safe', concentrations (Backhaus, 2014). One study on the chemical mixtures detected in Brazilian surface waters found that, while algae were most vulnerable to acute effects, fish were more sensitive to sublethal effects (Reis et al., 2021).

To begin to address the mixtures issue at a basic level, co-exposure studies are used to test the specific effects of binary mixtures, using drug combinations selected based on evidence for their potential to interact. This approach can help elucidate the mechanisms behind effects seen in more complex environmental mixtures, and/or highlight new potential risks. There are numerous fish studies on the effects of mixtures of same-class pharmaceuticals, such as oestrogenic compounds (Petersen & Tollefsen, 2011; Serra *et al.*, 2019) or other steroid hormone mixtures (Schmid et al., 2020). However, studies on combinations of compounds from different classes are less common. Nonetheless, different classes of compounds have been found to have interactive effects. For example, the fungicide ketoconazole has been reported to exacerbate the oestrogenic effects of BPA in male wild type zebrafish but increase anti-oestrogenic activity in female fish. In this study, the two contaminants were selected based on the potential for ketoconazole to potentiate the toxic effects of BPA through inhibition of its CYP-mediated metabolism, a hypothesis which appears to be supported by the data (Ji et al., 2019). This illustrates the potential for pharmaceuticals to modulate the detoxification of other contaminants, and furthermore how binary mixture studies can help to understand the mechanisms at play in more complex environmental mixtures.

Other studies have selected combinations of pharmaceuticals based on those which are most commonly detected together in surface waters. Metformin (anti-diabetic), bisoprolol and sotalol (beta-blockers), and ranitidine (histamine 2-receptor blocker) are all popular pharmaceuticals with little to no metabolism and poor removal from wastewater, and hence are commonly detected in combination in effluents and surface waters. Godoy *et al.* (2019) chose this mixture to test the accuracy of the commonly used mathematical models, concentration addition and independent action, and to test the combined toxicity to zebrafish and

daphnia. While no effect was found on the zebrafish, daphnia revealed that basing an ERA on the effects of individual pharmaceuticals risks underestimating the risk of the mixtures (Godoy *et al.*, 2019).

TG models are becoming more popular for the study of mixture effects. Hinfray *et al.* used a Cyp19a1b-GFP model to find that oestrogen (E2) and the phytoestrogen genistein had antagonistic effects on radial glial cells. This interaction is not fully understood but believed to be due to differences in ER recruitment between the two compounds. The Cyp19a1b-GFP model is not as sensitive to oestrogen lignads as *in vitro* cell lines, but allows for incorporation of factors such as bioavailability and compound metabolism (Hinfray *et al.*, 2018), providing more comprehensive data on the biological effects of this mixture.

More recently, Cooper *et al.* used the ERE-GFP zebrafish to assess the oestrogenicity of wastewater effluent (known to contain a mixture of steroids and other EDCs) (Cooper et al., 2021a) and for exposures during vulnerable developmental life stages (Cooper et al., 2021b). Differing tissue response patterns also highlighted the variability of steroid mixtures and concentrations between effluent sources and across time (Cooper et al., 2021a).

TG fish have also been applied to studying the effects of nanoparticles (reviewed in (Chakraborty *et al.*, 2016)) and nanoparticles in combination with chemicals, notably for effects on the immune response and vasculature. For example, the combination of silica nanoparticles and methyl mercury was found to be more toxic than either pollutant alone, as shown by exacerbated vascular endothelial damage in the TG model fli1-GFP and activated OS and inflammatory response in mpo-GFP neutrophils (Duan *et al.*, 2016). A similar interaction was observed in Fli1-GFP larvae exposed to a combination of cadmium selenium quantum dots (QDs) and copper ions, as the QDs assisted transport of the ions (Zhang et al., 2012).It is not only drug-drug interactions which give cause for concern, as other environmental factors, notably the physicochemistry of the water, have also commonly been found to influence the toxicity of pollutants (reviewed in (Pinheiro et al., 2021)).

*Table 1.4* ***Abiotic water variables and the mechanisms by which they are known to influence bioavailability and toxicity of pollutants****, adapted from Pinheiro et al. 2021*

| Variable | Mechanism |
|---|---|
| **pH** | Chemical speciation<br>Alters trans-epithelial electric potential (TEP) |
| **Temperature** | Metabolism<br>Degradation, volatilisation, and transport of compound |
| **Oxygen** | Behaviour<br>Respiratory physiology<br>Uptake rate |
| **Salinity** | Chemical fate and transport<br>Alters TEP<br>Physiological responses<br>Solubility |
| **Carbon dioxide** | Chemical speciation (via changes in pH)<br>Alters TEP (via changes in pH)<br>Alters internal physiology/biochemistry |
| **Cations/Anions** | Competition for uptake binding site<br>Complexation<br>Membrane permeability<br>Alters TEP |
| **Carbonate Alkalinity** | Metal complexation<br>Metal speciation<br>Moderating response to CO2 |
| **Dissolved organic matter** | Charge transfer<br>Complexation<br>Covalent bonding<br>Hydrogen ion binding<br>Hydrophobic adsorption<br>Ion exchange<br>Partitioning<br>Alters TEP |

As Table 1.4 shows, physicochemical features of the environment can markedly affect the properties of the chemical compounds themselves, including their rates of degradation by temperature (Op de Beeck et al., 2017). Physical or chemical properties of the aquatic environment can also directly affect the animals physiology to then affect how they respond to toxins, such as hypoxia-driven increased ventilation which draws more water and therefore potentially more pollutants over the gills, in turn increasing pollutant uptake (Pinheiro *et al.*, 2021).

These variables are set to become ever more changeable and more extreme with climate change, particularly in the case of temperature (in turn affecting oxygen content, for example), potentially increasing the risk of pharmaceuticals currently not of concern in the environment. There is a wealth of evidence suggesting that realistic future temperatures may exacerbate drug toxicity in the aquatic environment (Almeida et al., 2021; Maulvault et al., 2018a; Mehdi et al., 2019), either by undermining the animals' defence mechanisms through increased stress, or by enhanced uptake of the toxin.

Despite their growing popularity in mixture effects studies, TG zebrafish are currently underrepresented in physical-chemical stressor interaction studies. There are limited examples where TG models have been applied in the study of physical stressors. Examples of this include for embryotoxic effect of temperature (Lantz-Mcpeak *et al.*, 2015) and understanding the cold tolerance mechanism (Wang et al., 2014). There are even fewer examples where TG fish have been used to investigate interactions between pollutants and environmental conditions. The few studies which have been conducted in this area appear to focus on nanoparticles. The TG lines Tg(isl2B:GFP) for specific neurons, and Tg(fli1:EGFP) for vasculature visualisation, have been used to find that dissolved organic matter can mitigate acute and cross-generational effects of zinc oxide nanoparticles (Kteeba *et al.*, 2018). However, to our knowledge, no studies have used a TG zebrafish model to investigate the influence of an environmental/physical stressor on the toxicity of an environmental pharmaceutical.

## 1.7 Project Aims

Despite their growing popularity in the field of ecotoxicology, there are scant studies making use of TG zebrafish to understand how chemicals of different classes may interact, or the interaction between chemical toxicants and physical

stressors. To my knowledge, none have used TG zebrafish to understand the effect of temperature on pharmaceutical toxicity. In this thesis, I set out to establish how OS is influenced by a range of environmental pharmaceuticals and stressors through the advancing the use of TG zebrafish and bioimaging in chemical effects assessments. This began with developing the use of a new semi-automated imaging platform for its use in ecotoxicology: the Acquifer, and characterisation of a novel OS TG model, EpRE:mCherry. Developed by Mourabit *et al.* (2019), this TG fish model had previously been tested against a small range of chemicals, but not for application in HTS, or for mixture effects studies. After establishing the methodology for the imaging methods and TG model, my thesis work set out to use the TG model to test the anti-oxidative effects of oestrogenic chemicals, and then subsequently to investigate the effect of temperature on drug-induced OS using the TG EpRE: mCherry zebrafish.

Chapter 2 sets out the main methods applied to fish husbandry and chemical exposures used in each data chapter. It also describes the analytical chemistry techniques employed to complement the bioimaging data, along with methods used for statistical analyses. Techniques used for image acquisition and analysis are briefly outlined, but their methodology is developed in chapter 3.

The aims for the following thesis chapters were as follows:

**Chapter 3 - Imaging tools for chemical effects assessment**

The first data chapter assessed the utility of the Acquifer and optimised the methodology for its application in the assessment of chemicals effects in TG zebrafish embryo-larvae for the rest of the thesis.

Aims:

a) Assess how novel high throughput imaging platform (Acquifer) can be used for chemical effects assessment with TG embryo-larval zebrafish.

b) Characterise the benefits and limitations of the Acquifer.

c) Compare the utility of the Acquifer against a higher content, but lower throughput platform (confocal microscopy).

. This began with applying the Acquifer to assess for oestrogenic responses to a common and potent environmental oestrogen, EE2, in the TG zebrafish

ERE:GFP. The Acquifer was tested for its capacity for time-lapse imaging to capture the ontogeny of the oestrogenic response on daily and hourly scales. Once optimised for capturing the fluorescence of TG embryo-larvae at this life stage, the Acquifer system was then tested against the OS TG model EpRE:mCherry to investigate the OS response to a reference compound, paracetamol (APAP; a known pro-oxidant). In the last section of this chapter, the Acquifer was compared with confocal microscopy, a higher content imaging platform. The responses of the pronephric tubule to APAP and of neuromasts to cisplatin were used as case studies to compare the resolution of the 2 imaging platforms, and how this influences interpretation of the responses recorded.

**Chapter 4: Application of the EpRE:mCherry transgenic fish model to study OS responses for pharmaceutical exposures**

Having established that the known pro-oxidant APAP could induce a detectable response in the EpRE:mCherry model, I aimed to develop the application of the model further as a tool for screening pharmaceuticals of environmental concern for their potential to induce OS. I hypothesised that the following environmental pharmaceuticals could induce OS in the model: clarithromycin, cisplatin, cyclophosphamide, clozapine, diclofenac, doxorubicin and ibuprofen. I tested this hypothesis by exposing EpRE:mCherry embryolarvae to the individual chemicals (as well as APAP as a positive control and atenolol as a negative control) at a range of concentrations and measured the tissue-specific mCherry fluorescence.

Aims:

a) Assess the EpRE:mCherry model for its application in screening environmental pharmaceuticals for oxidative responses.
b) Acquire baseline data for the oxidative response visualised in the EpRE:mCherry model.
c) Select relevant pharmaceuticals for further investigation for mixture effects analyses.

The EpRE:mCherry model was characterised and used to optimise of chemical exposure protocols based on the reference compound APAP. The model was then used to screen 8 different pharmaceuticals at a range of concentration designed to approach human therapeutic concentrations (HTPC) but avoid overt toxicity.

To begin to understand the responses observed in the zebrafish larvae, liquid chromatography with tandem mass spectrometry (LC-MS/MS) was used to quantify uptake of the compounds. This allowed measured internal pharmaceutical concentrations to be compared against predicted plasma concentrations (based on lipophilicity) and against HTPCs using the fish plasma model (FPM).

Chapters 5 and 6 used the methods and tools developed in the above chapters to further our understanding of how pharmaceutical- induced OS can be influenced by environmental stressors.

**Chapter 5: Interactions of oestrogen with OS measured in the EpRE:mCherry transgenic zebrafish model**

This chapter set out to investigate the interactive mechanisms between oestrogen and OS induced by pharmaceutical exposure. Based on *in vitro* data in the literature, I hypothesised that a xenoestrogen would be able to buffer APAP-induced OS. To test this, I first established that an exogenous compound could reduce mCherry fluorescence in the EpRE:mCherry model using known antioxidants to optimise a positive control and dosing regimen. EpRE:mCherry larvae were then aqueously exposed to a mixture of APAP and the potent oestrogenic compound EE2. The resulting expression of mCherry fluorescence (and therefore OS induction) was compared with that in larvae exposed to paracetamol alone. I also hypothesised that endogenous oestrogen plays a role in buffering pharmaceutical-induced OS and this was tested by exposing larvae to a combination of APAP and the ER antagonist ICI 182, 780.

Aims:

a) Identify an antioxidative control and confirm if a reduction in OS can be quantified in the EpRE:mCherry model.
b) Optimise an exposure protocol to assess the antioxidative capacity of EE2 and compare this against the positive control
c) Assess the role of endogenous oestrogen in buffering OS by inhibiting oestrogen receptors and quantifying the effect on APAP-induced OS.

**Chapter 6: Interaction of temperature and pharmaceutical-induced OS as measured in the EpRE:mCherry model**

This chapter set out to investigate the interactive effects between a physical stressor, temperature, and drug induced OS. I hypothesised that elevated temperatures would exacerbate pharmaceutical-induced OS. This was tested by incubating EpRE:mCherry larvae at temperatures higher than standard husbandry practice during aqueous exposure to a pharmaceutical. I also hypothesised that this interaction would be driven by more rapid uptake of the drug, and so this was tested using LC-MS/MS to measure the internal APAP concentrations in larvae at different time points throughout the exposure period.

Aims:

a) Assess the effect of temperature on basal redox state of EpRE:mCherry embryos and confirm if this can be quantified in the TG model.
b) Assess the effect of environmentally realistic temperature increases on the pro-oxidative action of a range of compounds with varying potencies and modes of action.
c) Use analytical chemistry to assess how toxicokinetics of the reference compound, APAP, is affected by elevated temperature.

In this work, it was first established that the EpRE:mCherry model could be used to visualise OS induced by temperature, and to assess how the proposed study temperatures affected the rates of development and growth of the embryos. The effect of temperature on drug-induced OS was then assessed across a range of temperatures for the 3 main target organs (pronephric tubule, pronephric duct, and liver). This was demonstrated for 3 different drugs: APAP, diclofenac, and doxorubicin. The toxicodynamics of APAP under different temperature treatments were quantified using LC-MS/MS.

**Chapter 7: General discussion**

This chapter provides a critical appraisal of the main thesis findings and their implications and sets out a vision for future research in the application of TG fish models for mixtures assessments, risk assessment and environmental protection.

# Chapter 2- Methods and Materials

## 2.1 Ethics statement

All experimental procedures conducted with zebrafish in this thesis were in accordance with U.K. Home Office regulations for the use of animals in scientific procedures and followed local ethical review guidelines ensuring their humane treatment.

## 2.1 Zebrafish husbandry

Adult zebrafish were held in flow through aquaria at the University of Exeter Aquatic Resource Centre, at 28 ± 1 °C. Breeding stocks were kept in 8L plastic tanks, maximum 30 adults at an approximately 50:50 male:female ratio and maintained under a 14h:10h light:dark regime. Aquarium system water comprised mains tap water filtered by reverse osmosis (Environmental Water Systems UK Ltd.) and reconstituted with Analar-grade mineral salts to a standard synthetic freshwater composition (final ion concentrations: 117mg/L CaCl22H20, 25.0 mg/L NaHCO3, 50mg/L MgSO47H20, 2.3mg/L KCl, 1.25mg/L Tropic Marine Sea Salt, giving a conductivity of 300mS). Fish were fed *Artemia nauplii* twice a day, alongside one dry feed (Zebrafeed, Sparos).

## 2.2 Embryo surface sanitation (bleaching) for zebrafish line regeneration

For biosecurity reasons, each generation of zebrafish breeding stock was sanitised as 1 dpf embryos using sodium hypochlorite in order to remove surface microbes before being raised in the ARC. Up to 250 embryos at a time were rinsed in a sieve with aquarium system water for 30 seconds and washed in 500ml 0.045 % sodium hypochlorite for 8 minutes, with gentle agitation to ensure all embryo surface were covered. Embryos were then transferred to 500ml 0.7 g/l sodium thiosulfate in order to neutralise the sodium hypochlorite and washed for 30 seconds, again with gentle agitation, and then rinsed with system water before being transferred to a petri dish in fresh system water.

## 2.3 Embryo collection

For embryo collection, sexually mature adults were transferred to break-out chambers in 5 groups of 6 (3:3 males and females) the evening before collection.

On the day of collection, embryos were collected 30 minutes after dawn and pooled to avoid batch effects. They were then sorted for fertilisation and normal development using a stereo microscope. All embryos from the breeding stock expressed the transgenes so pre-screening for fluorescence was not necessary.

## 2.4 Chemical exposure

Exposure concentration ranges used are detailed in the relevant chapters. All exposure solutions were made up in aquarium system water on the day of exposure. Stock solutions were pH adjusted to 7-7.6 and diluted to 1.2 x the nominal exposure concentrations. 1ml of this exposure solution was then added to 1 embryo in 200µl system water to provide 1 embryo per well in 1.2 ml exposure media in a 24 well plate. Plates were kept in a 14hr:10hr light:dark cycle at 28°C (±1°C). Where dimethyl sulfoxide (DMSO) was needed as a solvent, stock solutions of the compound were made in 0.5 % DMSO and diluted using a mixture of system water and DMSO so dosing solutions always contained 0.05 % DMSO, regardless of compound concentrations. 0.05 % DMSO was therefore used as a solvent control. Where a solvent was not needed, the negative control was clean aquarium system water (clean water; CW).

All embryo chemical exposures began at 6 hpf (unless otherwise stated). At 6 hpf the germ ring and embryonic shield is very clear from the animal pole (Kimmel et al., 1995), and so chemical exposures began at this age as fertilised, normally developing embryos can be selected and any showing abnormal development can be excluded.

After method optimisation in Chapter 4, the standard exposure regimen chosen was a 4 day exposure. Exceptions to this regimen are stated in the methods section of the relevant chapter. Sample sizes (N) were selected based on a combination of similar experiments found in the literature and what was practical depending on the spawning success of that day. Sample sizes are therefore a minimum of 12 embryos (with the exception of primary screens) from one spawning event and are stated in the figure legend for each experiment.

At the end of the exposure period, after image acquisition, larvae are terminated using an overdose of benzocaine. For larvae >5 dpf, death was confirmed by destruction of the brain.

The compounds used in this thesis for chemical exposure assays were:

- *Paracetamol (APAP)*

Paracetamol (CAS no. 103-90-2; Sigma-Aldrich, Dorset, UK). Dissolved in 0.5% DMSO to make 50 mM stock.

- *Diclofenac (DCF)*

Diclofenac sodium (CAS no. 15307-79-6; Sigma-Aldrich, Dorset, UK). Dissolved in 0.5% DMSO to make 500 mg/L (1.7 mM) stock.

- *Ibuprofen (IBF)*

Ibuprofen (CAS no. 15687-27-1; Sigma-Aldrich, Dorset, UK). Dissolved in 100% DMSO to make 500 mg/L (2.4 mM) stock.

- *Doxorubicin (Dox)*

Doxorubicin hydrochloride (CAS no. 25316-40-9; Sigma-Aldrich, Dorset, UK). Dissolved without the use of a solvent to make 500mg/L (0.9 mM) stock.

- *Cisplatin (Cis)*

Cisplatin (CAS no. 15663-27-1; Merck, Darmstadt, Germany). Dissolved in 0.5% DMSO to make 500 mg/L (1.7 mM) stock.

- *Cyclophosphamide (CP)*

Cyclophosphamide (CAS no. 6055-19-2; Sigma-Aldrich, Dorset, UK). System water added directly to ISOPAC bottle to make 5 g/L (19.2 mM) stock.

- *Clarithromycin (CAM)*

Clarithromycin (CAS no. 81103-11-9; Sigma-Aldrich (Dorset, UK). Dissolved using 1.5% DMSO to make 1 mM stock.

- *Clozapine (Cloz)*

Clozapine (CAS no. 5786-21-0; Sigma-Aldrich, Dorset, UK). Dissolved in 0.5% DMSO to make 500 mg/L (1.5 mM) stock

- *Desmethyl clozapine (DMC)*

N-desmethylclozapine (CAS number 6104-71-8; Sigma-Aldrich, Dorset, UK)

(also known as norclozapine) 250 mg/L (0.8 mM) stock made in 0.5% DMSO.

- *Atenolol (ATL)*

Atenolol (CAS no. 29122-68-7; AstraZeneca, Macclesfield, UK). Dissolved without the use of a solvent to make 500 mg/L (1.9 mM) stock.

- *Ethinyl Estradiol (EE2)*

Ethinyl estradiol (CAS no. 57-63-6; Sigma-Aldrich, Dorset, UK). Dissolved in 100% methanol to make 220 mg/L (0.7 mM) stock.

- *Fulvestrant (ICI 182, 780)*

Fulvestrant (ICI) (CAS number 129453-61-8; Sigma-Aldrich, Dorset, UK). Dissolved in 100% DMSO to make 20 mM stock and diluted down to 0.5 % DMSO for dosing solution.

- *NAC*

N-acetyl-L-cysteine (NAC) (CAS number 616-91-1; Sigma-Aldrich, Dorset, UK) 60 mM stock made without the use of a solvent.

- *NACA*

N-acetylcysteine amide (NACA) (CAS number 38520-9; Sigma-Aldrich, Dorset, UK). 50 mM stock made without the use of a solvent.

- *LGR*

L-glutathione reduced (LGR) (CAS number 70-18-8; Sigma-Aldrich, Dorset, UK). 50mM stock made without the use of a solvent.

## 2.5 Acquifer image acquisition

On the day of imaging, embryos were anaesthetised using 0.4 g/L MS222 (Sigma-Aldrich; CAS number 886-86-2) and mounted in a 96 well plate pre-prepared with agarose to facilitate uniform orientation of the embryos. 70 µl of 1.5 % low melting point agarose had been transferred into each well and moulded into grooves using a 3D-printed orientation tool (Wittbrodt *et al.*, 2014) which was stamped into the agarose and left to set in 4°C. The 96 well plate was loaded into the Acquifer (Ditabis, Germany) and images acquired under brightfield and 595 nm (red fluorescence) or 470 nm (green fluorescence) channels from an LED light source. Light intensity and integration was consistent across the plate but optimised for each experiment to maximise sensitivity of the system and avoid oversaturation of the signal. A Z-stack of 11 Z-slices with dZ=8 µm was captured for each embryo on 4x or 10x magnification. The development of these methods is explored in detail in Chapter 3.

For daily imaging, embryos were recovered and returned to fresh dosing solution in between time points. Larvae that were used in time-lapse imaging over 3-24 hours were left in the 96-well plate containing 1.5 % low melting point agarose

made up with 0.4 g/L MS222 and the plate was sealed to prevent evaporation. When embryos had not hatched in time for imaging, such as 2 dpf embryos, they were manually dechorinated using forceps.

## 2.6 Confocal image acquisition

Larvae were anaesthetised using 0.4 g/L MS222 and embedded in 70 µl 1 % low melting point agarose made up with 0.1 g/L MS222. Larvae were embedded on their left lateral side in order to optimise visualisation of the liver along with the pronephros. Z stacks of the samples were acquired using a Nikon Ti A1plus confocal microscope (Nikon, Japan), using a 561 nm laser for excitation of the mCherry fluorophore and/or a 488 nm laser for visualisation of the PT-yellow or DASPEI stains. Objective used was selected depending on the experiment and specified in figure legends.

## 2.7 Image analysis

The methods for image analysis are detailed in chapter 3, but briefly, Fiji (ImageJ) (Abràmoff et al., 2004) was used to measure the mean pixel intensity within regions of interest (ROIs) drawn around the target organs, and the background values for each well was subtracted. For each figure, the legend describes if a data point represents the mean pixel intensity for the organ of an individual larva, or the mean value of all larvae in the treatment group.

## 2.8 LC- MS/MS

Larval exposure was performed by me, sample preparation was divided by myself and Maciej Trznadel, and LC-MS/MS was performed by Maciej Trznadel.

### 2.8.1 Sample preparation

Zebrafish larvae were terminated using an overdose of tricaine and transferred in 300 µL test solution to a 96 well MultiScreen$_{HTS}$ BV Filter Plate (Merck Millipore, Ireland). The test solution was removed under a vacuum and larvae were washed 12 times using pure water to eliminate residual test solution. Larvae were transferred in 300 µL pure water to a 96 deep well plate (Porvair Sciences, UK) and 300 µL HPLC- grade acetonitrile (containing an Internal Standard), was added to each well. Samples were then homogenised to extract analytes. 900 µL LCMS grade water was added to each well, the plate was mixed and then centrifuged at 4000 rpm for 30 mins. The resulting supernatant from each well was then sampled for LC-MS/MS analysis.

### 2.8.2 LC-MS/MS method

Analysis was performed on a TSQ Vantage triple quadrupole mass spectrometer equipped with heated electrospray (HESI II) source coupled to Surveyor MS Pump Plus HPLC pump with HTPC PAL autosampler (all Thermo Fisher Scientific, San Jose, CA). Chromatographic separation was achieved using reversed-phase, 3 µm particle size, C18 Hypersil GOLD column 50 mm × 2.1 mm i.d. (Thermo Scientific, San Jose CA, USA). All analytes apart from clarithromycin were separated using a linear gradient of water and methanol, both containing 0.1% of formic acid. For separation of clarithromycin, methanol and water were spiked with aqueous ammonia at 0.1%. The initial conditions for the gradient comprised 20% of methanol with formic acid, which was increased to 100% in 1.5 min and maintained for another 1.5 min before returning to the initial 20%. The flow rate was 500µL/min. A slightly altered programme was used for separation of APAP, which started with 5% of solvent and increased to 100% in 1.5 min. This was maintained for 1.5 min and returned to initial conditions for another minute, with a flow rate of 400 µL/min.Temperature of the autosampler was set at 6˚C, while the column was kept at a room temperature.

The HESI probe was operated in both positive mode with an ion-spray voltage of 3.75 kV and negative mode with 2.7 kV. The heated capillary temperature was set at 275°C and the vaporizer temperature was 350°C. Nitrogen was used as sheath and auxiliary gas at a pressure of 60 and 2 arbitrary units, respectively. The argon CID gas was used at a pressure of 1.5 mTorr and the optimum collision energy (CE) for each MS-MS transition was automatically optimised by the software. Quantification of the analytes was performed using characteristic multiple reaction monitoring (MRM) transitions of precursor/product ions for each compound as listed in Table 2.2. Internal concentrations were quantified using an Internal Standard method.

*Table 2.1* ***Multiple reaction monitoring (MRM) transitions of precursor ions of compounds of interest.***

| Compound | Parent ion (*m/z*) | Product ion (*m/z*) | Collision energy (eV) | Ionisation Mode |
|---|---|---|---|---|
| Atenolol | 267.2 | 145.2 | 26 | + |
| Ibuprofen | 205.1 | 161.4 | 5 | - |
| Cyclophosphamide | 261.0 | 140.1 | 21 | + |
| Clozapine | 327.1 | 270.1 | 22 | + |
| Desmethyl clozapine | 313.1 | 192.1 | 41 | + |
| Doxorubicin | 544.2 | 397.1 | 12 | + |
| Diclofenac | 294.0 | 250.2 | 14 | - |
| Clarithromycin | 748.5 | 158.1 | 29 | + |
| Paracetamol | 152.1 | 110.1 | 17 | + |

## 2.9 Statistical analysis

All data analyses were performed using GraphPad Prism (version 9.3.0 for Windows, GraphPad Software, San Diego, California USA, www.graphpad.com). Data were first tested for normality using the Shapiro-Wilk test. Data that passed were then analysed using a one-way ANOVA followed by Tukey's multiple comparisons test to compare every treatment group with every other group, or Dunnett's to compare experimental treatment groups with the control only. When only a specific set of treatment groups are compared, (e.g., comparing temperature treatments within time points) the Bonferroni test is used. Data with more than one independent variable are analysed using a two-way ANOVA followed by Bonferroni or Dunnett's test.

Where data failed the normality test, they were analysed using non-parametric Kruskal-Wallis tests followed by Dunn's multiple comparison test. Results of multiple comparisons are reported as multiplicity adjusted P values in order to account for the number of comparisons and minimise the false discovery rate.

Experiments consisting of only 2 treatment groups were tested using a t-test, or nonparametric data was tested using Mann-Whitney.

Statistical analysis tests used on each experiment are specified in figure legends, as are the sample sizes and number of replicates. With the exception of data presented in Chapter 6 (where replicates are collated into one figure), experimental replicates are presented separately.

# Chapter 3- Imaging tools for chemical effects assessment

## 3.1 Introduction

As explored in Chapter 1, TG zebrafish are a popular tool for the assessment of chemical effects, and there are a range of imaging platforms available for their assessment, each with their own advantages and caveats. (Semi-) automated platforms can be used for HTS, for example via automatic loading of the embryos using microfluidics such as in the VAST system, which allows for more samples to be assessed more rapidly (Chang et al., 2012). More recently, the Acquifer (Acquifer, Karlsruhe, Germany) has been developed which can achieve high throughput through semi-automation, and has previously been used to screen pharmaceuticals, for example, for developmental nephrotoxicity (Westhoff *et al.*, 2020). One of the main advantages of the Acquifer is the rapid, uniformed orientation of the samples which is achieved with a 3D printed orientation tool (Wittbrodt *et al.*, 2014). This streamlines the mounting process as the wells are pre-prepared with agarose grooves, so embryo-larvae do not have to be individually embedded in agarose, and the animals can be conveniently manipulated into the same orientation which also allows for rapid and consistent visualisation. Additionally, the plate sits on a fixed stage and the camera itself moves, meaning the samples are not disturbed during image acquisition (see Fig. 3.1). The Acquifer can also be pre-programmed with auto-focus and positioning protocols, allowing a 96-well plate to be scanned automatically in as little as 20 minutes. Where only one z-slice and one channel (e.g., brightfield) is needed, with no autofocus and just a pre-set z-centre, a plate can be scanned in 2 minutes.

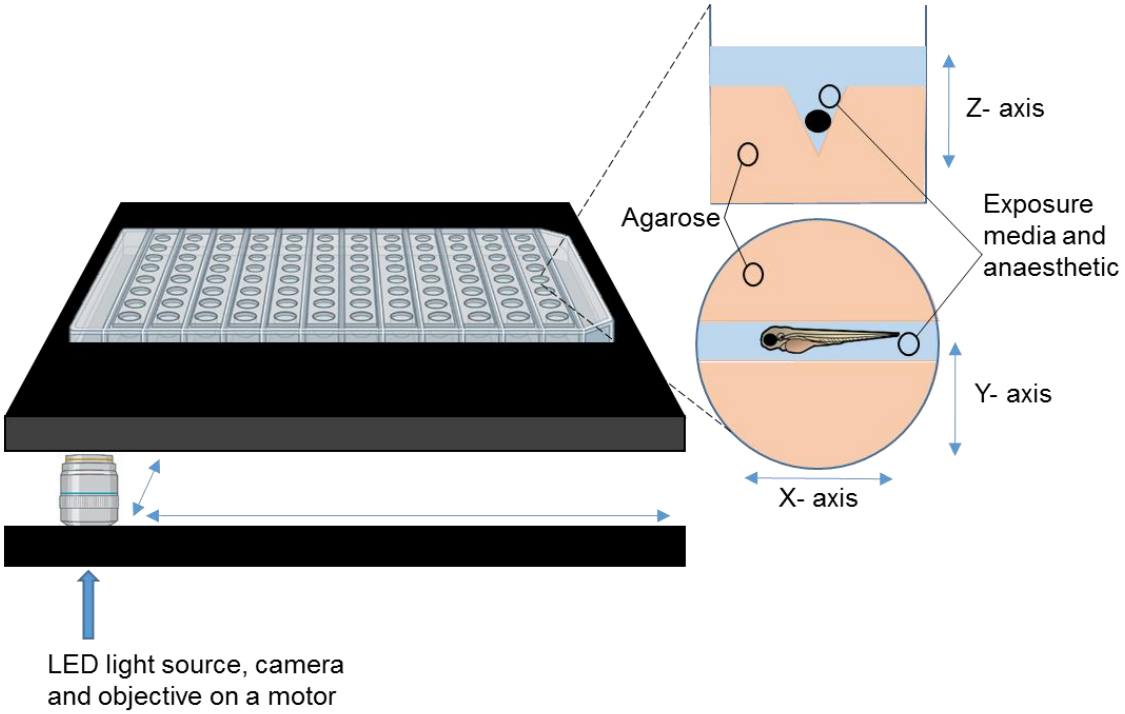


*Figure 3.1* ***Diagram of Acquifer set up****, showing the moving optics block on a linear motor below the fixed stage, and the larva positioned in an agarose groove.*

However, as discussed in Chapter 1, HTS platforms often achieve rapid image acquisition at the expense of resolution. Therefore, the application of the Acquifer was compared against a confocal microscope (Nikon, Japan). The confocal is a popular high content platform and can achieve <micron resolution with a high signal:noise ratio (Jemielita *et al.*, 2013). In contrast with the Acquifer which uses an LED fluorescence excitation light source for widefield imaging of the whole sample (Westhoff *et al.*, 2020), the confocal scans the sample using a focussed laser beam to excite the fluorophores, and a pinhole to block out-of-focus light (Jonkman et al., 2020). The result is a higher resolution image with improved signal:noise ratio and better Z- resolution, but a slower acquisition time. Additionally, the throughput of a confocal microscope is limited due to the time-consuming process of embedding the embryo-larva in agarose.

In the current chapter, two TG zebrafish models were used to optimise and refine the application of the Acquifer. ERE:GFP, generated by (Lee et al., 2012a), uses the GFP reporter gene the expression of which is driven by the oestrogen response element (ERE) promoter, along with the Gal4ff-UAS amplification system, to visualise activation of ERs. This model is well established, having been used to answer a myriad of questions about the risk of oestrogenic compounds in the environment since 2012. These include identifying vulnerable target organs

(Lee et al., 2012a) and more recently assessing the oestrogenicity of environmental samples (Cooper et al., 2021b), showing continuous use of the model.

The second model, EpRE:mCherry, is a novel TG model developed by Mourabit *et al.* 2019 to visualise the OS response. This model consists of a red fluorescent reporter (mCherry), the expression of which is driven by the EpRE, a gene which is part of the Nrf2/Keap1 signalling cascade that plays a significant role in mediating the anti-oxidative defence system (Osburn & Kensler, 2008). This model is still relatively new, having so far only been tested on a limited range of chemicals (Mourabit *et al.*, 2019), but crucially, OS is a common initiating mechanism in a wide range of organ specific toxicological responses.

2 key reference compounds with well characterised effects were used to develop the imaging methods applied in the rest of the project, including in the identification of target organs and tracking the development of a fluorescent signal over time. The first reference compound was EE2, a potent oestrogen used in the contraceptive pill which is frequently detected in surface waters (Laurenson et al., 2014). The presence of EE2 in the environment is of significant concern as it has been linked to the feminisation of fish (Jobling *et al.*, 2002; Lange & Paull, 2009) with possible population-level effects (Hamilton *et al.*, 2015). EE2 has also been found to interfere with many physiological process in a range of species including brain development in mice (Derouiche et al., 2015), heart function in bullfrog tadpoles (Salla *et al.*, 2016) and tissue regeneration in zebrafish larvae (Sun *et al.*, 2018). Here, EE2 was used to induce an oestrogenic response, and hence elevated expression of GFP in the ERE:GFP TG zebrafish.

The second pharmaceutical was paracetamol (APAP), a known pro-oxidant used previously to develop the EpRE:mCherry model (Mourabit *et al.*, 2019), and used here to develop methods for imaging the OS model as it is a known pro-oxidant shown to induce OS in a range of species (Gómez-Oliván et al., 2012; Nogueira & Nunes, 2021; Wang et al., 2017). APAP is one of the most popular drugs globally, and among the top 3 prescribed drugs in the UK by weight (Sebastine & Wakeman, 2003). Although it is easily biotransformed and not very persistent in the environment, APAP's continuous influx into the aquatic environment via sewage exceeds its rate of transformation (Santos *et al.*, 2013) and so APAP can be considered pseudo-persistent. Hence, it has been detected in concentrations

up to 0.04 µM in European waste water treatment plant (WWTP) effluent (Ternes, 1998), and up to 0.43 µM in a UK river (Roberts & Thomas, 2006).

The efficacy of the Acquifer was then compared against that of a confocal microscope by focussing on 2 types of tissue which can be challenging to visualise in a 4 dpf larva without a suitable microscope: the pronephric kidney and neuromasts.

The pronephros is a simple primitive renal structure comprising a central single glomerulus, with two renal tubules that run down each flank of the animal (pronephric convoluted tubules; PCTs) leading into pronephric ducts (PDs) (Fig. 3.2). It is a major sight of detoxification and hence vulnerable to OS induction by APAP. Each segment of the tubule has a specialised role, broadly mirroring the functional segmentation of the more advance mesonephros and mature kidney of high vertebrates (Wingert & Davidson, 2008). Proximal tubule cells, for example, are particularly vulnerable to the effects of OS as their role is to reabsorb solutes and so preferentially concentrate toxins from the filtrate (Basile et al., 2012; Sanz et al., 2008), in addition to their reliance on aerobic respiration which makes them further susceptible to OS (Chevalier, 2016).

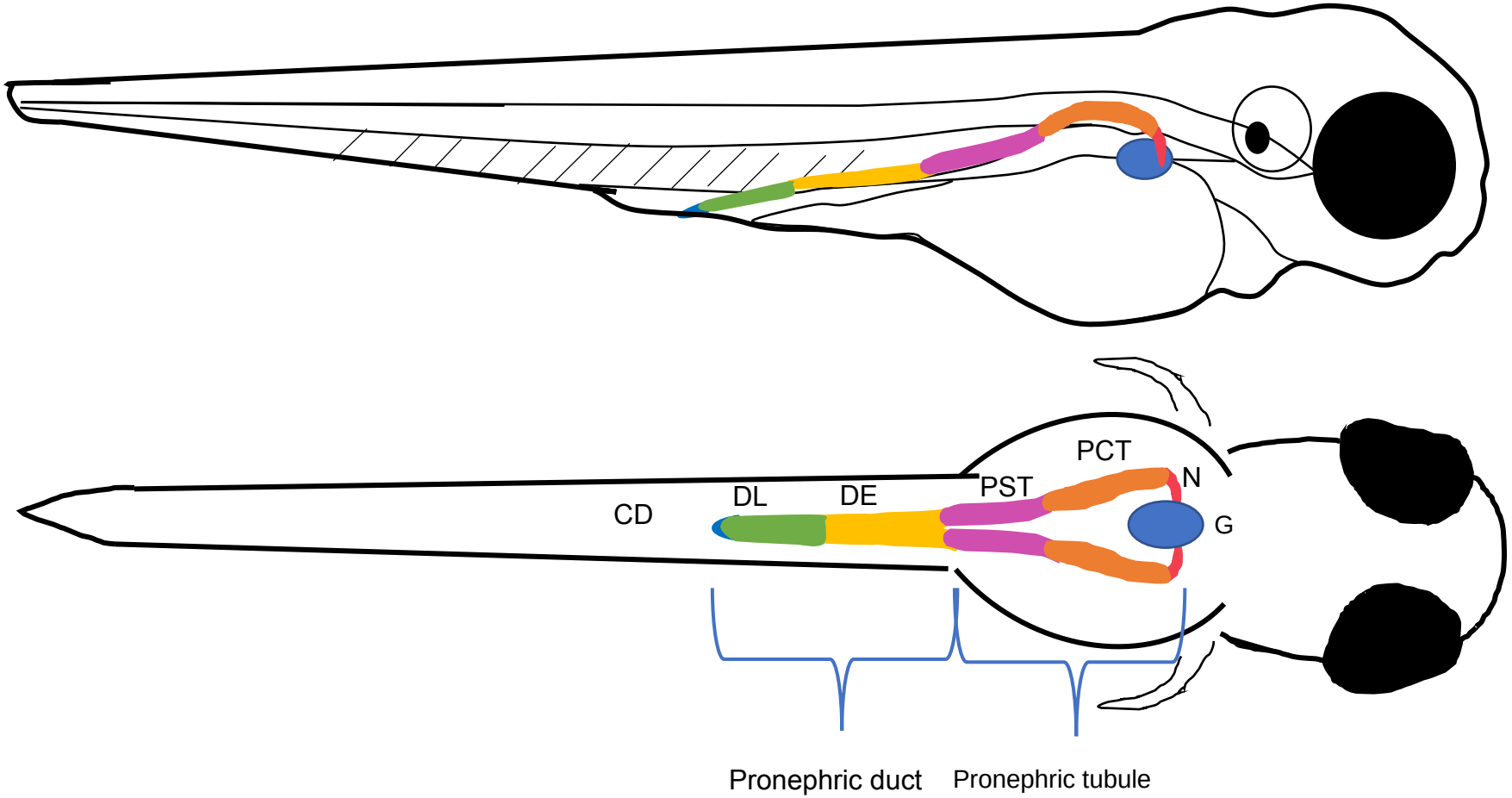


*Figure 3.2* ***Segmentation of the zebrafish pronephros from a [top] lateral and [bottom] ventral view****. (G) Glomerulus, (N) neck, (PCT) pronephric proximal tubule, (PST) pronephric straight tubule, (DE) distal early, (DL) distal late, (CD) collecting duct. Adapted from Drummond and Davidson 2010.*

The pronephric tubules (PTs) can be challenging to visually distinguish in a developing larva as they are small, relatively transparent and located deep within the larva adjacent to the spinal column. To overcome this, a fluorescent stain, PT-yellow (Sander *et al.*, 2015), was used to allow easier visualisation of the tubule and better determine the location of the OS mCherry signal in APAP-treated EpRE:mCherry larvae. In addition, the preferential staining of the proximal convoluted tubule (PCT) by PT-yellow allows delineation between the PCT and glomerulus. These images were compared with those acquired using the Acquifer to assess the resolution of the higher throughput platform.

Neuromasts are mechanosensory organs comprising a ring of supporting cells around a central cluster of mechanosensory hair cells, functionally equivalent to those found in the inner ear of mammals, present at several points along the lateral line of bony fish (Fig. 3.3) (Froehlicher et al., 2009; Ghysen & Dambly-Chaudière, 2004; Metcalfe et al., 1985). The lateral line detects water movement and low frequency vibrations, essential for prey detection and predator avoidance (Buck et al., 2012; Ghysen & Dambly-Chaudière, 2004).

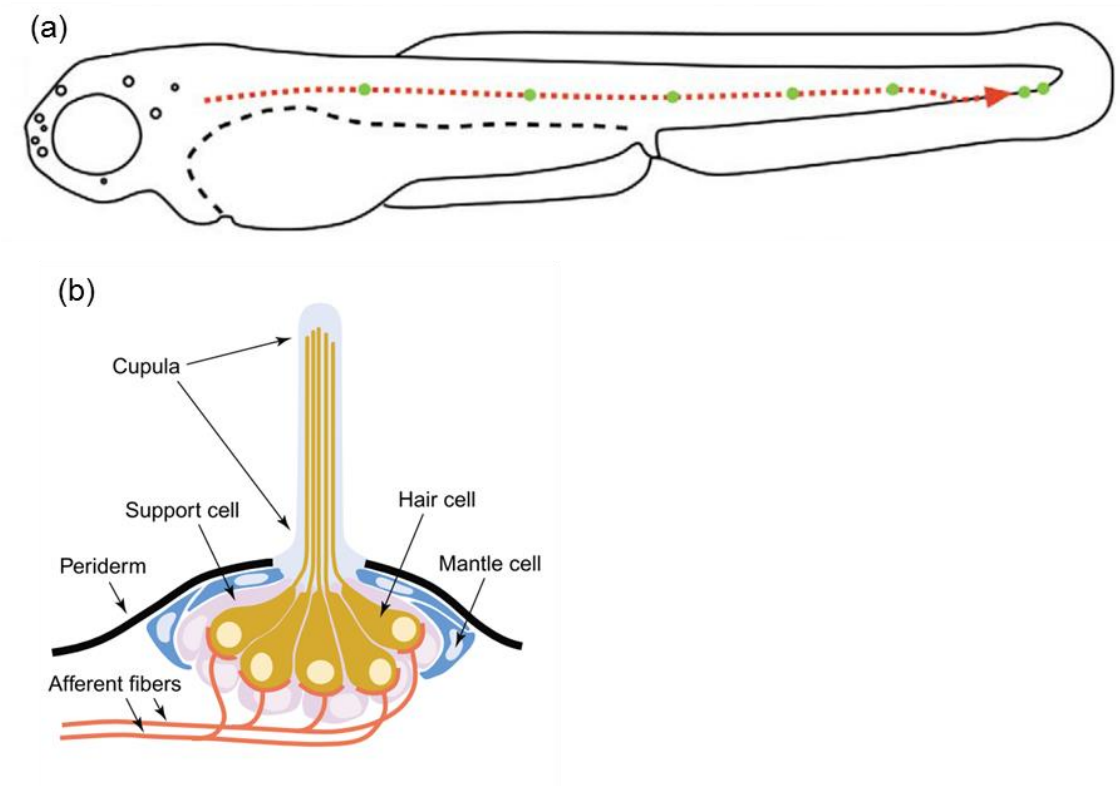


*Figure 3.3* ***The fish lateral line*** *[a] Pattern of primary neuromasts (green dots) deposited along the lateral line by the end of embryogenesis [B] Diagram of the neuromast, showing the hair cell surrounded by support cells. Taken from Ghysen and Dambly-Chaudièr, 2004*

Ototoxic (hearing-damaging) drugs, such as aminoglycoside antibiotics, are known damage these cells (Buck *et al.*, 2012; Owens *et al.*, 2009) and so the zebrafish lateral line has become a popular surrogate for ototoxicity (Froehlicher *et al.*, 2009). The chemotherapeutic drug cisplatin (Cis), which is detected in European surface waters in the low pM range (Queirós et al., 2021), has previously been shown to induce OS in the neuromasts of the EpRE:mCherry model, detected using confocal microscopy (Mourabit *et al.*, 2019). As neuromasts occur at distinct points along the body of the larva and can be difficult to visualise, the fluorescent stain DASPEI, which stains the pronephric tubule, was used here to aid identification and provide a diffuse fluorescent signal to challenge the sensitivity/resolution of the Acquifer.

The Acquifer has received little use in the field of ecotoxicology and so here, the methods for its application for TG model assessment were optimised. The method was furthermore compared with confocal microscopic assessment, using a range of chemicals and TG models to refine their applications. To direct this work, there were three main questions:

a. How can a novel high throughput imaging platform (the Acquifer) be effectively applied for chemical effects assessment?
b. What are the benefits and limitations of the Acquifer as an imaging acquisition system?
c. How does the application of the Acquifer compare with confocal microscopy (as a higher content, but lower throughput platform)?

## 3.2 Methods

### 3.2.1 Fish husbandry

All OS measurements were conducted using EpRE:mCherry zebrafish and the oestrogenic response was assessed in ERE:GFP zebrafish larvae. Both strains of zebrafish were maintained under the same conditions (see Chapter 2, section 2.1).

### 3.2.2 Chemical exposure

Unless stated otherwise, embryos were exposed to the drug of interest from 6 hpf (hours post fertilisation) and anaesthetised using 0.4 g/L MS222 before imaging at 3, 4, or 5 dpf (days post fertilisation). In order to optimise the parameters for

assessing mCherry fluorescence on the Acquifer, it was used to assess a known response and so the first APAP assay follows the protocol used by the researchers who first developed the EpRE:mCherry model (Mourabit *et al.*, 2019) in that embryos were dechorionated and exposed from 2 to 4 dpf. For full details of exposure methods used, see Chapter 2 section 2.4.

Ethinyl estradiol (CAS no. 57-63-6) was purchased from Sigma-Aldrich, Dorset, UK, dissolved in 100 % methanol to make 0.7 mM stock, stored in -20°C, and dissolved in system water on day of exposure. Paracetamol (APAP) (CAS no. 103-90-2) was purchased from Sigma-Aldrich, Dorset, UK and dissolved in 0.5 % DMSO on day of exposure to make 50 mM stock. Cisplatin (CAS no. 15663-27-1) was purchased from Merck, Darmstadt, Germany, dissolved in 0.5 % DMSO to make 1.7 mM stock, stored in -20°C, and diluted in system water on day of exposure.

For time-lapse imaging of embryo-larvae in which larvae were cultured in the Acquifer for up to 19 hours, the 1.5 % agarose used in the 96-well plate (see section 3.2.3) was also impregnated with 0.4 g/L MS222 and the corresponding concentration of EE2 to avoid leaching of the compounds which may have altered the exposure concentrations.

### 3.2.3 Staining

Larvae exposed to Cis were also stained on day of imaging using DASPEI (2-(4-(dimethylamino)styryl) -N-Ethylpyridinium Iodide) (CAS no. 3785-01-1; Sigma-Aldrich, Dorset, UK) to visualise the neuromasts. Larvae were removed from dosing solution and incubated in 0.005% DASPEI (1 larvae per well of a 96 well plate in 2ml solution) for 20 minutes. Larvae were then washed in clean system water 3 times and then anaesthetised and imaged using either a 470 nm light on the Acquifer or 488 nm laser on the confocal microscope.

To identify the PT, 3 dpf larvae exposed to APAP were stained with BDNCA3-D2 (PT-yellow) (Generon, Slough, UK) and imaged the next day. 100 µM stock in 56 % DMSO was made up prior to the experiment and stored in a -20°C freezer. After method optimisation adapted from (Sander *et al.*, 2015), 72 hpf larvae were incubated for one hour in 100 nM (0.06 % DMSO) of the stain. Larvae were then washed three times and returned to exposure media until imaging at 96 hpf. The use of 100 nM was higher than recommended by (Sander *et al.*, 2015) and the

stain was visible in the yolk and gastrointestinal tract (GI) in addition to the PCT, but this was the only concentration at which the tubule could be clearly seen. On day of imaging, the stain could be visualised under 488 nm laser on the confocal microscope.

### 3.2.4 Image acquisition on the Acquifer

Exposed larvae anaesthetised using 0.4 g/L MS222 were transferred in 100µl exposure media to a 96-well microtiter plate containing agarose imprinted using a 3D printed moulding tool to create grooves (Wittbrodt *et al.*, 2014) (Fig. 3.4). Embryos were manoeuvred into these grooves to ensure uniform orientation on their left lateral side for optimum visualisation of the pronephros and liver.

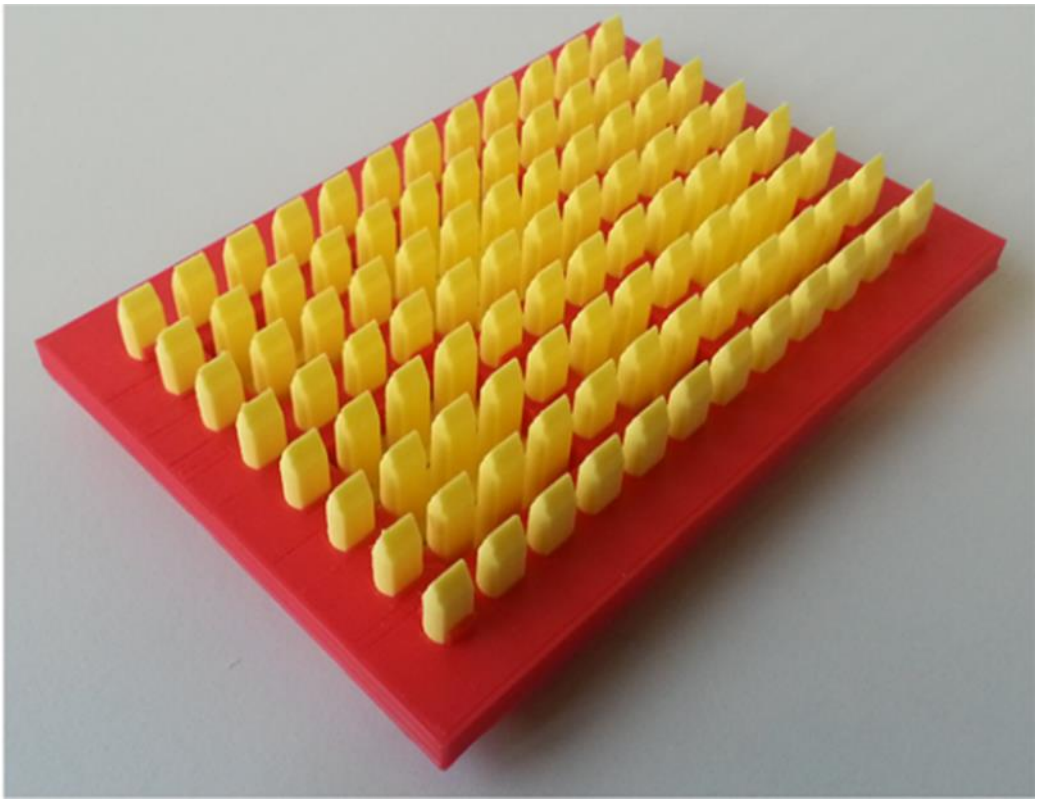

*Figure 3.4* ***Photo of example orientation tool****. Taken from Wittbrodt et al. 2014*

The plate was first scanned on 2x objective using no fluorescence channels and only 1 z slice, with no focussing. This allowed for an entire 96 well plate to be scanned in two minutes and facilitated a rapid assessment of the larvae so incorrectly positioned or phenotypically aberrant (in which the fluorescence could not be accurately measured) larvae could be deselected prior to the higher content scan. At this stage, the exact positioning of the larvae on the X and Y-axis in the well could be selected using the centring tool (Fig. 3.5). Using this function, the desired field of view for a higher magnification could be pre-selected

for each individual larva and programmed into the script for a follow-up higher content scan.

The plate was then scanned a second time using 4x or 10x magnification, and the relevant fluorescent channel (595 nm for red fluorescence to capture the mCherry fluorophore, and 470 nm for green fluorescence to capture the GFP), in addition to brightfield. The intensity and integration for the fluorescence channels were optimised for each experiment to compromise between maximum sensitivity (i.e., in order to capture the weakest fluorescence) and avoiding oversaturation of the signal, which would negate efforts to measure a concentration-dependent response and potentially mask more subtle signals. Therefore, absolute values in intensity cannot be compared across experiments, but relative changes between control and experiment treatment groups can be.

During the second scan, an autofocus protocol was used to automate acquisition. This autofocus script was optimised using trial-and-error to compensate for variation between samples in position on the Z-axis used 15 z-slices at dZ=75µm, 1x1 binning under brightfield at 50% intensity and 50ms integration. Once the algorithm had selected a suitable Z-centre, a Z-stack of 11 Z-slices with dZ=8 µm was captured, optimised to capture the whole depth of the pronephros and liver.

### 3.2.5 Image acquisition on the confocal microscope

Anaesthetised larvae were embedded in 1 % agarose and imaged manually. For full details see Chapter 2 section 2.6.

### 3.2.6 Image analysis

Images were analysed using Fiji (ImageJ) (Abràmoff *et al.* 2004). After efforts to automate image analysis proved unviable, the images were analysed manually. This was due to high levels of noise particularly in the EpRE:mCherry model, along with natural variation in the larvae and in their position in the Z- axis (Jeremy Metz, *personal communication*). Using the selection tools, regions of interest (ROIs) were drawn around each of the target organs (liver, PT, PD, GI, and heart) plus an agarose only selection to provide a background measurement. After extensive method optimisation these ‘templates’ were designed to be slightly oversized to ensure the whole organ was captured, and the same templates between treatment groups, in order to avoid bias by only drawing around obvious fluorescence. The mean fluorescence within these ROIs was taken, and the background fluorescence for each well subtracted from each ROI.

Other methods for image analysis were considered, such as the use of thresholding for pixel selection, however the methods described above were found to be the most time-efficient, reproducible and least bias.

For images of the PT-yellow stain acquired using the confocal microscope, a co-localisation analysis was performed using the JACoP plug-in (Bolte & Cordelières, 2006) on Fiji to quantify the overlap in pixels between images of the same sample taken using a red laser and a green laser.

### 3.2.7 Statistical analysis

See Chapter 2 section 2.9.

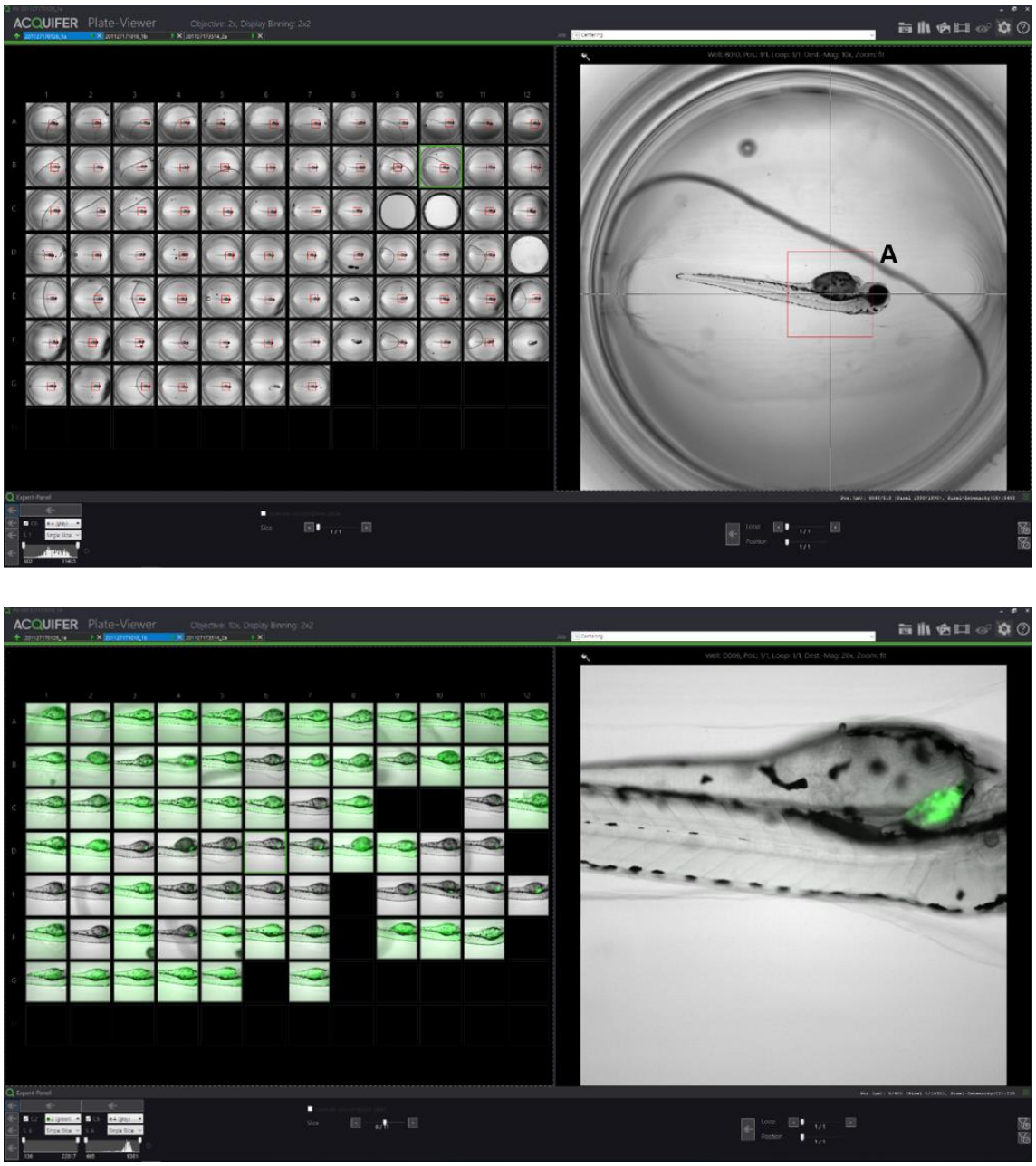


*Figure 3.5* ***Screenshot of the Acquifer Plate-Viewer V1.7.1.*** *[Top]The Plate-Viewer can be used for rapid assessment of the larvae on low magnification and selection of the field of view (marked by A) for a follow-up scan using a higher magnification. [Below] The plate has been scanned on a higher magnification using the field of view selected in (A), and a Z-stack has been captured for each well. The images show an overlay of the bright field and green channels for 4 dpf ERE:GFP larvae, with ERE activation indicated by green fluorescence in the liver.*

## 3.3 Results

### 3.3.1 Response of ERE:GFP to EE2

The Acquifer was first used to assess the oestrogenic response to EE2 in the ERE:GFP model at 4 dpf. This allowed the rapid identification of the liver as a target organ, which reliably exhibited detectable, concentration-dependent fluorescence in response to EE2 exposure at 0.034 nM (Fig. 3.6).

The heart also expressed GFP, although it did not appear as sensitive as the liver it was only significant at 0.067 nM EE2. The signal was also much weaker compared to the liver and not consistently detectable.

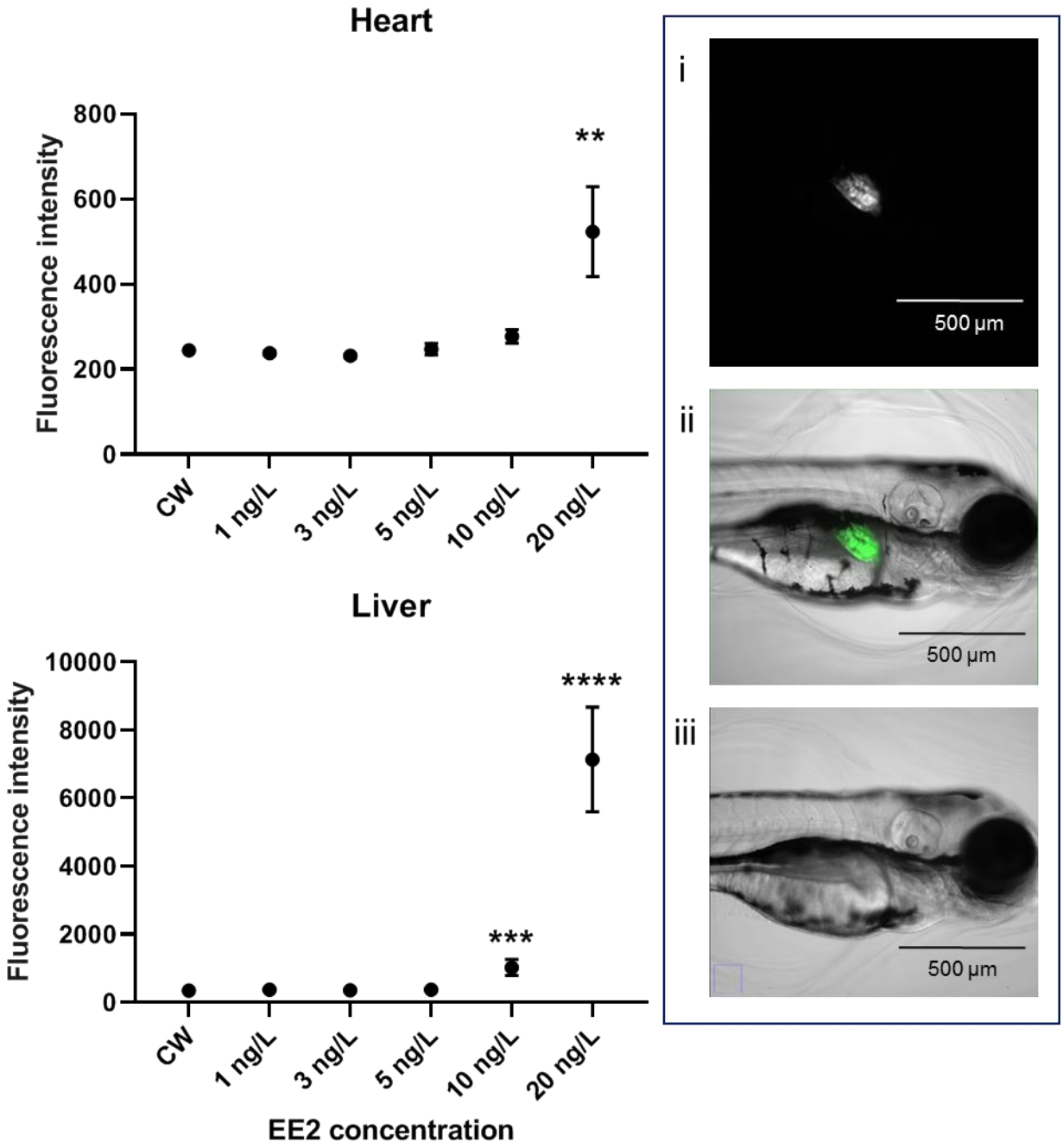


*Figure 3.6* ***Fluorescence response in 96 hpf ERE:GFP larvae aqueosly exposed to EE2.*** *Data points show the mean values of the mean pixel intensity within the heart or liver for 12 larvae per treatment group, error bars show the SEM. Data were not normally distributed and so analysed using a Kruskal-Wallis test followed by Dunn's multiple comparison test. Asterisks represent significant difference from the clean water control (CW): * = P<0.05, ** = P<0.005, *** = P<0.0005, **** = P<0.0001. Insert shows 96 hpf larva exposed to 0.067 nM EE2 as [i] green channel only and [ii] composite image. [iii] shows composite image of an ERE:GFP larva exposed to CW only as a comparison. Scale bar shows 500 µm. The heart is not as easily visualised as the liver.*

The ERE:GFP model was then imaged daily under a range of EE2 concentrations to understand the temporal profile of the oestrogenic response (Fig. 3.7). Again, no significant fluorescence was detected in the 0.017 nM treatment group. Interestingly, an oestrogen response was detected in the 0.034 nM group as early as 2 dpf, but not in the 0.067 nM until 3 dpf. The most dramatic increase in fluorescence intensity was seen in the top 2 concentrations between 3 and 4 dpf. Again, the heart did not show a concentration-dependent response, and a signal was not detected at all in the heart until 4 dpf.

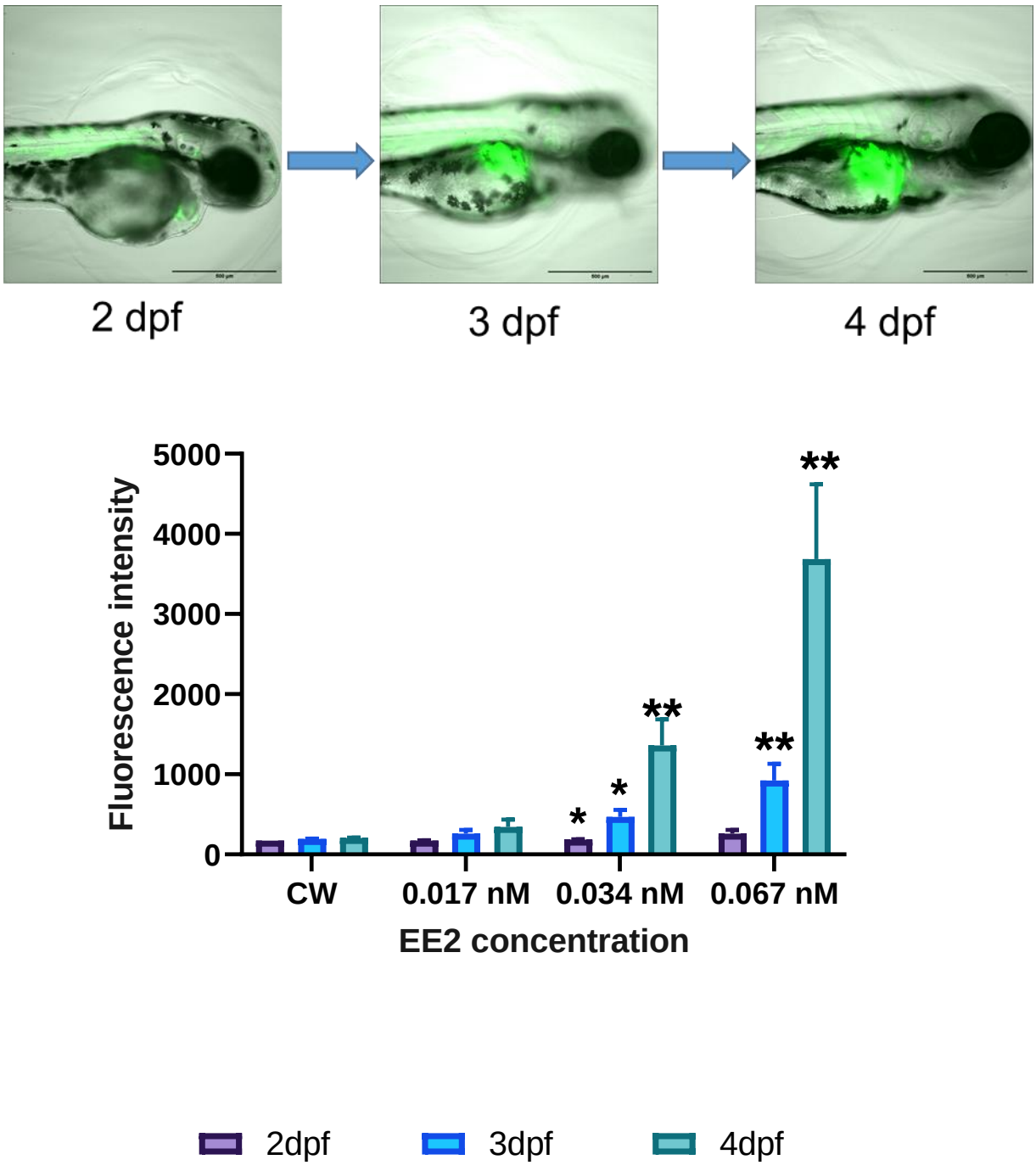


*Figure 3.7* ***Fluorescence response over time in the liver of ERE:GFP larvae treated with EE2*** *[Top] Example images of ERE:GFP larvae aqueously exposed to 0.067 nM EE2. Scale bars show 500 µm. [Bottom] The same larvae were imaged at 2, 3 and 4 dpf, and were transferred to fresh exposure media in between each time point. Data shows the mean values for mean pixel intensity within the liver of 20 larvae, error bars show the SEM. Data was normally distributed with equal variance and so analysed using an ANOVA followed by Dunnett's test. Asterisks indicate significant difference from the clean water control group for the corresponding time point: * = P<0.05, ** = P<0.005.*

The daily imaging highlighted 3-4 dpf as the time period of greatest increase in ER response from the previous time point (Fig. 3.7). The temporal resolution of the imaging system was then tested by taking hourly images of the larvae during and around this window (Fig. 3.8), to find if the profile of the ER response could be tracked in even finer detail. A continuous imaging period of 24 hours was attempted, however, after 6 – 17 hours in the anaesthetic, larvae began to show necrotic brain tissue, and cardiac oedemas could be observed after a minimum of 3 hours in all larvae regardless of chemical treatment (Fig. 3.9). The experiment was therefore terminated after 19 hours.

Fig. 3.9 shows an example 4 dpf larvae from the time lapse experiment along with the cumulative frequency distribution showing how rapidly cardiac oedema or necrotic brain tissue were first noticed. Not all larvae developed oedemas, or were angled in a way that made the development of an oedema clear, hence this value has a smaller N. The histogram also illustrates that oedemas began to develop before brain necrosis was clear. The median value for onset of the oedemas was 9 hours, while for the brain necrosis this was at 12 hours.

No significant changes in the oestrogenic response were detected during this time, although some individuals in the 0.034 nM and 0.067 nM EE2 treatment groups showed a downward trend in fluorescence intensity (Fig. 3.8).

Subsequent time-lapse experiments were limited to 10 hours, and although the larvae did not show such a severe reaction to the extended anaesthesia (only 47 % of larvae developed oedemas during the period, and no tissue necrosis was observed), no change in GFP fluorescence was detected (Fig. 3.8).

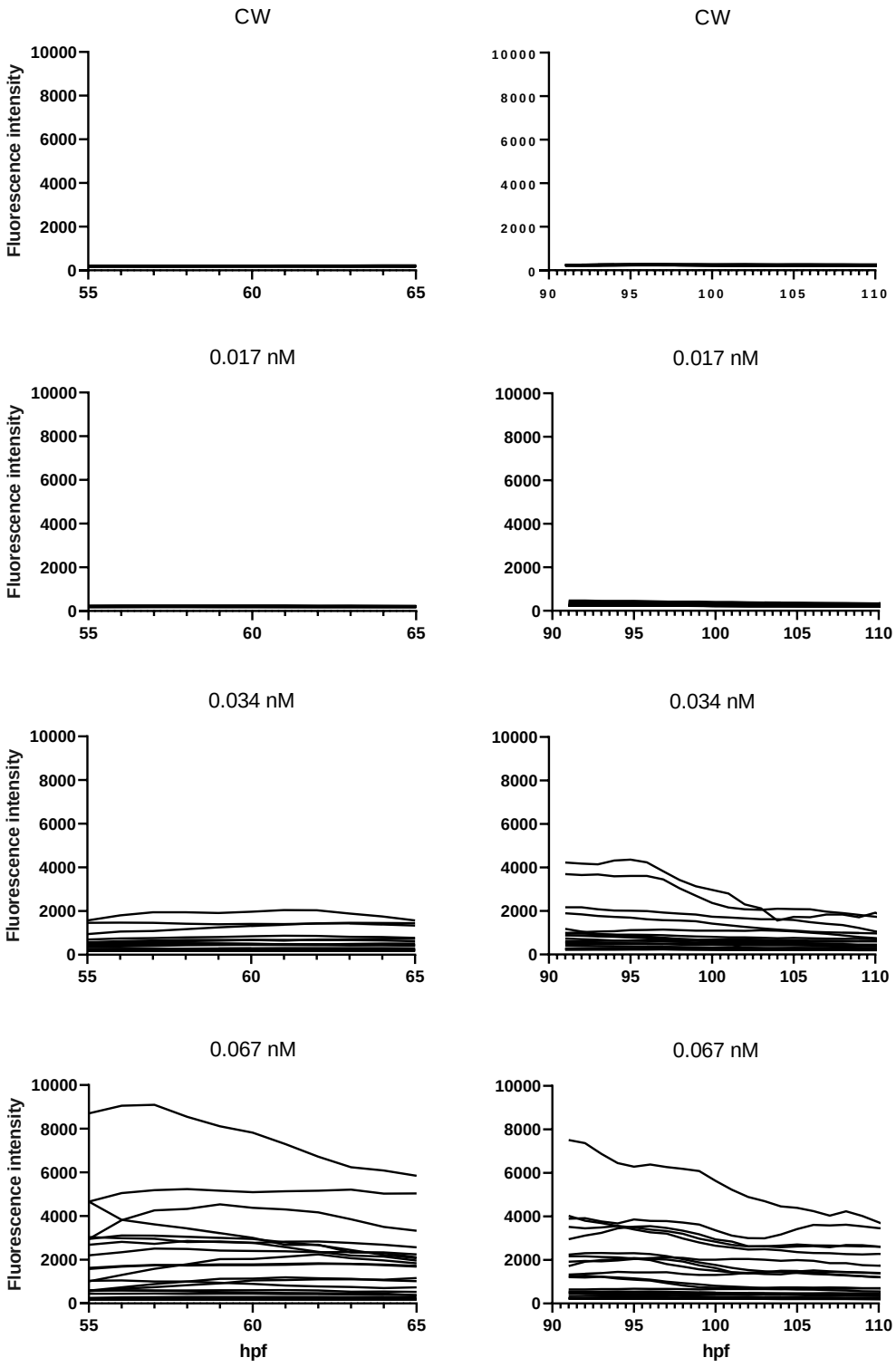


*Figure 3.8* ***Hourly imaging of ERE:GFP larvae aqueously exposed to a range of EE2 concentrations from 6 hpf****. Each line shows the mean pixel intensity within the liver of an individual larva (12 larvae total per treatment group).*

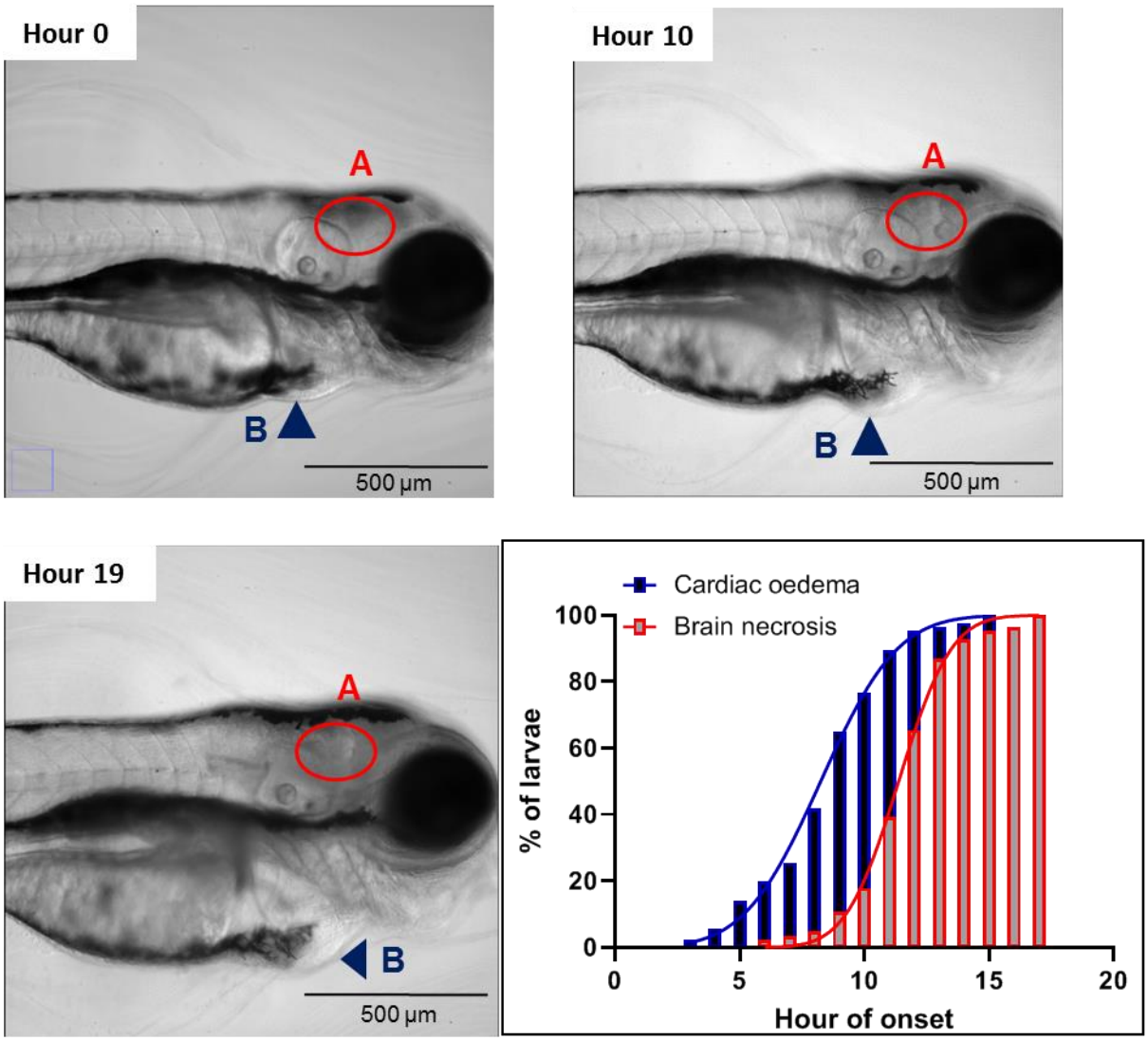


*Figure 3.9* ***One example 4 dpf ERE:GFP larva aqueously exposed to 0.067 nM EE2 from 6 hpf, shown at 3 time points from the start of the time lapse to 19hrs of continued anaesthetic exposure on the Acquifer (brightfield channel only)****. Of particular interest is [A] the darker tissue in brain which also becomes more swollen, indicating necrosis, and [B] the swelling of the membrane around the pericardial sac, indicating an oedema. Necrotising tissue and declining optical clarity hindered the accurate measurement of tissue-specific fluorescence. Insert shows a cumulative frequency distribution histogram for the hour of onset for cardiac oedema and brain necrosis in the larvae presented in fig. 3.8 (i.e., total 96 larvae anaesthetised at 4 dpf for 19 hours).*

### 3.3.2. Response of EpRE:mCherry to APAP

The pronephros (PT and PD) and liver were confirmed as tissues vulnerable to APAP-induced OS in the EpRE:mCherry model. A significant level of OS was observed in the liver at 2.5 and 5 mM APAP, but not at 1.25 mM APAP (Fig. 3.10).

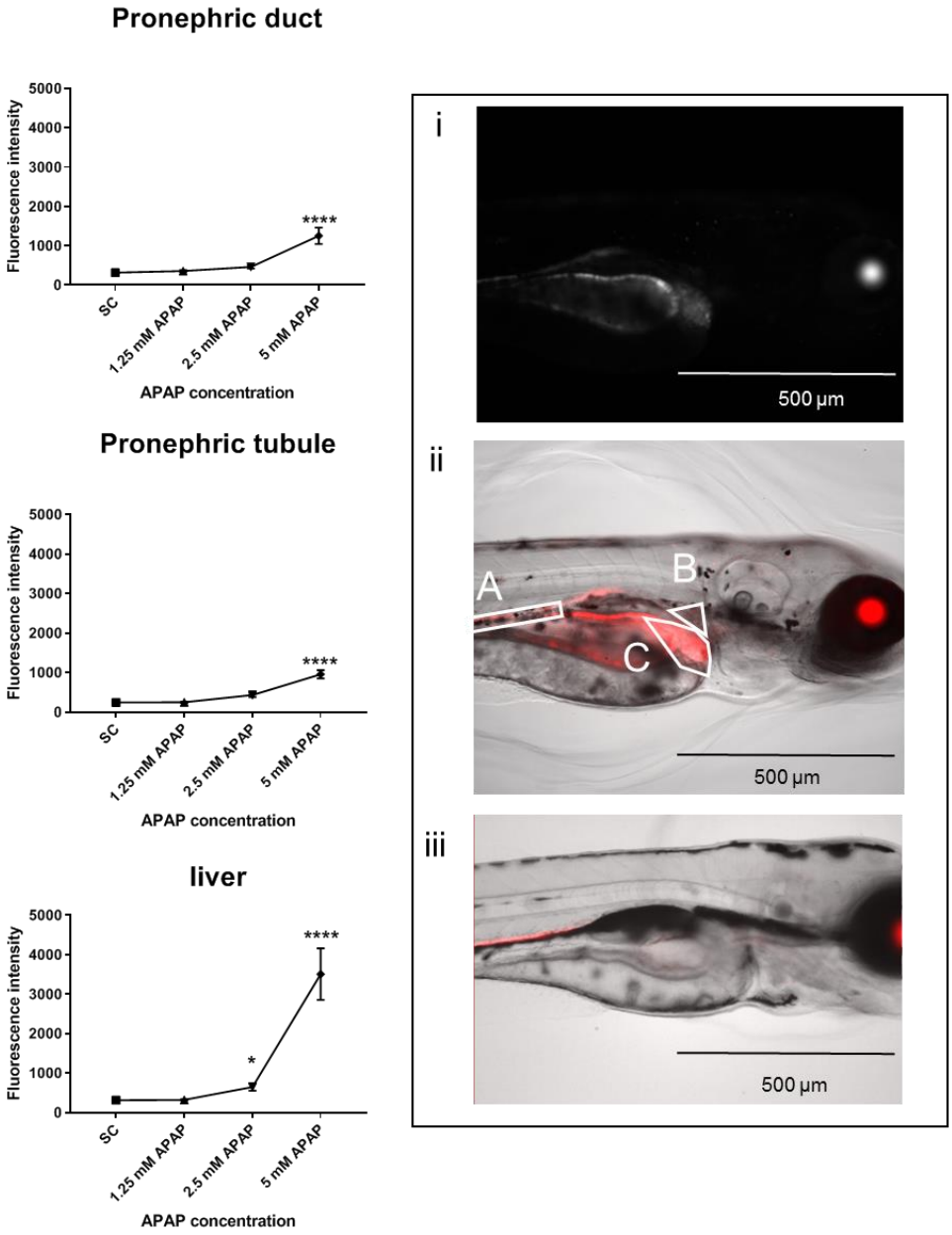


*Figure 3.10* ***Fluorescence response in 4 dpf EpRE:mCherry larvae exposed to APAP, imaged using an Acquifer****. Embryos here were exposed using the same protocol as Mourabit et al. 2019: embryos dechorionated and exposed to APAP at 2 dpf. [Left] Data shows the mean values (+/-SEM) of mean pixel intensity within the organ for 12 larvae per treatment group. Data were non-normally distributed so analysed using a Kruskal-Wallis test followed by Dunn's multiple comparison test * = P<0.05, ** = P<0.005, *** = P<0.0005, **** = P<0.0001. [Insert] [i] red channel only and [ii] Composite image of 4 dpf EpRE:mCherry larva exposed to 5 mM APAP from 2 dpf, showing strong fluorescence in the [A] PD; [B] PT; [C] liver. A strong red signal in the eye is a marker for the TG line and is present regardless of chemical treatment. [iii] shows a composite image of an EpRE:mCherry larvae exposed to SC (0.5% DMSO) only for comparison.*

### 3.3.3. Comparison of Acquifer with confocal microscopy

#### *3.3.3.1 Tissue identification and signal localisation*

In order to confirm the identity of the organ labelled [B] in Fig. 3.11, the fluorescent stain PT-yellow was used, which is taken up by the PCT and appears green. (Sander *et al.*, 2015). Fig. 3.11 confirms that OS is detected in the head of the pronephros, but a strong red signal can also be seen in the tissue adjacent to the stained PCT. This tissue is believed to be the glomerulus, as the stain is excluded from the tissue and by moving through the Z stack, the PCT can be seen leading medially into it.

When the PCT and glomerulus were analysed separately, a stronger fluorescent signal for OS appeared to be detected in the glomerulus than the PCT, both in SC and APAP-treated larvae (Fig. 3.12). However, the red fluorescent signal also appeared to follow the green fluorescence (i.e., the stain) intensity profile closely across the PCT until the glomerulus where the green fluorescence vanishes and the red fluorescence reaches its strongest peak (Fig. 3.12). Further, a co-localisation analysis of the PCT and glomerulus together (from now on collectively referred to as the pronephric tubule) captured on the confocal, using JACoP on ImageJ gives a mean Pearson's coefficient of 0.474 (SEM 0.0326; N=20), indicating a weak but positive correlation between the 2 fluorescent signals and therefore suggesting co-localisation.

#### *3.3.3.2 Resolution of the Acquifer versus confocal microscopy: pronephros*

Fig. 3.11 shows that the Acquifer can detect the fluorescence emitted by the PT-yellow stain in the PCT [A]. However, the organ is less clearly defined in the Acquifer images compared with the confocal, and it is more difficult to track the PCT laterally or medially to find where it joins with the glomerulus (based on the images acquired by the confocal, this is assumed to be [B]). This complicated the precise identification of the tissue which is emitting the red fluorescence (i.e., experiencing OS).

To test the resolution of the Acquifer whilst still achieving medium-high throughput, the stained embryos were automatically imaged using the standard protocol with some adjustments made to the auto-focus parameters to optimise resolution. However, only 8 out of 59 embryos imaged on 10x magnification showed clear visualisation on the PCT on the green channel (considered as

showing sharp edges of the tubule). Given the success of the stain when embryos were imaged on the confocal, this unlikely to be due to poor uptake of the stain. At 20x magnification, even manual focussing could only achieve poor visualisation of the PT.

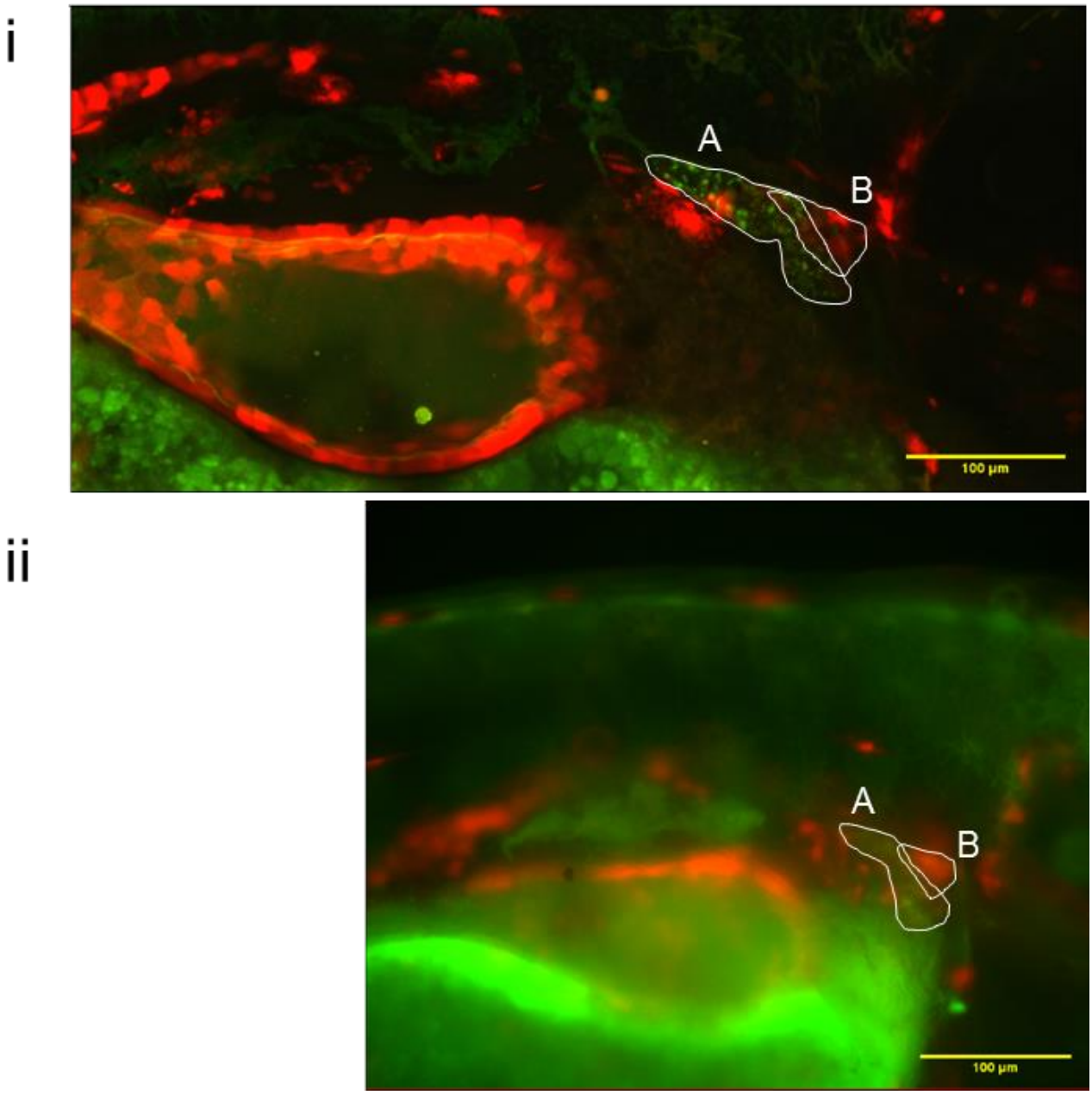


*Figure 3.11* ***4 dpf EpRE:mCherry larva exposed to 2.5 mM APAP from 6 hpf and stained using 500nM PT-yellow, imaged on [i] confocal and [ii] Acquifer.*** *The PT-yellow stain is shown in green and mCherry fluorescence is shown in red. The PT-yellow stains the PCT [A] but is excluded from the glomerulus. Scale bar shows 100 µm and images are uncropped; they are different dimensions due to the differing platforms used.*

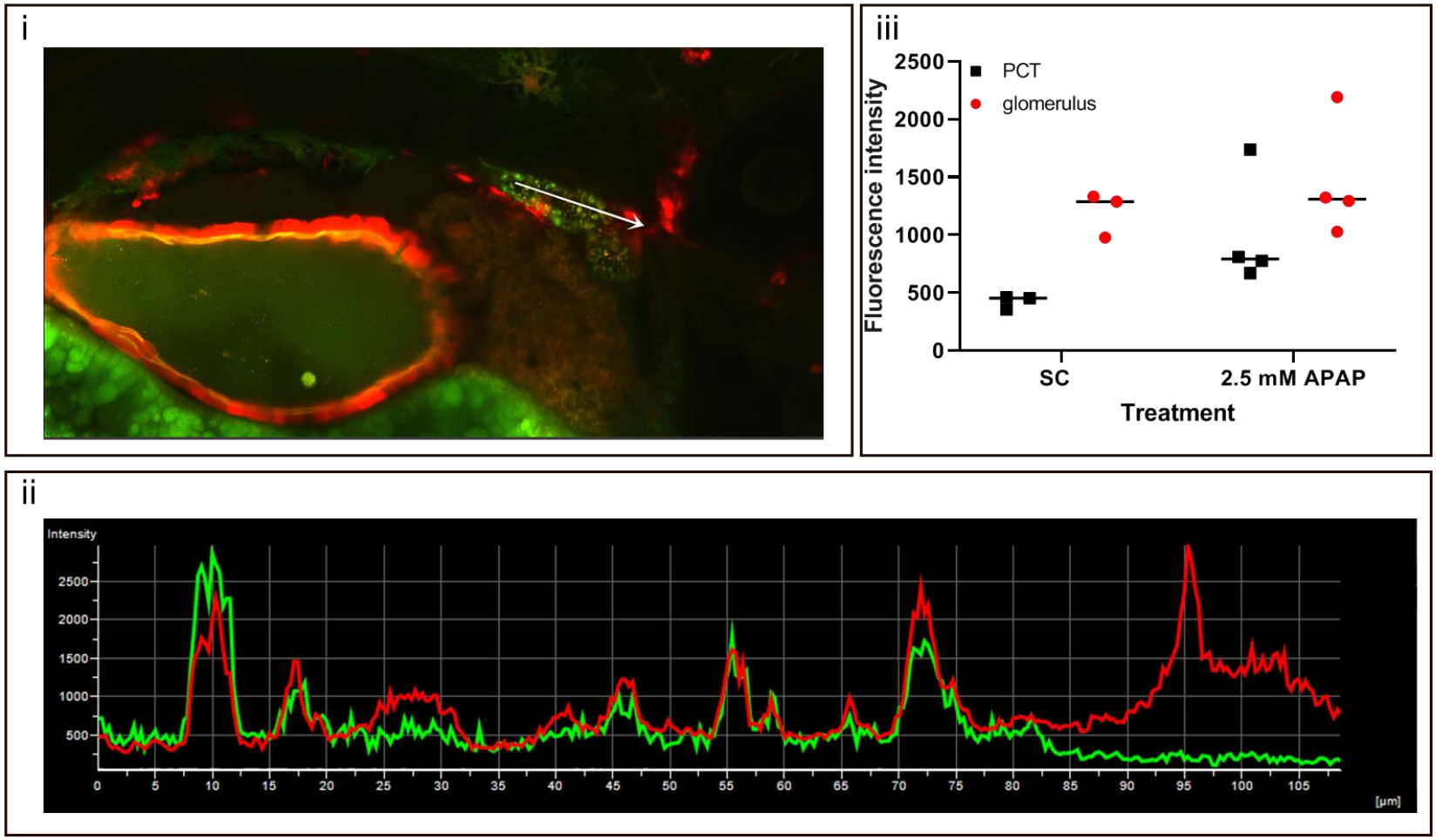


*Figure 3.12* ***Difference in mCherry fluorescence intensity between the glomerulus and the PCT.*** *[i] Confocal image of a 4 dpf larva exposed to 2.5 mM APAP from 6 hpf and stained with 500 nM PT-yellow, and [ii] the corresponding intensity profile of the red fluorescence (OS) and green fluorescence (PT-yellow stain) along the white arrow. [iii] Mean pixel intensity of the PCT and glomerulus in 4 dpf larvae exposed to a solvent control (SC) or 2.5 mM APAP (each data point represents an individual larva). Line shows median value, N=4.*

#### *3.3.3.3 Resolution of the Acquifer versus confocal: neuromasts*

In further investigation of the resolution of the Acquifer, this system was used to image the neuromasts of 4 dpf EpRE:mCherry larvae following exposure to Cis, a known ototoxin which had previously been shown to induce significant OS neuromasts of the EpRE:mCherry model (Mourabit *et al.*, 2019).

Although the neuromasts were visible using the DASPEI stain on the Acquifer (Fig. 3.13) as well as the confocal (Fig. 3.14), no change could be detected in the red fluorescence channel (i.e., OS) on the Acquifer. Fig 3.15 shows that larvae imaged using the Acquifer show no significant OS, signified by no change in the mCherry signal, whereas the confocal images suggest there was a significant increase in OS in embryos exposed to 0.3 µM versus the SC group. Further, the confocal shows that at 10x this concentration the red fluorescence was significantly lower than the control, and no neuromasts could be identified using the DASPEI stain (suggesting they had been destroyed).

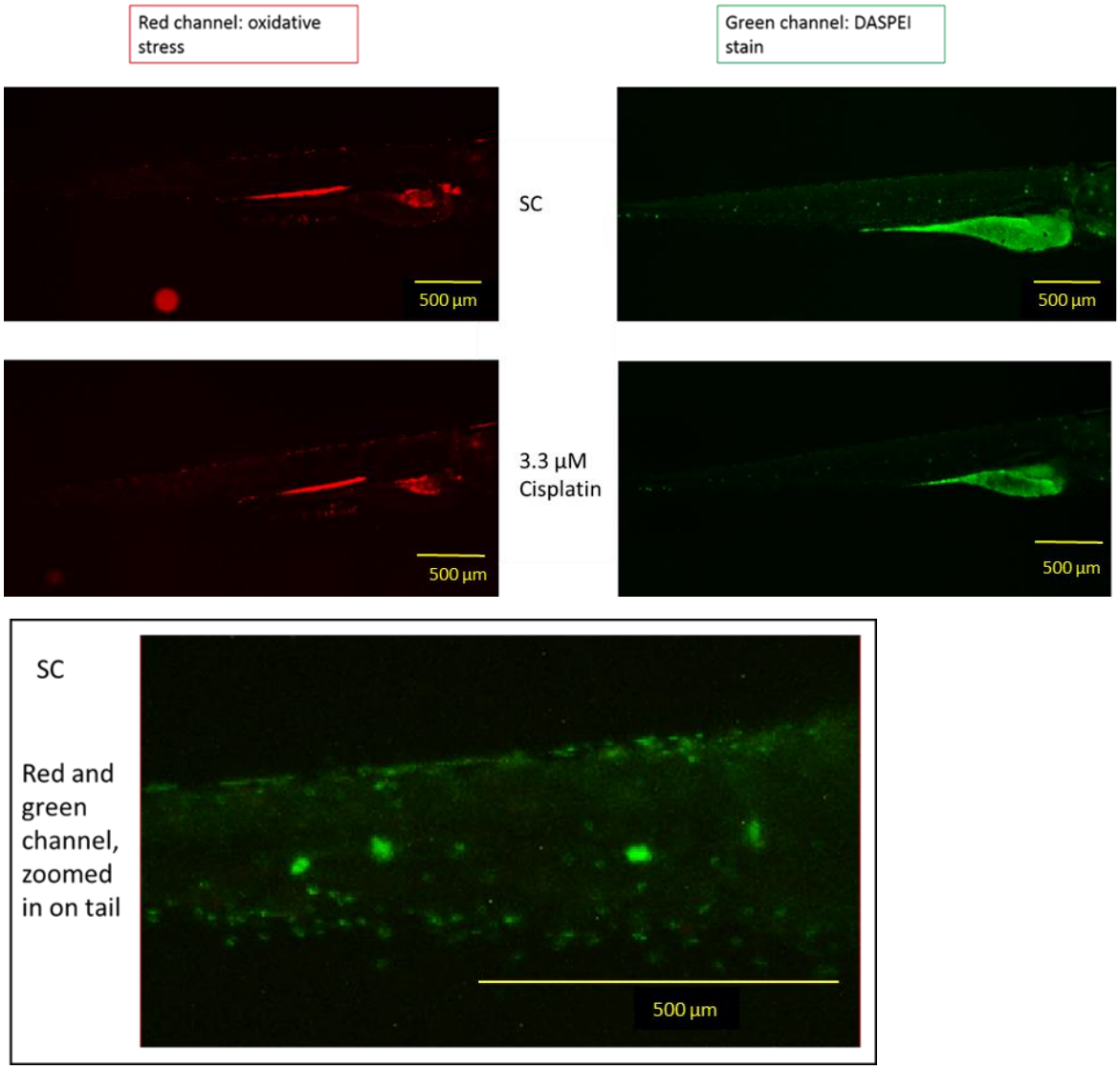


*Figure 3.13* ***4 dpf EpRE:mCherry larvae exposed to cisplatin or SC from 6 hpf and stained with DASPEI to identify neuromasts and imaged on Acquifer on 4x magnification.*** *[Left] red channel shows oxidative channel and [right] green channel shows DASPEI stain. Scale bar shows 500µm. Insert shows a larva from SC treatment group, shown as an overlay of red and green images, focussed on the tail. Contrast of images have been modified to aid visualisation*

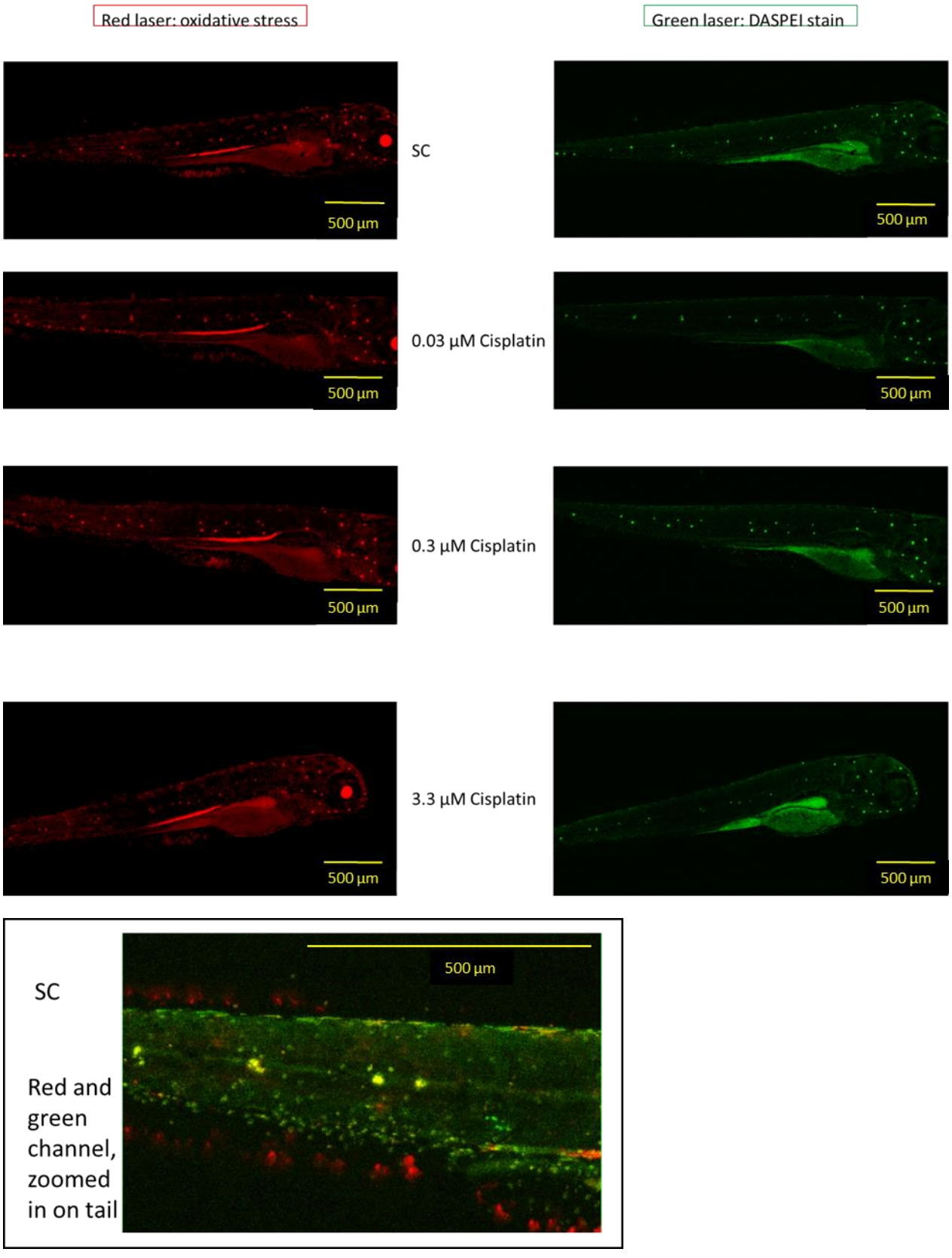


*Figure 3.14* ***4 dpf EpRE:mCherry larvae exposed to cisplatin or SC from 6 hpf and stained with DASPEI to identify neuromasts and imaged on confocal on 4x magnification.*** *[Left] red channel shows oxidative channel and [right] green channel shows DASPEI stain. Scale bar shows 500µm. Insert shows a larva from SC treatment group, shown as an overlay of red and green images, focussed on the tail. Contrast of images have been modified to aid visualisation*

Confocal

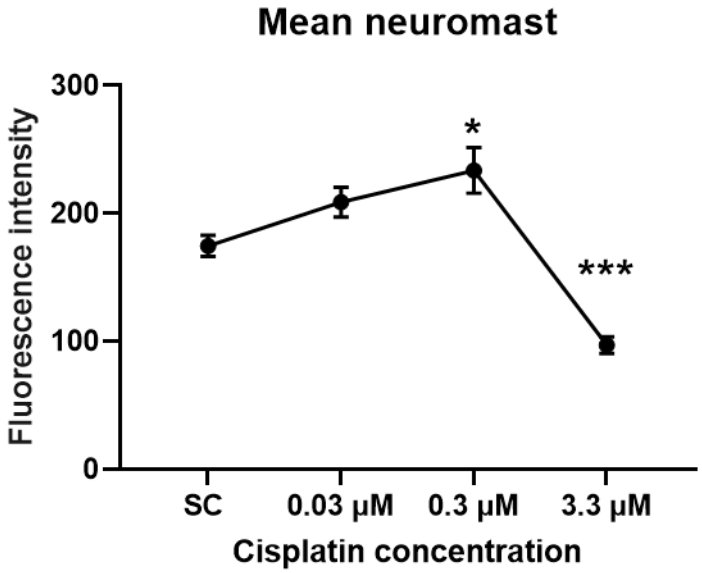


Acquifer

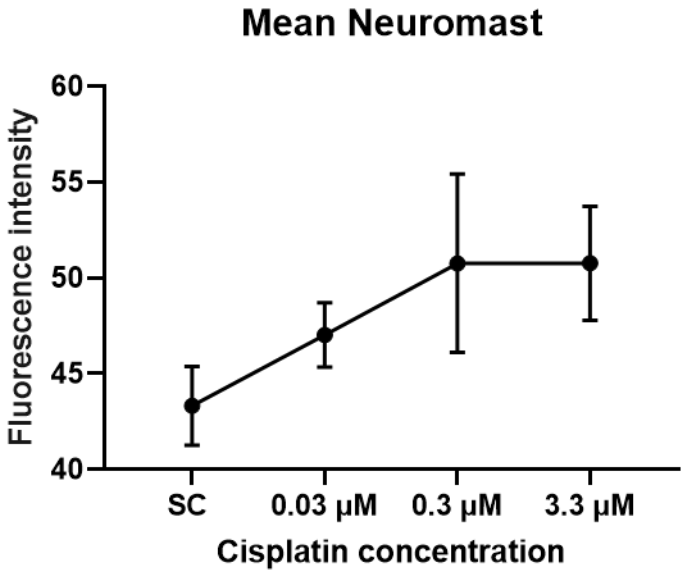


*Figure 3.15* ***Difference in OS levels in neuromasts of 4 dpf EpRE:mCherry larvae exposed to cisplatin from 6 hpf, detected using confocal microscopy compared with the Acquifer.*** *Fluorescence intensity is measured as the mean pixel intensity within 6 neuromasts, and given as the mean values (+/- SEM) from 12 larvae per treatment group. Imaged on [top] confocal and [bottom] Acquifer. Data were not normally distributed and therefore analysed using a Kruskal-Wallis test followed by Dunn's multiple comparison test * = P<0.05, ** = P<0.005, *** = P<0.0005, **** = P<0.0001.*

## 3.4 Discussion

The data presented in this chapter showed that the Acquifer is suitable for chemical affects assessment of TG zebrafish and has demonstrated this using two TG models: ERE:GFP using EE2 and EpRE:mCherry using APAP. The mounting process in agarose grooves make it suitable for rapid assessment of a large number of embryo-larvae, whilst also allowing for repeated imaging of the same individuals across multiple days. However, the closed static system is not suitable for long term culturing of embryo-larvae to achieve time-series data. As expected, the Acquifer also cannot achieve the same level of sensitivity in terms of fluorescence detection as confocal microscopy, nor spatial resolution.

### 3.4.1 Chemical effects assessment of ERE:GFP and EpRE:mCherry zebrafish

#### *3.4.1.1 ERE:GFP*

The system tested here was not as sensitive as previous responses detected using the ERE:GFP model: significant GFP induction from 0.034 nM EE2 exposure (Fig 3.6; well above environmental concentrations (Laurenson *et al.*, 2014)) compared to 0.003 nM EE2 reported by Lee *et al.* (2012). This difference in sensitivity may be due to the different imaging platforms used (Lee *et al.* used a confocal microscope) or the use of a later generation in the present study compared to Lee *et al*'s. Later generations of TG models can experience progressive reduction in transgene expression through successive generations of animals, caused by a range of mechanisms. TG lines which incorporate Gal4/UAS amplification systems, as the ERE:GFP model does, are particularly vulnerable to epigenetic gene silencing over generations due to methylation of the UAS copy (Goll *et al.*, 2009). Methylation of UAS could be confirmed using a variety of methods intended for analysis of DNA methylation of specific genes of interest, such as digestion-based assay followed by PCR or qPCR, or bisulphite conversion followed by sequencing (Kurdyukov & Bullock, 2016).

The identification of the liver as a target organ of EE2 is consistent with previous reports using this TG model (Lee et al., 2012a) and other TG models such as ERE-Kaede-casper (Green *et al.*, 2018). Additionally, Hao *et al.* 2013 reported that most 17β-estradiol (E2)-responsive genes at this age, including those encoding vitellogenin, were predominantly located in the liver (Hao *et al.*, 2013). In contrast with the data presented here, Hao *et al.* also observed E2-induced GFP and upregulation of oestrogen-responsive genes in the pancreas. A pancreatic signal could not be seen in the ERE:GFP model used here, although

it is possible that the bright signal from the liver masked the pancreas, as the 2 tissues are located close to each other.

The detection of a fluorescent signal in the heart is also in line with what is known about the impact of oestrogenic compounds on heart valves. There is strong evidence in the literature for the influence of oestrogenic compounds on heart valve development (Brown et al., 2019; Green et al., 2018; Moreman et al., 2018), including observation of fluorescence in the heart in this model previously (Lee et al., 2012a). Previous studies have suggested that the heart valves are more sensitive than the liver (Moreman *et al.*, 2018). The weaker and less consistent signal observed here may be a result of pigmentation covering the pericardial sac blocking the area of fluorescence characteristic of the heart valves. The ERE:GFP model has also been developed in a pigment-free casper background (Green *et al.*, 2016), which avoids this problem, however this line spawned less reliably and produced larvae that less frequently expressed fluorescence and so was not suitable for the development of the Acquifer methods in the present study.

#### *3.4.1.2 EpRE:mCherry*

A significant level of OS was detected in the PT, PD and liver of EpRE:mCherry larvae at an APAP concentration of 2.5 mM (Fig. 3.10), although this model previously had shown a response in the liver at concentrations as low as 1.3 mM (Mourabit *et al.*, 2019). This suggests either that the Acquifer is not as sensitive as the confocal (as used by Mourabit *et al.*), or the model has lost sensitivity over the generations, similar to the ERE:GFP model. However, throughout the course of this project, new generations of EpRE:mCherry zebrafish were compared against their parents for APAP-induced fluorescence intensity and sensitivity (Chapter 4 section 4.3.1), and these were found to be consistent. Later, it was found that the model could detect lower APAP concentrations when exposed from 6 hpf as opposed to 48 hpf, and this provided a standard protocol with a known response against which the effects of other pharmaceuticals could be compared (see Chapter 4 for development of the model).

### 3.4.2 Application of the Acquifer for capturing time-series data

The Acquifer facilitated daily imaging of EE2-exposed larvae, with easy recovery of the animals and minimal stress between time points. This allowed the visualisation of a response profile over time to understand the ontogeny of the

oestrogenic response. The detection of a signal as early as 2 dpf (Fig. 3.6) is largely in line with what is known about the expression of oestrogen-responsive genes during embryo development. For example, previous studies have reported upregulated oestrogen-responsive genes and activation of ERE in the brain, liver and pancreas from 2 dpf (Gorelick & Halpern, 2011; Hao et al., 2013; Lee et al., 2012a). The heart valves exhibit weak ERE-dependent GFP from 4 dpf, with a stronger signal at 5 dpf (Bondesson et al., 2015; Moreman et al., 2018). This is in line with the data shown here, as a signal was not detected at all in the heart until 4 dpf, confirming the applicability of the Acquifer as a HTS tool for responses in the heart.

Characterisation of the ontogeny of ER expression primarily divides the process into 3 stages: *esr*2b, maternally loaded into the oocyte, is expressed until 6 hpf, at which point there is no ER expression until 48 hpf when all ERs, but particularly *esr*1, are expressed (Bardet et al., 2002). However, Lassiter *et al.* detected *esr*2a transcripts between 24 and 48 hpf (Lassiter et al., 2002). It would have been interesting to use the ERE:GFP model to test for an oestrogenic response at 24 hpf, but this was not possible due to the fragility and morphology of the embryo at this stage, as it could not be positioned in the agarose mould for imaging.

One of the advantages of the Acquifer over previous HTSs (e.g. the ArrayScan (Green *et al.*, 2018)) is the mounting process, which consists of agarose grooves shaped using an orientation tool (Wittbrodt *et al.*, 2014) into which the anaesthetised larva can be placed (still in the exposure media) and positioned uniformly across all the wells. The rapid, uniform orientation facilitates convenient, automated imaging of all the embryos, and leaving the larvae in exposure media instead of embedding them in agarose means they can be easily recovered and re-exposed in fresh media for further imaging later. Therefore, the response profiles of individuals can be tracked. Additionally, this methods avoids the risk of growth restriction and malformations which can arise from long-term embedding in agarose, a rigid media which does not allow for movement or growth of the embryo-larva (Kaufmann et al., 2012). However, because the embryos are not embedded in the agarose, they can sometimes move within the well, particularly at 4 dpf or older when the swim bladder is beginning to inflate and the larvae generally become more active, causing the larva to roll or float to the surface. Additionally, the auto-focus algorithm functions only within a pre-

determined z-axis, therefore any larvae sat outside of this range will not be in focus. Consequently, to ensure a minimum sample size is always achieved, more larvae must be used in order to compensate for the small number which will not be useable.

The Acquifer can also be used to track the development of a response over time using repeated imaging. However, although the Acquifer successfully acquired daily images with recovery intervals, larvae could not be held in the system for longer than around 9 hours before they began to develop oedemas or tissue necrosis (Fig. 3.9). The darker tissue and malformations may account for the apparent decline in ER response over time (Fig. 3.8), as they began to attenuate the fluorescent signal. Additionally, although the agarose was impregnated with MS-222 and EE2 to avoid either chemical leaching out of the exposure media, the anaesthetic did begin to lose effect for some larvae, allowing them to move within the well and impairing the auto-focus.

The degradation of the samples may be a result of the extended anaesthetic, and/or the closed, static system: the plate was sealed to prevent evaporation and consequently oxygen and EE2 could not be replenished, just as waste could not be removed. Therefore, the Acquifer system proved unsuitable for longer term immobilisation for smaller-interval time lapses. A more suitable platform for this kind of experiment could be 'fish-on-a-chip' tools (discussed in Chapter 1) or other microfluidics devices which allow long term culturing for time-lapse imaging of embryo development (Zhu *et al.*, 2019) by refreshing the levels of oxygen and test compound, and removing waste.

Besides the issues of limited oxygen in a static system, there is also the question of how representative the response of an anaesthetised larva is of that of a conscious larva free to move and with unimpaired physiological processes. Although gill ventilation is not necessary in larvae until around 14 dpf for oxygen uptake and until 7 dpf for ionoregulation (Rombough, 2002), the larval heart rate may have been reduced by the anaesthetic, as has been shown with adult zebrafish (Huang *et al.*, 2010). This potentially limited the distribution of the EE2 around the body, as well as resulting in the necrotic tissue (Fig. 3.9). The metabolic demand of an anaesthetised/immobilised larva may also be reduced, which consequently may alter the interaction of the test organism with the pharmaceutical via metabolism, excretion, absorption or distribution.

### 3.4.3 Assessment of tissue-specific fluorescence

The combination of the stain and confocal microscopy in Figs. 3.11 and 3.12 has served two purposes: firstly, they have confirmed that the signal observed using the Acquifer was located in the proximal part of the PT. For this thesis, the PCT and glomerulus are considered collectively as the PT, as both tissues fulfil similar functions and previous studies also do not delineate between the PCT and glomerulus (including in previous use of the EpRE:mCherry model by Mourabit *et al.* 2019). Secondly, the stain and confocal images reveals that the response to APAP is even more localised, as the strongest OS is detected in the glomerulus rather than the PCT.

The co-localisation value of 0.474 implying a weak but positive correlation between the stain and OS within the PCT is only an approximation and should be interpreted with some caution; the maximum absorbance for the PT-yellow stain is at 548 nm (Sander *et al.*, 2015) but here was imaged using a 488 nm laser (for EGFP) due to availability, while mCherry was visualised using a 561 nm laser. Hence, it is possible that a weak signal from the stain was also detected in the mCherry image. Nevertheless, the co-localisation value can be used to imply some overlap between the two fluorescence signals, supporting the observation that some, but not all, the red fluorescence detected is localised in the PCT. In further support of this, the intensity profiles of the two fluorescence signals across the PCT follow each other closely as it travels laterally until the glomerulus, where the stain is excluded and the OS peaks. Analysis of the PCT and glomerulus separately also shows a greater level of fluorescence intensity in the glomerulus (Fig. 3.12). However, the stronger signal in the glomerulus may simply be consequence of the structure of the organ combined with the angle of imaging. The glomerulus is a very dense organ, and so contains a high number of cells which may undergo OS, and it sits in the middle of the body and spreads over multiple z planes (Fig. 3.2). The PCT, in contrast, is a comparatively narrow organ which spreads laterally along the body, occupying a narrower range of z slices and representing a less dense collection of cells. Therefore, from a lateral imaging angle, more cells of the glomerulus are likely to be captured in a given area, generating a stronger fluorescence signal when assessing mean or maximum intensity projections.

Interestingly, the difference in intensity between the PCT and glomerulus is reduced in larvae that have been exposed to APAP (Fig. 3.12). This suggests that, while the glomerulus has a higher background level of OS, the PCT may be more vulnerable to drug-induced OS. However, the small sample size (N=4) prevents a firm conclusion from being drawn. A future study with a focus on the pronephros and the differing roles/vulnerability of its segments may benefit from using the EpRE:mCherry model in combination with confocal microscopy to investigate this further.

In contrast, the images acquired using the Acquifer do not allow the precise segmentation of the proximal part of the PTs. At higher magnifications on the Acquifer, the fluorescence of deeper tissues became more blurred than features on the surface such as pigmentation or topography of the skin, suggesting the Acquifer is limited in its penetration of deeper tissue. This is likely to be related to the use of an epifluorescence LED light source in the Acquifer, which illuminates the entire sample, as opposed to the laser used in the confocal which excites one z plane at a time. In combination with a pinhole to block unfocussed light, confocal imaging can use point illumination to reduce background fluorescence (Nwaneshiudu *et al.*, 2012). This contrasts with the Acquifer in which fluorescence can bleed through the different Z-slices, resulting in poorer resolution and blurring the signal of deeper tissue (see Table 3.1).

The Acquifer has previously been shown to achieve cellular-resolution imaging of zebrafish embryos, but these were only at 48 hpf and therefore more transparent (Peravali *et al.*, 2011). Pilot studies had previously established that the Acquifer could not easily image larvae ≥ 5 dpf as the swim bladder causes the sample to float out of position, and the impaired capability of the Acquifer to penetrate deeper or more opaque tissue may provide another reason it should be used to image older larvae with more caution. To test this, a future study could use manual embedding of the fish in agarose to test the Acquifer on older, and therefore more optically opaque, larvae. However, this would be more time consuming and reduce the throughput of the platform, undermining the main advantage of the Acquifer.

The Acquifer was recently used to screen drugs for developmental nephrotoxicity using a TG wt1b:EGFP zebrafish. In their study, Westhoff *et al.* were able to visualise the entire pronephros with clear distinction of the glomerulus by using a

dorsal view of a 48 hpf embryo (Westhoff *et al.*, 2020). However, a dorsal view of a 96 hpf EpRE:mCherry in the present study gave inferior visualisation of the pronephros (on the confocal and Acquifer) due to the opacity and pigmentation of the older larvae. If the primary aim of the study was to study nephrotoxicity, the Acquifer would necessitate the use of a younger embryo, or perhaps the breeding of the model in a pigment-free casper background. However, there are some data to suggest a mitochondrial dysfunction in casper zebrafish (D'Agati *et al.*, 2017). This would compromise the utility of an OS TG model as the mitochondrial electron transport chain is the main intracellular source of ROS, and mitochondrial dysfunction itself can be a mechanism of drug toxicity (Jaeschke et al., 2012). For further exploration of the utility of the EpRE:mCherry model, see Chapter 4.

The limitations in sensitivity for the Acquifer were also illustrated in the imaging of neuromasts. Although the neuromasts were visible using the DASPEI stain on both imaging platforms (Fig. 3.13 and 3.14), no change could be detected in the red fluorescence channel of the Acquifer whereas changes were detected in the confocal images. It is possible that the different responses relate to the different batches of embryos used on the different imaging platforms but, this result was repeatable in Chapter 4 (section 4.3.3.4). This suggests that the Acquifer does have the resolution to detect fluorescence in the neuromasts, but not the sensitivity to detect subtle changes in the red fluorescence in these tissues. This could also be related to the sensitivity of the cameras attached to the imaging platforms (Table 3.1): the Acquifer uses a camera (Hamamatsu sCMOS), while the confocal uses a combination of photosensitive detectors, such as a gallium arsenide phosphide (GsAsP) photomultiplier tube (PMT), which are highly efficient at detecting fluorescent wavelengths (http://cste.sut.ac.th/2014/wp-content/uploads/2013/12/Confocal-Microscope-A1-Plus-A1R-Plus-8.pdf Accessed 4/11/2021).

Fig. 3.15 shows that the confocal microscope detected significant induction of mCherry fluorescence at 0.3 µM Cis (compared to the control larvae), but at 10x this concentration, the fluorescence intensity showed a sudden drop and was significantly lower than the control. This suggests that Cis does induce OS in the neuromasts, but at high concentrations, Cis impairs the development of the neuromasts, so there is no tissue to emit a fluorescence signal. This is supported

by the fact that, at 3.3 µM, no neuromasts could be identified using the DASPEI stain. This is in contrast to the results published by Mourabit *et al.* 2019, who detected fluorescence in the PT and neuromasts in response to 50µM and 100µM. This difference may be due to the differing exposure regimens; Mourabit *et al.* exposed the embryos only from 2-4 dpf, whereas the embryos in the present study were exposed from 6hpf for 4 days. Neuromast development begins around 18 hpf with the appearance of the cranial placode from which the neuromasts will eventually arise (Sarrazin *et al.*, 2010), and they are deposited along the posterior lateral line which is complete at 48hpf (Nuñez *et al.*, 2009). 3.3 µM Cis from 6 hpf could have interfered with this process, whereas exposure from 2 dpf has a reduced effect on neuromasts as they are already established. The toxicity of Cis and its effect on the EpRE:mCherry model is further explored in Chapter 4.

Together with the images of the pronephros, these data indicate that while the Acquifer can be used to identify signals in gross landmarks of the embryo at high throughput, it is limited in its resolution and therefore struggles to capture more nuanced changes in fluorescence in smaller or more nebulous tissues.

*Table 3.1* ***Comparison of the key features of the Acquifer and confocal microscopy***

| | Acquifer | Pros and cons | Confocal | Pros and cons |
|---|---|---|---|---|
| **Acquisition time (for 2 fluorescence channels, with a z-stack of 11 slices):** | 96 well plate in 23 mins (14 secs per embryo) | Rapid and requires minimal human intervention. | 1 min 40 secs per embryo | Slower and not all locations/tissues can be imaged |
| **sample preparation time (excluding agarose preparation)** | 1 hr to mount and orientate 96 embryos (38 secs per embryo) | Rapid; allows many samples to be prepared at once. However, older larvae are more likely to move or float out of position. | 3 mins to embed one embryo | Less dependent on age of larva, but more time and labour intensive |
| **Total time to mount, orientate and image 96 larvae** | 1.5 hours | Rapid assessment for high throughput screening of multiple compounds/conditions. Can detect changes in fluorescence intensity and morphological changes in major organs. | 6 hours | Far slower; cannot achieve the same throughput but can detect subtle changes in fluorescence in smaller or more diffuse tissues that the Acquifer struggles to visualise. |
| **Stage** | Fixed; optics block moves | Samples are not disturbed during imaging, ideal as embryo-larvae are resting in exposure media and agarose grooves. | Mobile; camera is stationary | Samples are embedded in agarose, so it is less crucial that embryos are not moved during imaging. |
| **Detector** | Hamamatsu sCMOS 2k x 2k camera | Less sensitive | Photomultiplier tube (PMT) detectors and a Nikon A1 camera | More sensitive |
| **Autofocus?** | yes | Removes need for human intervention; reducing opportunities for bias and allowing automation to increase throughput. However, depending on the age and quality of samples, up to 10 % of samples fall out of the autofocus range and so more embryos must be used to compensate for those which may not be imaged in focus. | No | Manual focus on each sample impedes throughput and risks bias in the selection of the focal plane, but doesn't require the use of extra samples |
| **Light source** | LED | Whole sample is illuminated at once, allowing rapid image acquisition, but light from entire sample is captured at once, so noise cannot be filtered out and fluorescence can bleed through the different planes. At higher magnification this results in poorer resolution and smaller tissue penetration depth. | laser | One plane is excited at a time, so all light can be focussed and reduces background noise. This allows superior resolution and penetration depth, but slower acquisition time. |

### 3.4.4 Biological implications of a fluorescent signal in the transgenic model

The Acquifer was able to assess the tissue-specific, concentration-dependent response of two different TG models in a rapid and convenient manner. The information derived from the fluorescence response profiles can be used to better our understanding of receptor-specific response to chemical exposure.

#### *3.4.4.1 Oestrogenic response*

The present data cannot be used to confirm which ER subtype (ESR) is responsible for mediating the oestrogenic response to EE2 exposure observed in the ERE:GFP model. This is due to a caveat of the TG model being that the fluorescence is mediated via the upregulation of the oestrogen response element (ERE), which can be activated by any one of the 3 ESRs (esr1, esrb or esr2a (Filby & Tyler, 2005)). However, previous studies have combined the use of the ERE:GFP model with other molecular techniques such as morpholinos in which specific ER subtypes are knocked down to delineate the subtype-specific responses (Moreman *et al.*, 2018).

Existing data in the literature can be used to make inferences about the role of specific ESRs in the oestrogenic response observed in the present study, but there exists conflicting data on the tissue-specific expression of different ESRs. mRNA for all three subtypes have been detected in the liver of zebrafish, although only *esr1* was found to be upregulated by estradiol exposure, while *esr1a* was downregulated and *esr2b* was unchanged (Menuet *et al.*, 2004). In contrast, RNA *in situ* hybridisation of 5 dpf zebrafish showed *esr1* transcripts in heart valves, but *esr2a* in the liver (Gorelick *et al.*, 2014). In adult fathead minnow, *esr1* and *esr2b* are expressed mainly in the liver, while *esr2a* expression was lowest. Although there is some overlap in the distribution of the subtypes, they are believed to have distinct physiological functions (Filby & Tyler, 2005). Esr*1* is known to be expressed in the liver of many adult fish species (including zebrafish) where it mediates oestrogen-responsive genes (Moreman *et al.*, 2018), and so on balance, the response seen in the liver ERE:GFP model here is most likely mediated via esr1. GFP expression detected in the heart is also believed to be mediated specifically via esr1 and/or esr2 (Brown et al., 2019; Gorelick et al., 2014). However, it is also known that various oestrogenic compounds can result in distinct tissue-response profiles due to differing interactions with different esrs. For instance, BPA has been shown to mostly activate esr1, and to a lesser extent esr2a, in zebrafish liver cell lines (Cosnefroy *et al.*, 2012). Indeed, another

ERE:GFP zebrafish model has been used to show the differing patterns of ER activation by different samples of environmental oestrogens (Gorelick *et al.*, 2014).

Oestrogen-dependent fluorescence in ERE:GFP showed a particularly dramatic increase between 3 and 4 days (Fig. 3.7). This is in concordance with results published by (Hao *et al.*, 2013) who used RT-qPCR and microarray analysis to show that *esr1* was significantly upregulated in response to EE2 exposure, with a particular peak at 4 dpf compared to any earlier time points. In contrast, *esr2a* and *esr2b* expression remained mostly stable across the 4 day exposure and did not change compared to unexposed embryos (Hao *et al.*, 2013). This also further supports the conclusion that the response seen in the liver of the ERE:GFP model was mediated primarily by the esr1 receptor.

Exposure to EE2 has been shown to increase vitellogenin levels in the plasma and liver of rainbow trout (Skillman et al., 2006) and directly linked to adverse outcomes for the liver; chronic exposure to EE2 induced concentration-dependent liver damage zebrafish (Van den Belt et al., 2001) and in least killifish (*Heterandria formosa*) (Jackson et al., 2019). This damage includes nuclear hypertrophy, cell lysis and vacuolisation of hepatic cells (Jackson *et al.*, 2019), and also indicates that the effects are translatable at least across teleost species. This damage may result in reduced enzyme activity such as oxygenases required for detoxification, potentially impairing the animal's ability to respond to future toxic exposures as well as exacerbating the impact of endocrine disruption on reproduction (Jackson *et al.*, 2019).

The fact that the fluorescence signals are only visible in ERE:GFP after treatment with exogenous oestrogens suggest either that endogenous oestrogen levels are too low to induce GFP expression, or that the ligands are not expressed in these tissues during early development, despite the expression of the receptors (Bondesson *et al.*, 2015). Either way, the ERE:GFP model confirms the presence of ERs at this early life stage and hence that the larva is vulnerable to the effects of environmental oestrogens at this age

#### *3.4.4.2 Oxidative stress*

The detection of APAP- induced OS in the liver and pronephros is in line with data previously reported on the EpRE:mCherry model (Mourabit *et al.*, 2019).

This is also in keeping with what is known about the role of OS in APAP toxicity, reviewed in (Wang et al., 2017). APAP is metabolised via CYP450 enzymes to produce the toxic intermediate N-acetyl-p-benzoquinone imine (NAPQI), which is conjugated by the antioxidant GSH. When cellular stores of GSH are depleted, such as by APAP overdose, NAPQI can go on to react with other proteins, resulting in OS (Wang et al., 2017). OS can cause tissue damage via damage to lipids, proteins and DNA, ultimately leading to cell death via apoptosis or necrosis (Wang et al., 2017).

OS can cause liver damage specifically via lipid peroxidation (Wendel et al., 1982). Hepatotoxicity is a well-documented consequence of APAP overdose in humans, and is the leading cause of drug induced liver injury in the US (Rotundo & Pyrsopoulos, 2020; Yoon et al., 2016). Liver toxicity has also been reported in other fish species after chronic (Choi et al., 2018) and subchronic APAP exposure (Guiloski *et al.*, 2017). The findings of the present study may also be translatable to human health as, although the structure of the zebrafish liver is different to that of a mammalian liver, the main physiological processes are well conserved, such as the role of hepatocytes in CYP P450 metabolism (Vliegenthart et al., 2014). Indeed, the zebrafish is a popular model for studying drug-induced liver injury in clinical applications.

Lipid peroxidation as a result of OS is also implicated in nephrotoxicity (Abdul Hamid *et al.*, 2012; Canayakin *et al.*, 2016) and the data from the confocal microscopy images here can be used to better our understanding of the mechanism by delineating the tissue-specific fluorescence of the EpRE:mCherry model. The glomerulus appeared to have a higher background level of OS, indicated by the stronger fluorescent signal localised in the glomerulus of chemically treated and untreated larvae compared to the PCT (Figs. 3.11 and 3.12). APAP has previously been reported to cause ultrastructural damage in the glomerulus of rats treated with an APAP overdose (Dallak *et al.*, 2020) and prolonged APAP exposure (Ucheya & Igweh, 2010). However, the localisation of the mCherry fluorescence in the glomerulus is more likely to be related to its dense structure (discussed in section 3.4.3) rather than its vulnerability to APAP toxicity as there is stronger evidence in the literature for OS induction in the PCT. Indeed, the PCT showed a greater relative increase in OS detected than the glomerulus when larvae were treated with APAP (compared to the control) (Fig.

3.12) (albeit the small sample size used here precludes a firm conclusion). This is in line with what is known about the distinct functions of the different compartments of the pronephros: blood filtration occurs in the glomerulus while the PCT is responsible for recovering important molecules such as salt, sugars and small proteins, making it vulnerable to toxic insults (Drummond & Davidson, 2010; Sander *et al.*, 2015). The PCT also contains a particularly dense concentration of mitochondria and hence has high rates of oxygen consumption, in addition to relatively low levels of endogenous antioxidants compared with the glomerulus, making it particularly vulnerable to oxidative damage (Chevalier, 2016). The PCT has also been identified as the primary target of injury in kidney damage or disease in humans, and damage to the PCT is considered to be the major link between acute kidney injury and chronic kidney disease (Chevalier, 2016). Further, nephrotoxicity in patients caused by APAP overdose is typically mediated via damage to the PT, where toxic conjugates have been found to result in tubular epithelial cell necrosis in proximal and distal parts of the tubules (Mazer & Perrone, 2008).

## 3.5 Conclusions

In this chapter I optimised the methods and parameters for image acquisition using the Acquifer and image analysis using Fiji in a way that would allow consistent, rapid and reliable data acquisition for the following chapters. The Acquifer was able to capture the fluorescent signal of two fluorophores (GFP and mCherry) reliably and rapidly across a range of tissues. However, it could not detect a fluorescent signal in the ERE:GFP or EpRE:mCherry models at drug concentrations as low as previously reported using other imaging platforms, although in the case of the ERE:GFP model, this could be a result of gene silencing in later generations rather than a limitation of the imaging platform. I have shown that the Acquifer can be used to repeatedly image the same larva to track the development of a fluorescent response over a number of days (at least up to 5 dpf) but is not suitable for continuous long term culturing/imaging of larvae as the exposure media cannot be refreshed. Additionally, although the Acquifer could be used to identify more difficult to discern organs such as the neuromasts, it could not capture the more subtle changes in fluorescence (in contrast to the confocal, which could). However, the time-consuming embedding process required for confocal microscopy and its lack of auto-focus or automated imaging

drastically limit its throughput compared to the Acquifer (Table 3.1). Future studies could therefore refine their experiments by using the Acquifer to screen a high number of samples to select exposure compounds/samples for more detailed imaging on the confocal

The images in Figs. 3.11 and 3.12 also suggest that the Acquifer cannot be used to delineate fluorescent signal derived from the glomerulus and PCT in a 4 dpf larva, unlike confocal microscopy. Therefore, if information was needed on glomerulus or PCT specifically, the Acquifer may not be suitable. However, the Acquifer can still be used to assess tissue-specific OS, including in the pronephros, as the PT-yellow stain and confocal images confirmed the that the signal observed in Acquifer images came from the proximal region of the PT. Additionally, based on the literature, kidney damage most often involves both the PCT and glomerulus. Indeed, APAP exposure in zebrafish has been linked to both malformed PCTs and glomerulus (Peng *et al.*, 2010).

As expected, the Acquifer cannot achieve the same level of sensitivity or resolution as confocal microscopy, but for the purpose of this thesis (i.e., the assessment of how multiple different conditions and compounds affect OS), this deficit is negligible and easily made up for by the higher throughput of the Acquifer.

# Chapter 4- Characterisation of the TG EpRE:mCherry model

## 4.1 Introduction

OS occurs when reactive oxygen species (ROS) generation exceeds antioxidant capacity leading to oxidative damage such as lipid peroxidation and DNA damage (see General Introduction, section 1.4.3.1 for more detail). OS is a major mechanism by which many compounds, including pharmaceuticals, exert toxic effects as free radicals can be produced as a result of phase I metabolism (Liska, 1998). Traditional methods for quantifying OS include immunologic techniques to measure products of lipid peroxidation such as malonic dialdehyde (MDA) however, this method is quite non-specific (Lushchak, 2016). Other common biomarkers include levels of oxidatively modified proteins, which can be a more meaningful indicator than oxidised lipids as the proteins have specific roles and so their levels of oxidation can reveal perturbation of function. Additionally, the end products of protein oxidation are fairly stable (Lushchak, 2016). Another biomarker of OS frequently used in ecotoxicology studies is the activity of key antioxidant enzymes such as CAT, SOD, GPx, and the ratio of GSH:GSSG which can be monitored using enzyme activity assays (Birnie-Gauvin *et al.*, 2017) (see Table 1.1 in General Introduction for a full summary). As discussed in the General Introduction, many of these techniques are labour intensive and/or result in sample destruction. These biomarkers also cannot provide real-time, *in vivo* visualisation of the OS response across a range of tissues and so provide a narrow view of the response both temporally and spatially, unlike the fluorescence response of a TG model.

The TG(EpRE:mCherry) model, briefly introduced in Chapter 3, indicates OS through the induction of red fluorescence via upregulation of the element EpRE. The EpRE is upregulated via the Nrf2/Keap1 complex as a result of excess ROS generation (Fig. 4.1). Under normal conditions, Keap1 binds to Nrf2 in the cytoplasm, targeting it for ubiquitylation, which results in its degradation and so keeps cellular levels of Nrf2 low. Under OS, inducers alter the structure of this complex, resulting in the dissociation of Keap1 and allowing Nrf2 to accumulate and translocate to the nucleus. Here, Nrf2 can activate the EpRE (also known as

antioxidant response element; ARE) and thereby upregulate a suite of antioxidant genes (Lee & Hu, 2020).

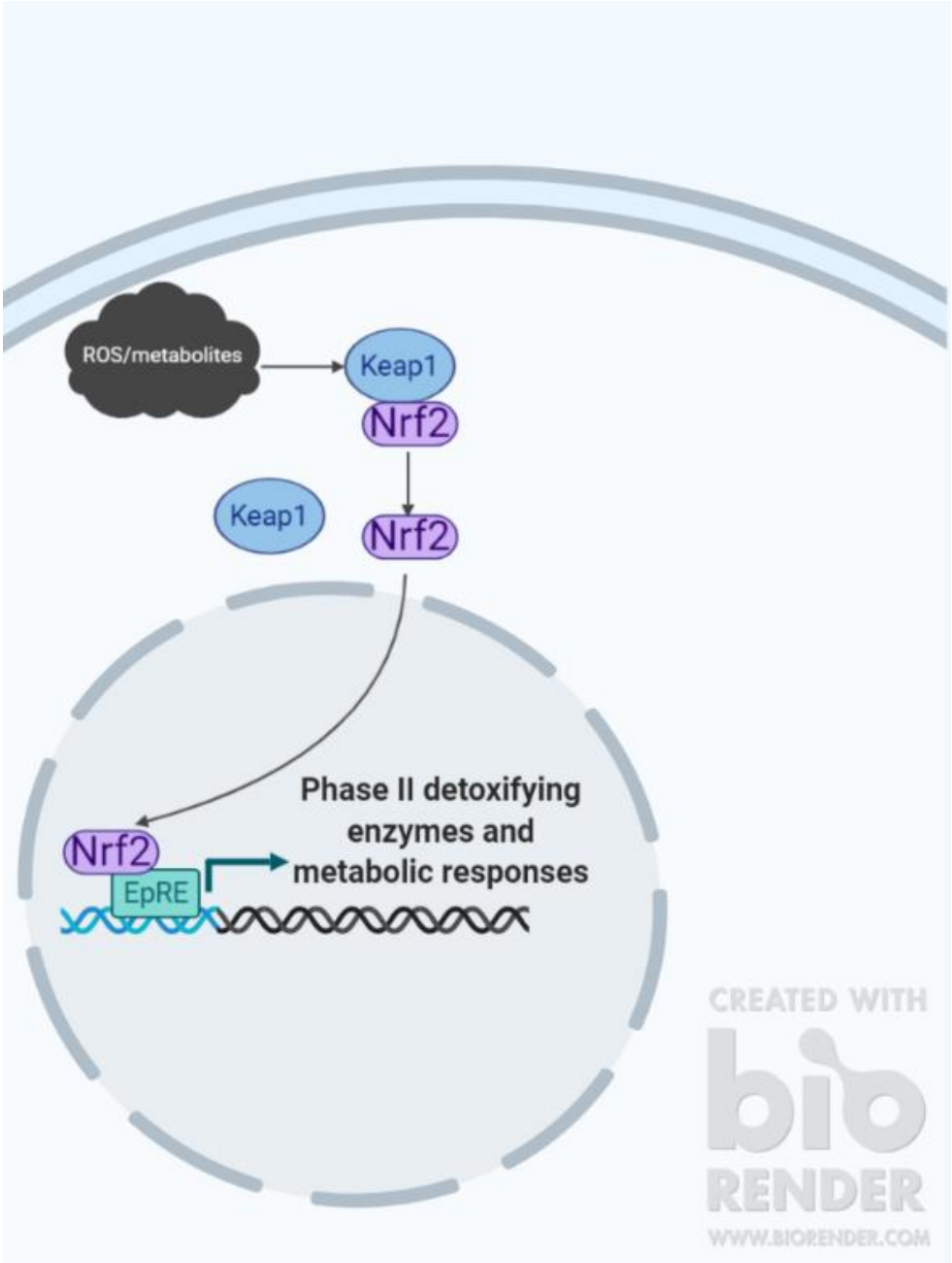


*Figure 4.1* ***Schematic of how an excess of ROS can activate Nrf2*** *so it can translocate to the nucleus and bind to the EpRE, consequently upregulating the expression of phase II enzymes and other metabolic responses as part of the antioxidant defence system*

Chapter 3 showed the development of the Acquifer method for the assessment of responses in this TG zebrafish larvae. The EpRE:mCherry model has previously been assessed using confocal microscopy in response to a limited range of chemicals (including only two pharmaceuticals) but has not been assessed as a tool for HTS of pharmaceuticals for potential oxidative action. In

this chapter, the application of the EpRE:mCherry model for screening pharmaceuticals for their capacity to induce oxidative action was evaluated. To achieve this, the study was guided by three main aims:

a. Acquire baseline data for the oxidative response quantified in the EpRE:mCherry model, and assess the consistency of the response across generations and experiments.
b. Assess the EpRE model for its application in screening environmental pharmaceuticals for oxidative responses and optimise methodology for its use in chemical effects assays.
c. Select relevant pharmaceuticals for further investigation for chemical mixture effects analyses.

Changes in fluorescence intensity in the EpRE:mCherry model were used to indicate pro-oxidative action for 9 pharmaceuticals. The pharmaceuticals included in the screen were chosen to represent a range of chemical classes with varying potencies. Selection was based primarily on evidence found in the literature for their capacity to affect cellular redox state, and also on the prevalence of the drug in European surface waters (thus presenting a potential environmental concern). Table 4.1 shows a summary of the pharmaceuticals including their class, environmental concentration and other key data. The exposure ranges were selected to cover or exceed human therapeutic plasma concentrations (HTPC) whilst avoiding concentrations that are expected to induce overt toxicity, i.e. changes in the phenotype. This is for two reasons: a) changes in the phenotype such as malformations risk obscuring the fluorescent signal, resulting in imprecise measurements of tissue-specific OS; and b) to improve conformance to the 3Rs by avoiding more severe endpoints, thereby testing the EpRE:mCherry model's application as a sensitive biomarker of toxicity.

The whole embryo was assessed for fluorescence induction, but image analysis focussed on the liver, PD and PT. The pronephros and liver are the key sites for detoxification and drug metabolism in fish larvae (Sousa Borges et al., 2020) and so it follows that these tissues would be among the most responsive to drug-induced OS. These tissues were indeed shown to be convenient (easily located), rapid indicators of OS that consistently responded to APAP, the known pro-oxidant and reference compound (see Chapter 3). Focus was then widened to

identify any other organs responding to specific drugs, with particular attention paid to tissue types where previous studies had reported ROS production or other toxic effects (e.g., the neuromasts in response to Cis (Mourabit et al., 2019; Ou et al., 2007), or heart in response to doxorubicin (Cappetta *et al.*, 2017; Songbo *et al.*, 2019)).

To help interpret the chemical responses seen in the EpRE:mCherry model, the internal concentration of the exposure pharmaceuticals were measured using liquid chromatography mass spectrometry (LC-MS/MS). Analytical chemistry is often used in tandem with chemical effects analyses to understand how the compound partitions from the aquatic environment into the tissue of the animal, and how this relates to receptor responses or adverse outcomes. The measured internal drug concentrations were also compared with the fish steady state plasma concentration (FssPC) calculated using the fish plasma model (FPM) in order to provide helpful context to internal drug concentrations and aid in the interpretation of the data.

Further analytical chemistry techniques which are beginning to be applied in ecotoxicological studies include mass spectrometry imaging (MSI). MSI is an emerging tool for label-free imaging and quantification of drugs and their metabolites in tissue with excellent spatial and mass resolution. It has so far been primarily applied in drug discovery and development to identify drug accumulation in non-target organs, which could lead to toxicological effects. Also, it is used to ensure drug penetration of the target organ, which may not be accurately represented by plasma levels (Prideaux & Stoeckli, 2012). MSI is beginning to be used to elucidate the pharmacometabolome *in situ*, through its application to track and distinguish parent drugs from their metabolites through a tissue sample (Swales et al., 2019). The application of MSI to assess the environmental risks of pharmaceuticals is growing, but very much still in its infancy.

In this thesis work, desorption electrospray ionisation (DESI) was used to visualise the distribution of clozapine and its metabolites within the body of zebrafish larvae in an attempt to relate this to the response profile observed in the TG model. This series of experiments explored the potential of DESI (and MSI more generally) in supporting TG zebrafish larvae exposure assays.

*Table 4.1* ***Pharmaceuticals screened using the EpRE:mCherry model****, including evidence for their ability to alter the redox state of cells, environmental concentration, and concentrations tested. Human therapeutic blood plasma concentrations (Cmin and Cmax) are taken from* (Schulz et al., 2012)*, except for Cis which is taken from* (Charlier et al., 2004)*.*

| **Pharmaceutical** | **Class** | **Example evidence for affecting redox status** | **Environmental concentration (µM)** | **Human therapeutic blood plasma concentration (Cmin-Cmax) (µM)** | **Concentration range tested (µM)** |
|---|---|---|---|---|---|
| Paracetamol (APAP) | Analgesic | OS in liver and pronephros of zebrafish larvae (Mourabit *et al.* 2019)<br>OS in Hediste diversicolor (Nogueira and Nunes 2021)<br>OS in Hyalella azteca (Gómez-Oliván *et al.* 2012) | 430 nM (Roberts and Thomas 2006) | 66.16 – 165.39 | 1250 - 5000 |
| Atenolol (ATL) | Betablocker | N/A | Up to 0.2 nM in surface waters in Welsh river (Kasprzyk-Hordern *et al.* 2009) | 0.38 – 3.76 | 0.004 - 400 |
| Diclofenac (DCF) | Analgesic | OS in brain, liver, gill and blood of common carp (Islas-Flores *et al.* 2013.<br>Altered antioxidant enzyme activities in 96hpf zebrafish larvae (Bio and Nunes 2020)<br>OS in Galaxius maculatus (McRae *et al.* 2018)<br>OS in Dapnia magna (Gomez-Olivan *et al.* 2014)<br>OS in Hyalella Azteca (Oviedo-Gómez *et al.* 2010) | pM - low nM range (Lonappan *et al.* 2016) | 1.69 – 10.13 | 0.003 - 34 |
| Ibuprofen (IBF) | Analgesic | OS in common carp (Gutiérrez-Noya *et al.* 2020)<br>OS in Hyalella Azteca (Gómez-Oliván, Neri-Cruz, *et al.* 2014)<br>OS in Daphnia magna (Gómez-Oliván, Galar-Martínez, *et al.* 2014)<br>OS in common carp (Cyprinus carpio) (Islas-Flores *et al.* 2014) | Up to 0.06 µM in Spanish surface waters (Gutiérrez-Noya *et al.* 2020) | 72.71 – 145.43 | 0.005 - 50 |

| | | | | | |
|---|---|---|---|---|---|
| Doxorubicin (Dox) | Chemotherapeutic | ROS formation in cardiomyocytes (Raschi *et al.* 2010) | Predicted environmental concentration (PEC) in low pM range, but frequently below level of detection (Franquet-Griell *et al.* 2015) | 0.011 – 0.037 | 0.0018 - 1.8 |
| Cisplatin (Cis) | Chemotherapeutic | OS in neuromasts and pronephros of zebrafish larvae (Mourabit *et al.* 2019) | Low pM range in European surface waters (Queirós *et al.* 2021) | 3.32 – 16.61 | 0.03 - 33.2 |
| Cyclophosphamide (CP) | Chemotherapeutic | Upregulation of antioxidants in zebrafish larvae (Aderemi *et al.* 2020)<br>Inhibited antioxidant enzymes and DNA damage in Nereis diversicolor (Fonseca at al. 2018) | pM - nM range (Fonseca *et al.* 2018) | 38.30 – 95.75 | 0.0004 - 383 |
| Clozapine (Cloz) | Atypical antipsychotic | Anti-oxidative action by blocking ERK phosphorylation in vitro (Magliaro and Saldanha 2009)<br>Increased GSH and reduced lipid peroxidation in patients (Hendouei *et al.* 2018)<br>ROS formation in zebrafish larvae (Zhang *et al.* 2021) | Up to 3.24 µM in treated effluent (Escudero *et al.* 2021) | 1.07 – 1.84 | 0.003 - 30.6 |
| Clarithromycin (CAM) | Macrolide antibiotic | Anti-oxidative action by protecting ROS balance of human epithelial cells in vitro (Iwayama *et al.* 2017 and 2018).<br>Increased ROS levels in microalgae (Guo *et al.* 2020)<br>Increase ROS levels in zebrafish ovaries (Qiu *et al.* 2020) | Up to 0.7 nM in WWTP effluent (Baumann *et al.* 2015) | 0.28 – 2.67 | 5 - 400 |

APAP was first tested on the EpRE:mCherry model to characterise the response of the model to a known/reference pro-oxidant and optimise the exposure protocol. APAP, therefore, was used as a positive control against which other pharmaceuticals were compared. To achieve this, a time- and concentration-dependent response profile for APAP was built to understand the ontogeny of the OS response and relate this to the onset of a general indicator of overt toxicity: pericardial oedema.

Atenolol (ATL) was used as a negative control to confirm that the EpRE:mCherry model does not respond indiscriminately to chemical exposure. ATL is a beta-blocker used to treat heart disease and high blood pressure frequently detected in surface waters, reaching 0.2 nM in a Welsh river upstream of WWTP effluent (Kasprzyk-Hordern et al., 2009). However, ATL is perceived as a low risk in the environment, resulting in limited ecotoxicity data, having a PEC/PNEC risk quotient of 0.003 for *Daphnia magna* (Küster *et al.*, 2010). Additionally, there is limited evidence of ATL-induced OS in fish. GST, SOD and CAT in adult zebrafish showed reduced activity in response to 3.8 µM ATL and its photolysis by-products (Diniz *et al.*, 2015) but, beyond this, the data available does not imply OS. Exposure of fathead minnows up to 38 µM resulted in no changes in viability, hatching or growth (Winter *et al.*, 2008). A zebrafish embryo exposure from 0-4 dpf also showed concentrations up to 10mM had no effect on survival, phenotype or swimming behaviour (Bittner et al., 2018).

Diclofenac (DCF) has been shown to cause an increase in various OS biomarkers in response in zebrafish (Bio & Nunes, 2020), other teleost species such as common galaxius (*Galaxius maculatus)* (McRae et al., 2018) and Eurasian carp (*Cyprinus carpio)* (Islas-Flores *et al.*, 2013), and invertebrates including *Hyalella Azteca* (Oviedo-Gómez et al., 2010) and *Daphnia magna* (Oliveira et al., 2015). However, a juvenile growth test using zebrafish found that DCF reported no effect on OS biomarkers, although only levels of glutathione S-transferase or glutathione reductase (GR) were measured (Praskova *et al.*, 2014).

There is evidence in the literature for the pro-oxidant action of ibuprofen (IBF), and it has also been reported as a hsp70 (heat shock protein) inducer (Gravel & Vijayan, 2007). IBF has been reported to induce OS in a range of taxonomic levels, from *Hyalella Azteca* (Gómez-Oliván et al., 2014b) and *Daphnia magna*

(Gómez-Oliván et al., 2014a), to common carp (*Cyprinus carpio*) (Islas-Flores *et al.*, 2014).

The anthracycline doxorubicin (Dox), a chemotherapeutic drug, induces ROS generation in cardiomyocytes (Cappetta *et al.*, 2017; Songbo *et al.*, 2019). Dox is frequently below the level of detection in waterways but is predicted to be present in the environment based on prescription rates, drug metabolism and wastewater elimination rates (Franquet-Griell et al., 2015).

Cis can induce OS in the pronephros and neuromasts (Mourabit *et al.*, 2019; Ou *et al.*, 2007) and is detected in surface waters in the pM range (Queirós *et al.*, 2021). In Chapter 3, section 3.3.3, Cis was shown to cause damage to the neuromasts, impairing their ability to express mCherry fluorescence. Therefore, the toxicity of this drug made it more challenging to test on the TG model and it was investigated in more detail.

The macrolide antibiotic clarithromycin (CAM) was included in the screen because it can increase ROS levels in microalgae (Guo et al., 2020) and zebrafish ovaries (Qiu *et al.*, 2020). However, there is also evidence that low levels of CAM can have a protective effect on cellular ROS balance (Iwayama *et al.*, 2018), by inhibiting hydrogen peroxide-induced depletion of cellular GSH (Iwayama *et al.*, 2017). To date, this has been shown in studies using human epithelial cells (Iwayama et al., 2017, 2018), and in rats (Özdemir et al., 2010). Conversely, CAM has been shown to affect the heart rate of zebrafish embryos without influencing antioxidant activities or MDA levels (Yan *et al.*, 2019). Therefore, CAM was screened using the EpRE:mCherry model to assess if the TG model could be used to better characterise the response profile (i.e., at what concentrations it may have a protective or antagonistic effect on the EpRE). CAM also presents an environmental concern because it is frequently detected in surface waters as the unchanged parent compound and its metabolites. It is not effectively removed from sewage by traditional treatment methods (Baumann *et al.*, 2015) and is highly persistent and resistant to photo- or bio-degradation, hence CAM has been detected in rivers in concentrations in the nM range (Guo et al., 2020).

The prodrugs cyclophosphamide (CP) and clozapine (Cloz) were also screened. CP is one of the oldest and most frequently prescribed cytotoxic anti-cancer drugs

and enters waterways both via domestic and hospital sewage, but its elimination at WWTPs is incomplete and therefore is detected in surface waters around the world in the pM - nM range (Fonseca *et al.*, 2018). CP has previously been reported as affecting the oxidative status of several species (Aderemi et al., 2020; Fonseca et al., 2018). Cloz is an atypical antipsychotic, and its metabolites have been linked to ROS generation (Thorn et al., 2018; Vredenburg et al., 2013). It has been detected in levels up to 3.24 µM in treated WWTP effluent (Escudero *et al.*, 2021) and 94 nM Cloz has been shown to significantly impact survival of fathead minnow larvae (Overturf *et al.*, 2012) but, little is known about the mechanism by which Cloz can be toxic to aquatic wildlife.

Cloz and CP are pro-drugs and thus require bioactivation to have a therapeutic effect (Griskevicius et al., 2003; Pereira & Dean, 2006; Pirmohamed et al., 1995). However, bioactivation of pharmaceuticals requires CYP P450 metabolism, and zebrafish larvae do not express the full complement of CYP genes until the end of organogenesis, or 5dpf (Fig. 4.2) (Goldstone *et al.*, 2010; Verbueken *et al.*, 2018). Additionally, there is conflicting evidence in the literature on the metabolic capacity of zebrafish embryo-larvae and different CYP transcripts have been shown to peak at different points throughout larval development (Fig 4.2) (Verbueken *et al.*, 2018). While most genes in CYP families 5 – 51 in zebrafish are direct orthologs of human CYPs, those involved in xenobiotic metabolism (families 1 – 3) are more diverse and show less conservation of sequence between zebrafish and humans (particularly in CYP 2) (Goldstone *et al.*, 2010). Despite this, there are functional similarities in metabolism between zebrafish and humans and zebrafish are an increasingly popular model for assessing xenobiotic metabolism and drug discovery (de Souza Anselmo et al., 2018). Hence, mammalian data on the metabolism of Cloz and CP may not be directly translatable to zebrafish larvae, but may be used to infer potential mechanisms behind effects seen in the TG model. To investigate the effect of bioactivation and its effect on the outcome of a drug screen, EpRE:mCherry larvae were exposed to either the synthesised metabolite (in the case of Cloz) or the parent compound as older larvae (8-10 dpf) (in the case of CP), when they are known to have fully developed CYP capacity.

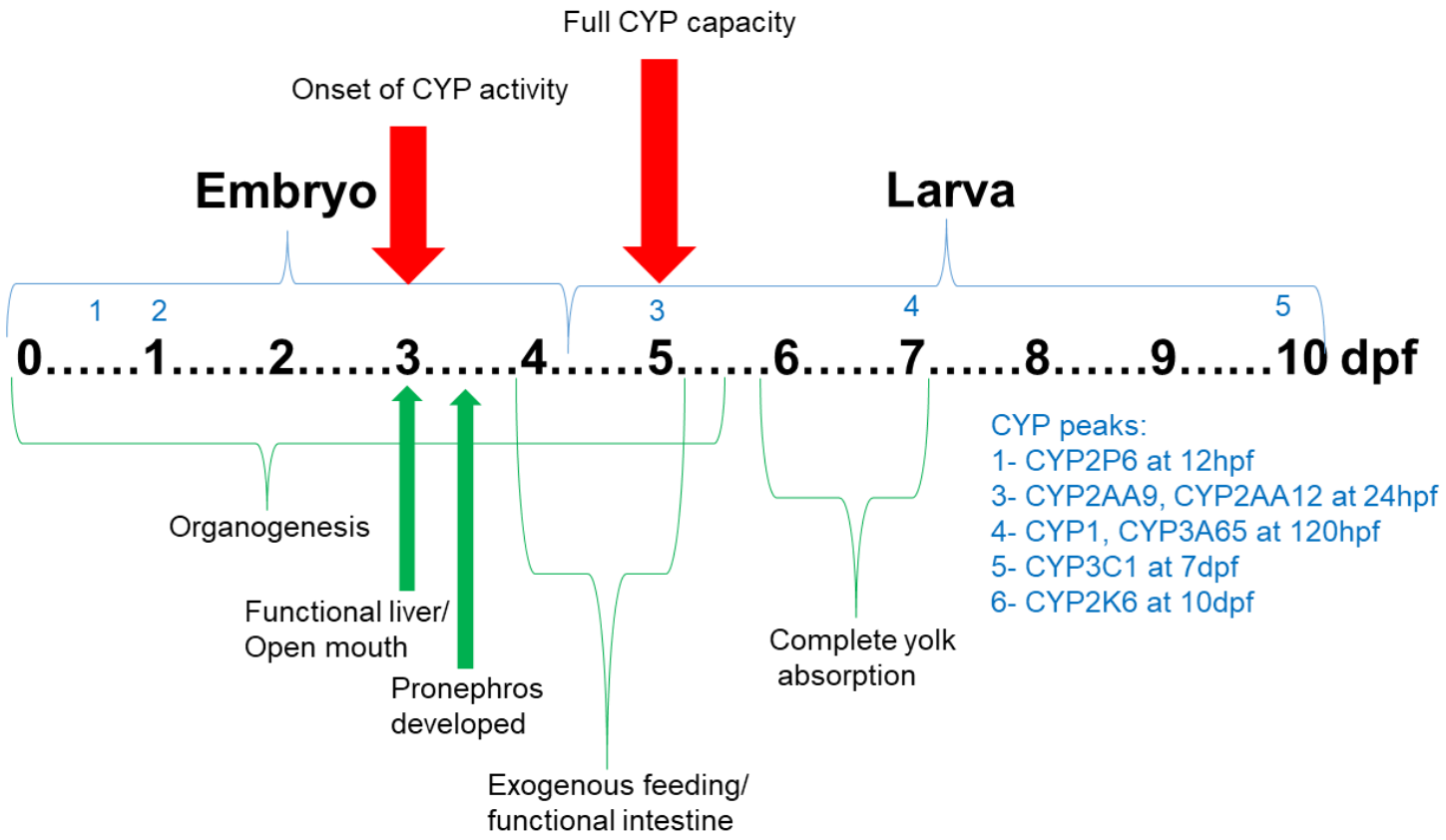


*Figure 4.2* ***Timeline of zebrafish development and CYP capacity****. Blue numbers indicate the time of peaks for select CYP transcripts involved in drug and contaminant metabolism, demonstrating the expression of different CYPs peak at different points throughout embryo-larval development. The liver and intestine are the main sites of CYP-mediated drug metabolism, and so zebrafish reach the full complement of CYPs in time for exogenous feeding, by which time the liver and intestine are functional. Adapted from Verbueken et al. 2018 and Goldstone et al. 2010.*

Finally, the internal concentration of the reference pro-oxidant, APAP, was measured over time following depuration and correlated to tissue-specific mCherry fluorescence to understand how the degradation of the fluorescence response is related to drug excretion. This is a variable not often reported in the development of TG models; to my knowledge, no previous study has directly linked the degradation of a fluorophore with the decreasing internal concentration of a toxicant. An understanding of the relationship between the up/down-regulation of the fluorophore and the internal toxicant concentration can allow the model to be used to elucidate more dynamic responses, such as those investigated in upcoming chapters.

This chapter set out to better our understanding of the EpRE:mCherry as a pharmaceutical screening tool and elucidate the dynamics of the OS responses to the selected drugs.

I hypothesised that the seven pharmaceuticals listed above could induce detectable OS in the EpRE:mCherry model.This was tested by exposing EpRE:mCherry larvae to a range of pharmaceuticals from 0-4 dpf and measuring the tissue-specific mCherry fluorescence. When two of the drugs tested, cyclophosphamide and clozapine, did not induce significant OS in the model, I hypothesised that this was due to lack of metabolic activation in the larvae at this early life stage, presenting a potential limitation of the model. Therefore, this was tested by exposing the larvae to either the synthesised metabolite (desmethyl clozapine) or by exposing the larvae to the parent drug (cyclophosphamide) at a later life stage (8-10 dpf) and comparing the OS induction with the standard exposure protocol. Analytical chemistry techniques (DESI, LC-MS/MS) were also applied in this work to quantify internal drug concentrations and/or distributions in order to compare them with the biological responses seen.

Data derived from this chapter were used to select pharmaceuticals for further study in chapter 6 where a range of pro-oxidants (identified in the present study) were tested for their interaction with a physical stressor in the EpRE mCherry model.

## 4.2 Methods

### 4.2.1 Fish husbandry

All imaging/OS measurements were conducted using EpRE:mCherry zebrafish. The supply of EpRE:mCherry zebrafish was limited and WIK embryos were therefore used for all LC-MS/MS and DESI methods to assess uptake of the drug. Both strains of zebrafish were maintained under the same conditions (see Chapter 2, section 2.1).

An important consideration in the application of TG zebrafish models is consistency of the fluorescence response and sensitivity of the model for different batches of embryos and across different generations. This is particularly true for work using fish over multiple years, as was the case for this thesis work.

Therefore, as a stock of EpRE:mCherry zebrafish adults aged beyond their optimum for breeding and the next generation was generated, embryos from the old and new generation were compared for their background levels of OS and chemically-induced levels of mCherry fluorescence. Additionally, control groups from different experiments were compared within generations to ensure larval responses exhibited consistent levels of baseline fluorescence between spawning events.

### 4.2.1 Embryo disinfection

Another potential issue in the application of the EpRE:mCherry model relates to how it responds to embryo bleaching/disinfection. Many laboratories employ the standard protocol of bleaching embryos using a disinfectant such as chloramine T at <6 hpf before an assay in order to disinfect the embryo surface, removing extra-ovum pathogens that may have been released during spawning (Alidadi Soleimani et al., 2017), including viruses and *Mycobacterium* sp. (Kent et al., 2014). However, observations made in early pilot studies had indicated that the mCherry fluorescence signal EpRE:mCherry model is easily influenced by early life conditions.

Therefore, to investigate if the chloramine T bleaching process induces an OS response which could disrupt the pharmaceutical exposure study analyses, embryos were bleached as per the standard protocol: 12 2 hpf embryos were washed in 10 g/L chloramine T for 1 minute with gentle agitation to ensure all embryo surface were covered. Embryos were then rinsed twice in CW for 1 min each and raised in clean system water until imaging at 4dpf.

Additionally, the embryos of each new generation of zebrafish were disinfected at 1 dpf using a sodium hypochlorite solution (as per the standard husbandry protocol used in the ARC; see Chapter 2, section 2.2 for details), so a transgenerational effect was also investigated. A parallel, unbleached line was raised simultaneously in a quarantined facility. When both lines reached maturity, their embryos were collected and exposed to a range of APAP concentrations to compare the background levels and drug-induced levels of OS between the two lines.

### 4.2.3 Chemical exposure

Pharmaceutical screens were performed according to the methods outlined in Chapter 2, section 4. Briefly, EpRE:mCherry embryos were exposed from 6 hpf

to the exposure solution made up in aquarium system water, 1 embryo per well of a 24-well plate in 1.2 ml exposure media. The following compounds were obtained from Sigma-Aldrich (Dorset, UK): paracetamol (CAS no. 103-90-2); diclofenac sodium (CAS no. 15307-79-6); ibuprofen (CAS no. 15687-27-1); doxorubicin hydrochloride (CAS no. 25316-40-9); cyclophosphamide (CAS no. 6055-19-2); clarithromycin (CAS no. 81103-11-9); Clozapine (CAS no. 5786-21-0); N-desmethylclozapine (CAS number 6104-71-8). Cis was purchased from Merck (Darmstadt, Germany) (CAS no. 15663-27-1) and ATL was obtained from AstraZeneca (Macclesfield, UK) (CAS no. 29122-68-7). For a flowchart of how the pharmaceutical screens and other experiments relate to one another, see Figs. 4.4 and 4.5.

For the comparison of the screening protocol used here with the protocol used by Mourabit *et al.* (2019), a selection of embryos was also exposed to Cis from 2 dpf. These embryos were kept in Petri dishes in 50 ml aquarium system water for 2 days, with 50 % water changes daily, before being transferred to 24-well plates for drug exposure.

To test the effect of a more developed metabolic capacity on the toxicity of CP, some larvae were exposed from 8 to 10 dpf, in accordance with UK Home Office regulations for the use of animals in scientific procedures. These embryo-larvae were kept in Petri dishes in 50 ml system water for 8 days, with 50 % water changes daily. From 5 dpf, larvae were fed zm-000 fry food (Zebrafish Management Ltd, Winchester, UK) in excess twice daily. On the day of exposure, larvae were transferred to a 24-well plate (1 larva per well in 1.2 ml exposure media). Larvae were not fed during the 2 day exposure period to avoid the absorption of CP by the food, potentially changing the exposure concentration and route of exposure (i.e. additional uptake via the chemical adsorbed to the food). After imaging, larvae were terminated using an overdose of anaesthetic (MS222) followed by destruction of the brain.

### 4.2.4 APAP depuration

Embryos were exposed to APAP from 6 hpf and manually dechorionated at 48 hpf. At 78 hpf (72 hours exposure), larvae were washed and transferred to fresh system water in clean 24-well plates and depurated for 24 hours. Wild Indian Karyotype zebrafish (WIKs) were used for the LC-MS/MS analysis of internal APAP concentrations, and samples were taken 1 hour pre-depuration,

immediately prior to depuration, and at 1, 2, 3, 4, 6, 10, 20 and 24 hours post depuration. EpRE:mCherry larvae were treated with the same dosing and depuration regimen but imaged using the Acquifer at 2 hours prior to depuration, and 1, 2, 4, 6, 20, and 24 hours post depuration. Different larvae were imaged for each timepoint, so larvae were not kept anaesthetised for an extended period. Fluorescence intensity values of APAP-treated larvae were normalised against control larvae (i.e., not exposed to APAP) to account for the increasing intensity of background fluorescence that can occur with advancing development.

To capture fluorescence changes over a longer period of time, embryos were exposed from 6 – 48 hpf to APAP and then underwent depuration for 48 hours. Larvae were manually dechorionated at 48 hpf and 54 hpf (2 days exposure), washed once in fresh system water and transferred to clean well plates in clean system water. These larvae were imaged using the Acquifer at 1, 24 and 48 hours post depuration. The same larvae were used for each time point: following image acquisition, they were recovered and transferred to fresh system water. Separately, WIK fish were treated with the same dosing/depuration regimen and sampled for LC-MS/MS analysis at the same time points as the EpRE:mCherry larvae were imaged.

### 4.2.5 LC-MS/MS

For details of LC-MS/MS methods used, see Chapter 2 section 2.8.

### 4.2.6 Image acquisition and analysis

All TG larvae image acquisition was performed using the Acquifer, other than experiments using larvae >5 dpf, which used confocal microscopy. For details on Acquifer methodology and image analysis, see Chapter 3, section 2. For details on confocal microscopy, see Chapter 2 section 9. Due to unavailability of the Acquifer, the initial CAM and CP screens were imaged using an Olympus SZX16 epifluorescent stereomicroscope (Tokyo, Japan) and an Andor Zyla sCMOS (UK) camera. Here, embryos were anaesthetised and mounted in agarose grooves as described in Chapter 3, section 2, and single z-slices were captured using a Nikon camera.

### 4.2.7 DESI-MSI

DESI methods are adapted from (Bäckström *et al.*, 2018). Embryo exposure and embedding was performed by me. Sectioning, imaging and data analysis were

performed by James Blades (undergraduate placement student working at AstraZeneca, Cambridge), supervised by Dr Gregory Hamm.

#### 4.2.7.1 Exposure

96 hpf WIK embryos were exposed to 100 µM (32.68 mg/L) Cloz for 20 minutes. They were then terminated in an overdose of tricaine and embedded in an HPMC-PVP 10 % micro block: the recommended embedding media for MSI. Embryos were embedded on either their right lateral side or ventral side and stored in -80°C.

#### 4.2.7.2 Sectioning

Larvae were sectioned (5 µm) using a CM3050 cryo-micro- tome (Leica Biosystems, Nussloch, Germany) and thaw- mounted onto Superfrost slides (Fisher Scientific, Loughborough, UK). Tissue section slides were stored at -80°C until analysis. After DESI analysis, samples were stained using hematoxylin and eosin (H&E) staining and visualized with ImageScope software (Aperio Tech.).

#### 4.2.7.3 DESI

MSI analysis was performed using desorption electrospray ionization (DESI) Q-Exactive (Thermo Fisher Scientific Inc., Bremen, Germany) mass spectrometer. Images were collected at spatial resolution of 30 µm in positive ion detection mode over a mass range of 80-900 Da and normalised using Root Mean Square. Molecular adduct ions for Cloz and its metabolites were profiled by accurate mass (Table 4.2).

*Table 4.2* ***Molecular adducts and their exact mass used by DESI to identify Cloz and its metabolites****.*

| **Compound** | **Adduct** | **Exact mass** |
|---|---|---|
| Clozapine | $[M+H]^+$ | 327.1371 |
| Desmethyl clozapine | $[M+K]^+$ | 351.077333 |
| Clozapine N-oxide | $[M+H]^+$ | 343.132015 |

#### 4.2.7.4 Data analysis

Data management, analysis, and visualization was performed using SCiLS Lab MVS 2018a software (SCiLS GmbH, Bremen, Germany). Different mass filters were selected based on the m/z of the Cloz and of known biomarkers to provide structural reference, such as haeme and phospholipids. These mass filters were applied to the image to visualise the distribution of the drug in context of the

animal's anatomy. Additionally, the images were segmented based on clustering of pixels with similar spectra. This allowed the distinction of tissue from background, and the distinction of certain regions within the tissue such as the brain. This facilitated the analysis of the mass spectra specific to those regions. Finally, the relative mean intensity of Cloz and its metabolites were assessed.

### 4.2.8 Fish plasma model (FPM)

The FPM is used to facilitate prioritisation of compounds for environmental risk assessment (ERA), using environmental drug concentrations and lipophilicity of the compound to predict the plasma concentration in fish in the environment. Based on the assumption that most drug targets are conserved across vertebrate phyla, the ratio of fish blood plasma drug concentration in the environment to human therapeutic plasma concentration (HTPC) can be used to predict the environmental risk of that drug (Huggett et al., 2003).The FPM, was used here to compare predicted drug FssPC in the body of exposed zebrafish larvae with human therapeutic plasma concentration (HTPC) (Fig. 4.3). This provided context to the concentration ranges used and allowed better understanding of the biological responses observed in the TG model. The FPM uses predicted partitioning values calculated using the equation from (Fitzsimmons et al., 2001) which describes the partitioning of a drug from the aqueous phase to the arterial blood in trout based on the lipophilicity of the drug:

$$\text{Log } P_{\text{Blood:Water}} = 0.73 \times \text{Log}K_{ow} - 0.88.$$

$\text{Log}D_{ow}$ was used here as a measure of lipophilicity instead of $\text{Log}K_{ow}$ as it accounts for ionisable compounds. Where $\text{Log}D_{ow}$ was not found in the literature, $\text{Log}K_{ow}$ used instead.

### 4.2.9 Statistical analysis

See Chapter 2 section 2.9.

Equations used

Predicted partitioning: $\text{Log } P_{\text{Blood:Water}} = 0.73 \times \text{Log } D_{ow}7.4 - 0.88$

- Fitzsimmons et al. 2001

FssPC = Effect concentration * ($P_{\text{Blood:Water}}$)

Effect ratio = HTC / FssPC

- Hugget et al. 2003

Worked example: APAP

Max. exposure concentration = 5000 µM

$\text{Log } D_{ow}7.4 = 0.4$

FPM predicted partitioning $= 10^{((0.73*0.4)-0.88)} = 0.258$

FssPC from FPM = 5000 * 0.258

Effect ratio from FPM (min HTPC) = 66.15 µM / 1291.13 µM

(max HTPC) = 165.384 µM / 1291.13 µM

*Figure 4.3 [Top]* ***Equations used to calculate predicted plasma concentration and effect ratio*** *[Bottom] Worked example using APAP. Exposure concentrations used are the maximum tested. Concentration of the drug in the exposure media at end of exposure period is unknown, so nominal exposure concentration is used instead. Predicted $LogD_{ow}$ values taken Chemspider.com [Accessed 10-11-21], generated using the ACD/Labs Percepta Platform – PhysChem module. A $LogD_{ow}$ value was not available for cisplatin, so $LogK_{ow}$ is used instead, taken from Dasari et al. 2014. HTPC for all drugs taken from Schulz et al. 2012, except cisplatin which is from Charlier et al. 2004.*

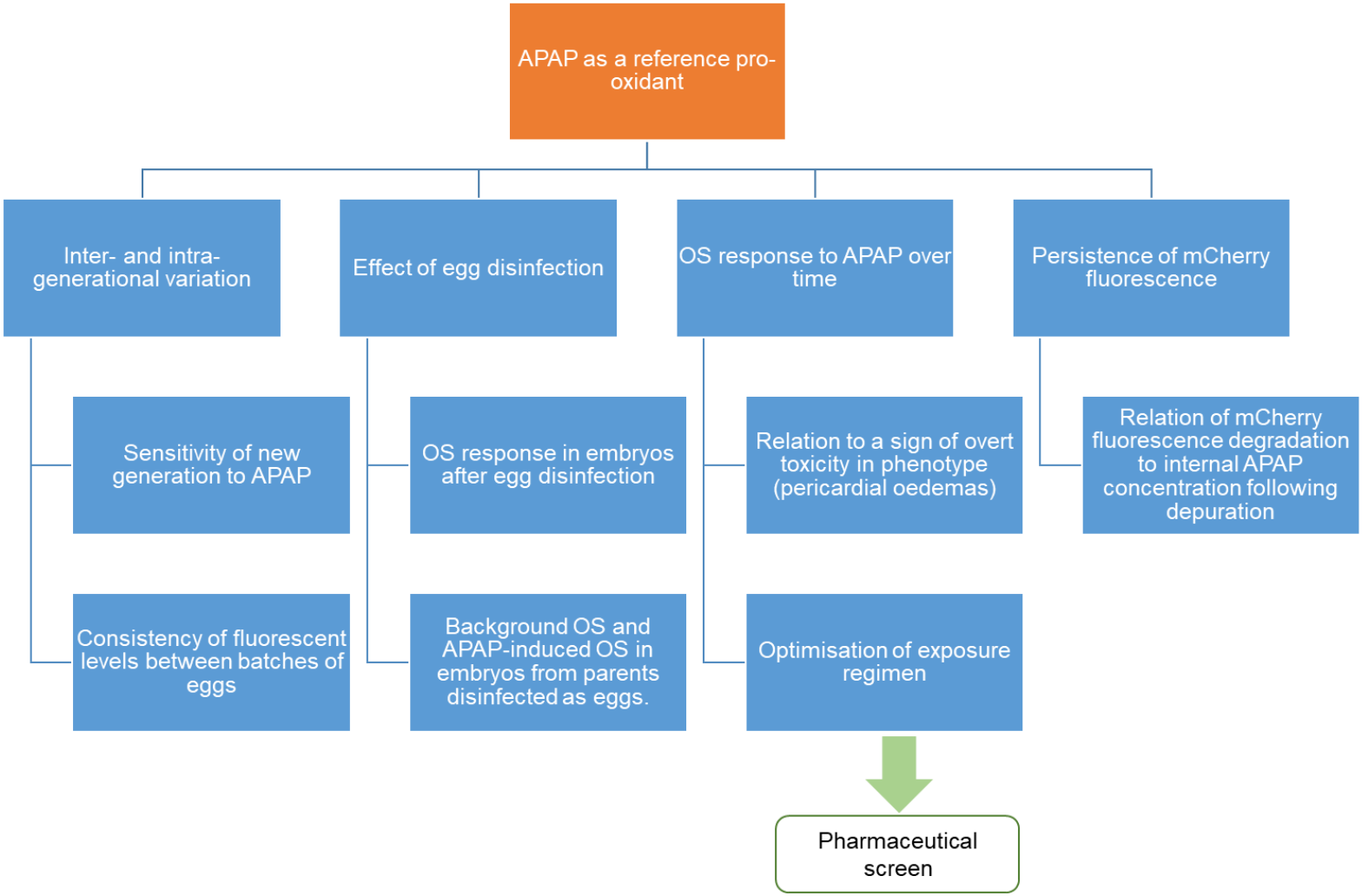


*Figure 4.4* ***Scheme showing the use of APAP as a reference pro-oxidant in the experiments performed in this chapter****. The optimisation of the exposure regimen went on to inform the pharmaceutical screen outlined in the next figure.*

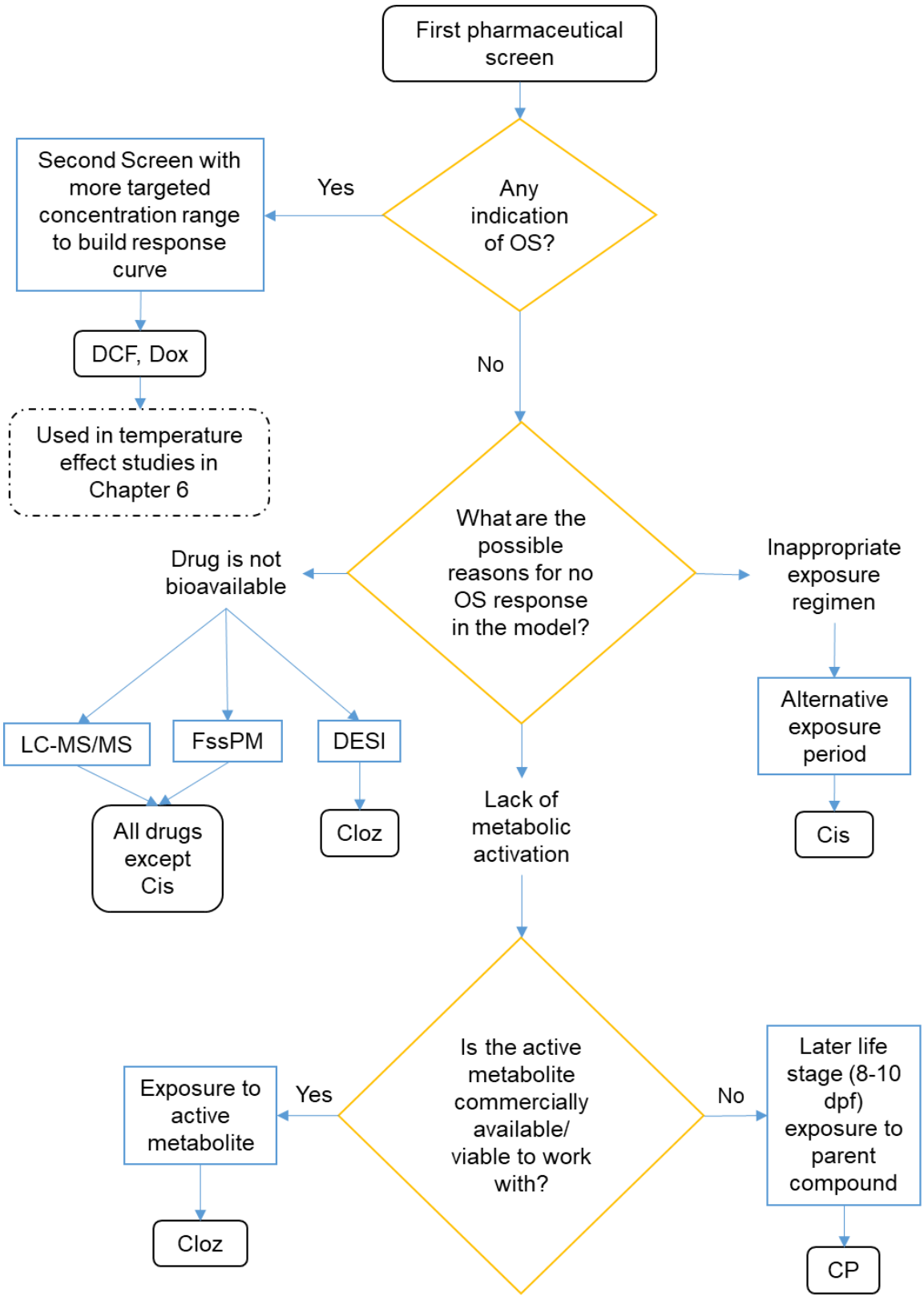


*Figure 4.5* ***Flowchart showing how the first pharmaceutical screen led to the selection of pharmaceuticals for further investigation in Chapter 6, and how the follow-up experiments relate to one another*** *to understand why the remaining drugs did not elicit the expected response in the EpRE:mCherry model.*

## 4.3 Results

### 4.3.1 Inter- and intra-generation variation

There was minimal inter-generation variation in background levels of OS or in APAP-induced OS for the generations used in this thesis work (F3, F4, F5 and F6). Fig. 4.6 shows an example of an assay to check for consistent sensitivity between the generations: the F4 generation showed the same level of sensitivity as the older F3 generation for OS induction in response to 2.5 mM APAP. Interestingly, larvae from the F4 generation showed greater levels of mCherry fluorescence in the liver than those from F3. F4 did not have significantly lower levels of OS under any treatment compared to the older, F3, generation, indicating no gene silencing occurred between the generations.

Some intra-generation variation was observed between control groups for the different spawning events/different experiments throughout the project (Figs. 4.7, 4.8 and 4.9). This is to be expected given the inherent variation of whole animal models and illustrates the importance of internal controls for each experiment against which relative changes in fluorescence expression can be compared. Variation in background mCherry fluorescence intensity among control individuals within each experiment was also fairly consistent within and between generations, ranging from approximately 20 – 40 % for each organ in most experiments, supporting the robustness and reliability of the model.

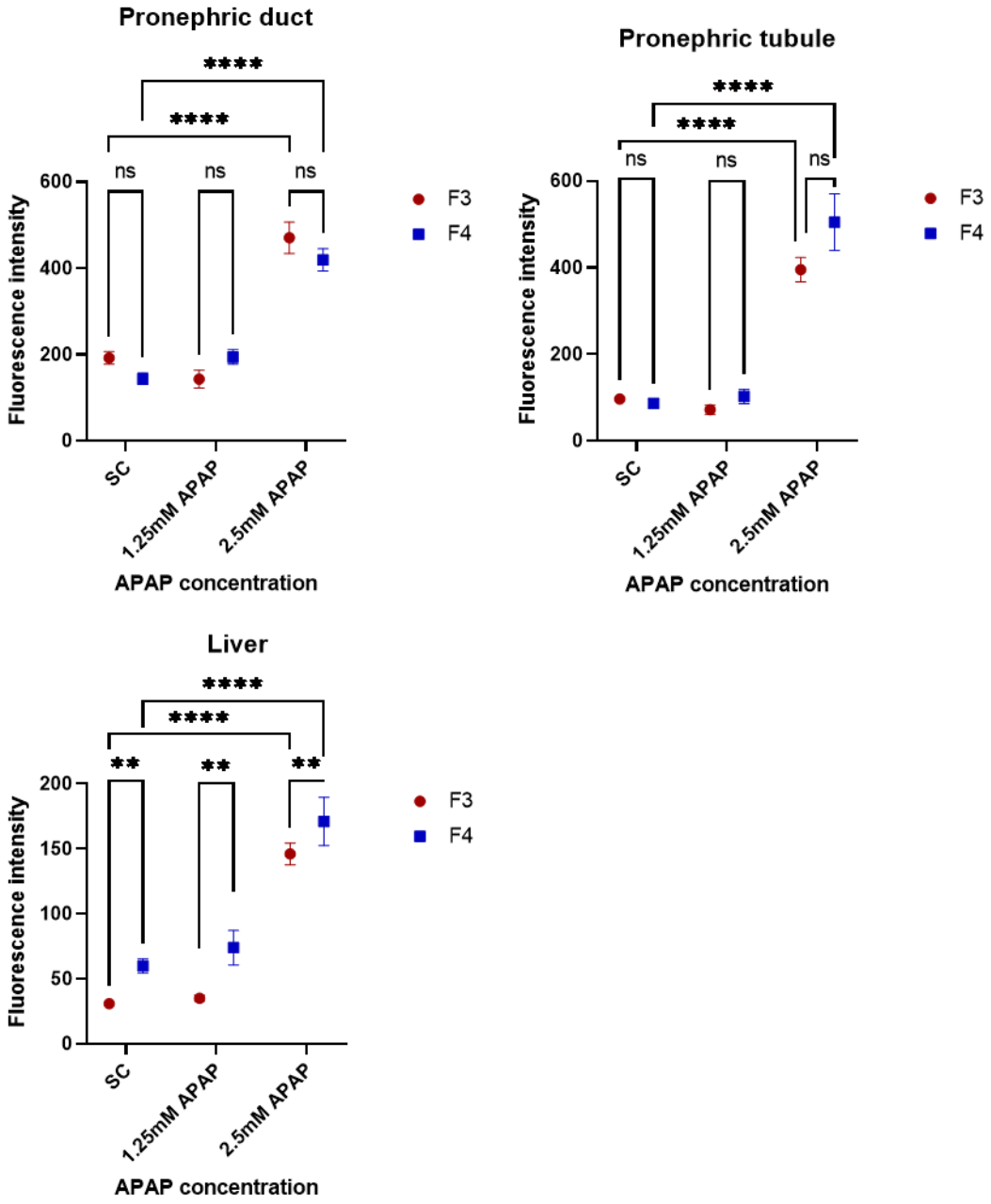


*Figure 4.6* ***Sensitivity and consistency of mCherry fluorescence response in EpRE:mCherry larvae across 2 generations, imaged using the Acquifer.*** *Embryos from F3 (red) and F4 (blue) were exposed from 6 hpf – 4 dpf to APAP and imaged using Acquifer. Data shows mean values (+/- SEM, N= 12) for the mean pixel intensity within the organ. Data were normally distributed so analysed using two-way ANOVA followed by Tukey's multiple comparison test.*

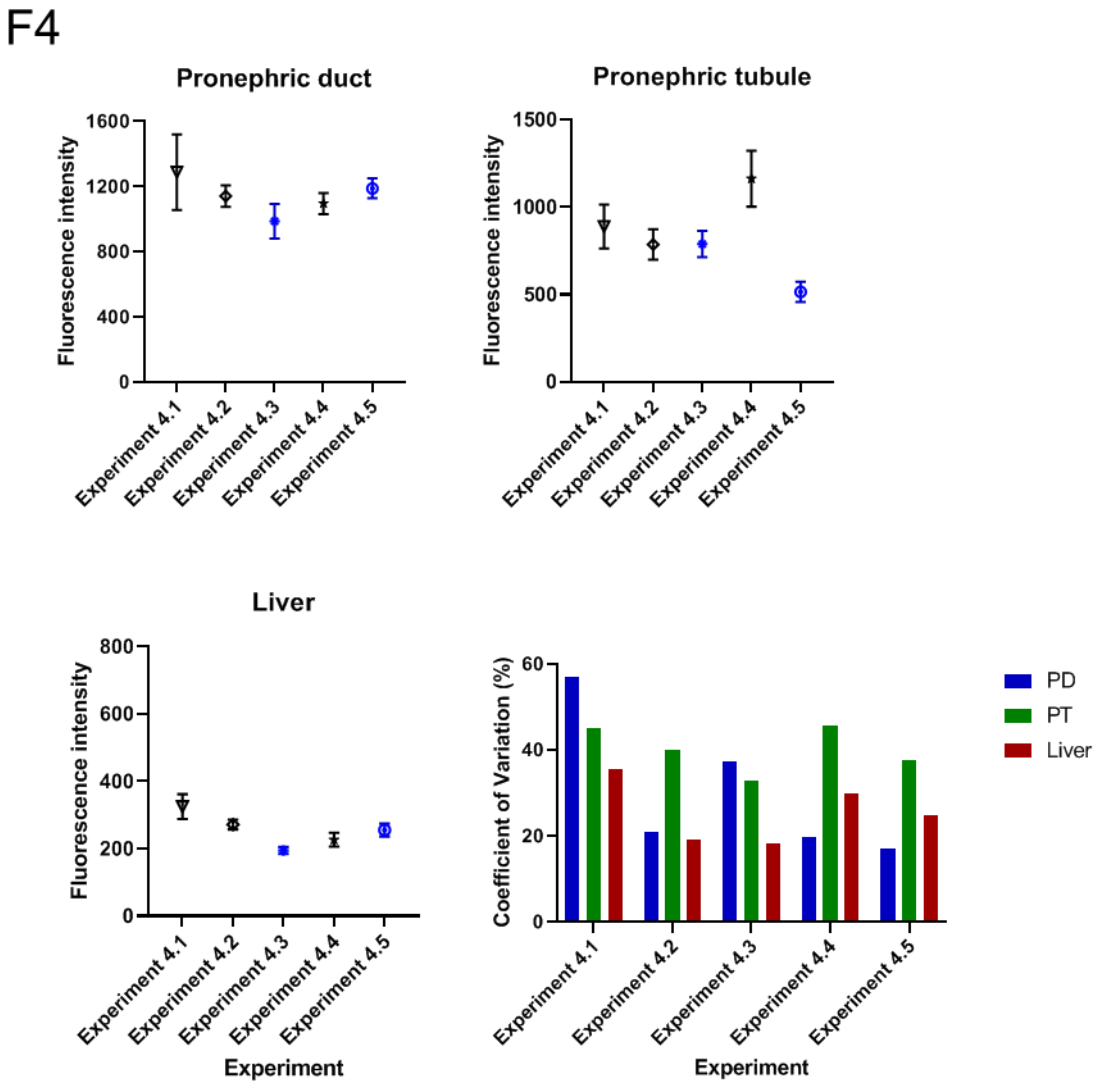


*Figure 4.7* ***Illustration of the relatively consistent response in control 4dpf larvae from the F4 generation, imaged using the Acquifer.*** *Data shows mean values (+/- SEM, N= 12) for the mean pixel intensity within the organ of 4 dpf larvae from a selection of experiments used in this thesis, taken from [blue] clean water controls, or [black] SCs. The bottom right panel shows the coefficient of variation, calculated as standard deviation/mean, illustrating relatively consistent variation in control embryos from this generation.*

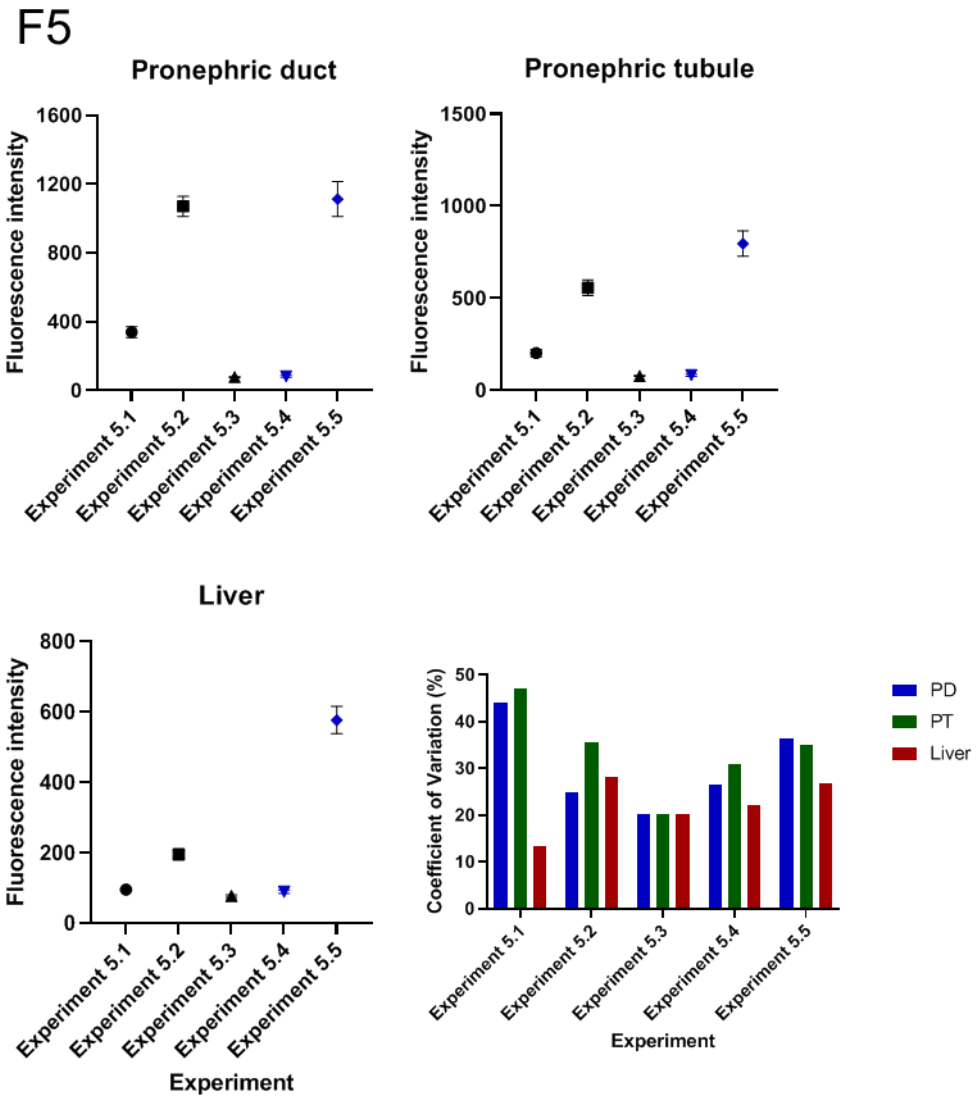


*Figure 4.8* ***Illustration of the relatively consistent response in control 4dpf larvae from the F5 generation, imaged using the Acquifer.*** *Data shows mean values (+/- SEM, N= 12) for the mean pixel intensity within the organ from a selection of experiments used in this thesis, taken from [blue] clean water controls, or [black] SCs. The bottom right panel shows the coefficient of variation, calculated as standard deviation/mean, illustrating relatively consistent variation in control embryos from this generation.*

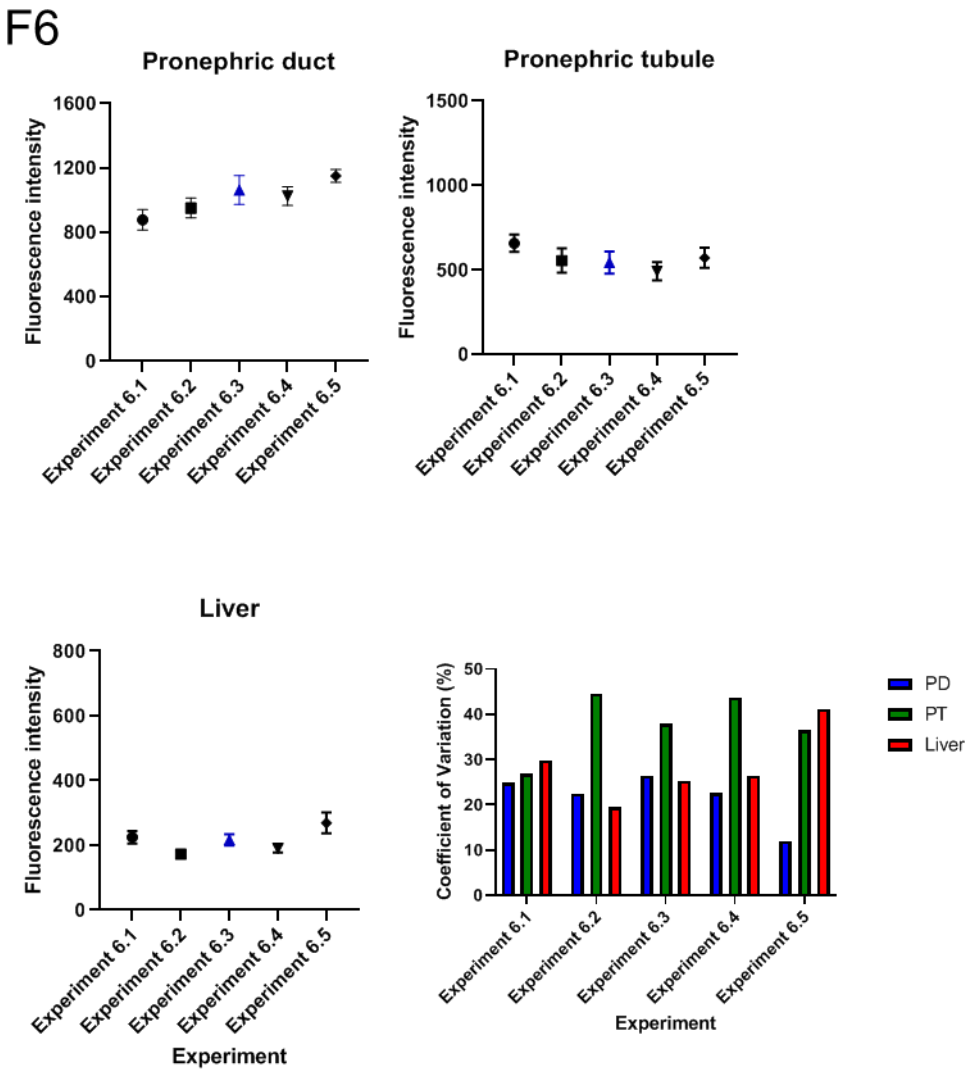


*Figure 4.9* ***Illustration of the relatively consistent response in control 4dpf larvae from the F6 generation, imaged using the Acquifer.*** *Data shows mean values (+/- SEM, N= 12) for the mean pixel intensity within the organ of 4 dpf larvae from a selection of experiments used in this thesis, taken from [blue] clean water controls, or [black] SCs. The bottom right panel shows the coefficient of variation, calculated as standard deviation/mean, illustrating relatively consistent variation in control embryos from this generation.*

### 4.3.2 Effect of embryo disinfection

As Fig. 4.10 shows, bleaching the EpRE:mCherry embryos using the popular disinfectant chloramine T resulted in a significant level of OS, despite the fact that embryos were rinsed thoroughly and raised in CW following the 1 minute bleach exposure. The fluorescent signal was particularly clear in the ionocytes and jaw, indicating that surfaces in direct contact with the media, namely the skin and inside of the mouth, were irritated. This could potentially link to the jaw malformations reported by Kant *et al.*, which were observed in 5 dpf zebrafish following longer exposure (up to 10 mins) to high concentrations of chlorine at 6hpf (Kent *et al.*, 2014). Interestingly, Kent *et al.* also found that different strains of zebrafish showed different levels of susceptibility to chlorine treatment (Kent *et al.*, 2014), so while this treatment was not appropriate for the EpRE:mCherry model, these results do not necessarily indicate the treatment will impact other lines of zebrafish.

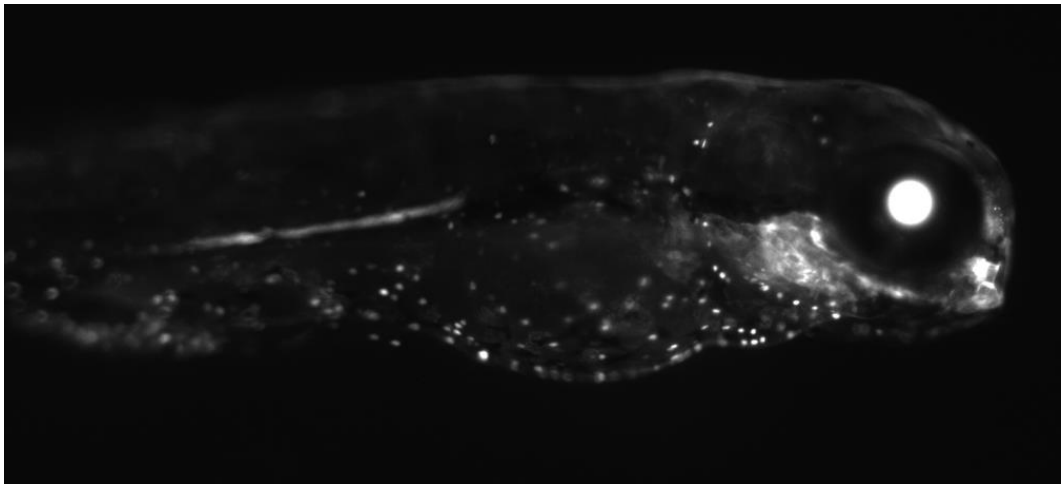

*Figure 4.10* ***4 dpf EpRE:mCherry larvae treated as an embryo using a short disinfection protocol.*** *Embryos were bleached using 10 g/L chloramine T for 1 minute at 2hpf and then rinsed twice and raised in clean system water until imaging at 4dpf. 6 out of the 12 embryos bleached also showed delayed hatching compared to unbleached embryos.*

Fig. 4.11 shows that there was no difference in OS response (background or drug-induced) between embryos taken from adults that were bleached as embryos versus those that were taken from the unbleached line, indicating that the sodium hypochlorite disinfection process did not have any transgenerational effects on the offspring. Consequently, the following experiments continued to use embryos taken from the bleached line due to the greater number of adults available in this brood stock, but embryos were not bleached prior to assays.

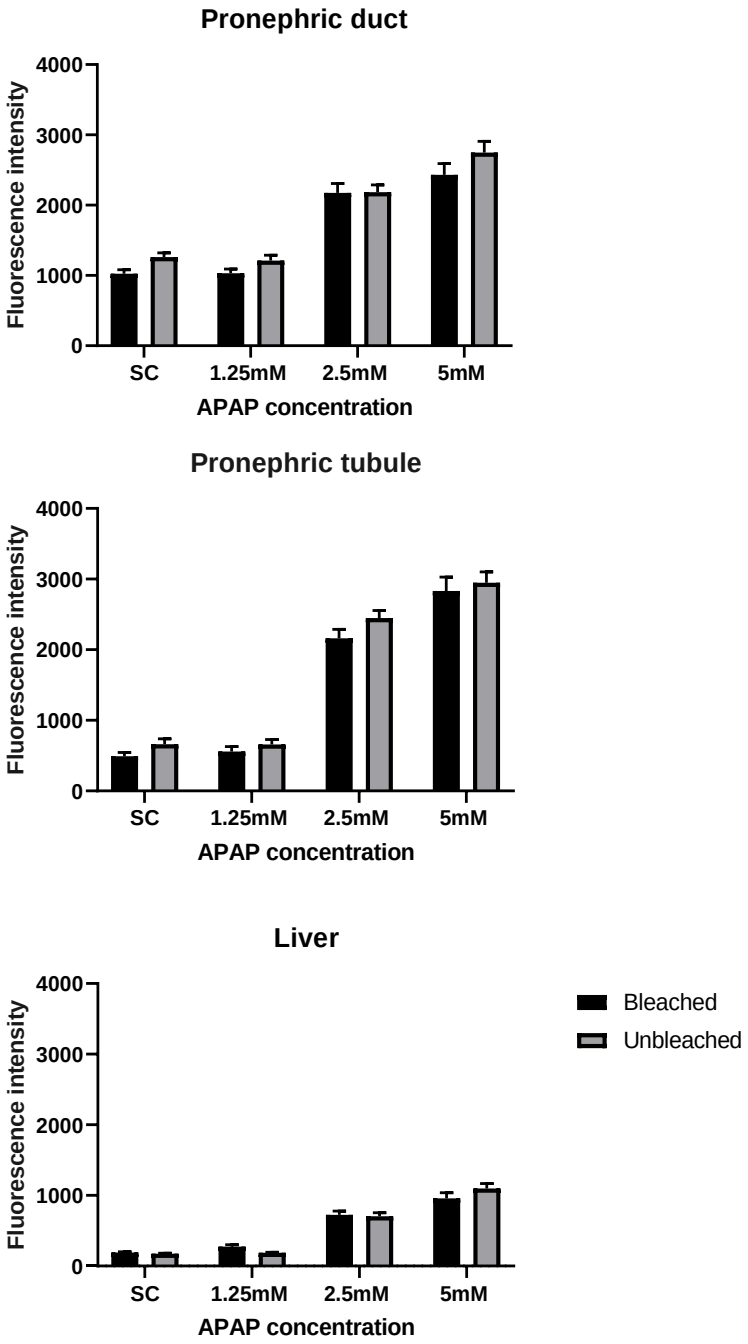


*Figure 4.11* ***Background and APAP-induced OS response of 4 dpf EpRE:mCherry embryos taken from [black] parents bleached as 1 dpf embryos compared with those from [grey] unbleached parents, imaged using the Acquifer.*** *Data shows mean values (+/- SEM, N= 16) for the mean pixel intensity within the organs of 4 dpf larvae exposed to APAP or SC from 6 hpf. . No significant differences between the two lines.*

### 4.3.3 Pharmaceutical screen

#### *4.3.3.1 Positive control: APAP*

The screening work began with the application of a positive control, APAP, which had been confirmed in the previous chapter to induce concentration-dependent OS. Fig. 4.12 shows that a significant level of OS was detected in response to APAP concentrations as low as 1.25 mM following exposure from 6 hpf. This was a more sensitive response than that measured in chapter 3 section 3.2, which followed the protocol used by (Mourabit *et al.* 2019), suggesting that dechorionation of the embryo was not required for the drug to be taken up by the animal if exposed from 6 hpf.

This experiment also revealed that the most dramatic increase in OS was between 3 and 4 dpf. Comparatively, there was only minimal increase in drug-induced OS between 4 and 5 dpf, confirming that there was little to be gained by using a protected animal over an unprotected larva. Together, this information facilitated the optimisation of an exposure protocol for the following drugs screens, designed to capture the most vulnerable window of response and capture the greatest level of sensitivity possible within the system.

Fig. 4.12 also appears to suggest that 5mM APAP resulted in reduced OS compared to 2.5 mM, however, 5 mM APAP induced malformations such as pericardial oedemas and necrotic tissue which obscured part of the fluorescent signal (inset of Fig. 4.12). 2.5 mM APAP reliably induced significant OS without resulting in overt toxicity, allowing the accurate measurement of tissue-specific fluorescence and so this was selected as the reference concentration for future experiments. Although pericardial oedemas are a general indication of toxicity and can be caused by any number of mechanisms, it is interesting to note that OS can be measured in this model at concentrations lower than those at which overt toxicity can be observed in the phenotype, supporting the use of this model as a sensitive biomarker.

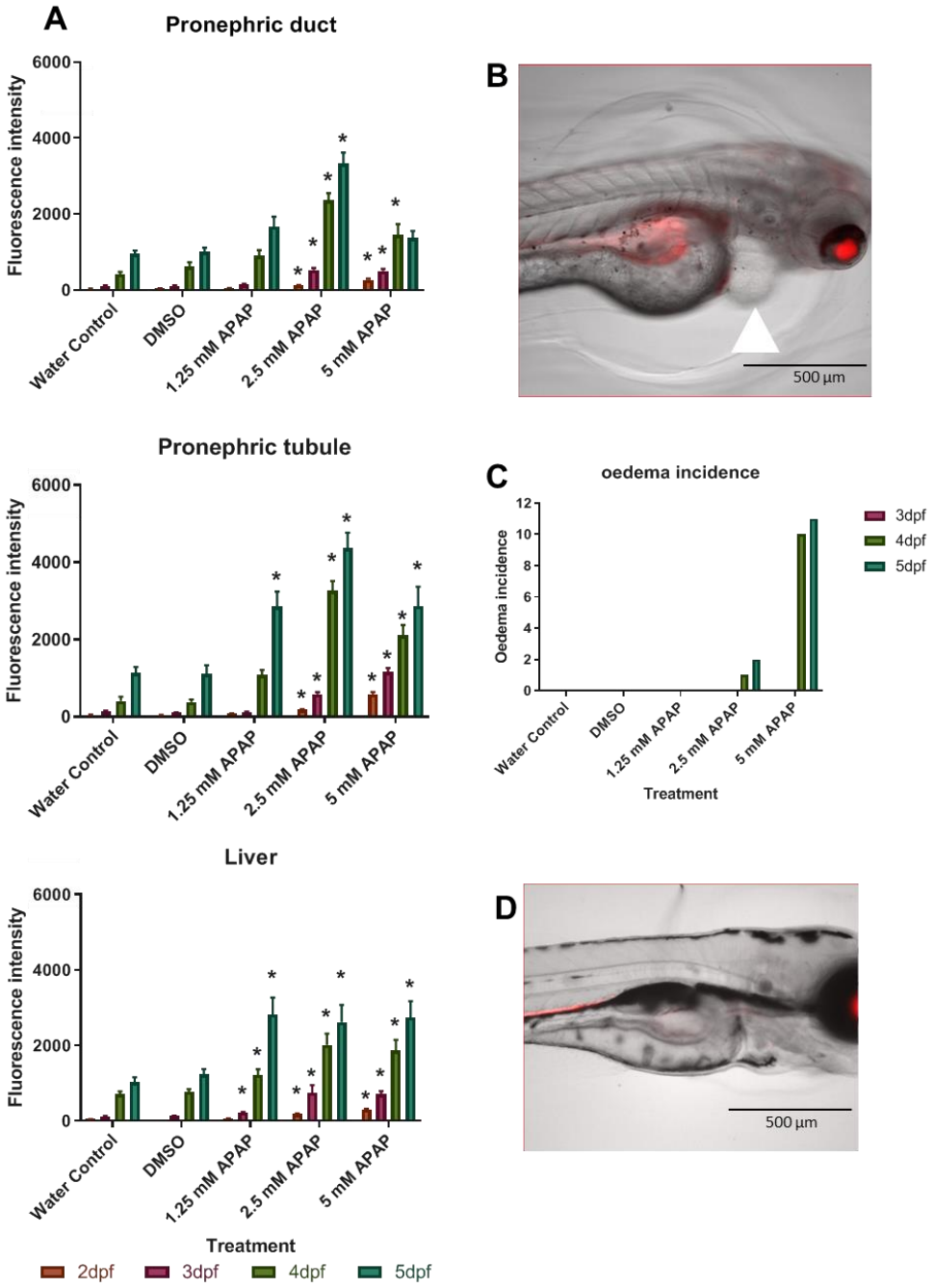


*Figure 4.12* ***Effect of APAP exposure on OS over time, imaged using the Acquifer*** *[A] Data shows mean values (+/- SEM, N= 12 per treatment) for the mean pixel intensity within the organs of EpRE:mCherry larvae exposed to water, DMSO control or APAP from 6 hpf, imaged daily on the Acquifer from 2-5 dpf. Data were not normally distributed and so were analysed using a Kruskal-Wallis followed by Dunn's multiple comparisons test. Asterisks represent significant difference (P<0.05) compared to the water control for the corresponding time point. [B] 4 dpf larva exposed to 5 mM APAP from 6 hpf. Arrow indicates large pericardial oedema typical of this treatment group. [C] Incidence of pericardial oedemas observed in larvae exposed to a range of APAP concentrations. [D] 4 dpf EpRE:mCherry larva exposed to CW only as a comparison*

#### *4.3.3.2 Negative control: ATL*

As expected, no OS was detected at any concentration of ATL (Fig. 4.13) and no phenotypic responses were observed.

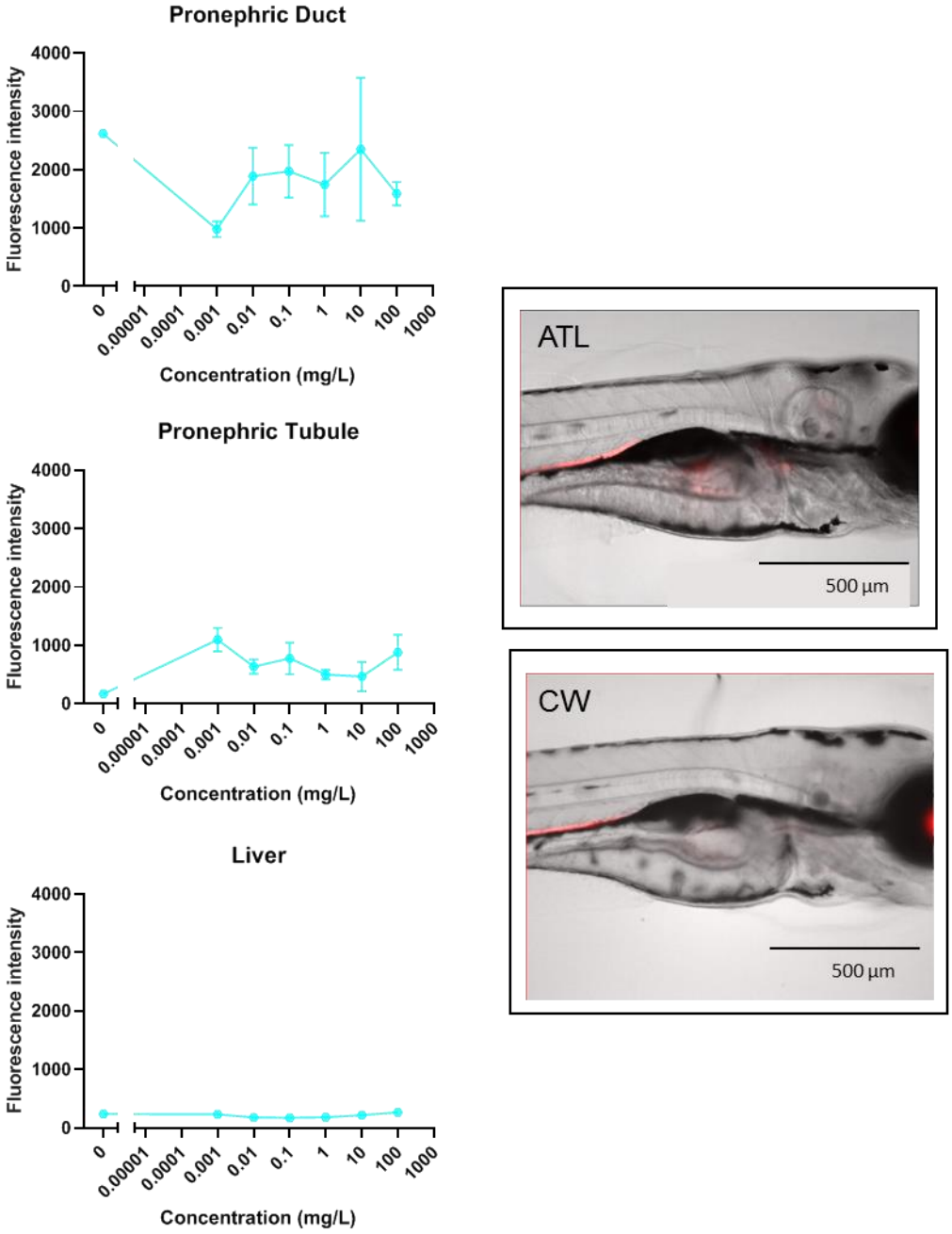


*Figure 4.13* ***Effect of the negative control, ATL exposure on OS levels, imaged using the Acquifer****. Data shows mean values (+/- SEM, N= 5) for the mean pixel intensity within the organs of 4 dpf larvae exposed to ATL or a clean water control (CW) from 6 hpf. Inset: 375 µM ATL. No malformations or mortalities were observed in any treatment group, and there were no significant changes in OS.*

#### *4.3.3.3 Analgesics*

Fig. 4.14 shows the results for a screen of the analgesics DCF and IBF. DCF elicited what appeared to be a detectable level of OS in the PT and liver (but this was not statistically significant), and so was tested again at a narrower concentration range and with a larger number of animal replicate (Fig. 4.15). At 3.4 µM, DCF also resulted in a significant number of pericardial oedemas. IBF did not cause detectable OS in any organs analysed.

In the repeated DCF assay, a significant level of OS was induced from 1.4 µM in the PD and liver, and from 2.0 µM in the PT (Fig. 4.15). The liver was also identified as the most responsive organ, with a particularly dramatic increase in OS across the relatively narrow concentration range. At 3.4 µM, all embryos were either hugely deformed with oedemas or they remained unhatched, so could not be measured for fluorescence intensity.

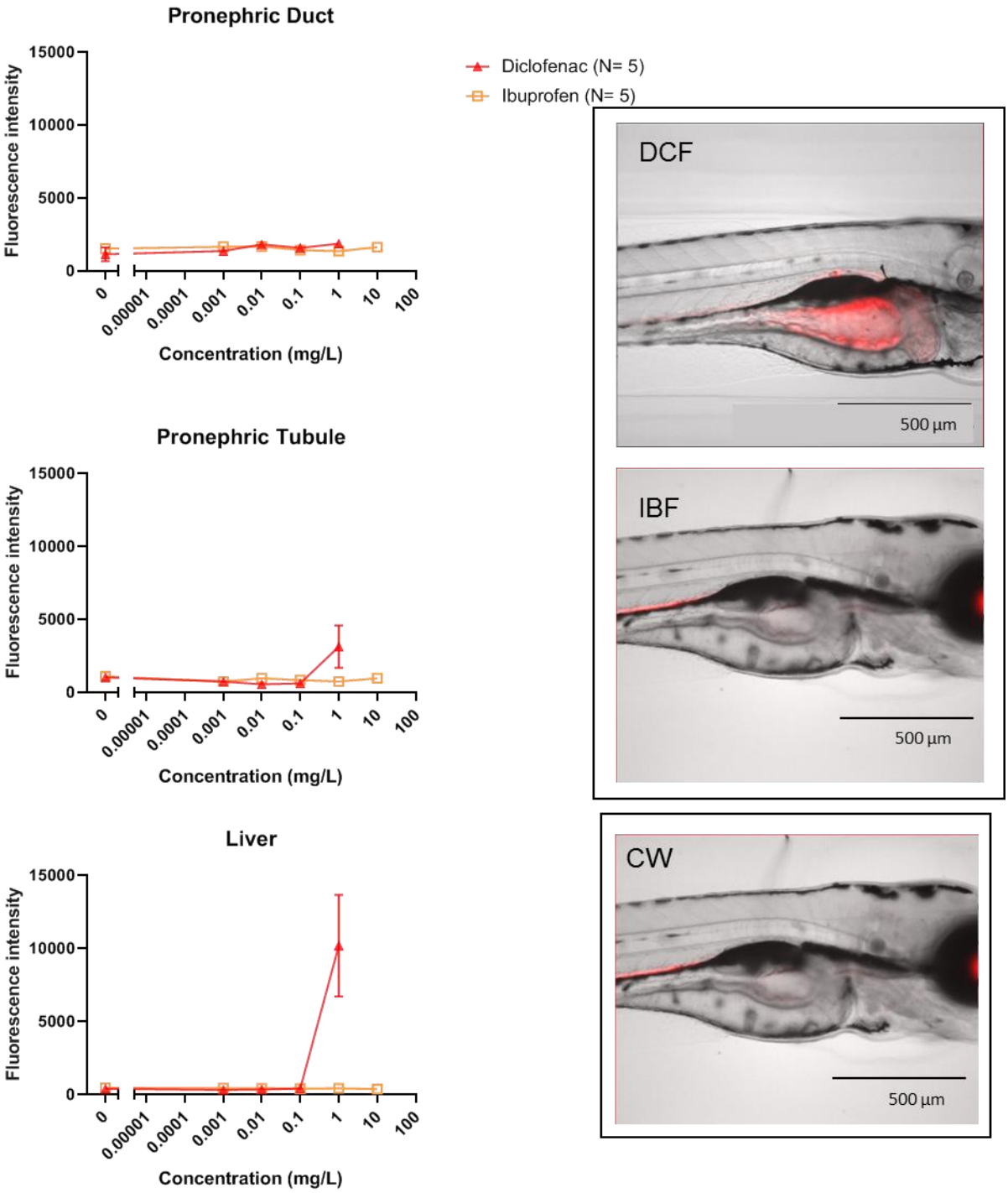


*Figure 4.14* ***Analgesics exposure: effect of DCF and IBF on OS levels, imaged using the Acquifer.*** *Data shows mean values (+/- SEM, N= 5) for the mean pixel intensity within the organs of 4 dpf larvae exposed to DCF, IBF or SC from 6 hpf. Inset: [top] 2.7 µM DCF, [bottom] 50 µM IBF. DCF was also tested at 3.4 µM, which resulted in 100 % mortality, and some pericardial oedemas were observed in 3.4 µM larvae. IBF did not result in any malformations or mortalities*

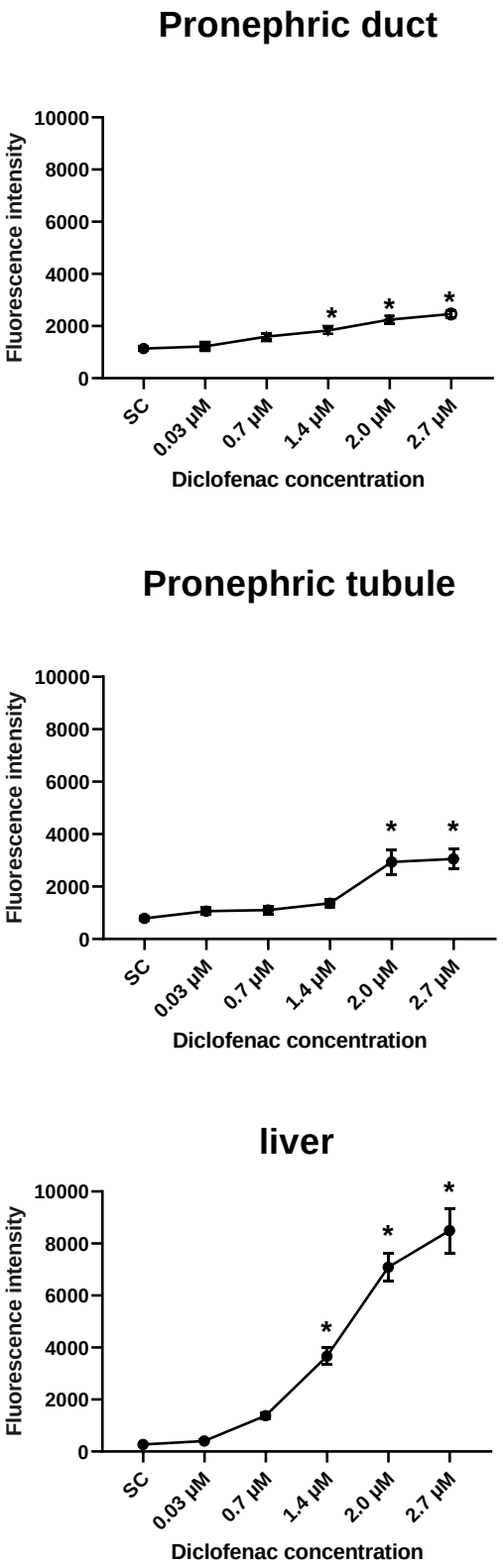


*Figure 4.15* ***Concentration-dependent fluorescence response to DCF, imaged using the Acquifer****. Data shows mean values (+/- SEM, N= 13) for the mean pixel intensity within the organs of 4 dpf larvae exposed to DCF or SC from 6 hpf. Data were not normally distributed and so were analysed using Kruskal-Wallis followed by Dunn's multiple comparisons. *=P<0.05, **=P<0.005, ***=P<0.0005, ****= P<0.0001*

#### *4.3.3.4 Chemotherapeutics*

Fig. 4.16 shows the responses of a range of chemotherapeutics, CP, Dox, and Cis. At the concentration ranges tested, Dox was the only drug that appeared to induce a detectable level of OS in the target organs (particularly the liver), although this response was not statistically significant, and the drug was therefore tested again at a more targeted concentration range (Fig. 4.17).

OS was detected in the liver at 1.1 µM and 1.8 µM Dox, and in the GI from 0.4 µM (Fig. 4.17). In the GI tract, the model shows a concentration-dependent increase in OS between 0.4 µM and 1.1 µM, but this levelled off between 1.1 µM and 1.6 µM. Reasons for this are unclear, as no signs of overt toxicity were observed in the images of these larvae (i.e. no oedemas or necrotic tissue) that might block the fluorescent signal of the GI tract. Image analysis was also expanded here to include the heart due to the strong evidence for ROS generation in cardiomyocytes (Sawyer et al., 2010) and the common cardiotoxicity observed in patients treated with Dox (Octavia *et al.*, 2012; Raschi *et al.*, 2010), but no OS was detected.

Interestingly, unlike almost every other drug screened here which showed any level of OS, Dox did not appear to induce OS in the pronephros. Although later experiments using Dox did show some OS in the PT (see chapter 6), this was only seen at even higher concentrations than tested here and the pronephros was still not nearly as affected as the liver or GI.

The absence of a detectable response in the model to Cis exposure was unexpected given the known ototoxicity (Buck et al., 2012; Choi et al., 2013; Hung et al., 2019; Lee et al., 2004; Ou et al., 2007; Shahab et al., 2021) and nephrotoxicity of Cis (Hentschel et al., 2005; Kruidering et al., 1997). Data in Chapter 3 showed that the Acquifer does not have the sensitivity to detect subtle changes in fluorescence in small organs such as the neuromasts, but the Acquifer can detect changes in fluorescence in the PT, which has previously been shown to exhibit OS in the EpRE:mCherry model in response to Cis (Mourabit *et al.*, 2019). Therefore, to determine if the lack of response was due to reduced sensitivity of a later generation of the EpRE:mCherry model, or a result of the different exposure regimen, the experiment was repeated again using a higher top concentration (up to 33.2 µM) and exposure from 0 dpf was compared against the effect of exposure from 2 dpf (as was used by Mourabit *et al.*).

After a 4 day exposure, Cis was still not found to induce a significant level of OS in any organ analysed. However, it did result in a reduced level of mCherry fluorescence in the liver, PD, and GI (Fig. 4.18). This also corresponds with the development of pericardial oedemas significantly larger for exposures to concentrations at and above 0.3 µM compared to the SC. Larvae exposed to 3.3 µM and 33.2 µM from 0 dpf also exhibited delayed hatching by at least 24 hours. In contrast, larvae exposed from 2- 4 dpf exhibited no overt signs of toxicity, except in the top concentration where pericardial oedemas were significantly larger. Additionally, 33.2 µM Cis induced a significant level of OS in the PT and PD compared to a minimum effect concentration of 50 µM in the PT reported by Mourabit *et al.* In the neuromasts, identified using the DASPEI stain, no significant changes in OS were detected, although larvae exposed from 0 dpf showed a downward trend in OS with increasing concentration, while larvae exposed from 2 dpf showed an upward trend.

The correlation between oedema size and OS in larvae exposed from 0 dpf indicates that the overt toxicity and corresponding phenotypic changes may have obscured the fluorescence and/or damaged the tissue to the extent it can no longer produce the fluorophore (e.g., as was shown in chapter 3 when Cis destroyed the neuromasts and so no OS could be measured).

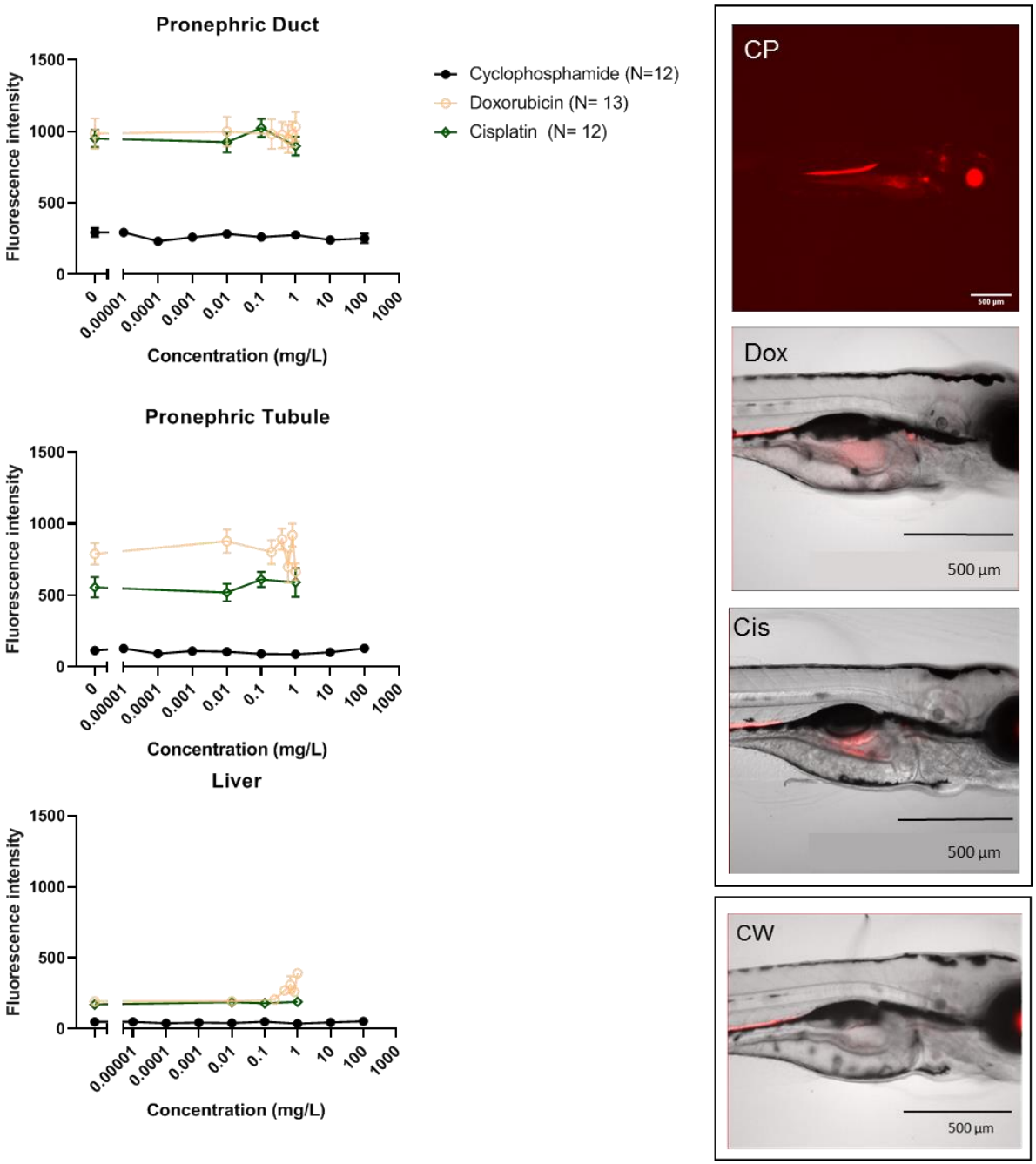


*Figure 4.16* ***Chemotherapeutic drugs exposure: effect of CP, Dox and Cis on OS levels, imaged using the Acquifer.*** *Data shows mean values (+/- SEM) for the mean pixel intensity within the organs of 4 dpf larvae exposed to CP, Dox, Cis or CW (or an SC in the case of Cis) from 6 hpf. Inset: [top] CP was first screened on an Olympus stereomicroscope, the image shown has had the contrast altered to aid visualisation of the larva [middle] 1.8 µM Dox [bottom] 3.3 µM Cis. Cis was tested at higher concentrations, but deformities were observed at 33.2 µM and delayed hatching at 332 µM. Doxorubicin was tested at 184 µM, which resulted in 100 % mortality, and 18.4 µM which resulted in malformations and deaths. No malformations or mortality was associated with any concentration of CP.*

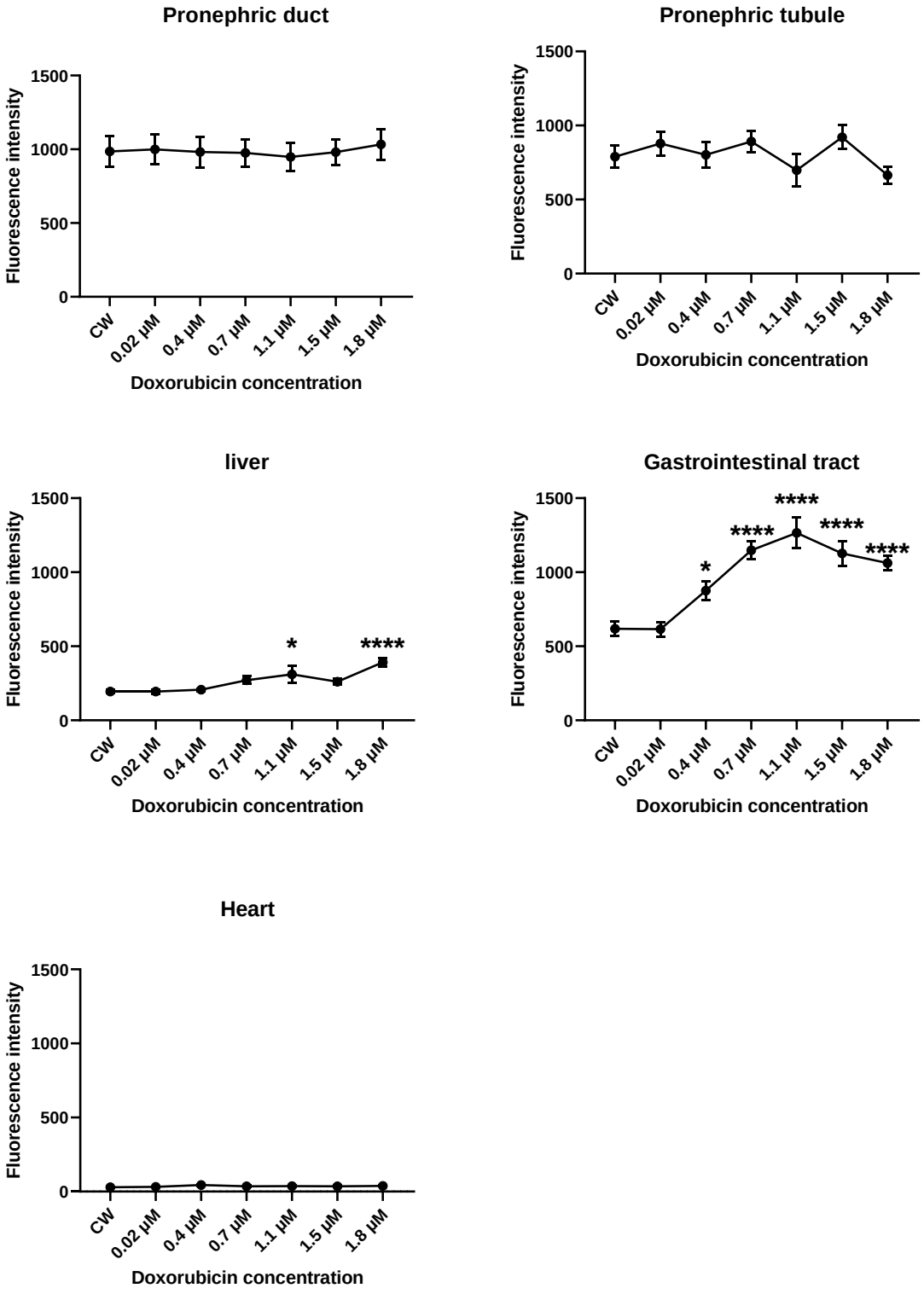


*Figure 4.17* ***Concentration-dependent OS induced by Dox, imaged using the Acquifer****. Data shows mean values (+/- SEM, N= 13) for the mean pixel intensity within the organs of 4 dpf larvae exposed to Dox or CW from 6 hpf. Data were not normally distributed and so were analysed using Kruskal-Wallis followed by Dunn's multiple comparisons. *=P<0.05, **=P<0.005, ***=P<0.0005, ****= P<0.0001.*

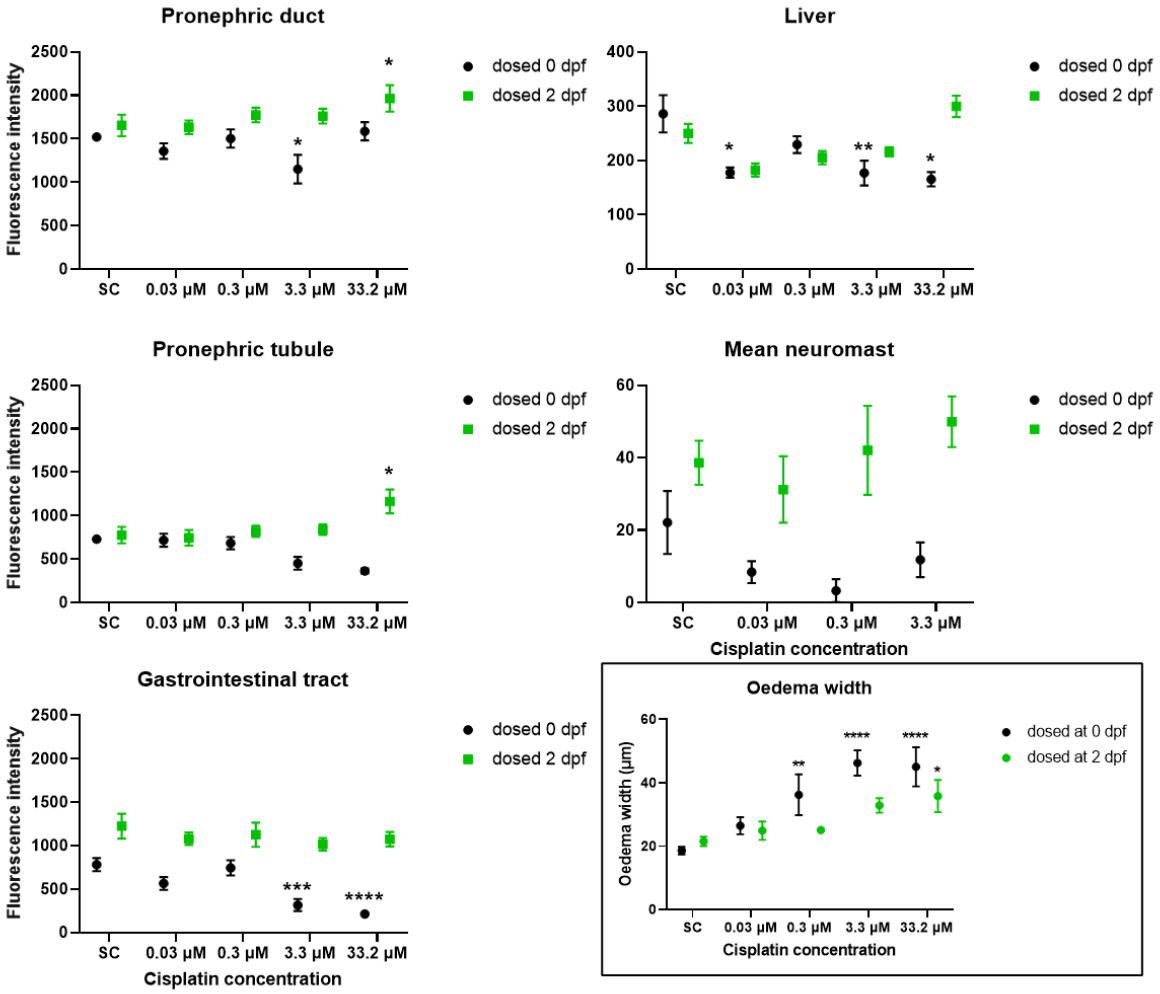


*Figure 4.18* ***Comparison of the OS induced by Cis when embryos are exposed on 0 dpf versus 2 dpf, imaged using the Acquifer****. Data shows mean values (+/- SEM, N= 12) for the mean pixel intensity within the organs of 4 dpf larvae exposed to Cis or SC from 6 hpf or 2 dpf. Inset shows the width of pericardial oedemas for these larvae, indicating an overt toxic reaction and phenotypic change which may be responsible for the perceived decrease in OS measured in larvae exposed at 0 dpf.. Data was not normally distributed and so was analysed using Kruskal-Wallis followed by Dunn's multiple comparisons. *=P<0.05, **=P<0.005, ***=P<0.0005, ****= P<0.0001*

#### *4.3.3.5 CAM*

At the concentrations tested here, CAM did not appear to induce or buffer against OS (Fig. 4.19).

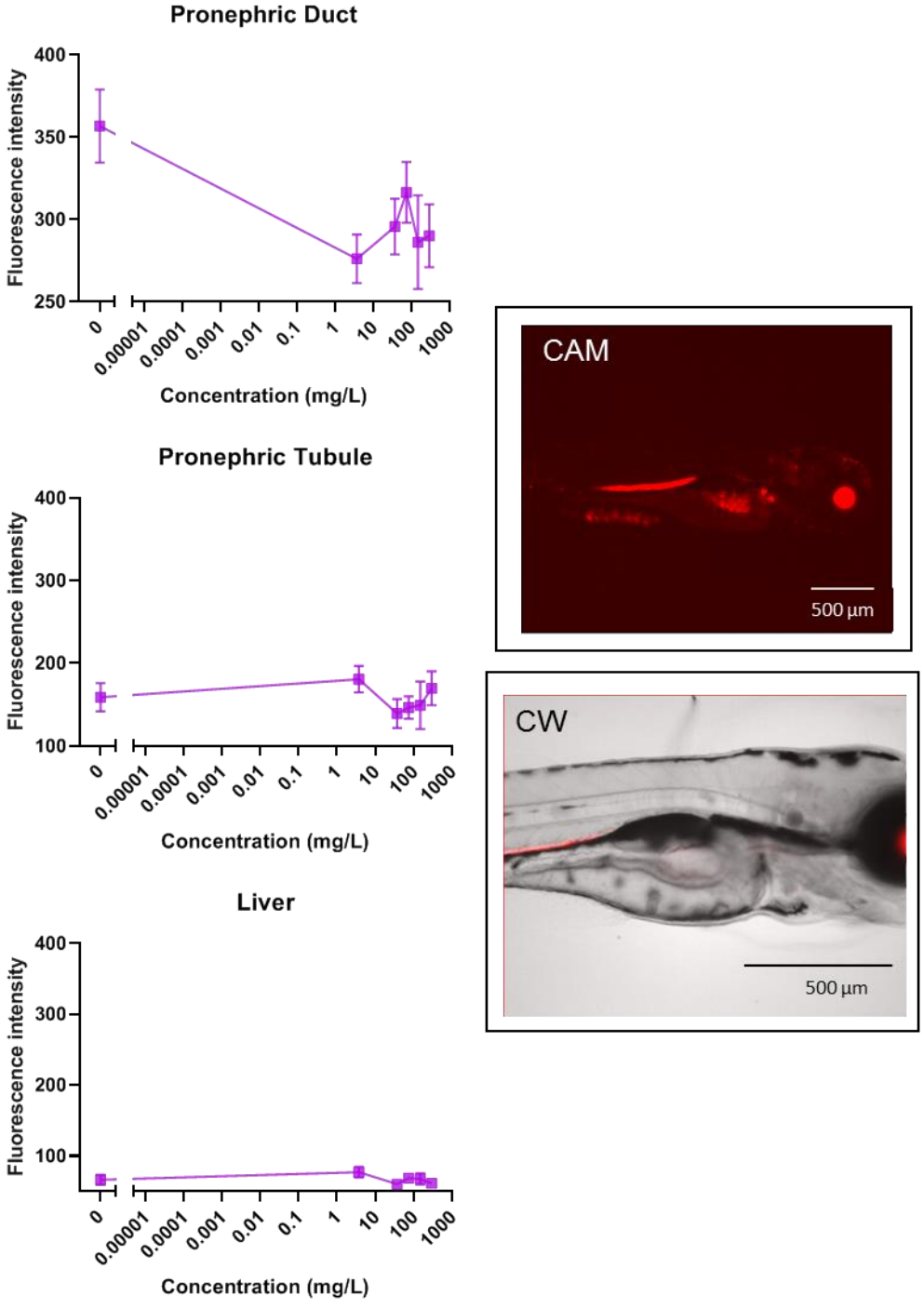


*Figure 4.19* ***Effect of CAM exposure on OS levels, imaged using the Acquifer.*** *Data shows mean values (+/- SEM, N= 12) for the mean pixel intensity within the organs of 4 dpf larvae exposed to CAM or SC from 6 hpf. Inset: 400 µM CAM, imaged on Olympus, contrast altered to better visualise larvae. Mortality or malformation incidence was not above background.*

### *4.3.3.6 Cloz*

Cloz did not induce significant OS in any of the tissues analysed at any of the concentrations tested (Fig. 4.20). A slight positive trend was observed in the liver at 30.6 µM, but this was not significant.

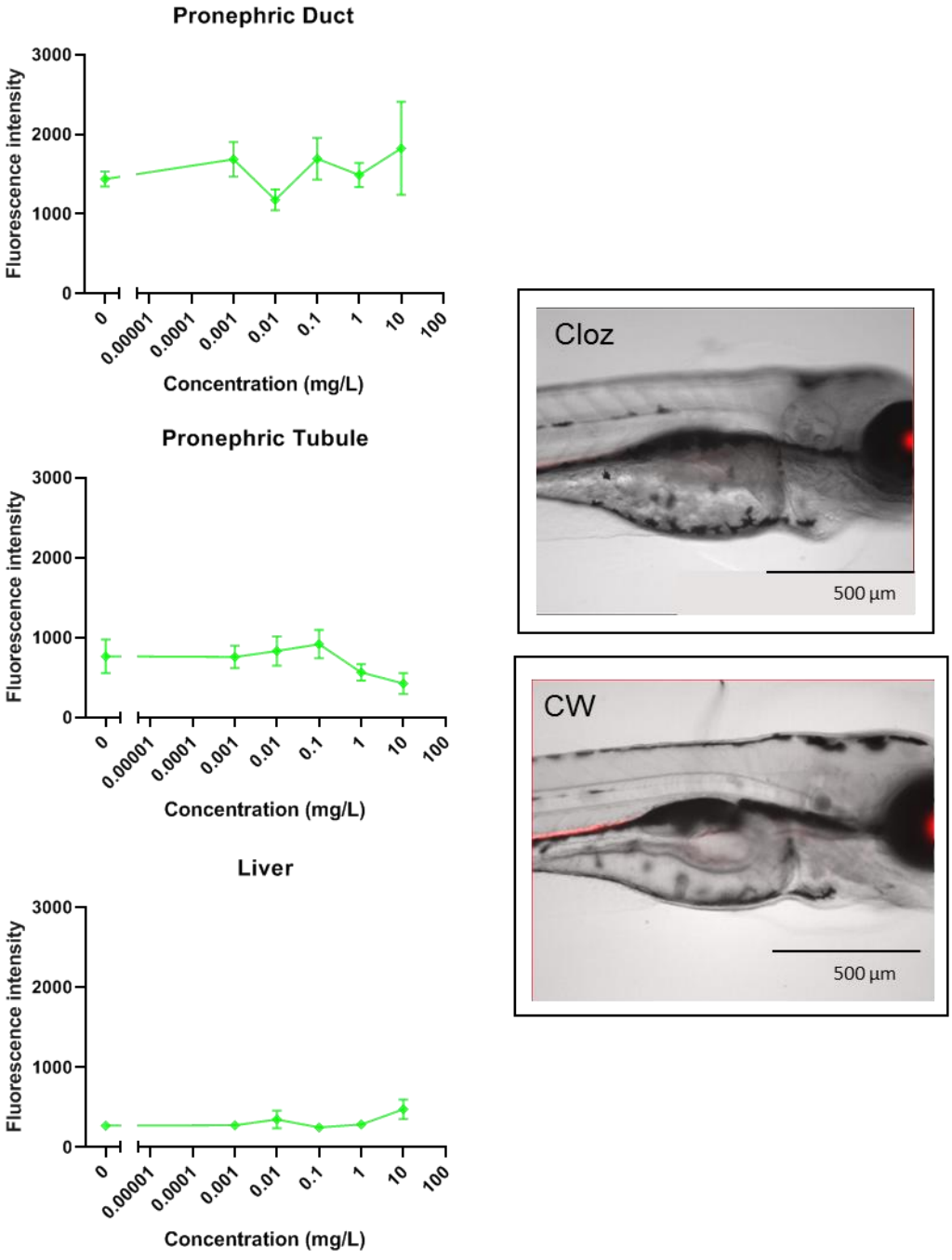


*Figure 4.20* ***Effect of Cloz on OS levels, imaged using the Acquifer.*** *Data shows mean values (+/- SEM, N= 5) for the mean pixel intensity within the organs of 4 dpf larvae exposed to Cloz or SC from 6 hpf. Inset: 30.6 µM cloz, showing necrotic tissue and a pericardial oedema. Oedemas were not observed at any other concentrations, and no mortalities were observed.*

### 4.3.4 Internal pharmaceutical concentration

To better understand the chemical responses (or lack thereof) observed in the TG model, plasma drug concentration was predicted using the FssPC. Analytical chemistry was also used to measure the internal concentrations of pharmaceuticals following 4 day exposures.

The FPM was used to predict if the pharmaceuticals used were likely to have an effect on the zebrafish larvae based on a FssPC:HTPC ratio of <1 (Table 4.3). The FssPC has been calculated based on the FPM predicted partitioning, calculated using the $LogD_{ow}$ values (Fig. 4.3). Based on the lipophilicity of the compound, every drug was predicted to reach therapeutic concentrations in the plasma of exposed larvae, except for Cis and IBF.

The results of the FPM are consistent with the internal concentrations measured using LC-MS/MS (Table 4.4). As expected, the positive control, APAP, was taken up by the larvae. The negative control, ATL, was also detected in the body of the larvae, although it did show low uptake (1.4 %). DCF and Dox were both below the limit of quantification (LOQ) for the method used. This could be due to a variety of reasons, including poor MS sensitivity, and does not necessarily reflect low uptake of the drugs, particularly as both had a clear effect on the model

For 7 of the 9 drugs tested, the predicted internal concentration (based on FPM) exceeds or reaches the HTPC. The internal concentration of Cis could not be measured, but previous studies have reported relatively low uptake of 3-4 % (Mourabit *et al.*, 2019) and it was not predicted to reach HTPC in the larvae. Despite this, it did elicit a response in the model at this concentration range (albeit OS induction was only significantly higher when exposed to the top concentration from 0-2 dpf, hence the response has been classed as ‘weak’ in Table 4.3).

Interestingly, IBF was detected in the body of the larvae and showed the second-highest uptake of the drugs tested (140%). However, the maximum internal concentration detected (41 µM) still did not reach HTPC (48.48 µM; Table 4.3) and it did not induce significant OS in the EpRE:mCherry model. The FPM model also did not predict that internal IBF concentration would reach therapeutic levels

(Table 4.3). However, due to the poor solubility of IBF, a higher exposure solution could not be tested.

Only two of the 5 drugs predicted to reach HTPC, CAM and Cloz, did not behave as expected. The internal concentration of CAM and Cloz were predicted to exceed HTPC (confirmed by LC-MS/MS) and hence represent examples of a compound where uptake or FPM could not be used to predict its effect on the EpRE:mCherry model. Cloz is a pro-drug and hence needed further investigation.

*Table 4.3* ***Effect ratio for each drug tested based on FPM.*** *Calculated from the human therapeutic concentration (HTPC) and estimated fish steady state plasma concentration (FssPC), based on the fish plasma model (FPM) predicted partitioning calculated from the $LogD_{ow}$. Red in the 'conclusion on predicted fish plasma concentration' column indicates predicted to reach or exceed HTPC, green indicates that it is not predicted to reach HTPC. Red in the 'response seen in model at 4dpf?' column indicates that a response was seen, green indicates no response, and yellow indicates a weak response under specific exposure conditions.*

| Compound | LogDow pH 7.4 | FPM predicted partitioning | HTPC (µM) | | Max exposure concentration (µM) | FssPC from FPM (µM) | Effect ratio | | Conclusion on predicted fish plasma concentration | Response seen in model at 4dpf? |
|---|---|---|---|---|---|---|---|---|---|---|
| | | | Min | Max | | | Min HTPC | Max HTPC | | |
| **Paracetamol (APAP)** | 0.40 | 0.26 | 66.15 | 165.38 | 5000.00 | 1291.13 | 0.05 | 0.13 | Exceeds therapeutic range | Yes |
| **Atenolol (ATL)** | -1.85 | 0.01 | 0.38 | 3.76 | 375.47 | 2.21 | 0.17 | 1.70 | Within therapeutic range | No |
| **Diclofenac (DCF)** | 1.37 | 1.32 | 1.69 | 10.13 | 33.77 | 44.53 | 0.04 | 0.23 | Exceeds therapeutic range | Yes |
| **Ibuprofen (IBF)** | 0.45 | 0.28 | 72.71 | 145.43 | 48.48 | 13.62 | 5.34 | 10.68 | Not predicted to reach therapeutic range | No |
| **Doxorubicin (Dox)** | -0.79 | 0.04 | 0.01 | 0.04 | 183.99 | 6.43 | <0.01 | 0.01 | Exceeds therapeutic range | Yes |
| **Cisplatin (Cis)** | -2.19 | 0.13 | 3.32 | 16.61 | 332.12 | 1.10 | 3.01 | 15.05 | Not predicted to reach therapeutic range | Weak |
| **Cyclo-phosphamide (CP)** | 0.53 | 0.32 | 38.30 | 95.75 | 3830.00 | 1230.55 | 0.03 | 0.08 | Exceeds therapeutic range | yes |
| **Clarithromycin (CAM)** | 2.38 | 7.20 | 0.27 | 2.67 | 400.00 | 2880.45 | <0.01 | <0.01 | Exceeds therapeutic range | No |
| **Clozapine (Cloz)** | 2.72 | 12.75 | 1.07 | 1.84 | 30.59 | 390.10 | <0.01 | 0.01 | Exceeds therapeutic range | No |

*Table 4.4* ***Internal pharmaceutical concentrations measured using LC-MS/MS****. Cis could not be measured. DCF and doxorubicin were below the LOQ. Values are given to two significant figures.*

| Compound | Nominal concentration (μM) | Mean concentration per larva (μM) | Uptake (%) Mean | SEM |
|---|---|---|---|---|
| Paracetamol (APAP) | 2500 | 740 | 29 | 1.5 |
| Atenolol (ATL) | 188 | 2.7 | 1.4 | 0.56 |
| | 375 | 5.3 | 1.4 | 0.38 |
| Diclofenac (DCF) | 1 | <LOQ | | |
| | 2 | <LOQ | | |
| Ibuprofen (IBF) | 25 | 33 | 140 | 17 |
| | 50 | 41 | 85 | 9.7 |
| Doxorubicin (Dox) | 9.2 | <LOQ | | |
| | 18.4 | <LOQ | | |
| Cyclophosphamide (CP) | 383 | 9.1 | 2.4 | 0.34 |
| | 3830 | 220 | 5.7 | 0.48 |
| Cisplatin (Cis) | N/A | | | |
| Clarithromycin (CAM) | 200 | 14 | 7.2 | 2.0 |
| | 400 | 53 | 13 | 0.92 |
| Clozapine (Cloz) | 30.6 | 1900 | 6300 | 380 |

### 4.3.5 Bioactivation of pro-drugs and influence of metabolism on drug toxicity

When drug uptake and FssPC could not explain the lack of effect several of the drugs had on the EpRE:mCherry model, attention was turned to the metabolic capacity of 4 dpf zebrafish. Cloz and CP are both pro-dugs, and thus require bio-activation to exert their therapeutic effect. Therefore, these compounds were further investigated to determine how developmental stage or metabolic activation may influence their OS potency, to better understand why they did not give a positive result in the initial screen.

#### *4.3.5.1 Cloz*

Cloz is metabolised by CYP P450 to produce the pharmaceutically active metabolite desmethyl clozapine (DMC) and clozapine-N-oxide (Fig. 4.21). DMC exposure had no effect on OS in the model (Fig. 4.22); although a detectable reduction was observed in the PT at 0.003 µM, this was not observed at any other concentration and is more likely to be an artefact from imaging. Table 4.5 shows an uptake between 270 – 550 %, (for exposure concentrations of 3.2 µM and 32 µM, respectively), suggesting uptake was not responsible for a lack of response.

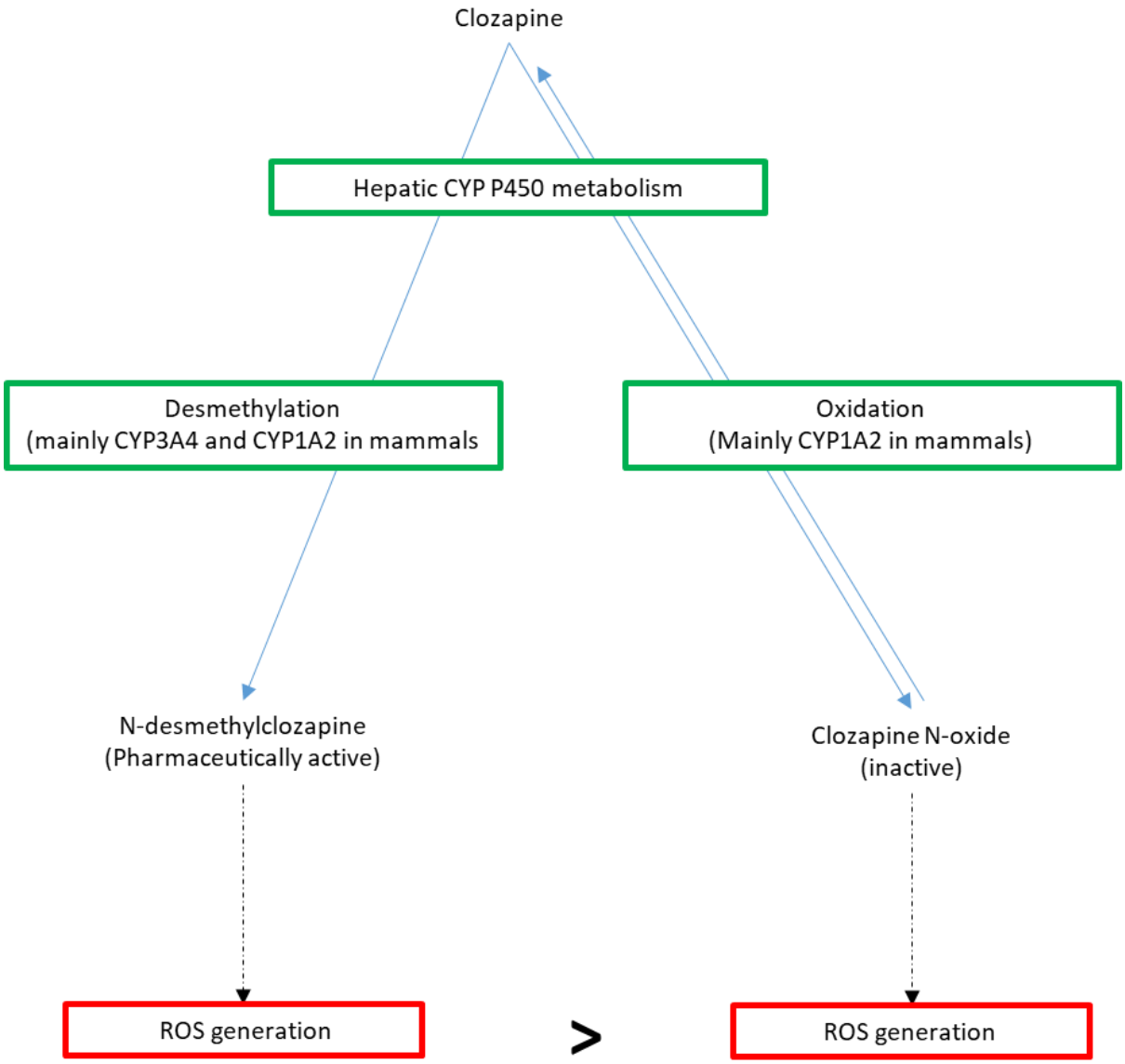


*Figure 4.21* ***Scheme of metabolism pathway for Cloz.*** *Adapted from Thorn et al. 2018 and Vredenburg et al. 2013*

Chemical analysis of embryos exposed to Cloz for 96 hours detected significant levels of DMC (around 50 % of the internal Cloz concentration) (Table 4.5), indicating that these larvae did metabolise the drug. One disadvantage of LC-MS/MS is that it measures the concentration of the compound in the whole body and cannot distinguish between different compartments within the larva. Therefore, MSI was attempted to assess the distribution of the parent and its two main metabolites in 4 dpf larvae. Sectioning of early life stage larvae is extremely challenging; therefore, it was not possible within the timescale to obtain ideal images in terms of quantity or perfect sections. However, the images obtained do provide some useful information:

Fig. 4.23a suggests Cloz extensively adhered to the outside of the larvae as well as some evidence for tail muscle (or notochord), eyes and, to a lesser extent, other parts of the upper body. Fig 4.23b show the distribution of Cloz and its two major metabolites; clozapine N-oxide and DMC, detected by accurate mass measurement. There is good spatial correlation between parent and N-oxide which were detected mainly in the brain and eyes of the larvae. DMC can only be 'tentatively' identified in these images as it was measured in lower levels compared to the other molecules and was less localised to specific tissues, suggesting it is barely above background noise. However, all three masses were shown to be significantly above the control background (Fig. 4.32c) providing evidence that the parent compound can be taken up into larvae, partition from the blood to other body tissue, and be metabolised by zebrafish larvae at this age. Unfortunately, for this evaluation, there were no sections containing other major organs of interest such as liver or pronephros, and so the distribution of the drug or its metabolites cannot be correlated to mCherry fluorescence intensity in these tissues.

Given some evidence for metabolism indicated by the DESI data, it was decided to modify the generic LC-MS/MS method to assess larvae exposed to Cloz for only 20 minutes. This confirmed metabolism of the drug after just 20 minute-exposure by detecting the presence of DMC, albeit naturally at lower levels compared to larvae exposed to Cloz for 4 days (Table 4.5; 8% compared to 50 % of the measured internal Cloz concentration). This data also provided more evidence in support of the identity of DMC in the DESI images.

Together, these data confirm that Cloz was a) bioavailable to the larval tissue and b) metabolised by the 4 dpf larvae, ruling these out as possible reasons for lack of response in the EpRE:mCherry model to Cloz exposure.

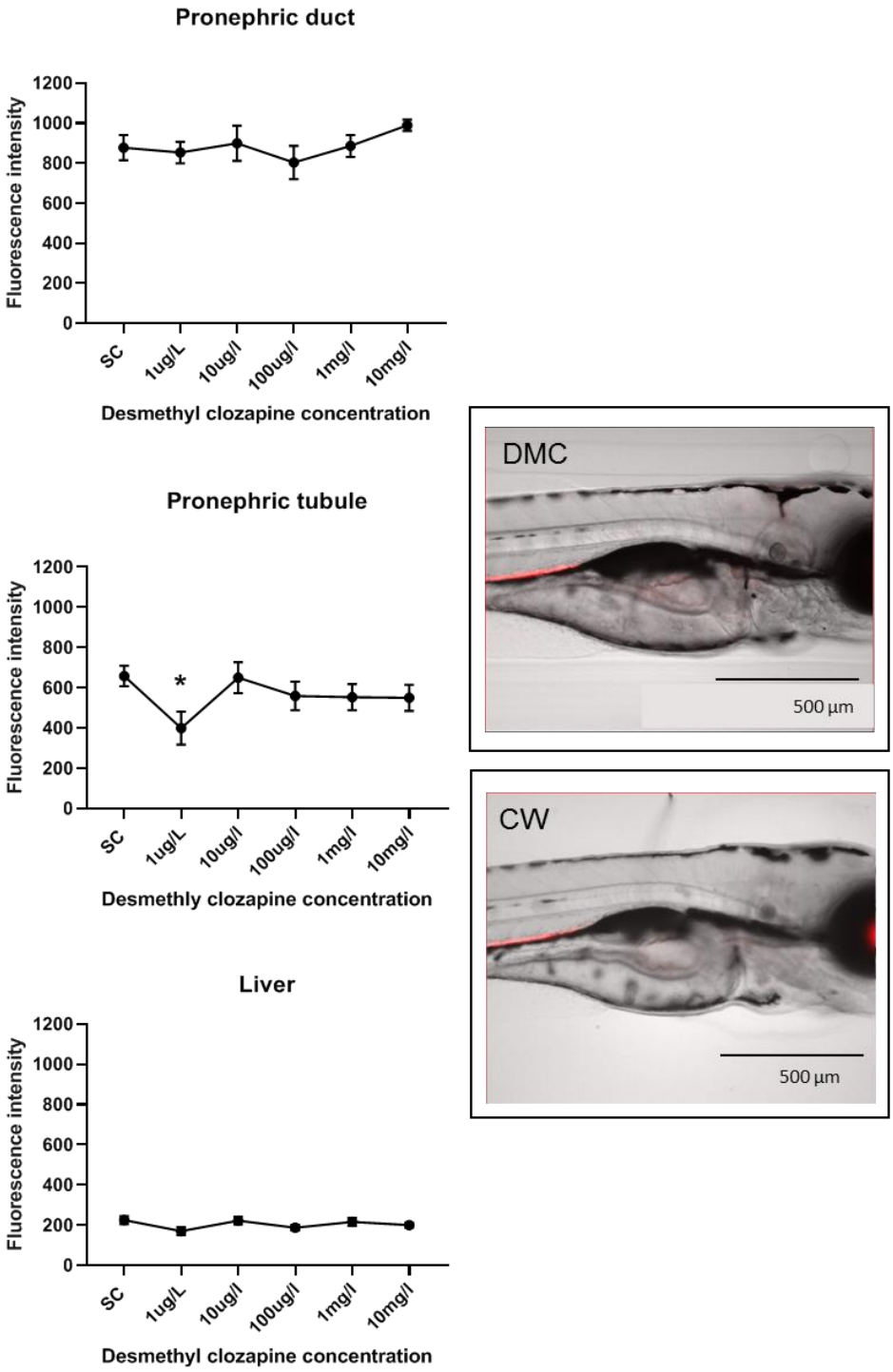


*Figure 4.22* ***Effect of DMC exposure on OS levels, imaged using the Acquifer****. Data shows mean values (+/- SEM, N= 12) for the mean pixel intensity within the organs of 4 dpf larvae exposed to DMC or SC from 6 hpf. Data was not normally distributed and so was analysed using Kruskal-Wallis followed by Dunn's multiple comparisons. *=P<0.05, **=P<0.005, ***=P<0.0005, ****= P<0.0001. Inset shows 32 µM DMC*

*Table 4.5* ***LC-MS/MS analysis showing uptake of Cloz and its synthesised metabolite, DMC,*** *alongside the proportion of DC produced following exposure to the parent compound. Values given to 2 significant figures.*

| Compound | Nominal concentration µM | Mean concentration per larva µM | Mean uptake % | SEM | DMC as a % of internal Cloz concentration Mean | SEM |
|---|---|---|---|---|---|---|
| Clozapine (Cloz) | 30.60 | 1900 | 6300 | 380 | 51 | 4.3 |
| 20 min exp. | 30.60 | 180 | 600 | 40 | | |
| 20 min exp. | 122.00 | 1000 | 830 | 44 | 7.9 | 0.42 |
| Desmethyl clozapine | 3.20 | 8.7 | 270 | 26 | | |
| (DMC) | 32.00 | 180 | 550 | 29 | | |

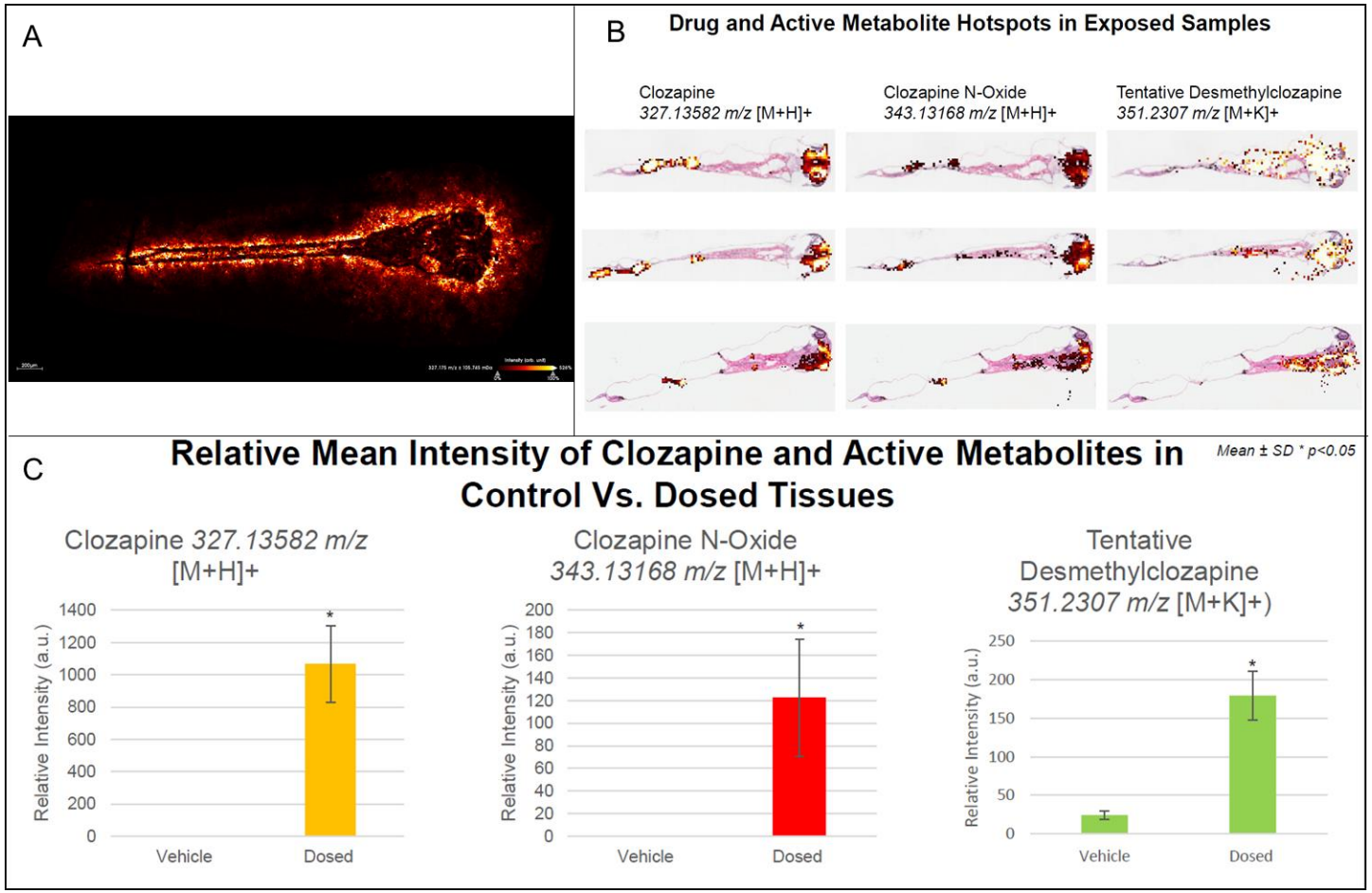


*Figure 4.23* ***DESI analysis of Cloz*** *[A] Coronal section of 4 dpf WIK embryos exposed to 100 µM Cloz for 20 minutes, imaged using DESI to detect the parent compound. [B] Histological sections overlaid with DESI images of distribution of Cloz, and its metabolites clozapine-N-oxide and (tentatively) desmethyl clozapine. [C] Relative mean intensities of those molecules detected in whole tissue.*

#### *4.3.5.2 CP*

4-hydroxycyclophosphamide (the active metabolite of CP) is highly unstable in aqueous solution and it was not viable to work directly with its metabolites acrolein or phosphoramide mustard (Fig. 4.24). Instead, larvae were exposed to the parent compound from 8 dpf, when the animal's metabolism is well established. Exposure of EpRE:mCherry larvae to CP from 8-10 dpf did not reduce the response threshold of the model compared with exposure from 0-4 dpf, although the most vulnerable organs did change (Fig. 4.25). In both exposure scenarios, 3830 µM was the only concentration to induce a detectable level of OS, suggesting CP was less potent than initially suspected, and hence did not have an effect at the lower concentrations tested in the initial screen (Fig. 4.16). However, in 4 dpf larvae, the significant OS was detected in the PD and liver, whereas only the PT exhibited OS in the 10 dpf larvae (Fig. 4.25). Additionally, in the 4 dpf larvae, 100% of the larvae exhibited overt toxicity in the form of stunted tails, pericardial oedemas and curved spines, in addition to OS in the neuromasts (Fig. 4.25, Ai). In contrast, no phenotypic changes were observed in the 10 dpf larvae, but they did show OS in the ionocytes (skin cells) on the ventral side of the trunk, regardless of treatment (Fig. 4.25, Bi and Bii).

It is not known why the most vulnerable organs changed between the 2 dosing regimens (from the PD and liver in 4 dpf, to just the PT in 10 dpf larvae). This could relate to the overt toxicity and phenotypic changes observed in the 4 dpf larvae, as 3830 µM CP was seen to have a teratogenic effect. The phenotypic changes may have masked the fluorescent signal in the PT, as it is a smaller organ compared to the PD and more challenging to delineate. Additionally, the lack of a significant OS response in the liver in 10 dpf could be related to the increasing opacity of this organ, as it was noticeably darker in colour in 10 dpf larvae compared to 4 dpf. However, image Bi of Fig. 4.25 shows that a fluorescent signal could still be detected. Further study could also test the effect of later life drug exposure on other pharmaceuticals to find if this effect is specific to CP. A further complication to the measurement of organ-specific fluorescence in the 10 dpf came from the fluorescence emitted by the ionocytes on the surface on the body trunk. This signal was visible and consistent in the larvae regardless of drug treatment, suggesting it was not related to the CP, and potentially skewed fluorescence intensity measures for deeper situated body organs, particularly in the liver which had a relatively weak signal compared to the other target tissues.

OS in the ionocytes of this model had only been previously observed following embryo surface disinfection (Fig. 4.10), potentially indicating irritation of the skin by the external media. In support of this, trials using 10 dpf larvae in which the samples were anaesthetised but not embedded in agarose did not reveal any fluorescence in the skin cells. Other confocal images of 4 dpf larvae did not show fluorescence in the ionocytes, suggesting 10 dpf is particularly vulnerable to irritation by the warm agarose.

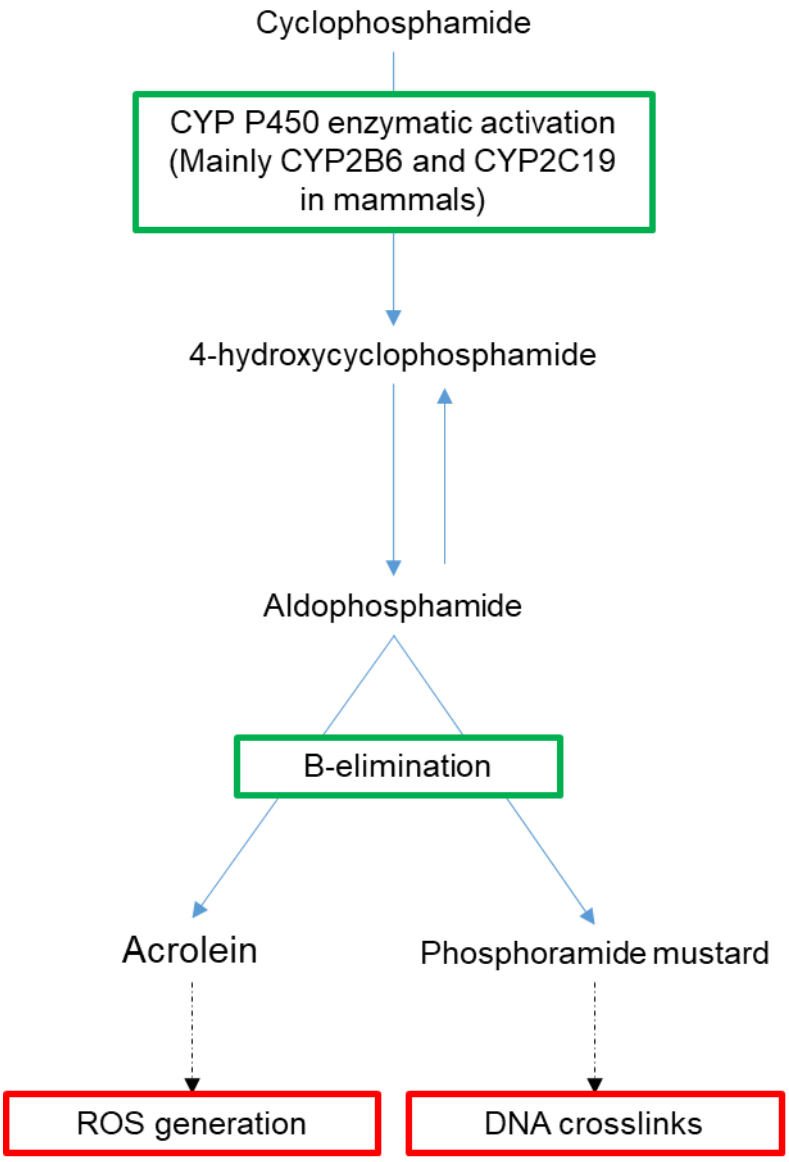


*Figure 4.24* ***Scheme of metabolism pathway for CP****. Adapted from Fonseca et al. 2018 and Kurauchi et al. 2017*

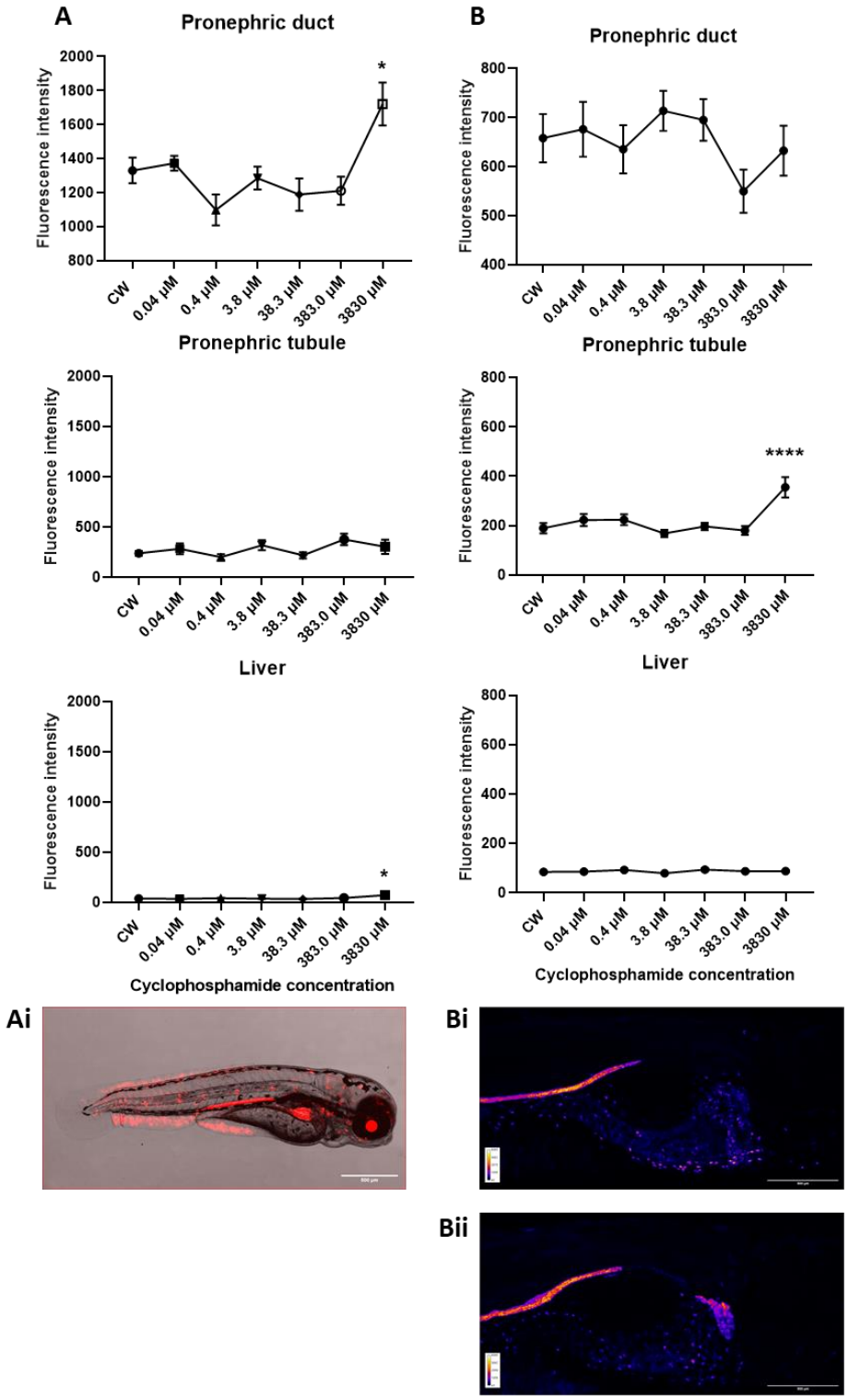


*Figure 4.25* ***Comparison of OS levels detected in larvae exposed to CP from [A] 0-4 dpf (N=12) or [B] 8-10 dpf (N=15),*** *both imaged on the confocal. Data shows mean values (+/- SEM) for the mean pixel intensity within the organs of EpRE:mCherry larvae. [Ai] 4 dpf larva exposed to 3830 µM CP, contrast altered to aid visualisation of the OS pattern, [Bi] 10 dpf larvae exposed to clean water control [Bii] 10 dpf larvae exposed to 3830 µM CP, both visualised using the 'fire' look up table.*

### 4.3.5 Persistence of the fluorescent signal following depuration

As part of characterising the EpRE:mCherry model, the persistence of the mCherry fluorescence in relation to depuration of the pro-oxidant was assessed. In two separate experiments, the concentration of APAP in the body of the larva drops rapidly during the first hour of depuration, then more steadily drops below the LOQ (which for this method was 13 nM) by 24 hours post depuration. The limit of detection for this method was approximately 5 nM, and some APAP could still be detected at 24 hours post depuration but, it could not be quantified. The mCherry fluorescence signal persisted, or even continued to increase, for up to 24 hours after the zebrafish was transferred out of the exposure media (Fig. 4.26 and Fig. 4.27) and only began to degrade after all APAP has been expelled (at around 24 hours post depuration). The fluorescence is still detectable for at least 24 hours after internal concentrations of the pro-oxidant have dropped below the LOQ, and in the case of the PT, can even remain at the level seen in the exposure for a period past this point (Figs. 4.26 and 4.27).

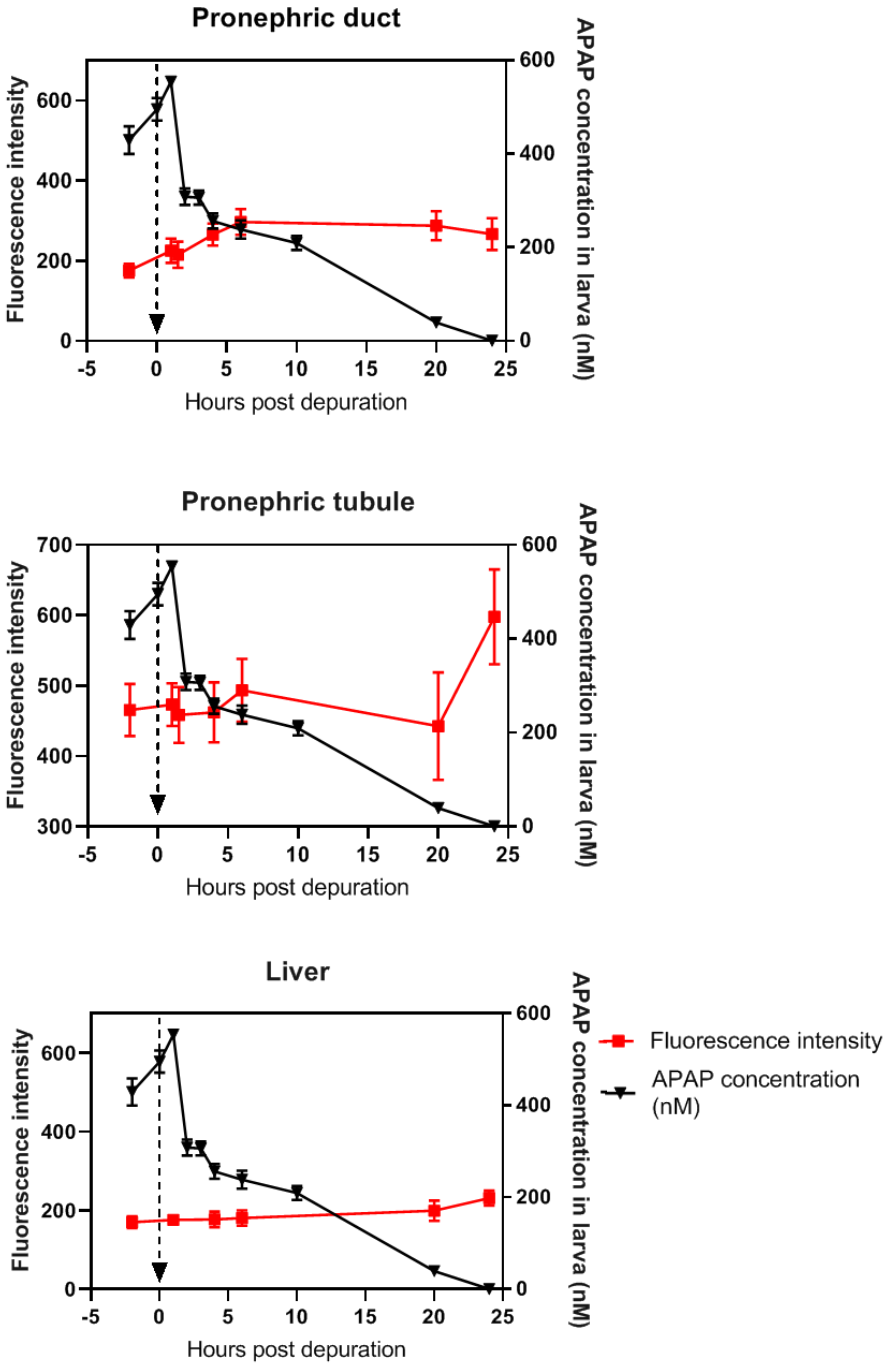


*Figure 4.26* ***Relationship between persistence of mCherry fluorescence and depuration of APAP from the larval body over 24 hours.*** *Relationship between depuration of APAP (black inverted triangles; internal APAP concentration measured in WIK larvae using LC-MS/MS and given as mean +/- SEM, N=6) and persistence of the fluorescence signal (red squares; measured in EpRE:mCherry larvae, imaged using the Acquifer) in 3-4 dpf larvae exposed to 2.5 mM APAP from 6 hpf. Dashed arrow indicates 3dpf/78 hours of exposure, the time point at which larva were washed and transferred from APAP to fresh water, time is given in hours post depuration. The fluorescence intensity is given as mean values (+/- SEM, N= 12) for the mean pixel intensity within the organs and has been baseline-corrected against an SC at the same time point to control for increase in background OS which occurs with embryo development.*

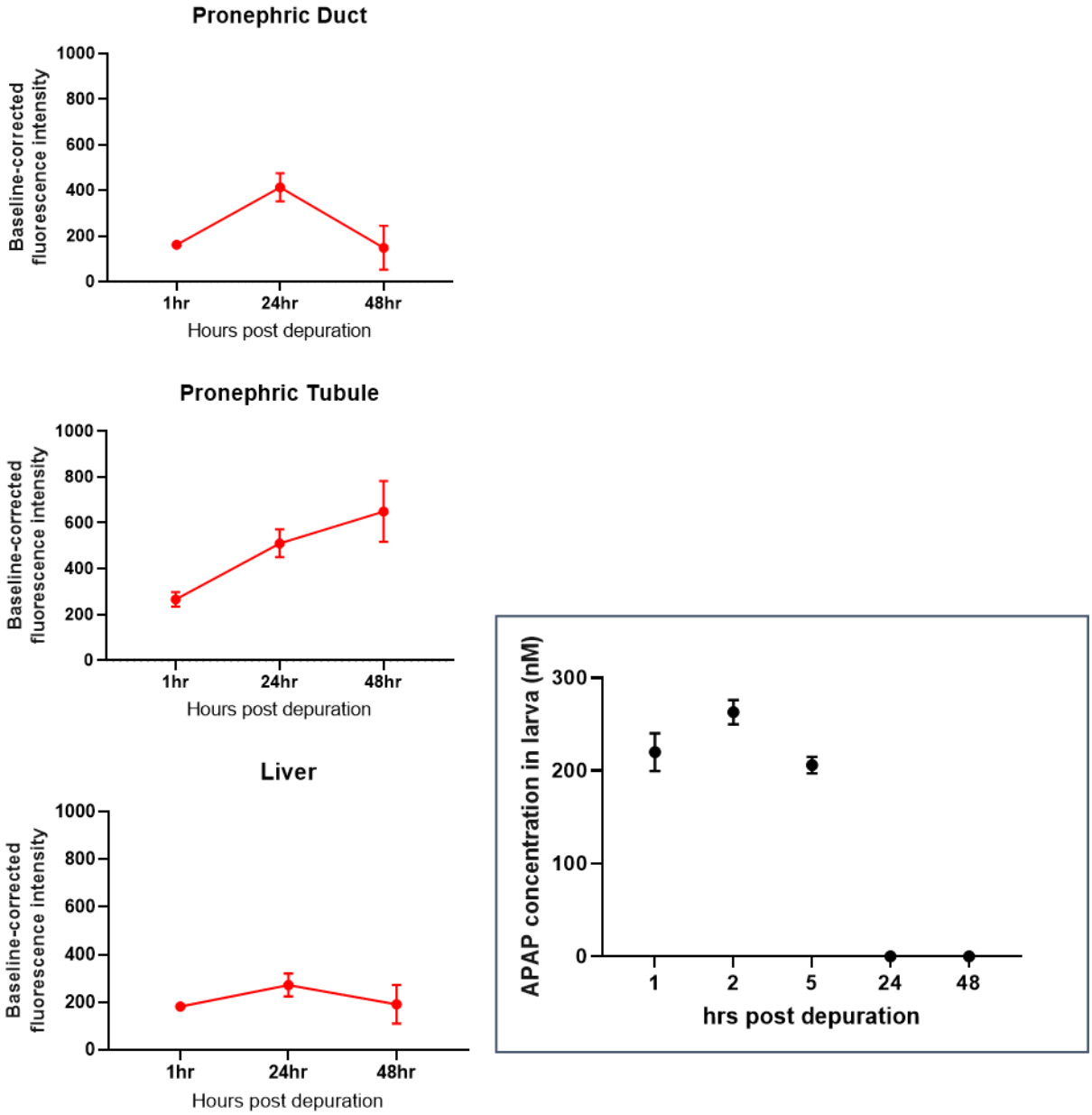


*Figure 4.27* ***Persistence of the mCherry fluorescent signal over 48 hours post depuration.*** *Larvae were exposed to 2.5mM APAP at 6hpf and transferred to clean water at 2dpf/48 hours exposure. Fluorescence intensity* is given as mean values (+/- SEM, N= 12) for the mean pixel intensity within the organs and has *been baseline corrected against SC to account for increase in background OS resulting from embryo development. Inset shows concentration of APAP detected using LC-MS/MS in WIK embryos exposed to 2.5 mM APAP and transferred to fresh water at 2 dpf.*

## 4.4 Discussion

This chapter sought demonstrate the utility of the EpRE:mCherry model as a convenient and rapid tool for the screening of pharmaceuticals for their potential to induce OS. Figs. 4.6, 4.7, 4.8 and 4.9 show that the model did not lose sensitivity between generations and control groups exhibited fairly consistent levels of mCherry fluorescence between spawning events, demonstrating a consistency and robustess of the EpRE:mCherry model.

The positive and negative controls behaved as expected, further supporting the validity of the model. APAP-induced OS was detected in the liver from 1.25 mM, in concordance with induction of OS by 1.3 mM APAP reported in the model previously (Mourabit *et al.*, 2019). As expected, no OS was detected at any concentration of ATL (Fig. 4.13), despite being predicted to reach HTPC in the larvae (Table 4.3). The ATL was also detected in the body of exposed larvae, albeit at very low levels (Table 4.4), and ATL has previously been observed circulating in the blood of zebrafish larvae (Fig. 4.28). This confirms that the EpRE:mCherry model responds specifically to pro-oxidants, and while it can be very sensitive to early life conditions (such as disinfection, Fig. 4.10, or a physical stressor as will be explored in chapter 6), it doesn't express fluorescence indiscriminately.

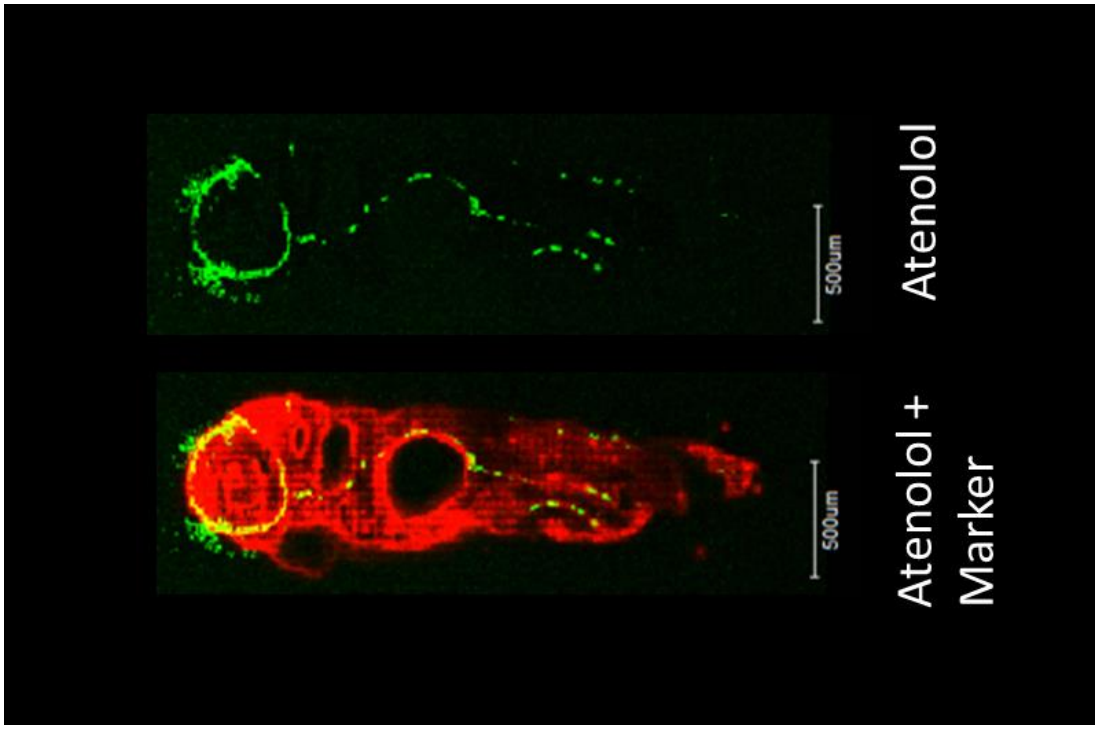


*Figure 4.28* ***MSI image showing ATL circulating in the plasma of a zebrafish larva.*** *Photo courtesy of Swales, Ball and Hetheridge.*

### 4.4.1 Convenience and throughput

The EpRE:mCherry model in combination with the HTS platform the Acquifer (discussed in the previous chapter) provided a convenient tool to screen nine pharmaceuticals for their pro-oxidative effect across a range of tissues in a whole-body animal. As discussed by Mourabit *et al.*, who first developed the model, the TG model visualises OS as mediated through the Nrf2/Keap1 pathway which can induce over 100 proteins in the antioxidant pathway, each with tissue-specific expression patterns (Mourabit *et al.*, 2019; Nakajima *et al.*, 2011). To achieve the same results using traditional gene regulation analysis methods (such as microarray analysis or RT-PCR) would be far more time consuming, more labour intensive and require analysis of multiple downstream genes from separate tissue samples. In comparison, one assay using the EpRE:mCherry model and a 20 min image acquisition using the Acquifer provided the OS response profile for a compound across all tissues in the 4 dpf zebrafish larva. Therefore, APAP, DCF and Dox were easily identified as pro-oxidants and their concentration-dependent effects on target tissues were characterised so these drugs could be carried forward for further investigation in later chapters.

Additionally, as detection OS in the EpRE mCherry model does not require the destruction of tissue, the onset of OS was measured repeatedly in the same individuals over time. Fig. 4.12 showed that significant OS was induced in the liver and pronephros as early as 2 dpf. Chemical OS induction over time has been studied previously, such as perturbation of the GSH:GSSG ratio in 72 hpf zebrafish larvae after 24, 48 and 72 hour exposure to dioxin-like 3,30,4,40,5-pentachlorobiphenyl (PCB126) (Liu et al., 2015). However, few studies have tracked OS induction from exposure at 0 dpf, and none appear to have been able to take repeated measures from the same individuals. This also facilitated the optimisation of an exposure protocol for the pharmaceutical screen by identifying the most vulnerable window of response (shown by the dramatic increase in fluorescence between days 3 and 4 of APAP exposure), capturing the greatest level of sensitivity possible within the system.

However, Fig. 4.18 indicates this protocol is not suitable for testing Cis, as 2-day exposure to 33.2 µM Cis resulted in significantly higher OS in the PD and PT, but a 4-day exposure to the same concentration range resulted in a decrease in OS in all organs measured (significantly so in the liver and GI). When compared with

the size of pericardial oedemas, the apparent decrease in mCherry fluorescence appears to be a result of overt toxicity, just as was seen for the toxic effects of 5 mM APAP that resulted in reduced mCherry fluorescence compared to 2.5 mM APAP (Fig. 4.12). In this instance, a 2-day exposure was more effective for assessing the pro-oxidative nature of Cis as a longer exposure period resulted in tissue damage before the OS could be assessed. This therefore highlights a caveat in the use of this model and of TG models in general as a pharmaceutical screen, as it cannot be used for compounds which are too potent that they may induce overtly toxic effects, causing tissue damage and therefore compromising the accuracy of any measurements of fluorescence intensity.

### 4.4.2 Identification of target organs

The EpRE:mCherry model allowed for the rapid identification of new target organs which had not previously been considered, such as the GI in response to Dox (Fig. 4.17). Dox has not previously been shown to induce OS in the GI, although it has been linked to adverse effects in the intestines of chemotherapy patients (Kaczmarek et al., 2012). The GI tract is known to be a site of metabolism and has even been proposed as the main site of detoxification for zebrafish larvae due to a higher level of induction of promotors related to phase I and II metabolism compared to the liver (Poon *et al.*, 2017). However, although CYPs are expressed in the intestine (Goldstone *et al.*, 2010), it contributes to CYP-mediated drug metabolism to a lesser extent compared to the liver (Verbueken *et al.*, 2017). In contrast to the fluorescence induction observed in Poon *et al.*'s TG larvae, the present pharmaceutical screen did not show the GI tract to respond as consistently, or as frequently, across the different drugs tested in comparison to the liver or pronephros, hence it was not included as default in initial screens of the drugs.

Interestingly, Dox did not appear to induce OS in the pronephros, unlike almost every other drug screened here which showed any level of OS. Although later experiments using Dox did show some OS in the PT (see Chapter 6), this was only seen at higher concentrations and the fluorescence detected in the PT was lower than the liver or GI. This could potentially be related to the greater increase in OS detected in the GI; inhibition of CYP1 activity has previously prevented Dox-induced cardiomyopathy in zebrafish larvae (Lam *et al.*, 2020), and CYP1A activity is first detected in the liver primordium at 56 hpf, followed closely by the

intestine at around 80 hpf (Otte et al., 2010). Indicating CYP1, and therefore the intestine, play key roles in the toxicity of Dox.

Historically, clinical studies to understand the mechanism of Dox toxicity have used primarily cardiac and liver cell lines (Wang et al., 2019). However, the significantly stronger signal observed in the GI tract here compared with the other tissues may indicate the GI as a target organ of this pharmaceutical which merits further study.

The EpRE:mCherry model also supports what has previously been reported on organ-specific vulnerability to DCF: the liver was identified as the most vulnerable of the three targeted organs, as indicated by the most dramatic increase in fluorescence intensity across the increasing concentration (Fig. 4.15). This is in line with the results reported by Islas-Florres (2013), who found the greatest increase in lipid peroxidation, a direct consequence of OS, and various antioxidant enzymes in the liver. This is likely because the liver is a major sight of biotransformation of DCF (Islas-Flores *et al.*, 2013).

### 4.4.3 Sensitivity

The EpRE model does not appear to be sufficiently sensitive for the detection of the pro-oxidative compounds studied here at environmentally relevant concentrations. The greatest level of sensitivity was achieved using Dox (0.4 µM) and DCF (1.4 µM), both of which are generally detected in the pM - nM range (Table 4.1). However, the internal concentration of both these compounds were below the LOQ, so while the TG model cannot be used at environmental levels, it is sensitive enough to show a response to very low internal concentrations of certain compounds. In particular, DCF showed an impressively steep concentration-response curve, starting with the onset of OS at 1.4 µM and reaching toxic effects (delayed hatching/mortality) at 3.4 µM (Fig 4.15).

While more traditional methods such as antioxidant activity assays or PCR of selected genes require destructive sampling and are not as integrative a biomarker as the EpRE:mCherry model, they can be more sensitive than the model. In an acute zebrafish exposure to DCF (from 5 – 96 hpf), Bio and Nunes found that the antioxidant enzymes GSTs were the most sensitive biomarker, with significantly reduced activity from 0.0015 µM DCF. This suggested a depletion of intracellular GSH, which is required as a conjugation substrate for GSTs but can

also be reduced through direct denaturation by ROS (Bio & Nunes, 2020). However, CAT activity was only significantly increased from 1.5 µM (Bio & Nunes, 2020), more in line with the results reported here (significant OS detected in the liver from 1.4 µM, Fig. 4.15). The upregulation of CAT suggests that at 1.5 µM DCF the cell is working harder to protect against the OS caused by the excess of ROS which GPx and GST failed to scavenge. CAT, along with GR, is often considered one of the more sensitive biomarkers for OS, and CAT could be considered the more biologically important biomarker due to its role in breaking down hydrogen peroxide, the precursor of the hydroxyl radical which is the most reactive ROS (Regoli *et al.*, 2002). In this way, perhaps CAT is a better biomarker (i.e., arguably more important) than other antioxidants as it is most strongly associated with oxidative damage. Therefore, true OS (in that ROS had overwhelmed the first line of cellular defences, necessitating the upregulation of CAT) was not reached in Bio and Nunes' study until the top concentration of 1.5 µM. Consequently, the EpRE:mCherry model arguably matched the sensitivity of this antioxidant activity assay, with the added advantage of identifying the exact tissues undergoing OS. It is not known how the degree of upregulation of EpRE in the model corresponds to relative activity of the different antioxidants. The EpRE:mCherry can indicate the degree of OS and the increased activity of downstream antioxidant enzymes but cannot be used to delineate the responses of specific enzymes. This could be an area of future study.

### 4.4.4 mCherry fluorescence degradation

The lag between the decline in internal concentration of a toxin and the decline of fluorescence intensity is important to consider regarding the use of this model for understanding more dynamic responses or changeable conditions (explored further in chapter 5). It is not known whether this is due to continued induction of the antioxidant defence system (i.e., the tissue is still recovering), a result of the half-life of the fluorophore, or an artefact of slow cellular or receptor turnover.

mCherry is very stable (Hebisch et al., 2013; Shaner et al., 2005), but this relates to how quickly it is photobleached under constant illumination, rather than how long it persists once generated. The red fluorophore also has a relatively short maturation time (the time between translation of the protein and formation of the chromophore) (Hebisch *et al.*, 2013), but little is known about how long the chromophore can persist once transcription/translation of the fluorescent protein

stops. mCherry can be used to visualise proteins with half-lives of 10 minutes to 8 hours (Doerr, 2012), indicating the fluorophore must also have a half-life of around 8 hours. This suggests that the fluorescent signal would persist at above-background levels after upregulation of EpRE (and particularly the downstream genes) have returned to normal levels for a matter of hours. Therefore, in the data presented, it is not possible to determine how quickly the tissue can recover from the OS based on how quickly the mCherry fluorescence degrades. To delineate these mechanisms, a future study could use an alternative measure of OS, such as SOD or CAT enzyme activity, to take time-series data during the depuration phase and compare the time taken for these levels to return to normal versus the fluorescence intensity.

In support of the hypothesis that slow recovery of the tissue from OS is the cause of this lag in fluorescence decline, rather than the fluorophore's half-life, the organs analysed do not show a uniform response. The fluorescence signal in the PT appears particularly persistent as it is the only tissue in which fluorescence intensity continues to increase past 7 hours post depuration (Figs. 4.26 and 4.27). In chapter 3, the sensitivity of the PT to OS was explored, including its relatively low levels of endogenous antioxidants and high concentration of mitochondria (Chevalier, 2016), in addition to its preferential accumulation of toxins (McKee & Wingert, 2015). This may explain the organ's slow recovery from oxidative damage.

As well as improving our interpretation of fluorescence detected in the EpRE:mCherry model, the ostensible persistence of OS for long after the stressor has been removed holds interesting implications for environmental risk assessments. If the prolonged mCherry expression truly reflects ongoing OS, this would imply that acute or pulse exposures to pro-oxidants can continue influencing an animal's redox status after the exposure period has ended, potentially impeding its fitness or ability to respond to subsequent stressors. Indeed, OS induction in zebrafish embryos has been shown to reduce their reproductive success as adults (Newman et al., 2015). Further, other chemical and receptor types have been used to show how early life exposure can enhance an animal's response to repeated or similar type of exposure later in life (Green *et al.*, 2018; Tiedeken & Ramsdell, 2007).

### 4.4.5 Understanding negative results from the EpRE:mCherry screen: why did CP, Cloz, CAM and IBF not induce OS as expected?

It has been established that Cis did not elicit the expected response in EpRE:mCherry larvae in the initial screen as 4 days was too long an exposure and likely caused too much damage before accurate levels of OS could be measured (see section 4.4.1). However, it is still unclear why the remaining pharmaceuticals, CP, Cloz, CAM, and IBF did not induce significant OS, as none of them exerted any obvious toxic effects, based on morphological features of the embryo-larvae (except for CP at the extremely high concentration of 3830 µM).

All four were taken up into the larval body (Table 4.4) and predicted by the FPM (Table 4.3) to reach therapeutic levels (except for IBF). As CAM, cloz and CP are known to be pro-drugs, it was originally postulated that 4 dpf zebrafish larvae may not have the necessary metabolic capacity to activate the compounds (Fig. 4.2). However, the present data appears to not support this hypothesis.

Cloz showed particularly high uptake (6300 %), in line with other studies which have shown its capacity to bioconcentrate in fish, particularly in the liver and kidney (Nallani *et al.*, 2016). Evidence in the literature indicates ROS generation is induced by DMC and clozapine N-oxide, which are produced by hepatic CYP P450 metabolism (Fig.4.21) (Thorn *et al.*, 2018; Vredenburg *et al.*, 2013). Therefore, it had been presumed that exposure to the active metabolite would have a more toxic effect than equimolar concentrations of the parent compound as it does not require bioactivation. However, although DMC was taken up by the larvae (albeit not as strongly as the parent drug) (Table 4.4), exposure to the synthesised metabolite also did not result in concentration-dependent OS (Fig. 4.22). Furthermore, LC-MS/MS also detected DMC in larvae that were only exposed to the parent drug (Table 4.5) and DESI detected clozapine-N-oxide in the tissue, showing that 4 dpf larvae are capable of metabolising Cloz. Unfortunately, DMC could only be ‘tentatively’ identified due to the noisy background created by an abundance of spectral peaks which can occur in the same mass range as the metabolite of interest. This could be mitigated by using the DESI with tandem mass spectrometry (MS/MS) to specifically target Cloz and its metabolites; however, this was not available within the timescale of this project.

4 dpf zebrafish larvae also appear to be able to metabolise CP, which is also activated by hepatic CYP P450 enzymes (Fig. 4.24), as exposure to CP at 8 dpf when the larva possesses the full complement of CYPS (Verbueken *et al.*, 2018) did not increase the toxicity of the drug. This is in contrast with data published by Busquet *et al.* 2008 who co-cultured embryos with CP and mammalian liver microsomes to develop a screening assay combining zebrafish embryos with exogenous mammalian metabolic activation. Embryos exposed to CP alone showed no changes, whereas those co-cultured with microsomes showed teratogenic effects at 3500 µM (Busquet *et al.*, 2008). Conversely, other studies have reported maximum non-lethal concentration (MNLC) of 4213 µM in 3-5 dpf larvae (He *et al.*, 2013) and teratogenic effects at 996 µM – 2999 µM in 0-3 dpf embryos without the external metabolic activation system (Weigt et al., 2011). Further, mRNA expression levels of CAT, SOD1 and SOD2 increased in zebrafish embryos exposed for 96 hrs to 1341 µM CP, although this did not translate to changes in actual enzymatic activity (Aderemi *et al.*, 2020).

On balance, the present data combined with the literature suggests that 4 dpf zebrafish larvae can metabolise CP and are vulnerable to its toxic effects. CP likely did not induce a response in the EpRE:mCherry model in the initial screen (Fig. 4.16) simply because the drug was less potent than expected, as 3830 µM later did induce OS in both 4 dpf and 10 dpf larvae. However, in the 4 dpf larvae, malformations were also observed at this concentration (e.g., stunted tails) (Fig. 4.25 Ai). This implies that, in keeping with the literature, CP can have teratogenic effects in early-stage embryo-larvae. However, unlike the other drugs tested here, CP appears to only induce significant OS at concentrations also high enough to cause overt toxicity, suggesting this is one example of a drug where EpRE:mCherry cannot be helpful. Indeed, Aderemi *et al.* also did not find any changes in CAT activity at sublethal concentrations (Aderemi *et al.*, 2020). Given the previous studies which showed toxic effects in the mM range (Aderemi *et al.*, 2020; Weigt *et al.*, 2011), it does not seem appropriate to test the EpRE:mCherry model at this concentration range as the malformations would impair measurements of tissue-specific OS. As mentioned in section 4.3.5.2, the change in most vulnerable organ from PD (in 4 dpf larvae) to PT (in 10 dpf larvae), may simply be a result of malformations in the 4 dpf larvae obscuring the PT

fluorescent signal. As with every drug which has induced malformations, the fluorescent signal should be interpreted with caution.

In contrast with CP, little is known about the mechanism by which Cloz can be toxic to aquatic wildlife. 0.09 µM Cloz has been shown to significantly impact survival of fathead minnow larvae (Overturf *et al.*, 2012), but the effect of Cloz on zebrafish has mostly been investigated in the context of screening drugs for possible side effects (de Alvarenga et al., 2017; Lee et al., 2013), and there are numerous *in vitro* and *in vivo* studies which have implicated OS in mediating toxic side effects in patients (Abdel-Wahab & Metwally, 2015; Hendouei *et al.*, 2018; Pereira & Dean, 2006; Reinke *et al.*, 2004). The data presented here suggests that Cloz does not have the potential to induce OS in the environment.

Together, the present data indicate that 4 dpf zebrafish are able to bioactivate CP and Cloz, and metabolism does not influence the pro-oxidative capacity of these two drugs at this life stage.

CAM is also mainly metabolised by CYP P450 isozymes (Rodvold, 1999) into its major metabolites 14-hydroxy(R)-clarithromycin (pharmaceutically active) and N-desmethyl-clarithromycin (inactive) (Baumann *et al.*, 2015). In contrast to IBF or CP, the evidence in the literature for the pro-oxidative action of CAM is much weaker. CAM has been reported to induce OS in green algae (Guo et al., 2020), and a mixture of 15 common environmental antibiotics at 3 nM, including CAM , induced ROS generation in the ovaries of adult zebrafish (Qiu *et al.*, 2020). Conversely, zebrafish embryos showed no OS (Yan *et al.*, 2019) and no toxic effects in response to CAM or its major metabolite 14-hydroxy(R)-clarithromycin (Baumann *et al.*, 2015). Therefore, the lack of response in the EpRE:mCherry model wasn't as unexpected as IBF or CP.

Although not tested in this chapter, evidence in the literature shows zebrafish at 72 – 96 hpf also appear to be able to metabolise IBF, as LC-MS/MS data shows 72hpf larvae exposed to IBF for 24 hours produce hydroxyl-ibuprofen (Jones et al., 2012), and the biotransformation of IBF by CYP2C9 can result in generation of ROS such as the hydroxyl radical and the superoxide anion (Uno et al., 2012).

Lack of metabolism is therefore not a likely reason for the absence of a response in the EpRE:mCherry model. A possible answer may be the internal IBF concentration because, although LC-MS/MS showed relatively high uptake of the

drug (up to 140 %; Table 4.4), it did not reach HTPC (up to 41 µM in the larvae compared to 73.71 µM $HTPC_{min)}$. Based on the lipophilicity of the drug, IBF was not predicted by the FPM to reach HTPC in exposed larvae (with a maximum effect ratio of 10.68; Table 4.3), but poor solubility had precluded the use of higher exposure concentrations. Naturally, HTPC does not always predict the response threshold for fish due to evolutionary divergence in, for example, drug-target activation or physiology (Brown et al., 2014). However, HTPC can be helpful by providing context to the fish plasma concentration.

Evidence in the literature appears to suggest IBF has highly variable bioavailability, with bioconcentration factors ranging from 0.08 – 1.4 L/Kg in fathead minnows and channel catfish (Nallani et al., 2011), and 9 L/Kg for rainbow trout after 48hr exposure (Brown et al., 2007). In the present study, IBF also partitioned into the embryo-larvae much more than had been predicted by the FPM, as has also been reported by previous studies (Huggett et al., 2004; Patel et al., 2016). This difference is expected to be due to the assumptions made by the FPM, namely that the drug has reached a steady state within the body of the larva, while the data presented represent a snapshot at the end of a 4-day exposure when the animal may have still been undergoing active/passive uptake. Additionally, FPM values based on $LogD_{ow}$ values assume that drug partitioning is driven purely by its lipophilicity and does not consider metabolism, excretion, or protein binding (Huggett *et al.*, 2003). FPM values should therefore be interpreted with caution.

IBF may not have induced OS in the model due to low potency/insufficient internal concentration, but previous studies have reported adverse effects caused by IBF at exposure concentrations lower than those tested here. Fathead minnow *(Pimephales promelas*) larvae exposed from 24-72 hpf showed therapeutic effects (reduced prostaglandin E metabolite levels) at 1.8 µM, well below HTPC (Patel *et al.*, 2016). Further, perturbed antioxidant levels and resultant teratogenic effects were shown in common carp (*Cyprinus carpio*) embryos at 7.3 nM IBF (Gutiérrez-Noya *et al.*, 2020). However, a chronic exposure of zebrafish to up to 121 µM IBF only showed an increase in GPx, but no change in GR or CAT activity, suggesting the OS response to IBF in zebrafish is more complex than indicated by other species (Bartoskova *et al.*, 2013). Even within one species, IBF has also

previously been found to have high inter-individual variation in concentration-dependent responses (Patel *et al.*, 2016).

Therefore, IBF either had not reached a sufficient internal concentration to cause an effect in the larvae or it has a very species-specific effect and does not induce OS in zebrafish larvae. In contrast, the evidence in the literature for OS-induction by Cloz or CAM so they may not exert toxicity through OS induction (see Table 4.1). Alternatively, any of these three drugs may induce OS via a different pathway not visualised by the EpRE-mediated mCherry, such as via inhibition of downstream antioxidants. Alternative OS pathways and the effects of antioxidants are explored more in chapter 5.

*Table 4.6* ***Summary of OS screen and uptake assays****, with postulated explanations on why each drug gave a weak or no response in the EpRE:mCherry model. Red indicates a response was observed in the model, green indicates there was no response, and yellow indicates a weak response only seen in specific exposure conditions.*

| Compound | Response seen in model at 4dpf? | Comments on weak or no response |
|---|---|---|
| **Paracetamol (APAP)** (positive control) | Yes | |
| **Atenolol (ATL)** (negative control) | No | LC-MS/MS shows the drug was taken up, but had no effect on OS. Functioned as a negative control. |
| **Diclofenac (DCF)** | Yes | |
| **Ibuprofen (IBF)** | No | Drug was taken up by larvae, but LC-MS/MS data and FPM indicate therapeutic plasma concentrations were not reached. Poor solubility limited the exposure concentration range, could therefore of insufficient concentration to exert effect, giving a false negative. Evidence in literature also suggests complex, species-dependent influence on OS, so could exert OS via pathway excluding the EpRE. |
| **Doxorubicin (Dox)** | Yes | |
| **Cisplatin (Cis)** | Weak | Narrow response range; 4 day exposure resulted in overt toxicity and tissue damage, impeding mCherry expression. OS only detected following 2 day exposure. |
| **Cyclophosphamide (CP)** | Weak | OS only detected at 1g/L, showing weak pro-oxidative action. Low uptake detected. No observed effect of later-stage exposure, assumed to be metabolised as early as 4 dpf. |
| **Clarithromycin (CAM)** | No | Evidence of OS induction in literature is weak. On balance, CAM probably does not induce OS in zebrafish embryos. |
| **Clozapine (Cloz)** | No | Evidence here of uptake and bio-activation at 4 dpf. Evidence in literature of OS induction, albeit limited in fish. May induce OS via pathway not involving the EpRE |

## 4.5 Conclusions

One of the biggest challenges currently facing the ecotoxicology field is sheer number and range of chemical pollutants in the environment, including emergent and legacy compounds. There is therefore an urgent need to develop tools and frameworks for the prioritisation of these compounds for risk assessment. Here, the EpRE:mCherry model has been demonstrated as a viable favourable system to rapidly screen pharmaceuticals for their potential to induce OS, thereby allowing their prioritisation for further study. The model can also be used to identify drug-specific vulnerable tissues, offering a means to refine future studies for more targeted assessments.

However, for the compounds tested it does not appear to have the sensitivity to detect these compounds at environmentally relevant exposure levels, albeit this may also be related to the lack of uptake for some for these compounds seen in these studies. It is also possible that some of the pharmaceuticals tested do not induce OS at environmental concentrations in the zebrafish. Thus, possible reasons for no OS detected in the EpRE:mCherry include: a) the pharmaceuticals are not pro-oxidative at the concentrations tested, b) OS is induced via a pathway not involving the EpRE, c) the compounds did not reach an effective concentration within the larvae. Lack of bio-activation was ruled out as a possible reason for the absence of a response for the drugs included in this screen.

Exposure to a synthetically activated pharmaceutical (DMC) or exposure of 8 dpf larvae (to CP) appeared to have no impact on the toxicity of the drugs. This suggests that, contrasting with the initial hypothesis, 4dpf larvae are capable of metabolising, and therefore activating, pro-drugs and so exposure to a metabolite or a parent drug at a later life stage had no impact on the potency of the response. This is further supported by the analytical chemistry data which detected DMC in the larvae following Cloz exposure.

The benefit of analytical chemistry in chemical effects assessments has also been demonstrated in this chapter by strengthening our understanding of how uptake of the compound relates to its toxicity profile. Regarding understanding the EpRE:mCherry model, chemical analyses have revealed that internal concentration (predicted and measured) did not always correlate to the response in the model for the compounds tested (Table 4.6), particularly in the case of pro-drugs. However, the FPM could provide a useful starting point for future studies

to establish exposure range for further testing of pharmaceuticals, which can be corroborated using LC-MS/MS to refine the study design. In the case of CAM and Cloz, the predicted and measured internal concentrations imply that, despite uptake into the larval body, these drugs may have not been bioavailable or have different mechanisms of toxicity which may not include OS.

Although limitations imposed by the pandemic limited exploration of the technique, the application of MSI was briefly demonstrated. Several studies have previously used MSI to localise pharmaceuticals in tissue (Reyzer and Caprioli 2007; Reyzer *et al.* 2003; Atkinson *et al.* 2007; Drexler *et al.* 2007; Signor *et al.* 2007). DESI, specifically, has been used to analyse adult zebrafish following chemical exposure (Perez et al., 2017), and to visualise lipid dynamics in zebrafish embryos (Pirro *et al.*, 2016). However, it has rarely been used to analyse zebrafish embryo-larvae due to the challenge of sectioning the small, fragile tissue samples (as demonstrated by the sections shown in Fig. 4.23). Due to time constraints, the methodology for DESI could not be further optimised and only Cloz was tested. Nevertheless, Fig. 4.23 does demonstrate the potential of MSI for visualising the distribution of pharmaceuticals and their metabolites in the body of zebrafish larvae, and how this could be related to the fluorescence response profile observed in a TG model. Future studies could usefully combine these tools to build a strong AOP by directly linking the presence of a compound in the tissue to the upregulation of a gene of interest, as visualised in the TG model.

One of the objectives for the use of the EpRE:mCherry model was also to provide a system for detecting OS induction in an intact organism without inducing significant harm. The work presented further supports that the fluorescence induction is sufficiently sensitive to indicate OS before overt toxicity is observed. The data also illustrates that, as an exposure regimen becomes overtly toxic, the induction of more severe effects such as tissue damage or malformations can impair the ability of an imaging platform to detect tissue-specific OS in the TG model. For instance, a longer period of Cis exposure resulted in tissue damage so it could no longer produce mCherry fluorescence, and 5 mM APAP resulted in malformations which obscured the fluorescent signal. However, this is a factor that most TG models must contend with in order to achieve accurate fluorescence analysis. Additionally, as the EpRE:mCherry model was designed as a biosensor

for non-toxic levels, overt toxicity can be avoided using careful concentration range and exposure period selection. For example, this was seen with DCF which was also highly potent and exhibited a very steep response curve in that OS began to be observed at 1.4 µM DCF exposure with no malformations, but less than a 3 x concentration increase resulted in pericardial oedemas and delayed hatching. Nevertheless, this is an important consideration to bear in mind when designing future experiments or interpreting concentration-responses.

# Chapter 5- Interactions of oestrogen with OS measured in the EpRE:mCherry transgenic zebrafish model

## 5.1 Introduction

Many compounds can act as oestrogens, including plasticisers (Mathieu-Denoncourt et al., 2015), fertilisers (Verderame et al., 2016) and pharmaceuticals (Badamasi et al., 2020; Corcoran et al., 2010). These chemicals enter waterways via sewage and run-off from agriculture, urban environments, and from land-fill sites (Adeel et al., 2017; Badamasi et al., 2020). As mentioned in Chapter 3, oestrogens in the environment are a concern as they have been linked to feminisation of fish and a range of other impacts on the development and reproductive functions of aquatic organisms. EE2 is a potent contraceptive oestrogen that is detected in waterways in the low ng/L range (Laurenson *et al.*, 2014) and has been proven to be associated with inducing feminised responses in wild fish populations (Tyler & Jobling, 2008).

Drugs are generally present in the environment as complex mixtures. Indeed, one monitoring study detected 56 pharmaceuticals in the effluent of US sewage treatment plants (Kostich et al., 2014). Similarly, a study on the effects of chemical pollutants in a Mediterranean river detected 57 pharmaceuticals from 14 different therapeutic groups (Proia *et al.*, 2013), thus illustrating the widespread presence of multiple types of active pharmaceutical ingredients (APIs) in the environment. This illustrates the need to consider co-exposure conditions in order to fully understand the potential environmental risks of exposure to pharmaceuticals in aquatic systems (Backhaus, 2016).

The issue of mixture effects is a rapidly growing field of study and there have been numerous studies on the effects of mixtures of oestrogenic chemicals. Using a zebrafish TG model for detecting brain aromatase (Cyp19a1b-GFP), it has shown that mixtures of EE2, estradiol (E2), oestrone (E1), BPA and 4-octyl phenol (OP) are additive in their biological effects (Petersen *et al.*, 2013). Conversely, Hinfray *et al.* (2018), also using the TG brain aromatase zebrafish

model, found an antagonistic effect between the natural oestrogen E2 and the phytoestrogen genistein (Hinfray *et al.*, 2018), illustrating that oestrogenic chemicals have potential for different interactive effects.

Data on the interactions of pollutants from different chemical classes or with different modes of toxicity are less common. Duan *et al.* (2016) used a combination of embryos from a wild type (WT) line, and TG lines fli-1:EGFP for detecting endothelial damage and mpo:GFP for detecting inflammatory responses mediated by neutrophils to demonstrate endothelial damage, inflammatory response and OS in response to co-exposure to silica nanoparticles and methyl mercury (Duan *et al.*, 2016). This further supports the need for studies to consider co-exposure effects, and illustrates the utility of TG models to facilitate this.

There is growing evidence that oestrogens can influence an array of physiological processes, not only those related to the endocrine system and fertility, but also the regulation of heartbeat (Romano *et al.*, 2017) and non-reproductive behaviours (Porseryd *et al.*, 2019). There is also some evidence derived from isolated liver mitochondria that oestrogens may protect against the effects of OS by upregulating antioxidant enzymes via intracellular signalling pathways (Borrás et al., 2010) (Fig. 5.1). In their study, Borrás *et al.* reported that normal levels of intracellular E2 prevented reactive oxygen species (ROS) formation and protected mitochondrial integrity via its interaction with ERs (as opposed to its phenolic structure). There is also evidence of the neuroprotective role of oestrogen through antioxidative action; inhibition of oestrogen has been shown to exacerbate OS in neuronal (but not glial-derived) cells derived from rats (Duong *et al.*, 2020). However, supplementation of oestrogen after an OS event resulted in exacerbation of the damage, suggesting oestrogen is not protective in an OS environment (Duong *et al.*, 2020). Additionally, clinical research indicates that, through maintenance of signalling cascades to minimise OS, oestrogen can potentially attenuate the progression of degenerative diseases such as Alzheimer's (Uddin *et al.*, 2020). However, there is scant data on the protective properties of oestrogen in fish.

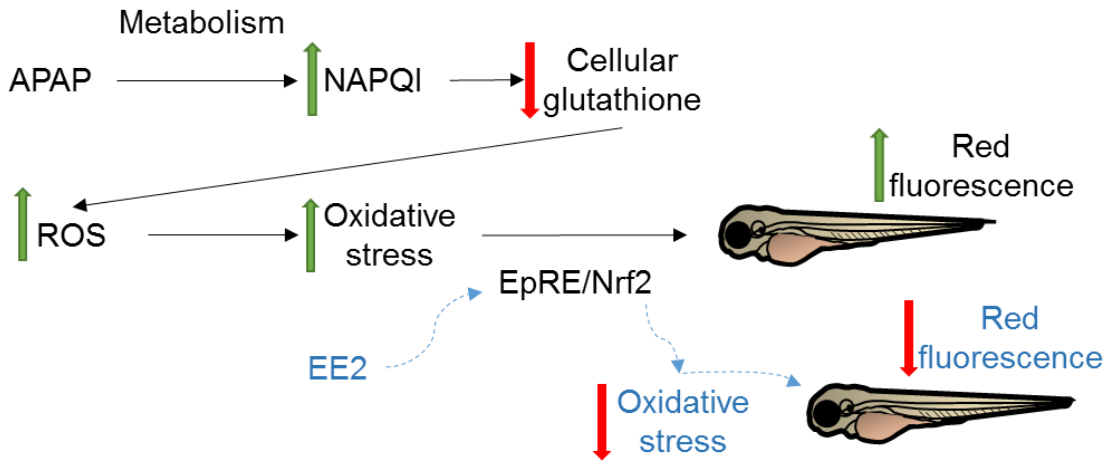


*Figure 5.1* ***Scheme illustrating the potential interaction between oestrogens and OS****. The known pathway by which APAP induces OS, and therefore red fluorescence, in the EpRE:mCherry model is shown in black. EE2 may reduce OS via the intracellular signalling pathways shown in blue.*

This also prompts the question: can xenoestrogens also buffer against OS? There are limited *in vivo* studies into this interaction, but genistein has been shown to upregulate antioxidant levels and reduce APAP-induced OS in mice (Wang et al., 2020a). Conversely, a study using Japanese sea bass (*Lateolabrax japonicas*) found a correlation between estradiol exposure and ROS generation in hepatic tissue (Thilagam et al., 2010).

This chapter set out to investigate the interaction between drug-induced OS and exposure to an exogenous oestrogen, as well as the presence of endogenous oestrogen in zebrafish *in vivo*. The main aims were:

d) Identify an antioxidative control and confirm if a reduction in OS can be quantified in the EpRE:mCherry model.
e) Optimise an exposure protocol to assess the antioxidative capacity of EE2 and compare this against the positive control
f) Assess the role of endogenous oestrogen in buffering OS by inhibiting oestrogen receptors and quantifying the effect on APAP-induced OS.

The first requirement was to establish an anti-oxidant positive control to confirm whether it was possible to reduce OS in zebrafish larvae through exposure to an exogenous antioxidant compound, and that this effect could be visualised in the EpRE:mCherry model. The three antioxidants tested as potential positive controls were N-acetylcysteine (NAC), N-acetylcysteine amide (NACA) and L-glutathione reduced (LGR). NAC is a precursor to the cellular antioxidant GSH, used to treat patients suffering from APAP-overdose and has been accepted as the most

effective therapy since the 1970s (Polson & Lee, 2005; Saito et al., 2010). NACA is a modified form of NAC in which the carboxyl group has been replaced with an amide, thereby improving its lipophilicity and rendering the compound more readily bioavailable (Ates et al., 2008). NACA has been found to be more effective at lower concentrations compared to NAC in buffering against APAP-induced OS in mice (Khayyat et al., 2016). NAC and NACA work by promoting hepatic GSH synthesis which contributes to NAPQI detoxification (Saito *et al.*, 2010). LGR, a synthetic version of GSH, is a thiol antioxidant shown previously to buffer OS in rabbits (Atakisi *et al.*, 2010) and in a Parkinson's TG zebrafish model (pink1:EGFP) (Priyadarshini et al., 2013).

After the optimisation of the application of a positive control and exposure regimen, the effect of EE2 and APAP (the reference pro-oxidative drug) co-exposure was assessed. EE2 was selected as being the most potent (synthetic) oestrogen (Adeel *et al.*, 2017) and a contaminant of significant environmental concern (Laurenson *et al.*, 2014). Furthermore, many other non-pharmaceutical oestrogens, such as plasticisers, have shown potential to induce OS in the environment (Mathieu-Denoncourt et al., 2015; Wu et al., 2011; Xu et al., 2013) and so they were unsuitable for this study as their toxicity may have complicated intrerpretation of the results. The concentration range for the exposures were selected at 0.017 – 0.067 nM EE2 based on the data in Chapter 3, where using the ERE:GFP model a strong oestrogenic response was seen at an exposure of 0.034 nM EE2. Higher concentrations were avoided to ensure absence of toxic effects, whereby the induction of malformations may complicate interpretation of the data; malformations have been observed in zebrafish embryos exposed to EE2 from 0 - 4 dpf, with an EC50 of 0.19 nM (Ramírez-Montero *et al.*, 2022).

The influence of endogenous oestrogen was investigated through co-culturing of embryos with APAP and an ER antagonist, ICI-182, 780 (ICI; also known as fulvestrant). ICI is a selective oestrogen receptor modulator (SERM) and can block activity of all 3 ER subtypes in zebrafish (Notch & Mayer, 2011). It has high affinity for ERs and competitively binds to them, preventing the receptor from locating to the nucleus (Osborne et al., 2004), in turn inhibiting oestrogen-dependent gene expression. ICI has been widely adopted for this purpose in many mammalian studies and fish research studies, including to inhibit GFP expression in the ERE:GFP model (Lee et al., 2012a). Early life aqueous

exposure to ICI has also been shown to result in feminising effects in adult male fathead minnows (Ali et al., 2018). It is also used to treat some forms of cancer (Jiang *et al.*, 2014). A multiple-target TG model expressing reporters for both the OS and oestrogenic response, EpRE:mCherry:ERE:GFP, was also tested for its capacity to visualise both the OS and oestrogenic pathways and any cross-talk between them. This multiple TG line was generated by crossing the EpRE:mCherry model with the ERE:GFP model introduced in Chapter 3.

These approaches were used to test the following hypotheses:

a) OS will be reduced in the presence of an exogenous antioxidant and this effect can be quantified in EpRE:mCherry.
b) EE2, an oestrogenic compound frequently detected in surface waters, can buffer pharmaceutically-induced OS.
c) The anti-oxidant action of EE2 is concentration-dependent and tissue-specific.
d) Endogenous oestrogen also has a role in buffering OS, and its inhibition can exacerbate OS.

## 5.2 Methods

### 5.2.1 Fish husbandry

All imaging/OS measurements were conducted using EpRE:mCherry zebrafish except for the final experiment testing the effect of ICI exposure, which used EpRE:mCherry:ERE:GFP embryo-larvae (Fig. 5.12). Both strains of zebrafish were maintained under the same conditions (see Chapter 2, section 2.1).

### 5.2.1 Compounds

All compounds used in this chapter were obtained from Sigma-Aldrich, Dorset, UK. All stocks other than APAP were made prior to the day of exposure and stored in -20°C. Exposure solutions were diluted in system water on the day of exposure. APAP (CAS no. 103-90-2) was dissolved in 0.5% DMSO to make 50 mM stock. EE2 (CAS no. 57-63-6) was dissolved in 100% methanol to make 220 mg/L (0.7 mM) stock. ICI (CAS number 129453-61-8) was dissolved in 100% DMSO to make 20 mM stock solution. Antioxidants were all dissolved without the use of a solvent. NAC (CAS number 616-91-1) was made to 60 mM stock. NACA (CAS number 38520-9) and LGR (CAS number 70-18-8) were made up in separate 50 mM stocks.

### 5.2.2 Larval assessment

Oestrogens have been postulated to exert their antioxidant effect through upregulation of antioxidants via intracellular signalling, based on mammalian *in vitro* (Borrás *et al.*, 2010) and *in vivo* (Wang et al., 2020a) data. Therefore, mCherry expression in the EpRE:mCherry larvae was analysed for changes fluorescence intensity, which would indicate changes in regulation of the EpRE (and therefore the redox status of the tissue). At the end of the exposure period (at 4 or 6 dpf), larvae were anaesthetised and imaged using the Acquifer, following the protocol described in Chapter 3, section 3.2.3. Image analysis focussed on the liver, PD and PT for three reasons: 1) they are major sites of detoxification and therefore vulnerable to the effects of chemical-induced OS (as explored in Chapters 3 and 4); 2) the liver had shown a strong response to EE2 in the ERE:GFP model (Chapter 3, section 3.3.1), and so was expected to show the greatest response to the antioxidative effects of EE2 compared to other organs; 3) the previous two chapters showed that the liver and pronephros always express mCherry fluorescence, including in chemically untreated larvae. This indicates that these tissues constantly experience a background level of OS, in keeping with what is known about the role of reactive oxygen species (ROS) in cell signalling and of antioxidants in maintaining homeostasis (discussed in Chapter 1). Therefore, the liver and pronephros were expected to respond to antioxidant supplementation, including when they have not been stressed by other chemical exposure.

Overtly toxic effects at the end of the exposure period were assessed by quantifying the degree of malformations observed which were scored from 0-5 (0 = normal development, 5 = extremely curved spine, large cardiac oedema and dark, necrotic tissue).

### 5.2.3 Chemical Exposure

#### *5.2.3.1 Antioxidant selection and optimisation of exposure regimen*

In order to identify and optimise the use of an antioxidant to act as a positive control, embryos were exposed from 6 hpf to either LGR, NAC or NACA for a period of 4 days. After the selection of the antioxidant, embryos were then exposed to a wider range of concentrations in order to select a suitable exposure concentration for the following experiments assessing the interactions between APAP induced OS and exposure to oestrogens.

#### *5.2.3.2 Antioxidant capacity of EE2*

In the first studies conducted to test for the anti-oxidative effect of EE2, embryos were exposed to 2.5 mM APAP and either 10 mM LGR (the positive control) or 0.008, 0.017, 0.034, or 0.067 nM EE2 simultaneously for 4 days (Fig. 5.2A). This however resulted in unexpected levels of OS and malformations (see Results). The exposure regimen using LGR was further optimised: embryos were exposed to 2.5 mM APAP from 0-2 dpf, placed in clean water (CW) and then immediately transferred to 10 mM LGR. The effect of the timing of LGR exposure was tested by keeping the larvae in CW after APAP exposure for either 6 minutes, 30 minutes, 1 hour, 2 hours, or 24 hours before being transferred to the LGR (see Fig. 5.2B).

Following the success of this exposure regimen, the rescue effect of EE2 was tested by exposing larvae to 2.5mM APAP from 0-2 dpf, followed by placing them in clean water, and then immediately transferring them to either CW, 10 mM LGR, or a range of different EE2 concentrations (Fig. 5.2C). This experiment was repeated twice, and a further time with a 4 day exposure to APAP followed by 2 day exposure to the rescue media: either CW, LGR or EE2 (Fig. 5.D).

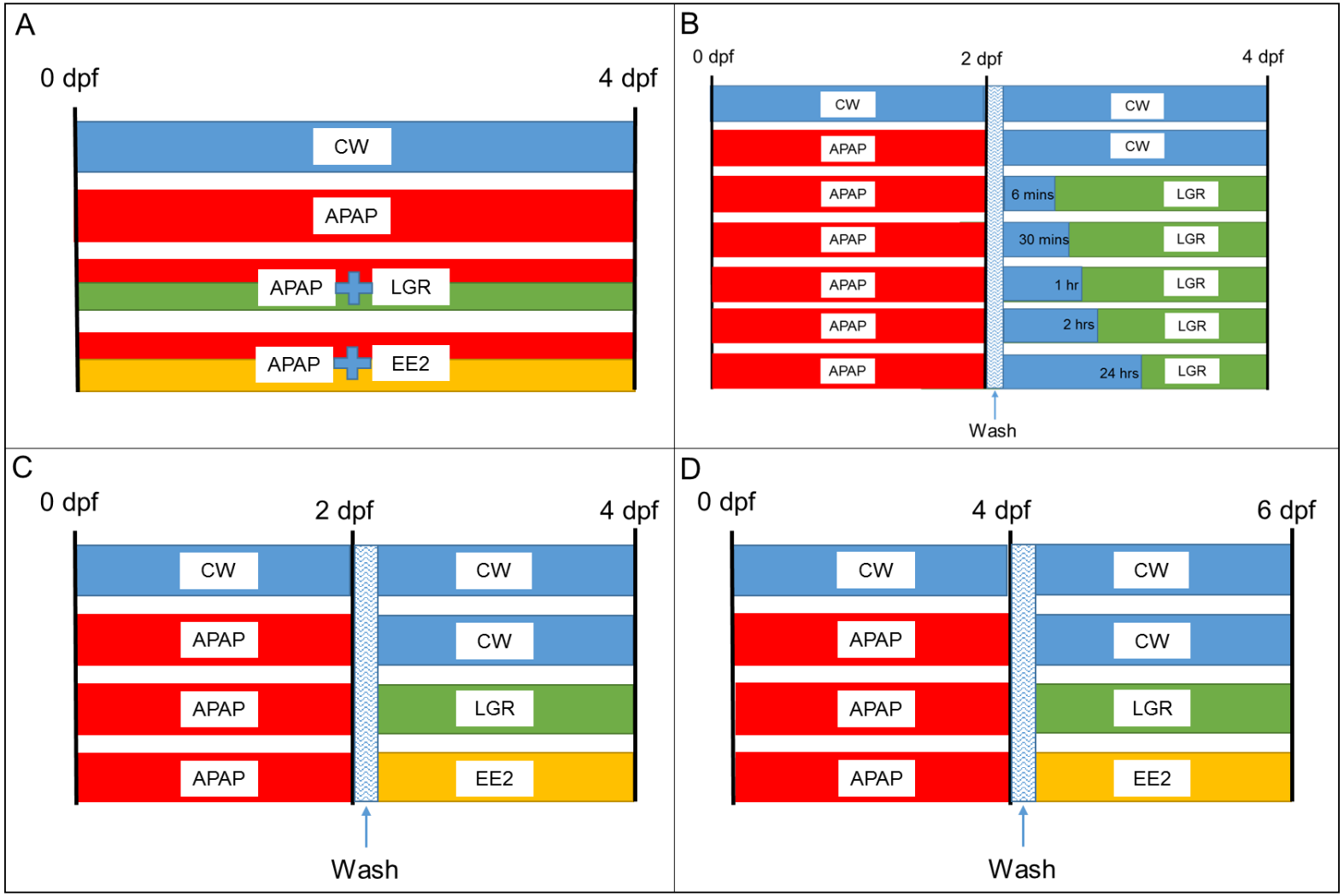


*Figure 5.2* ***Schemes of the various exposure regimens tested.*** *Embryos were exposed from 6hpf to [A] APAP (shown in red) and LGR (green) simultaneously, or APAP and EE2 (yellow) simultaneously; [B] APAP for 2 days and then washed and transferred to LGR after different time intervals in CW (blue); [C] APAP for 2 days and then washed and transferred to LGR or EE2; [D] APAP for 4 days and then washed and transferred to LGR or EE2.*

#### *5.2.3.3 Antioxidant capacity of endogenous oestrogen*

To investigate for the anti-oxidative effects of endogenous oestrogen, EpRE:mCherry embryos were simultaneously exposed to 1, 2 and 4 mM APAP in combination with 20 µM ICI and compared with the OS response induced by APAP exposure alone. In a separate experiment, embryos were exposed to one concentration of APAP only (2.5 mM), either alone or in combination with 20 µM ICI (Fig. 5.3). This exposure regimen was also tested on embryos from the mixed TG line EpRE:mCherry:ERE:GFP in order to confirm if ICI effectively blocked oestrogen (which would be indicated by reduced GFP expression) and if there was any correlation between GFP expression and mCherry expression, which would indicate a relationship between ER activation and EpRE response.

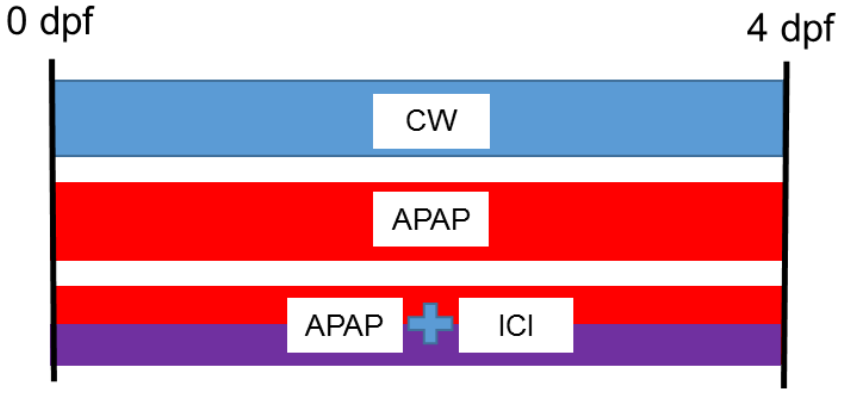


*Figure 5.3* ***Scheme of exposure regimen for testing the effect of the ER antagonist, ICI-182, 780 (ICI)***

### 5.2.3 Image Analysis and Acquisition

At the end of the exposure period, larvae were imaged using the Acquifer and the response quantified using ImageJ following the protocol described in Chapter 3 section 3.2.

Due to the unavailability of the Acquifer during a period of data gathering, the first five experiments were imaged using an Olympus SZX16 epifluorescent stereomicroscope (Tokyo, Japan) and an Andor Zyla sCMOS (UK) camera. Here, embryos were anaesthetised and mounted in agarose grooves using the same protocol as Acquifer imaging, and single z-slices were captured using a Nikon camera. These methods were used for optimisation of the antioxidant exposure regimen and the first experiment testing sequential exposure to APAP then EE2 (Figs. 5.4, 5.5, 5.6, 5.7, 5.8).

### 5.2.4 Statistical analysis

See Chapter 2 section 2.9.

## 5.3 Results

### 5.3.1 Antioxidant selection and optimisation of exposure regimen

NAC and its more bioavailable derivative, NACA, did not significantly affect the mCherry fluorescence intensity in the liver or pronephros compared to the CW control, indicating neither could reduce background levels of OS. LGR, however, did reduce background levels of OS ($P<0.05$) (Fig. 5.4). No oedemas or malformations were observed at any of the adopted concentrations, while 5 and 10 mM LGR were seen to be effective in significantly reducing background OS in most of the organs measured ($P<0.05$) (Fig. 5.5).

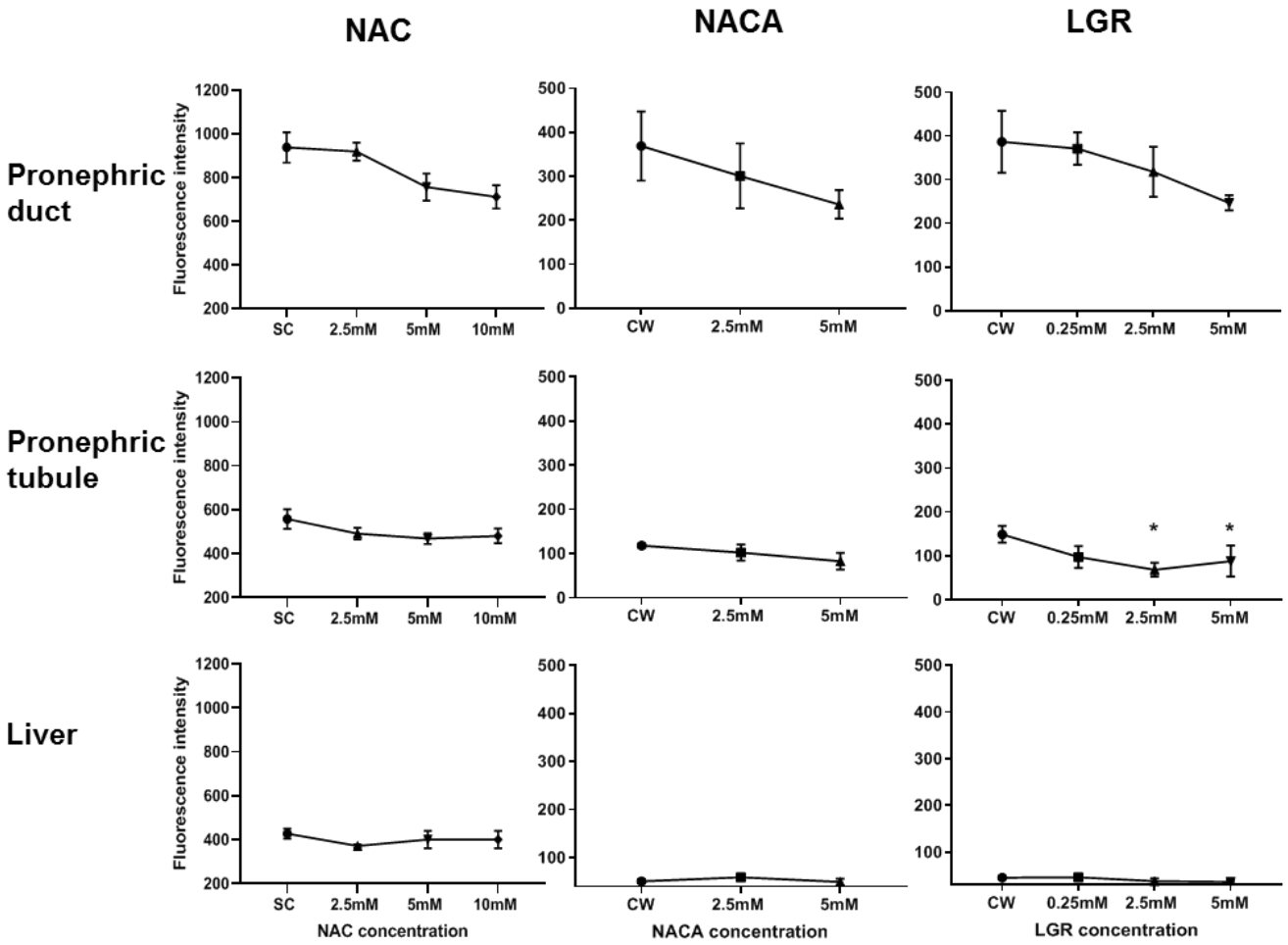


*Figure 5.4* ***Capacity of [left] NAC (N=20); [middle] NACA (N=6); or [right] LGR (N=6) to reduce the background levels of OS in the EpRE:mCherry model.*** *Data shows mean values (+/- SEM) for the mean pixel intensity within the organs of 4 dpf larvae exposed to an antioxidant, SC or CW from 6 hpf. Data was not normally distributed and so was analysed using a Kruskal-Wallis test followed by Dunn's multiple comparisons test, * = P<0.05. Imaged on Olympus epifluorescent stereomicroscope.*

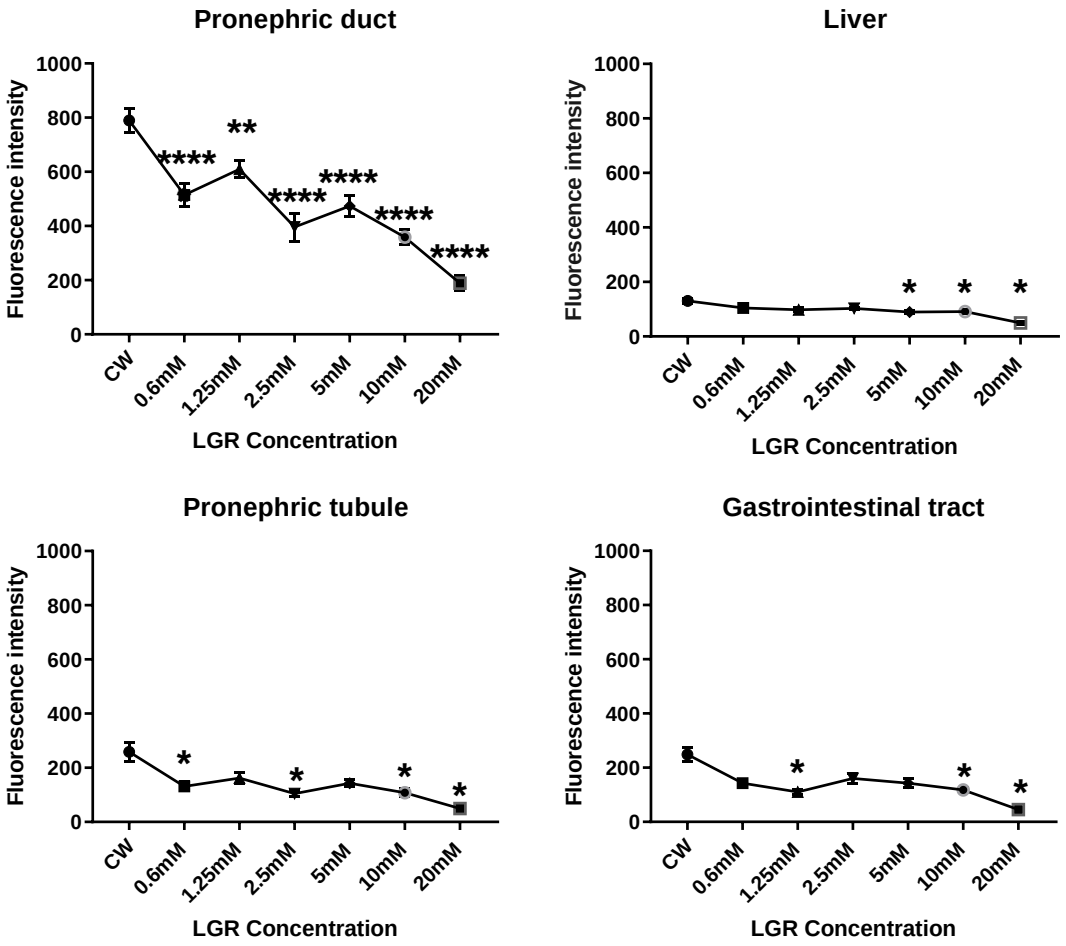


*Figure 5.5* ***Concentration-dependent effect of LGR on background OS.*** *Data shows mean values (+/- SEM, N= 20) for the mean pixel intensity within the organs of 4 dpf larvae exposed to LGR or CW from 6 hpf. Data were not normally distributed and so were analysed using a Kruskal-Wallis test, asterisks represent significant differences to the clean water control (CW). *= P< 0.05, **= P< 0.005, ***= P < 0.0005, ****= P<0.0001. Imaged on Olympus epifluorescent stereomicroscope.*

To test the capacity of LGR to buffer the OS effects of APAP, embryos were exposed to a combination of 2.5 mM APAP and 5 mM or 10 mM LGR at 6 hpf. After 4 days, co-exposure to APAP and 5 mM or 10 mM LGR resulted in similar OS levels to the exposure to APAP alone in the liver and PT. This was only seen in the PD at 10 mM LGR ($P<0.05$) (Fig. 5.6A'). Additionally, toxicity was observed in larvae co-exposed to APAP and LGR as indicated by malformations including curved spines and oedemas (Fig. 5.6B').

In contrast, drug- induced OS was significantly reduced without any malformations when embryos were 'rescued' by LGR exposure following OS induction by APAP. Here, embryos were exposed to APAP from 0 – 2 dpf, then washed once in clean water and immediately transferred to LGR for 2 more days. This exposure regimen was more effective in reducing OS than depuration in CW alone, specifically in the PD and PT. This is reflected in the OS level in the APAP-CW treatment group (in which embryos were left in clean water for 2 days following APAP exposure) which is significantly higher compared to the CW control ($P<0.05$), indicating the larvae were still undergoing OS caused by the APAP. However, the treatment groups in which embryos were transferred to LGR following APAP exposure were not significantly higher than the CW control ($P>0.05$), indicating OS levels had returned to background levels.

However, there was no difference in OS levels between regimens with different time intervals in CW between APAP and LGR exposure (Fig. 5.7).

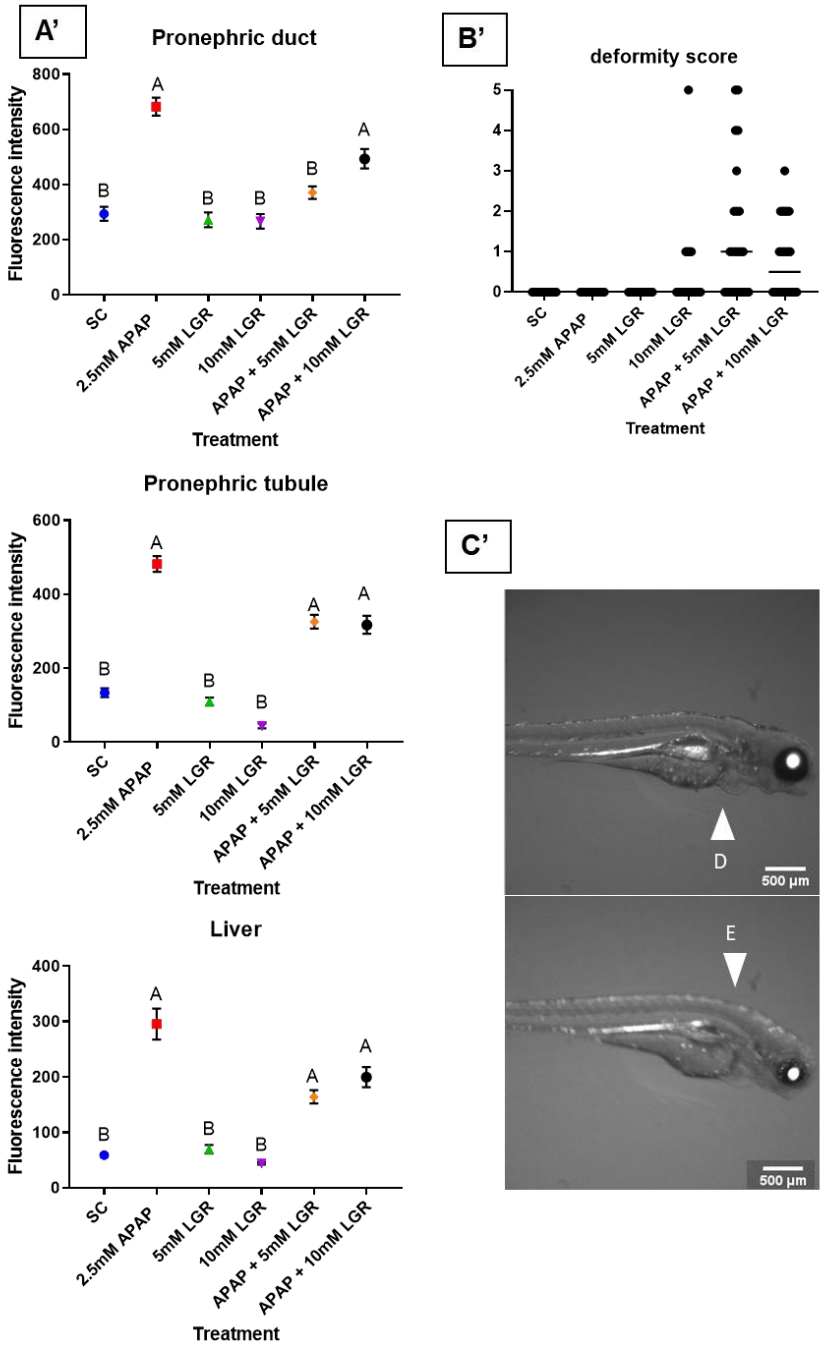


*Figure 5.6* ***Effect of co-exposure to APAP and LGR on OS levels and phenotype of EpRE:mCherry larvae.*** *[A'] Data shows mean values (+/- SEM, N= 24) for the mean pixel intensity within the organs of 4 dpf larvae exposed to APAP, LGR, or a combination of both from 6 hpf. Data were not normally distributed and so were analysed using Kruskal-wallis followed by Dunn's. . A= significant difference (P<0.05) compared to the solvent control-clean water treatment group, B= Significant difference compared to APAP-clean water. [B'] Deformity score for the same experiment. 0 = normal development, 5 = bent spine, large oedema and necrotic tissue. [C'] 4dpf larvae exposed simultaneously to 2.5 mM APAP and 10 mM LGR. [D] Pericardial oedema [E] bent spine. Imaged on Olympus.*

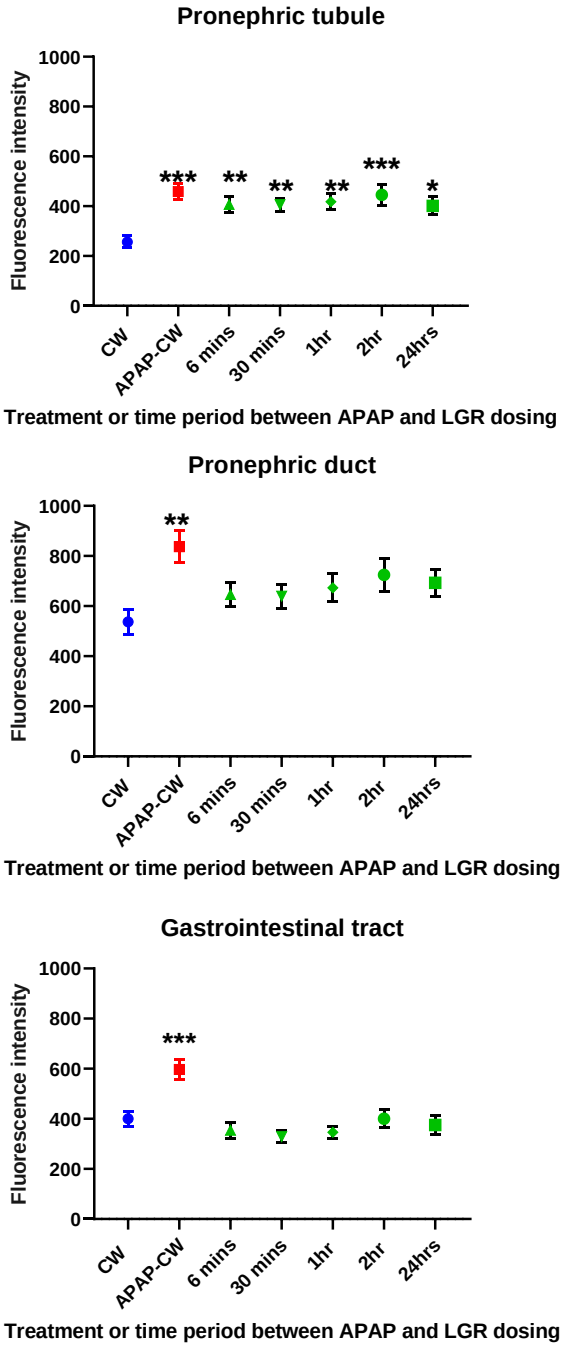


*Figure 5.7* ***Influence of the length of interval between removal of APAP at 2 dpf and addition of 10 mM LGR on the antioxidative action of LGR****. Data shows mean values (+/- SEM, N= 17) for the mean pixel intensity within the organs of 4 dpf larvae exposed to APAP or CW from 6 hpf-2 dpf, then LGR or CW from 2-4 dpf. [Blue] CW control; [red] embryos exposed to APAP for 2 days then left in CW for 2 days; [green] embryos exposed to APAP for 2 days then placed in CW for varying lengths of time and then transferred to LGR. Data were normally distributed with equal variance so analysed using ordinary one-way ANOVA followed by Dunnett's multiple comparison tests. Asterisks show significant difference compared to clean water; *= P< 0.05, **= P< 0.005, ***= P < 0.0005, ****= P<0.0001. Imaged on Olympus.*

### 5.3.2 Antioxidant capacity of EE2

Fig. 5.8 suggested EE2 may have shown some antioxidant action in the PD, shown by lower OS in the embryos treated with 0.017 nM EE2 for 2 days after APAP exposure compared with those left in CW after APAP exposure ($P<0.05$). However, this effect was not seen in repeat studies (Table 5.1). In the liver, no significant OS induction was observed and neither EE2 nor LGR had any effect on OS.

Fig. 5.9 shows the results of 4 day exposure to APAP, followed by 2 day exposure to EE2 or LGR. As data in Chapter 3 had shown that a higher level of OS induced by APAP is detected at 4 dpf compared to 2 dpf, the aim had been to achieve a greater degree of OS by exposing the larvae to APAP for longer, and therefore allow greater scope for OS reduction by an antioxidant. This was expected to reveal more subtle antioxidative effects of LGR or EE2. However, Fig.5.9 shows the extended exposure period had no effect. Additionally, APAP alone (followed by 2 days in CW) failed to induce a significant level of OS in the PD or liver. In contrast, 4 day APAP exposure followed by 2 day LGR or EE2 resulted in significant OS, potentially indicating that these compounds impaired the larvae's ability to recover at this age (even in the case of the positive control; LGR). However, as mentioned above, the negative control group (exposed to APAP and then depurated in clean water) did not behave as expected, suggesting these results should be interpreted with caution.

Most of the experiments follow the regimen of APAP exposure - wash - EE2 exposure because this was the regimen in which LGR was most effective in reducing APAP-induced OS (as discussed above). In order to find if EE2 was more effective when administered to the embryos at the same time as APAP, an assay was conducted in which embryo were exposed to APAP and EE2 simultaneously. However, EE2 again failed to influence OS induction. A summary of results for the statistical analyses for these experiments is shown in Table 5.1 (raw data of the repeated experiments are shown in Appendix 1).

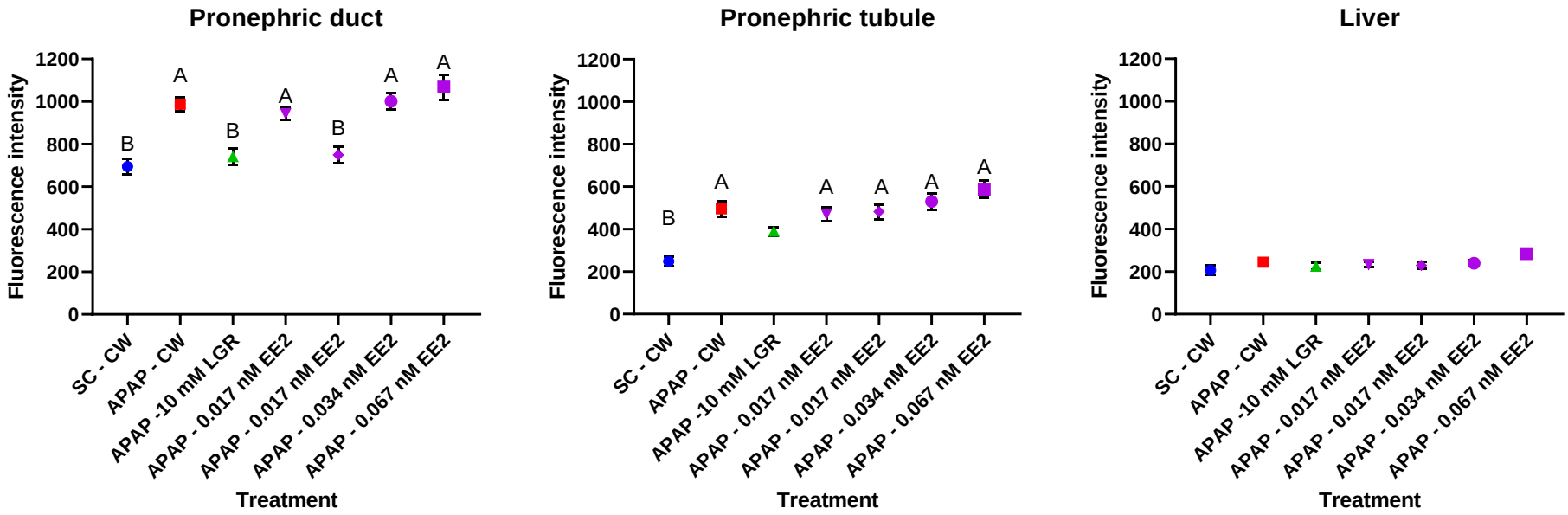


*Figure 5.8* ***Mean fluorescence intensity in 4 dpf larvae after 2 day APAP exposure from 6 hpf followed by 2 day exposure to rescue media (CW, LGR or EE2)*** *(N=24 per treatment). Data shows mean values (+/- SEM, N= 24) for the mean pixel intensity within the organs of 4 dpf larvae. Data were normally distributed with equal variance and so were analysed using a one-way ANOVA followed by Dunn's multiple comparisons test on Graphad Prism. A= significant difference (P<0.05) compared to the solvent control-clean water treatment group, B= Significant difference compared to APAP-clean water. Imaged on Olympus. Malformations were not above background level*

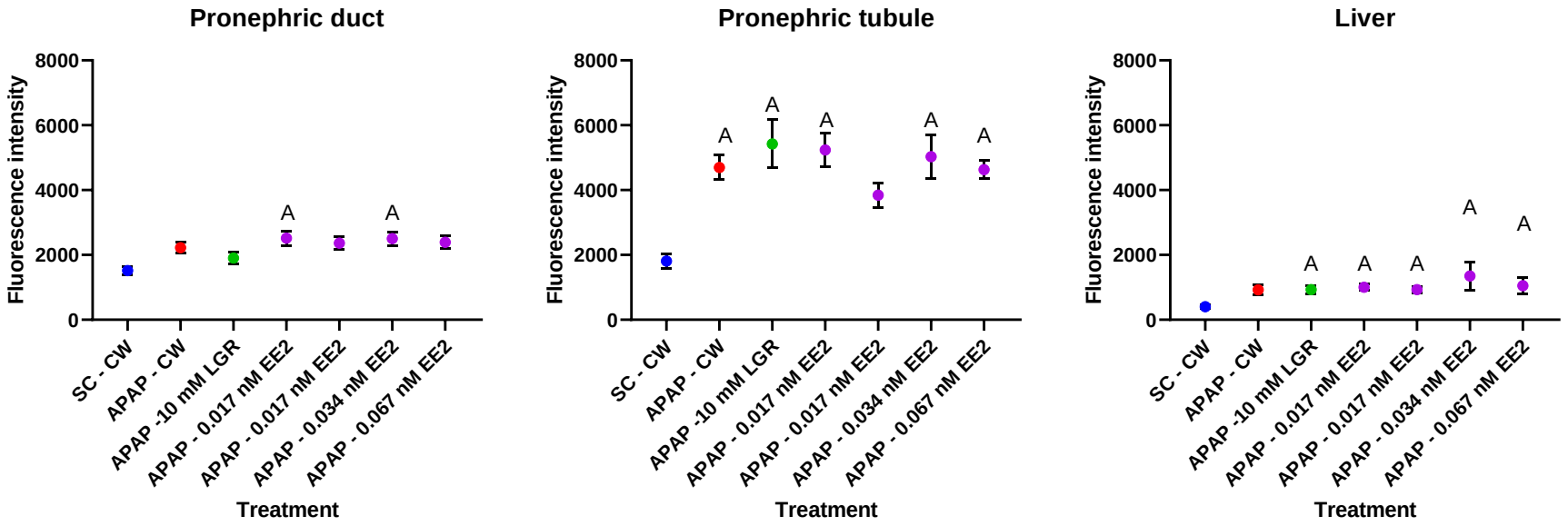


*Figure 5.9* ***Mean fluorescence intensity in 6 dpf larvae exposed to 2.5 mM APAP from 0-4 dpf, then a range of rescue media from 4-6dpf****. Data shows mean values (+/- SEM, N= 12) for the mean pixel intensity within the organs larvae. Data were not normally distributed and so were analysed using a Kruskal-Wallis test followed by Dunn's.. A= significant difference (P<0.05) compared to the solvent control-clean water treatment group. Imaged on Acquifer.*

| Experiment name | Tissue | Treatment group A | Treatment group B | significance |
|---|---|---|---|---|
| Rescue at 2 dpf | PD | SC - CW | APAP - CW | **** |
| | | SC - CW | APAP -10 mM LGR | ns |
| | | SC - CW | APAP - 0.008 nM EE2 | *** |
| | | SC - CW | APAP - 0.034 nM EE2 | **** |
| | | SC - CW | APAP - 0.067 nM EE2 | **** |
| | | APAP - CW | APAP -10 mM LGR | *** |
| | | APAP - CW | APAP - 0.017 nM EE2 | *** |
| | PT | SC - CW | APAP - CW | **** |
| | | SC - CW | APAP -10 mM LGR | ns |
| | | SC - CW | APAP - 0.008 nM EE2 | *** |
| | | SC - CW | APAP - 0.017 nM EE2 | **** |
| | | SC - CW | APAP - 0.034 nM EE2 | **** |
| | | SC - CW | APAP - 0.067 nM EE2 | **** |
| | | APAP - CW | any other treatment group | ns |
| | Liver | No significance | | |
| Rescue at 2 dpf repeat | PD | No significance | | |
| | PT | SC - CW | APAP - CW | **** |
| | | SC - CW | APAP -10 mM LGR | *** |
| | | SC - CW | APAP - 0.008 nM EE2 | **** |
| | | SC - CW | APAP - 0.017 nM EE2 | *** |
| | | SC - CW | APAP - 0.034 nM EE2 | **** |
| | | SC - CW | APAP - 0.067 nM EE2 | **** |
| | | APAP - CW | any other treatment group | ns |
| | Liver | SC - CW | APAP - CW | **** |
| | | SC - CW | APAP -10 mM LGR | ** |
| | | SC - CW | APAP - 0.008 nM EE2 | **** |
| | | SC - CW | APAP - 0.017 nM EE2 | **** |
| | | SC - CW | APAP - 0.034 nM EE2 | **** |
| | | SC - CW | APAP - 0.067 nM EE2 | ** |
| | | APAP - CW | any other treatment group | ns |
| Rescue at 4 dpf | PD | SC - CW | APAP - CW | ns |
| | | SC - CW | APAP -10 mM LGR | ns |
| | | SC - CW | APAP - 0.008 nM EE2 | ** |
| | | SC - CW | APAP - 0.017 nM EE2 | * |
| | | SC - CW | APAP - 0.034 nM EE2 | * |
| | | SC - CW | APAP - 0.067 nM EE2 | * |
| | | APAP - CW | any other treatment group | ns |
| | PT | SC - CW | APAP - CW | ** |
| | | SC - CW | APAP -10 mM LGR | *** |
| | | SC - CW | APAP - 0.008 nM EE2 | *** |
| | | SC - CW | APAP - 0.017 nM EE2 | ns |
| | | SC - CW | APAP - 0.034 nM EE2 | ** |
| | | SC - CW | APAP - 0.067 nM EE2 | ** |
| | | APAP - CW | any other treatment group | ns |
| | Liver | SC - CW | APAP - CW | ns |
| | | SC - CW | APAP -10 mM LGR | * |
| | | SC - CW | APAP - 0.008 nM EE2 | ** |
| | | SC - CW | APAP - 0.017 nM EE2 | * |
| | | SC - CW | APAP - 0.034 nM EE2 | ** |
| | | SC - CW | APAP - 0.067 nM EE2 | * |
| | | APAP - CW | any other treatment group | ns |
| Simultaneous dose 0-4 dpf | PD | SC | APAP | *** |
| | | SC | APAP + 0.013 nM EE2 | *** |
| | | SC | APAP + 0.017 nM EE2 | **** |
| | | SC | APAP + 0.020 nM EE2 | *** |
| | | SC | APAP + 0.024 nM EE2 | **** |
| | | APAP | any other treatment group | ns |
| | PT | SC | APAP | *** |
| | | SC | APAP + 0.013 nM EE2 | **** |
| | | SC | APAP + 0.017 nM EE2 | **** |
| | | SC | APAP + 0.020 nM EE2 | **** |
| | | SC | APAP + 0.024 nM EE2 | **** |
| | | APAP | any other treatment group | ns |
| | Liver | SC | APAP | * |
| | | SC | APAP + 0.013 nM EE2 | * |
| | | SC | APAP + 0.017 nM EE2 | ns |
| | | SC | APAP + 0.020 nM EE2 | * |
| | | SC | APAP + 0.024 nM EE2 | *** |
| | | APAP | any other treatment group | ns |

*Table 5.1* ***Results of statistical analyses of experiments in Figs. 5.8 and 5.9, including repeats.*** *Values highlighted in green indicate suppression of the OS response, while those highlighted in red indicate significant OS was not induced by APAP and so no conclusion can be drawn on the antioxidative effect of EE2 or LGR*

### 5.3.3 Antioxidant capacity of endogenous oestrogen

The data appears to suggest that endogenous oestrogen may play a protective role. This is particularly seen in the PT where OS induced by 1 mM and 4 mM APAP was exacerbated by co-exposure to the oestrogen blocker ICI (Fig. 5.10). However, this effect was not concentration-dependent and was not seen for the repeat studies (Fig. 5.11 and Table 5.2). Table 5.2 shows a summary of the statistical results for these experiments (raw data are shown in Appendix 1). The ER antagonist alone did not induce any visible malformations, and no differences were observed between embryos exposed to ICI at day 0 and those exposed at day 2 (data not shown).

The highest APAP concentration (alone and in combination with ICI) resulted in some oedemas and curved spines, which may have interfered with fluorescence measurements by blocking or attenuating the signal from deeper tissue (as discussed in Chapter 4). Additionally, in the experiment shown in Fig. 5.10, fluorescence was observed in the neuromasts in the embryos treated with 1mM APAP and ICI only (Fig. 5.10 insert), which had not been seen in previous APAP exposures.

The data in Fig. 5.10 does indicate an additive interaction between APAP and ICI, but there was high variation and it was not statistically significant. The larvae co-exposed to APAP and ICI appear to group into 2 sub-populations, which was particularly distinct for the liver and GI tract. ICI reduced GFP fluorescence in the liver of the multiple TG EpRE:mCherry:ERE:GFP model (Fig. 5.12), indicating the compound was effective in blocking the ER, but this did not correspond to a change in mCherry fluorescence. These data should be interpreted with caution as the embryos were spawned by a heterozygous adult stock.

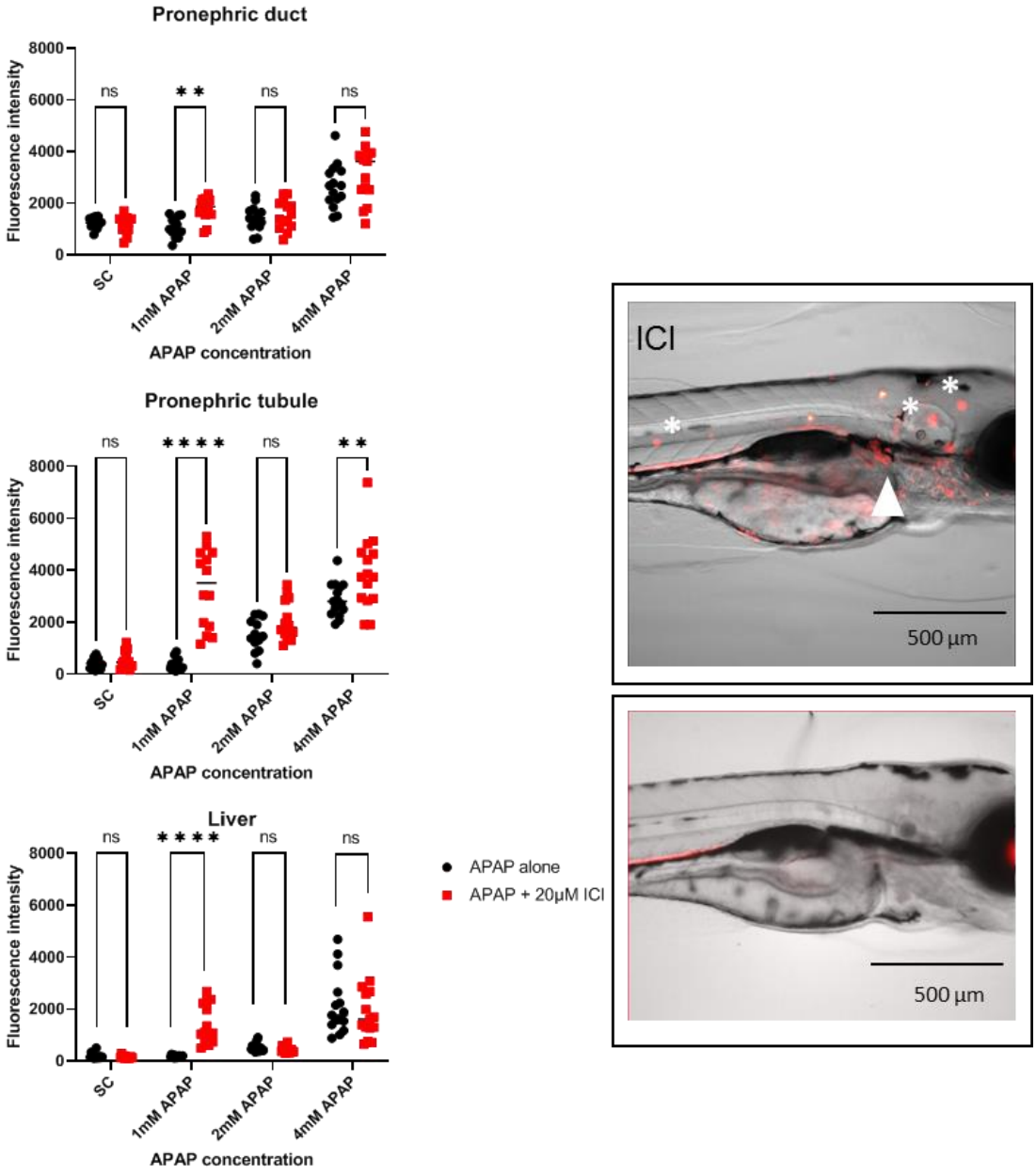


*Figure 5.10 OS* ***response to co-exposure to 20μM ICI and a range of concentrations of APAP****. Data shows mean values (+/- SEM, N= 15) for the mean pixel intensity within the organs of 4 dpf larvae exposed to APAP alone or in combination with ICI from 6 hpf. Data were normally distributed with equal variance and so analysed using an ANOVA followed by Bonferroni, or Mann-Whitney, asterisks show significant difference compared to solvent control (SC); *= P< 0.05, **= P< 0.005, ***= P < 0.0005, ****= P<0.0001. Embryos in the top concentration of APAP showed deformities such as oedemas and curved spines, which may have interfered with organ-specific fluorescence. 1mM APAP + ICI group interestingly also showed fluorescence in neuromasts. Insert shows 4dpf larvae exposed to 1mM APAP and 20μM ICI. Particularly clear in this image are the PT [arrow] and neuromasts on the head [*]*

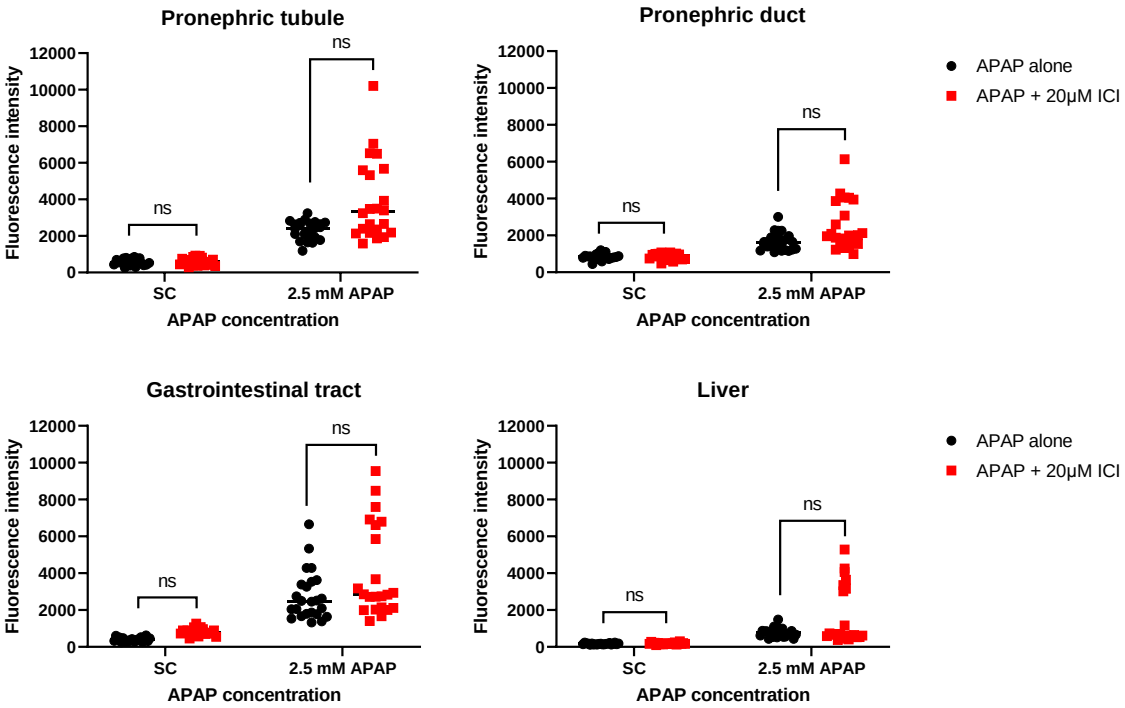


*Figure 5.11* ***OS response to co-exposure to 2.5 mM APAP and 20 μM ICI.*** *Data shows mean values (+/- SEM, N= 24) for the mean pixel intensity within the organs of 4 dpf larvae exposed to APAP alone or in combination with ICI from 6 hpf. Data were not normally distributed and so were analysed using Kruskal-Wallis and Dunn's, asterisks show significant difference compared to solvent control (SC); *= P< 0.05, **= P< 0.005, ***= P < 0.0005, ****= P<0.0001.*

*Table 5.2* ***Statistical analyses results for ICI experiments****. Values highlighted in green indicate exacerbation of APAP-induced OS by co-exposure with ICI*

| Experiment name | Tissue | Treatment group A | Treatment group B | significance |
|---|---|---|---|---|
| APAP vs ICI (shown in Fig. 5.11) | PT | SC | 2.5mM APAP | **** |
| | | SC | 20μM ICI | ns |
| | | 2.5mM APAP | 2.5mM APAP + 20μM ICI | ns |
| | PD | SC | 2.5mM APAP | **** |
| | | SC | 20μM ICI | ns |
| | | 2.5mM APAP | 2.5mM APAP + 20μM ICI | ns |
| | Liver | SC | 2.5mM APAP | **** |
| | | SC | 20μM ICI | ns |
| | | 2.5mM APAP | 2.5mM APAP + 20μM ICI | ns |
| | GI | SC | 2.5mM APAP | **** |
| | | SC | 20μM ICI | ns |
| | | 2.5mM APAP | 2.5mM APAP + 20μM ICI | ns |
| APAP vs ICI.2 | PD | SC | 2.5mM APAP | **** |
| | | SC | 20μM ICI | ns |
| | | 2.5mM APAP | 2.5mM APAP + 20μM ICI | * |
| | PT | SC | 2.5mM APAP | **** |
| | | SC | 20μM ICI | ns |
| | | 2.5mM APAP | 2.5mM APAP + 20μM ICI | ns |
| | Liver | SC | 2.5mM APAP | **** |
| | | SC | 20μM ICI | ns |
| | | 2.5mM APAP | 2.5mM APAP + 20μM ICI | ns |
| | GI | SC | 2.5mM APAP | **** |
| | | SC | 20μM ICI | ns |
| | | 2.5mM APAP | 2.5mM APAP + 20μM ICI | ns |
| APAP vs ICI .3 | PD | 1.25mM APAP | 1.25mM APAP + 20μM ICI | ns |
| | | 2.5mM APAP | 2.5mM APAP + 20μM ICI | * |
| | | 5mM APAP | 5mM APAP + 20μM ICI | ns |
| | PT | no significance | | |
| | Liver | no significance | | |
| | GI | no significance | | |
| APAP vs ICI .4 (shown in Fig. 5.10) | PD | 1.25mM APAP | 1.25mM APAP + 20μM ICI | ** |
| | | 2.5mM APAP | 2.5mM APAP + 20μM ICI | ns |
| | | 5mM APAP | 5mM APAP + 20μM ICI | ns |
| | PT | 1.25mM APAP | 1.25mM APAP + 20μM ICI | **** |
| | | 2.5mM APAP | 2.5mM APAP + 20μM ICI | ns |
| | | 5mM APAP | 5mM APAP + 20μM ICI | ** |
| | liver | 1.25mM APAP | 1.25mM APAP + 20μM ICI | **** |
| | | 2.5mM APAP | 2.5mM APAP + 20μM ICI | ns |
| | | 5mM APAP | 5mM APAP + 20μM ICI | ns |
| APAP vs ICI .5 | PD | 1.25mM APAP | 1.25mM APAP + 2μM ICI | ns |
| | | 2.5mM APAP | 2.5mM APAP + 2μM ICI | ns |
| | | 5mM APAP | 5mM APAP + 2μM ICI | ns |
| | PT | no significance | | |
| | Liver | no significance | | |
| | GI | no significance | | |

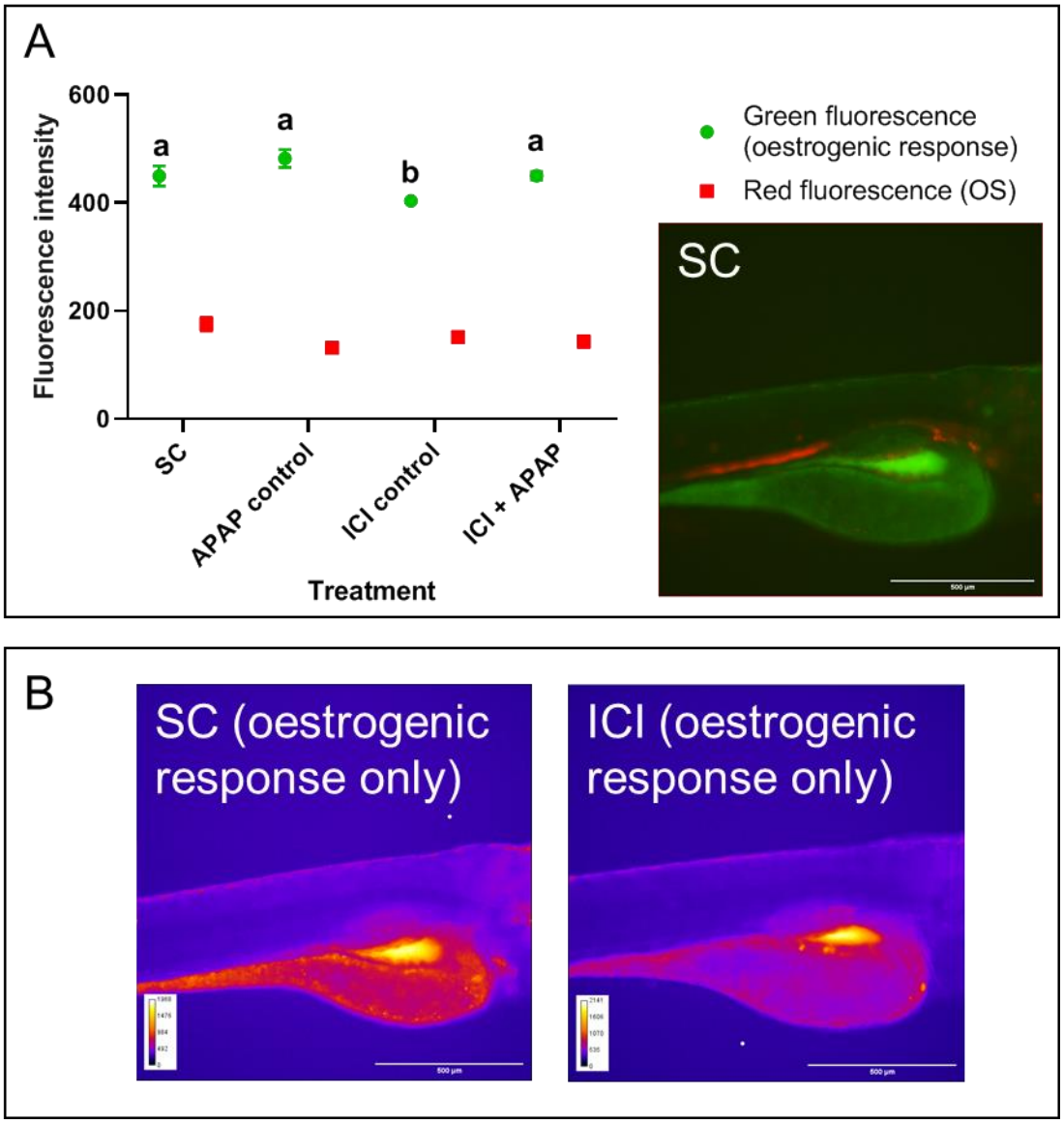


*Figure 5.12* ***Effect of ICI and APAP co-exposure on mCherry fluorescence in EpRE:mCherry:ERE:GFP larvae****. [A] TG(EpRE:mCherry:ERE:GFP) in response to 2.5mM APAP and/or 20µM ICI. Data shows mean values (+/- SEM, N= 24) for the mean pixel intensity within the organs of 4 dpf larvae exposed to APAP alone or in combination with ICI from 6 hpf. Data were normally distributed with equal variance and so were analysed using an ANOVA followed by Tukey's test. Different letters represent statistical significance (P<0.05). There was no statistical difference in the red fluorescence intensity between any of the treatment groups. Image shows an example larva from SC group, imaged on red and green fluorescent channels. [B] EpRE:mCherry:ERE:GFP larvae showing only oestrogenic (GFP) response, exposed to [left] SC, or [right] 20 µM ICI, presented using 'Fire' look up table. Scale bar shows 500 µm.*

## 5.4 Discussion

Data presented here shows OS in zebrafish larvae can be reduced through exposure to exogenous compounds, and this can be visualised as a reduction in mCherry fluorescence intensity in the EpRE:mCherry model. However, exposure to exogenous EE2 appears to not have an influence on drug-induced OS, at least as visualised in the EpRE:mCherry model. The data in this chapter also suggest that endogenous oestrogen may have some role in buffering OS, but the data are not conclusive and warrant further investigation.

### 5.4.1 Antioxidant exposure regimen optimisation

Background OS was reduced in a concentration-dependent manner by exposure to the antioxidant compounds NAC, NACA, and LGR (Fig. 5.4), but only LGR significantly reduced basal OS. Given the standard use of NAC in treating APAP overdose-induced nephrotoxicity, its inconsistent effect in this study was unexpected.

The data presented in Fig. 5.4 shows 2.5 mM LGR effectively reduced OS in the PT, while the same concentration of NAC or NACA had no effect. An assessment of the efficacy of NAC versus LGR (also known as GSH) administration in the treatment of APAP toxicity in mice has previously shown that, at equimolar concentrations, LGR was more effective in preventing APAP-induced liver injury (Saito *et al.*, 2010). This was put down to the 3-fold higher levels of amino acids found in LGR compared to NAC, as the difference in effectiveness disappeared when NAC was administered in higher concentrations (Saito *et al.*, 2010). The majority of amino acids supplied by NAC and LGR are used to enhance synthesis of hepatocellular GSH, which can go on to conjugate the toxic intermediate, NAPQI, preventing it from modifying cellular proteins (Corcoran & Wong, 1986; Lauterburg et al., 1983), while the surplus of amino acids supplied by LGR can be used as a mitochondrial energy substrate (Saito *et al.*, 2010).

Fig. 5.5 shows that LGR was effective in reducing OS in all the organs, and at concentrations as low as 0.6 mM in the PD. The oral administration of the reduced form of glutathione also successfully reduced background levels of OS in TG knock-in mice that had otherwise not been chemically treated (Izumi *et al.*, 2020). The data shown in Figs. 5.4 and 5.5 also suggest that all 3 antioxidants tested had the greatest effect on the pronephros, and little to no effect on the liver. This

is in keeping with what is known about the fish kidney, as it has lower endogenous antioxidant levels compared to the liver and is more susceptible to oxidative damage (Ahmad *et al.*, 2000). Hence, the larval pronephros here appears more responsive to antioxidant supplementation.

However, co-exposure to APAP and LGR resulted in overt toxicity in the form of curved spines and pericardial oedemas, and OS levels equal to or greater than APAP exposure alone (Fig. 5.6). To my knowledge, this effect has not been previously reported, as there is no evidence in the literature for LGR supplementation resulting in OS or other adverse outcomes. However, there is evidence that in the process of APAP metabolism, APAP-GSH conjugates or derivatives thereof can be nephrotoxic (Stern *et al.*, 2005). Furthermore, despite GSH being considered a detoxification molecule, there are examples of other compounds, such as haloalkenes and quinones, where the GSH conjugation of which results in the formation of toxic metabolites (Anders, 2004; Bolton et al., 2000). Exposing the embryos to APAP and LGR simultaneously may have driven production of APAP-GSH and its derivatives and depleted cellular stores of GSH needed to detoxify NAPQI. Indeed, treatment of mice with acetaminophen-cysteine (APAP-CYS), a metabolite derived from APAP-GSH, depleted renal GSH, predisposing the kidney (but not liver) to APAP-induced damage (Stern *et al.*, 2005). Further, this interaction may be specific to APAP, as a pilot study showed co-exposure of larvae for 4 days to 1.4 µM DCF and 10 mM LGR effectively prevented induction of OS in the liver and PD without causing more malformations than those observed in the control group.

In the present study, GSH rescue after exposure to APAP did not enhance toxicity. Chapter 4 showed that APAP is completely expelled from the body of a 2-3 dpf larvae after 24 hours depuration in clean water. Therefore, in the first 24 hours of LGR exposure there may be a direct interaction between APAP and LGR, but by the time the larvae are imaged (after 48 hours LGR exposure), any OS detected is a residual effect from pro-oxidant exposure. Given there was no difference in OS levels between the treatment groups with different time periods between APAP and LGR exposure, residual APAP in the depurated embryo doesn't seem to affect the rescue capacity of LGR. A future study could better our understanding of the GSH-APAP interaction by pre-treating the embryos with GSH, followed by APAP exposure.

In contrast, addition of GSH to zebrafish embryos co-cultured with APAP and a mammalian metabolic activation system (MAS; rat liver microsomes) has been shown to be sufficient to prevent any teratogenic effects seen in embryos exposed to 6mM APAP and the MAS (Weigt et al., 2010). That study was aimed at testing how metabolic activation of the drug by MAS affected the teratogenicity of APAP, but they found 72 hour exposure to 6 mM APAP alone (with no external metabolic activation) did not induce any malformations (Weigt *et al.*, 2010), which is in stark contrast with the data presented in this thesis which showed malformations at 4 mM APAP exposure, along with other papers (David & Pancharatna, 2009; Tao & Peng, 2009).

### 5.4.2 Oestrogen and Oxidative stress

The evidence appears not to support the hypothesis that exogenous oestrogen exposure can buffer OS, at least as visualised in the EpRE:mCherry model.

#### *5.4.2.1 Exogenous oestrogen*

In the various exposure regimens trialled: APAP exposure from 0 - 2 dpf followed by EE2 for 2 days, APAP exposure from 0 - 4 dpf followed by 2 day EE2 exposure, and co-exposure to APAP and EE2, EE2 was only seen to reduce APAP-induced OS for one EE2 exposure at 0.017 nM, for one occasion in the PD and one occasion in the PT (Table 5.1). This effect however was not repeatable. Evidence for the antioxidative activity of oestrogens have been reported in some mammalian studies, such as the phytoestrogen genistein which has been shown to protect against APAP induced hepatotoxicity in mice via Nrf2 signalling as a result of SIRT1 activation. Genistein supplementation attentuated the APAP-induced increase in OS biomarkers such as MDA and reversed the depletion of hepatic GSH stores. This was potentially through binding the ER, which can then bind to the promoter for SIRT1, increasing its activity (Wang et al., 2020a). Although, genistein is a known antioxidant with influence on many pathways involved in homeostasis (Ganai & Farooqi, 2015), including activation of adenosine monophosphate-activated protein kinase (AMPK) (Lee et al., 2019), and so its antioxidative role may not have been related to its oestrogenic function (Wang et al., 2020a).

To my knowledge, there are no studies which have reported antioxidant effects of xenoestrogens in fish but, EE2 exposure in fish has been linked to increased antioxidant activity as a tissue response to OS induction rather than a protective

role of the compound. In *Carassius auratus* (Crucian carp), EE2 exposure resulted in an increase in amino acids related to cysteine metabolism- a precursor to GSH and hence implying an upregulation of the antioxidant (Zhou et al., 2019). This increase in antioxidant defences is more likely an adaptive respones to OS induction by EE2, as other purtubations of the metabolome implied induction of OS (Zhou et al., 2019). Futher study is needed to quantify cellular GSH and products of OS, such as MDA, to confirm if the carp experienced OS. Oxidative damage and a resulting increase in antioxidant activity has also been reported in zebrafish embryos exposed to EE2, albeit at concentrations above those used in the present study (Ramírez-Montero *et al.*, 2022). Conversely, EE2 has recently been shown to inhibit superoxide dismutse (SOD) and CAT activity in *Pelteobagrus fulvidraco* (yellow catfish), in direct contrast to the hypothesis of this study, and resulted in increased levels of MDA (Mo *et al.*, 2019). These studies contrast with the findings of this chapter as EE2 did not induce OS either in combination with APAP or alone (as indicated in pilot studies), with the exception of 4 day APAP exposure followed by 2 days EE2 exposure (Table 5.1).

Extended APAP exposure (0-4 dpf) followed by 2 days in clean water did not induce significant OS. This could be a result of the more developed metabolic capacity of the larva (discussed in Chapter 4), allowing it to detoxify and expel the APAP more efficiently during the 2 days depuration period allowing the tissue to recover more rapidly. However, in the same experiment larvae which were transferred to EE2 or LGR after 4 day APAP exposure exhibited significantly higher OS compared with the clean water control. This could indicate that the second chemical exposure impaired the ability of the tissue to recover from OS. Alternatively, it could be due to the quality of image acquisition of the embryos which, at 6 dpf, is less sensitive due to increased opacity of the body and the challenge of embedding and orientating the embryos uniformly for the Acquifer. With more time, a follow-up study could use the confocal to image the older larvae and provide more accurate measurements of tissue-specific mCherry fluorescence.

Interestingly, the premise on which these studies have been built have been questioned by recent clinical studies linking EE2 to OS induction in women using the oral contraceptive pill (Cauci *et al.*, 2021).

#### *5.4.2.2 Endogenous Oestrogen*

While EE2 failed to rescue OS, the data presented appears to suggest that endogenous oestrogen may play a protective role against OS, particularly in the PT (Fig. 5.10), as the simultaneous exposure to APAP and ICI resulted in elevated OS compared to exposure to either compound individually. As a known ER antagonist, ICI potentially exerted its effect through suppression of the influence of ERs on the Nrf2/Keap1 pathway (Fig. 5.13); oestrogen has previously been shown to increase Nrf2 activity, particularly in studies on breast cancer research (Gorrini et al., 2014; Song et al., 2019; Wu et al., 2014). ICI alone did not induce a significant OS response (Figs. 5.10, 5.11 and Table 5.2), indicating the compound itself is unlikely to be a pro-oxidant, but more likley impairs the upregulation of the larva's natural antioxidant defences when stressed by another chemical. It is possible that ICI interacted with APAP to induce OS, rather than suppressed the antioxidant defences, but to my knowledge no previous studies have linked ICI with OS induction in any context.

The distribution of the present data points in Figs. 5.10 and 5.11 where there appears to be two data clusters (one showing no response to the addition of ICI and one showing a strong increase in APAP-induced OS) may hint at innate biological variation in the larvae influencing how they respond to the treatment. Given that the high variation in fluorescence intensity between individuals has been specifically observed in EpRE:mCherry larvae exposed to chemicals modulating the oestrogenic response, more so than in previous chapters, this is most likely related to variation in the oestrogenic pathway/response as opposed to the TG model itself or imaging platform. This variation could therefore perhaps come from an early form of sex-specific responses to oestrogen inhibition, although sexual differentiation isn't initiated until between 20 – 25 dpf (Kossack & Draper, 2019). Previous studies have also reported high variation among zebrafish juveniles in their responses to xenoestrogen exposure, attributed to ongoing gonad differentiation (Legler *et al.*, 2000). Sex difference in susceptibility to the consequences of OS have been indicated in mammalian studies. Females appear to be less vulnerable to OS in general, potenially linked to the properties of oestrogen, or alternatively related to variation in NADPH-oxidase activity between the sexes (Kander et al., 2017). OS is also an established mechanism of aging disorders and there are known sex-differences here as well, such as the pro-oxidative action of testosteron which can exacerbate OS via an androgen

receptor in certain brain regions, accounting for sex differences here (Duong *et al.*, 2020).

The process of sex determination is not fully understood in zebrafish but is influenced by a range of factors including rearing temperature, genetic factors and early life chemical exposure (von Hofsten & Olsson, 2005). A sex-specific response would therefore be difficult to prove in 4 dpf zebrafish larvae. There are currently no known sex markers at this life stage (Aharon & Marlow, 2022), and fish sex is particularly plastic as it can be altered by chemical exposure (Morthorst et al., 2010; Tyler & Jobling, 2008). A future study could potentially separate EpRE:mCherry larvae based on their response to ICI and APAP co-exposure (i.e a low response and a high response group) and raise them to adulthood in clean water. At this age, sex can be phenotypically and histologically determined, so differing sex ratios between the groups could indicate if their response to larval ICI exposure was influenced by sex.

Alternatively, the high variation could be a result of the poor solubility of ICI (9.53x10-6 mg/L in water) (National Center for Biotechnology Information, n.d.), resulting in inconstistent internal concentrations as the compound precipitated and/or less was taken up by the animal. However, this does not explain the two distinct subpopulations, and previous experiments have successfully used ICI via media exposure to treat zebrafish embryos (Lee et al., 2012b).

Unlike exogenous oestrogen exposure which did not have an effect on the liver, blocking endogenous oestrogen appeared to have a less tissue-specific response. The data in Figs. 5.10 and 5.11 appear to show an increase in OS resulting from APAP and ICI exposure (compared to APAP alone) in all the target organs (albeit this was not always statistically significant). This is in keeping with what is known about the wide distribution of ERs across different tissue types in fish including the liver and kidney (Filby & Tyler, 2005; Hao *et al.*, 2013) (as discussed in Chapter 3).

The data presented in Fig. 5.12 indicate there may not be a correlation between OS and endogenous oestrogen as ERE dependent GFP was reduced in larvae exposed to the ER antagonist, but OS-dependent mCherry fluorescence showed no significant change. However, although embryos were pre-screened for fluorescence, the larvae may have been heterozygous for the EpRE:mCherry,

ERE:Gal4ff, or UAS:GFP transgenes, impeding the sensitivity of the model. This may explain why larvae did not express increased mCherry fluorescence in response to APAP exposure, unlike larave from the EpRE:mCherry TG line. Therefore, as the APAP-only control did not elicit the expected response, no conclusion can be drawn about the effect of the various treatments on OS in the multiple TG model.

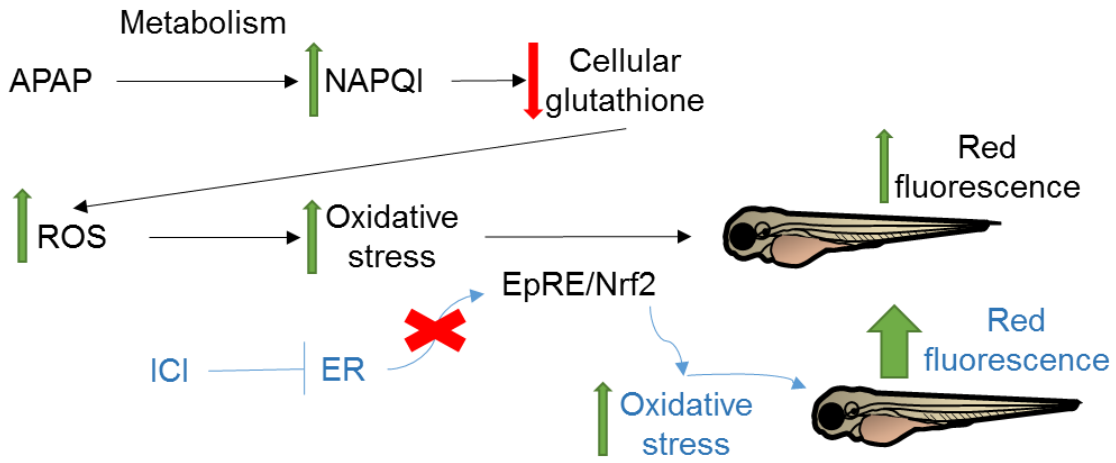


*Figure 5.13* ***Scheme of the proposed effect ICI may have on APAP-induced OS via inhibition of the ER.*** *The known pathway of OS induction by APAP is shown in black, and the pathway of ER inhibition is shown in blue. ICI is a known ER blocker and the data presented here suggests this can result in exacerbated APAP-induced OS, possibly via removal of the ERs influence on the Nrf2/Keap1 pathway, although more research is needed to elucidate this mechanism.*

## 5.5 Conclusions

There is a growing need for better understanding of how chemicals of different classes and with different modes of action interact but, knowing where to begin with mixture effect studies can be a challenge. To begin to tackle this issue, here two pharmaceuticals were selected based on *in vitro* evidence for their antagonistic interaction. However, the data presented does not support the hypothesis that EE2 has a buffering effect against OS. Despite this, the data presented does indicate endogenous oestrogen may have a protective role, but this requires further study to draw any firm conclusions.

There does not appear to be a consensus in the existing literature regarding the pro- or anti-oxidative properties of oestrogens. Evidence for the former has only been derived from *in vitro* or mammalian *in vivo* data, and the mechanism by which oestrogenic compounds may exert an antioxidant effect has not been fully

characterised but, the involvement of intracellular signalling pathways has been postulated. Unfortunately, the data in the present study does not seem to be able to clarify the issue due to the inconsistent responses seen in the EpRE:mCherry model. The data for OS levels in this chapter were more variable and less consistent when compared with the previous two chapters, potentially indicating an enhanced biological variability relating to the interaction between (xeno)-oestrogens and pharmaceutical-induced OS. This is particularly typified in the data showing the exacerbation of APAP-induced OS by the ER antagonist, in which the clustering of data into two subpopulations potentially implies sex-based differences.

Regarding realistic exposure scenarios in the environment, where aquatic wildlife may encounter xenoestrogens in combination with pro-oxidative compounds, it seems unlikely that the oestrogenic response would counteract any induced effects of OS. Indeed, existing ecotoxicity data heavily suggests environmental oestrogens induce OS. However, this chapter has only used one TG model to investigate this interaction, and so it is possible that EE2 may influence OS via a pathway not involving EpRE. Furthermore, there is evidence to suggest that EE2 may inhibit (Mo *et al.*, 2019) or increase (Ramírez-Montero *et al.*, 2022) the activity of antioxidants, and it is unknown how changing regulation of downstream antioxidants may feedback to the EpRE.

Additionally, the action of oestrogen is highly complex, with a wide range of roles and far-reaching effects. This chapter only tested its antioxidative effect in one system and under specific conditions and so it is highly possible that the EpRE:mCherry model was unable to represent the true extent of the interaction between OS and oestrogen.

# Chapter 6- Interaction of drug-induced OS and temperature

## 6.1 Introduction

Current environmental risk assessments are based on results of chemical effects assessments which are performed in laboratory conditions with strictly controlled parameters. In reality, wildlife are exposed to pharmaceuticals and other chemicals in highly variable environments, where environmental physicochemical factors such as pH, oxygen content, and temperature can vary temporally and spatially. These physicochemical conditions have the potential to affect how an animal responds to chemical stressors, both by impacting upon both biological processes and the chemical or physical properties of the water and pollutants (reviewed in (Pinheiro *et al.*, 2021). Additionally, different experimental parameters, including rearing temperature, have the potential to affect the predictability of zebrafish bioassays, for example as has been shown for effects on behaviour (Ogungbemi et al., 2019). Therefore, there is a need to better understand interactions between biomarkers of chemical exposure and abiotic conditions in order to more accurately assess the risk a pharmaceutical presents in the environment.

This chapter, therefore, focusses on interactions between temperature and chemical exposure, as this is of growing concern and there have been numerous studies showing elevated temperature can enhance the toxic effects of various pollutants (reviewed in (Noyes *et al.*, 2009). The main aims of the chapter were:

a) Assess the effect of temperature on basal redox state of EpRE:mCherry embryos and confirm if this can be quantified in the TG model.
b) Assess the effect of temperature on the pro-oxidative action of a range of compounds with varying potencies and modes of action.
c) Use analytical chemistry to assess how toxicokinetics of the reference compound, APAP, is affected by elevated temperature.

For zebrafish, there is evidence to suggest a temperature increase of just 5°C can enhance the effects of endocrine disrupting chemicals (EDCs) in the environment to drive population declines (Brown et al., 2015). There are a variety of mechanisms by which this can occur, such as by increased uptake of the

pollutant, altered toxicokinetics within the animal (e.g. affecting absorption, distribution, metabolism or excretion (ADME) of the drug), and altered homeostasis thereby rendering the animal more vulnerable to additional stressors. This is in addition to the ways in which temperature can change the chemical properties of water, such as by altering salinity or oxygen content. Finally, as poikilotherms, fish are more vulnerable to the impacts of environmental temperature change since their body temperature is almost entirely dependent on external conditions (Noyes *et al.*, 2009).

One of the main mechanisms by which elevated temperature can exacerbate toxicity in aquatic animals is via increased chemical uptake. Metabolic rate in poikilotherms increases two-fold with 10°C temperature increase, also known as the Q10 effect. This results in an increased oxygen demand which then drives an increase in ventilation, thereby drawing more pollutant into the body across the gills (Heugens *et al.*, 2003). Additionally, the higher level of kinetic energy provided by warmer temperatures can accelerate the diffusion or active transport of chemicals across membranes (Pinheiro *et al.*, 2021).

Conversely, a change in metabolic rate can also result in faster metabolism and excretion, potentially reducing the toxicity of a drug. This has been demonstrated for a range of pesticides, such as pyrimethanil, where a reduced toxic effect was linked to faster chemical metabolism and enhanced cellular repair in the embryos of the freshwater snail *Physella acuta* (Seeland et al., 2013). Evidence in the literature also suggests a drug can reduce the thermal tolerance of the animal. For example, chronic exposure to an antidepressant was shown to suppress the antioxidant defence response to temperature increase in adult zebrafish (Mehdi *et al.*, 2019).

To test the hypothesis of this chapter that elevated temperature can exacerbate drug-induced OS, APAP (1.0 – 3.0 mM), DCF (0.7 – 2.7 µM) and Dox (1.8 – 9.2 µM) (see Table 6.1) were selected as known environmental pro-oxidants based on the data from the drug screen in chapter 4 and their effects analysed for different temperature exposures. A relationship between elevated temperature and enhanced APAP toxicity has previously been shown in a variety of aquatic species, including medaka (*Oryzias latipes)* (Kataoka *et al.*, 2019) and *daphnia magna* (Kim et al., 2010). A similar relationship with temperature has been demonstrated for DCF in a freshwater shrimp (*Atyaephyra desmarestii*) (Nieto et

al., 2016), mussel (*Mytilus galloprovincialis*) (Freitas *et al.*, 2019), clams (*Ruditapes philippinarum* and *Ruditapes decussatus*) (Costa *et al.*, 2020) and seabass (*Dicenthrachus labrax*) (Maulvault et al., 2018a). Dox, however, has not yet been investigated for its interaction with environmental temperature. Data in chapter 4 indicated Dox induced either a weak or no OS in the standard organs tested (i.e., pronephros and liver) but a surprisingly strong OS in the GI. It was therefore included in this chapter to investigate how temperature could influence the OS induction of a drug with a different response profile.

To my knowledge, the interaction of temperature with the toxicity of these drugs have not previously been demonstrated in zebrafish, with the exception of DCF which showed increased uptake in zebrafish embryos at higher temperatures, possibly related to increased metabolism (Chen et al., 2015). Further, there are scant studies investigating how temperature specifically influences drug-induced OS. One of the few studies to achieve this in an *in vivo* model used the common goby (*Pomatoschistus microps*) to show how higher temperature can increase mercury accumulation and consequently oxidative damage in muscle tissue (Vieira *et al.*, 2021). Despite the growing interest in the mechanism driving interactions of temperature and drug toxicity, a TG fish larval model has not yet been utilised for this.

In this chapter, EpRE:mCherry embryos are first raised at 33°C with no chemical stressor to assess the OS induced by temperature alone. Embryos were then exposed to one of the three pro-oxidants at a range of concentrations and raised at 33°C or 28°C (the control) to investigate how temperature affects the minimum response threshold, in addition to enhancing the OS observed. 33°C was selected as a maximum temperature as it represents a realistic future temperature rise for spawning endogenous zebrafish populations (Brown et al., 2015) whilst remaining within their thermal tolerance range (Spence et al., 2006). The interaction is also tested across a range of temperatures to understand if the relationship between temperature and drug-induced OS is linear, or if a thermal threshold must be exceeded for temperature to exert its effect. This includes a temperature below the standard for zebrafish husbandry, 24°C, to find if a lower temperature has a suppressive effect for the induction of OS. Finally, this interaction was investigated over time to understand how temperature influences the ontogeny of the OS response or its rate of increase.

Temperature is known to affect the development rate of zebrafish (Parichy *et al.* 2009). Hence accelerated development of embryos raised at higher temperature could potentially result in larger organs at a given timepoint and therefore skew the measurement of tissue-specific OS. As a result, the body length of each larva was measured for each temperature experiment as an indicator of development rate.

I hypothesised that elevated, environmentally relevant temperatures can exacerbate pharmaceutical-induced OS. This was tested by incubating EpRE:mCherry larvae at temperatures higher than standard husbandry practice during aqueous exposure to a pharmaceutical. This interaction between temperature and drug-induced OS, based on the available literature, is hypothesised to be mediated primarily via increased uptake of the pharmaceutical from the exposure media. To test this, the influence of temperature on the toxicokinetics of the drug was also investigated using LC-MS/MS to measure the APAP concentration inside the larvae at different time points throughout the exposure period.

## 6.2 Methods

### 6.2.1 Fish husbandry

All imaging/OS measurements were conducted using EpRE:mCherry zebrafish. The supply of EpRE:mCherry zebrafish was limited and WIK embryos were therefore used for all LC-MS/MS to assess uptake of the drug across time points. Both strains of zebrafish were maintained under the same conditions (see Chapter 2, section 2.1).

### 6.2.2 Chemical exposure

All compounds used in this chapter were obtained from Sigma-Aldrich, Dorset, UK. All stocks other than APAP were made prior to the day of exposure and stored in -20°C. Exposure solutions were diluted in system water on the day of exposure. APAP (CAS no. 103-90-2) and DCF (CAS no. 15307-79-6) were dissolved in 0.5% DMSO and Dox (CAS no. 25316-40-9) was dissolved without the use of a solvent.

Embryos were raised at standard husbandry temperature (28°C) in CW in Petri dishes until 6 hpf, at which point they were exposed to the chemical in 24-well

plates and transferred to the test temperature regimen. See Chapter 2 section 2.4 for details on standard chemical exposure conditions.

Concentration ranges were selected based on the results of the concentration-dependent response curves shown in chapter 4 and were chosen in order to cause a detectable level of OS without inducing overt toxicity. Dox was tested for its interaction with temperature in a range-finding study at concentrations between 0.7 and 9.2 µM (see Appendix 2, Fig.1). Similar to the results shown in chapter 4, Dox concentrations below 1.8 µM only induced OS in the GI tract and liver but not the heart or pronephros. Subsequently, a concentration between 1.8 and 9.2 µM was used.

For experiments testing a range of pharmaceutical concentrations at a control or single experimental temperature, the concentrations used were: 1 mM, 2 mM, 3 mM APAP with a SC; 1.8, 3.7, 5.5, 7.4, 9.2 µM Dox with a CW control; 0.7, 1.4, 2.0, 2.7 µM DCF with a CW control (Table 6.1). For experiments testing the effects of a range of temperatures on a single concentration, 2.5 mM APAP and 2.0 µM DCF were used.

*Table 6.1 Pharmaceuticals tested for their interaction with temperature, and concentration ranges used*

| Drug | Concentration range (µM) |
|---|---|
| Paracetamol (APAP) | 1000, 2000, 3000 |
| Doxorubicin | 1.8, 3.7, 5.5, 7.4, 9.2 |
| Diclofenac (DCF) | 0.7, 1.4, 2.0, 2.7 |

### 6.2.4 Embryo culturing at different temperatures

Embryos cultured at test temperatures were kept in a Stuart SI60D digital incubator (Cole-Parmer, Cambridgeshire, UK) set to the desired temperature. An Elitech RC-5 data logger (Elitech, London, UK) was used to track and verify the temperature, and the transparent incubator was kept in the same room as the control zebrafish to ensure all embryos were exposed to the same light:dark cycle.

To avoid variable degrees of evaporation resulting from the different incubation temperatures which would otherwise affect the final exposure concentration, each 24-well plate was sealed using parafilm.

Embryonic development is known to be closely associated with temperature (Parichy et al., 2009), and pilot studies showed larvae raised at 33°C hatched up to 24 hours earlier than those raised at 28°C, and their swim bladders were also found to inflate earlier. This created two confounding factors for the comparison of OS between temperature groups: firstly, premature hatching may result in a different exposure scenario due to the removal of the protective barrier formed by the chorion, and secondly, larvae with larger swim bladders can be more difficult to image on the Acquifer as they are more likely float to out of position in the agarose grooves (as shown in chapter 3). Several steps were taken to account for these complications; manual dechorionation of the embryos at 2 dpf so all larvae effectively 'hatched' at the same time; exposure was also terminated at 3 dpf (when all larvae did not have fully inflated swim bladders) to ensure all larvae could be imaged. In a separate series of experiments, larvae were exposed for 4 days and imaged daily from 2 dpf so the development of the OS response over time could be compared between temperature regimens. In these experiments, additional numbers of embryos were used to compensate for the 10 % of 4 dpf embryos which may not be viable for imaging due larger swim bladders (thereby still achieving a final sample size of 24 larvae per treatment).

### 6.2.5 Image acquisition and analysis

All images were acquired using the Acquifer and tissue-specific fluorescence intensity analysed using ImageJ following the protocol described in Chapter 3. For every assay, body length was also measured on the bright field images from the end of the head to the caudal peduncle in order to assess if the different culturing temperatures resulted in differing body sizes (example results are shown in Fig. 6.2).

For experiments assessing the effects of elevated temperature across a drug concentration range or assessing the effect of a single concentration at several experimental temperatures, larvae were imaged at the end of a 3 day exposure period (from 0-3 dpf). For experiments assessing the development of the OS response over time at different temperatures, larvae were imaged at 2, 3 and 4 dpf and placed in fresh exposure media after each time point.

### 6.2.6 Drug uptake analysis

The rate of APAP uptake was measured in WIK embryo-larvae using LC-MS/MS. This experiment was performed using APAP only as DCF and Dox were not detectable at the concentrations used in the current methods (see Chapter 4). For full details of methods used, see Chapter 2 section 2.8. Uptake is given in amount of APAP per larva (nM), not concentration, as the volume of the unhatched embryo or larvae at each time point could not be confirmed. WIK embryos were pooled in order to obtain enough tissue for drug concentration to exceed the LOQ and therefore, each data point represents an N of 6, with 4 embryos per sample.

### 6.2.7 Statistical analysis

See Chapter 2 section 2.9.

## 6.3 Results

### 6.3.1 Temperature-induced oxidative stress

Fig. 6.1 shows that elevated temperature alone induces OS and this can be visualised in the EpRE:mCherry model. The two different treatment groups had different sample sizes because embryos raised at 33°C developed slightly faster and, with more inflated swim bladders, some of these animals floated out of the agarose grooves and in turn out of focus for the imaging so fluorescence intensity measurements could not be taken. This problem directed further temperature-based experiments to be carried out using embryos at 72 hpf for imaging (other than daily imaging experiments). This is when the differences in development are less pronounced and the swim bladder is not inflated to an extent that disrupts the imaging process.

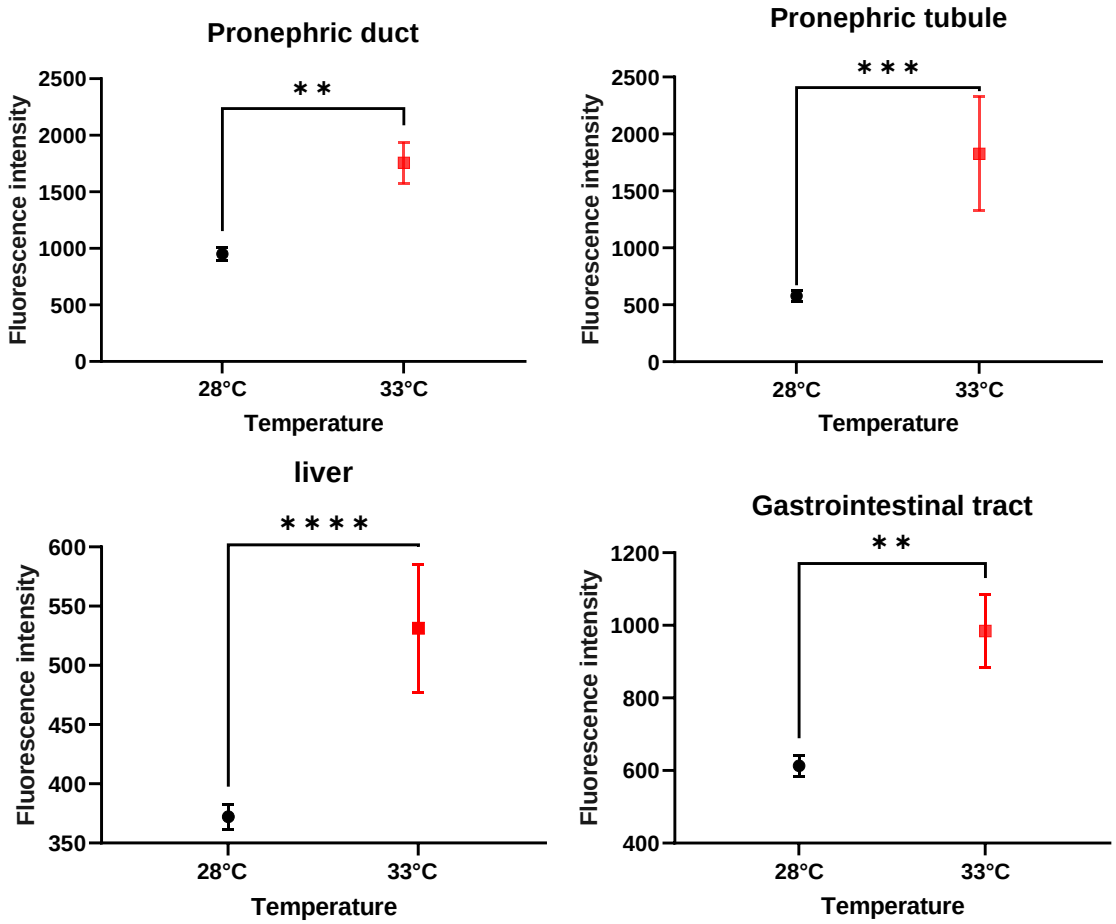


*Figure 6.1* ***Effect of elevated temperature on OS in non-chemically treated 4 dpf EpRE:mCherry larvae.*** *Data shows mean values (+/- SEM) for the mean pixel intensity within the organs of larvae. N= 15 for 28°C and N=6 for 33°C treatment groups. Data Data were not normally distributed and so were analysed using Mann-Whitney, * = P< 0.05, **= P< 0.005, **= P<0.0005, ****= P< 0.0001.*

### 6.3.2 Effect of temperature on embryo-larvae size

Embryo-larvae raised at 33°C were only significantly greater in length compared to 28°C at 2 dpf and this difference was not apparent at later life stages (Fig. 6.2). Therefore, the image analysis method (Chapter 3) was still valid as the larvae were not significantly different in size and so using the same templates to measure tissue-specific fluorescence intensity for each treatment group will still give reliable results.

A lower temperature of 24°C, however, was found to consistently result in significantly smaller sized larvae (Fig. 2), suggesting lower temperature delayed embryonic development. Therefore, the fluorescence intensity for larvae raised at this temperature were interpreted with caution as smaller organs could have affected the measurement of fluorescence intensity (see Discussion).

Neither APAP nor DCF alone had any effect on the growth of embryo-larvae at the exposure concentrations used.

Body length measurements were taken for each chemical exposure assay, and the same trend was seen each time: neither chemical exposure nor an increased temperature affected body length (except for 33°C at 2 dpf, where larval length was greater), however, a lower temperature did impede larval growth. Fig. 6.2 shows examples of these data.

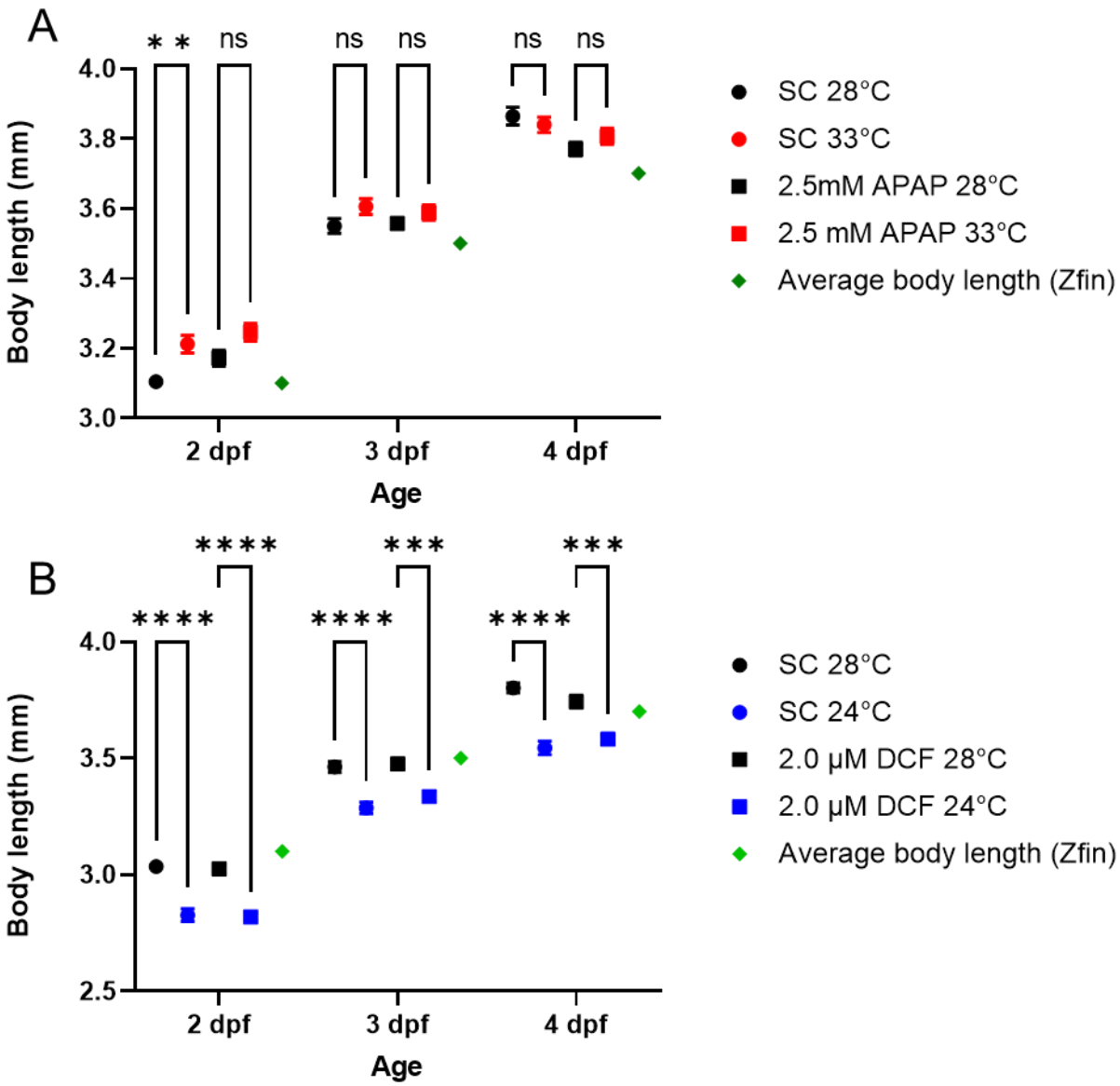


*Figure 6.2* ***Effect of [A] 33°C (N=12) and [B] 24°C (N=24) on body length of embryo-larvae at different developmental stages.*** *The average body length for 28 °C according to Zfin (https://zfin.org/zf_info/zfbook/stages/ Accessed 5/11/2021) are provided as a reference to show temperature did not unduly alter the growth rate of the larvae. Data is given as mean body lengths (+/- SEM). Data were normally distributed with equal variance and so were analyse using a two-way ANOVA followed by Tukey's multiple comparison test; * = P< 0.05, **= P< 0.005, **= P<0.0005, ****= P< 0.0001.*

### 6.3.3 Interaction of temperature and pharmaceutical-induced oxidative stress: across different concentrations

Embryo-larvae cultured at an elevated temperature exhibited enhanced pharmaceutical-induced OS compared to those raised at the standard 28°C. Additionally, the higher temperature was shown to reduce the concentration of compound needed to cause a significant level of OS (i.e. the lowest observable effect concentration (LOEC) was reduced) (Figs. 6.3, 6.4, 6.5).

For every drug tested, the GI tract showed the greatest increase in drug-induced OS when larvae were cultured at 33°C compared to 28°C. Other than the GI tract, the organs most affected by this interaction appear to be drug-specific and reflect the specific target organs identified in Chapter 4. For APAP, the elevated temperature resulted in a lower LOEC for the PT and PD, but not the liver (Fig. 6.3). In contrast, the liver and PD were affected in DCF-treated larvae (Fig. 6.4) while the pronephros appeared mostly unaffected by the temperature/Dox interaction, but the LOECs for the heart and liver were reduced (Fig. 6.5).

Despite being tested at the lowest and narrowest concentration range (0.7 – 2.7 µM DCF compared to 1.8 – 9.2 µM Dox and 1.0 – 3.0 mM APAP), larvae exposed to DCF exhibited the most dramatic increase in OS in response to different temperatures; no OS was observed in the 28°C treatment group at any DCF exposure (Fig. 6.4), while larvae in the 33°C group showed significant OS in the liver in response to 1.4 µM DCF, and in the GI tract from 0.7 µM (Fig. 6.5).

It is important to note that these experiments were performed on zebrafish embryos from different spawning events, and although the variability between control groups of different batches of embryos is small (see chapter 4), it is not appropriate to directly compare the absolute fluorescence intensity detected between experiments, but focus on the relative changes in fluorescence intensity within an experiment between treatment groups.

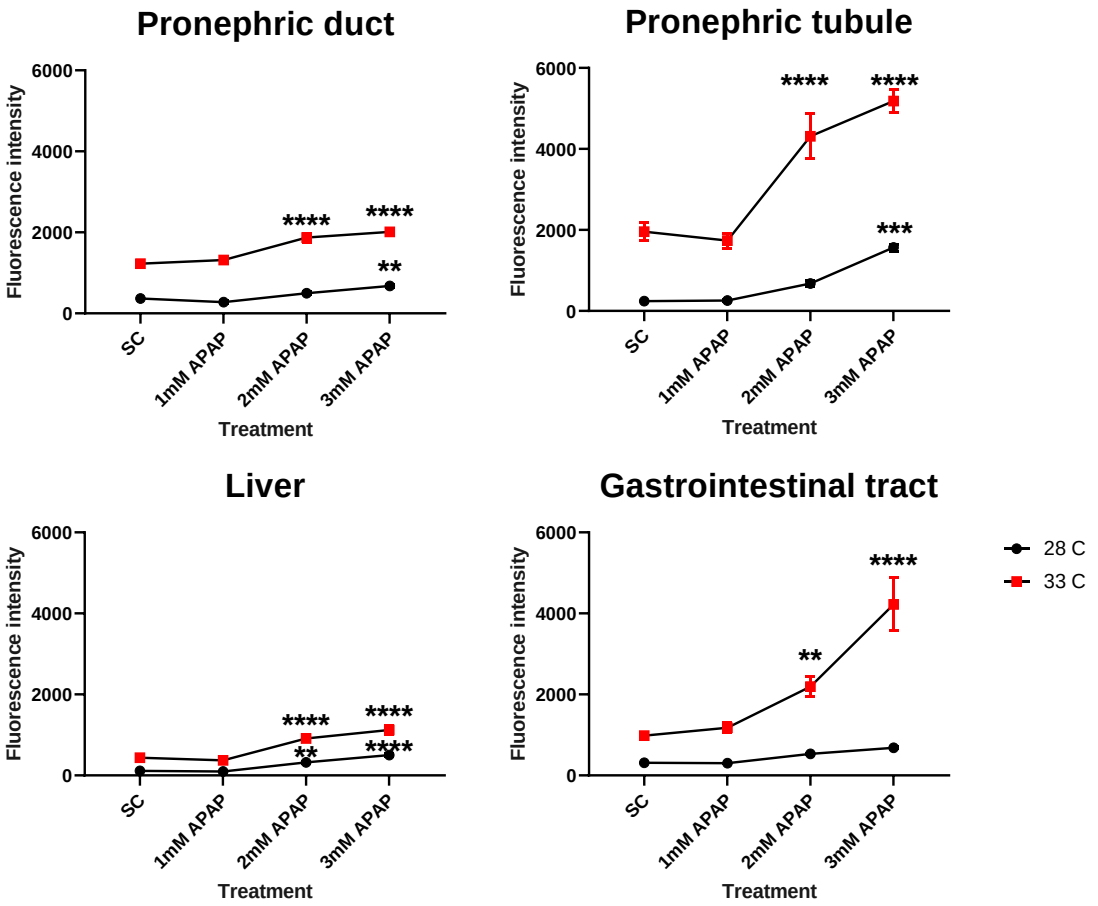


*Figure 6.3* ***Effect of temperature on APAP-induced OS****. Embryos were exposed from 6 hpf to 3 dpf to a range of APAP concentrations and raised at 28 or 33°C. Data shows mean values (+/- SEM, N= 18) for the mean pixel intensity within the organs of 3 dpf larvae. Asterisks show significant difference to the control of the same temperature group. Data were normally distributed and so were analysed using 2-way ANOVA followed by Dunnett's. The 2-way ANOVA also showed significant interaction between concentration and temperature (***).* = P< 0.05, **= P< 0.005, **= P<0.0005, ****= P< 0.0001*

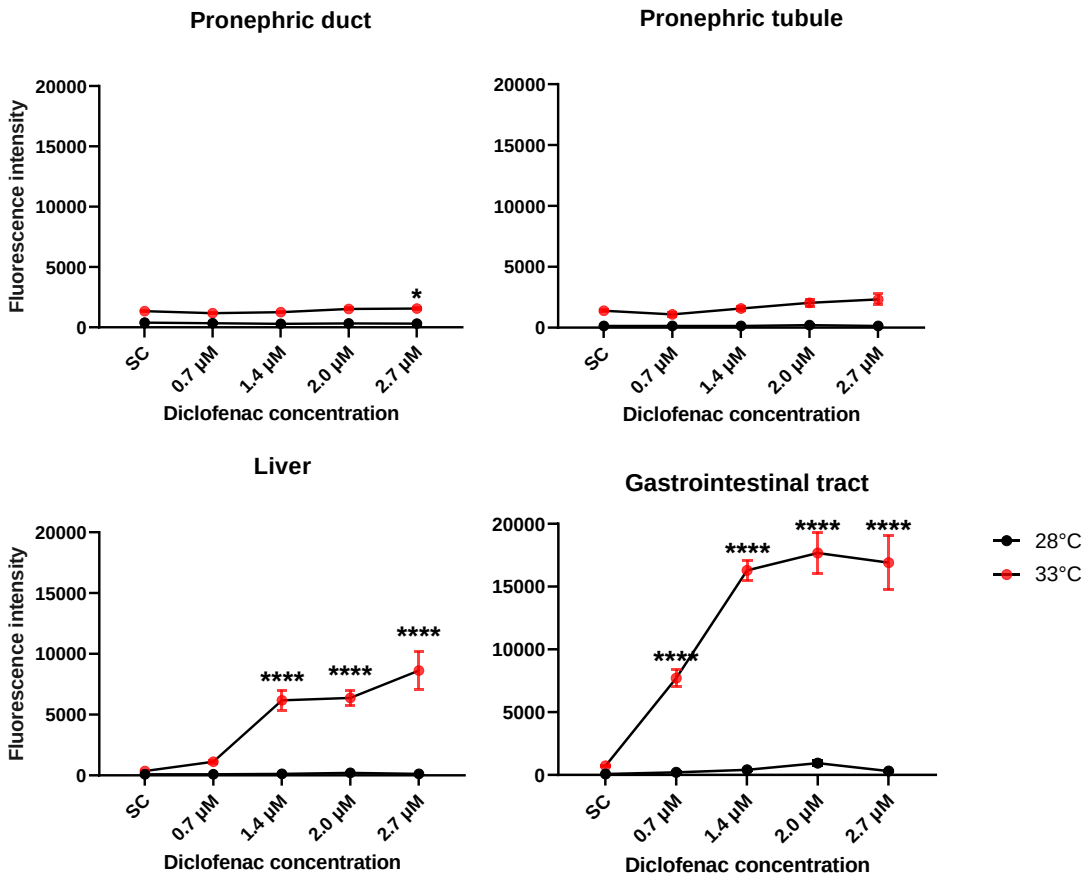


*Figure 6.4* ***Effect of temperature on DCF-induced OS.*** *Embryos were exposed from 6 hpf to 3 dpf to a range of DCF concentrations and raised at 28 or 33°C. Data shows mean values (+/- SEM, N= 18) for the mean pixel intensity within the organs of 3 dpf larvae. Asterisks show significant difference to the control of the same temperature group. Data were normally distributed with equal variance and so analysed using 2-way ANOVA, followed by dunnett's, except PT which was tested using separate Kruskal Wallis tests followed by Dunn's. * = P< 0.05, **= P< 0.005, **= P<0.0005, ****= P< 0.0001.*

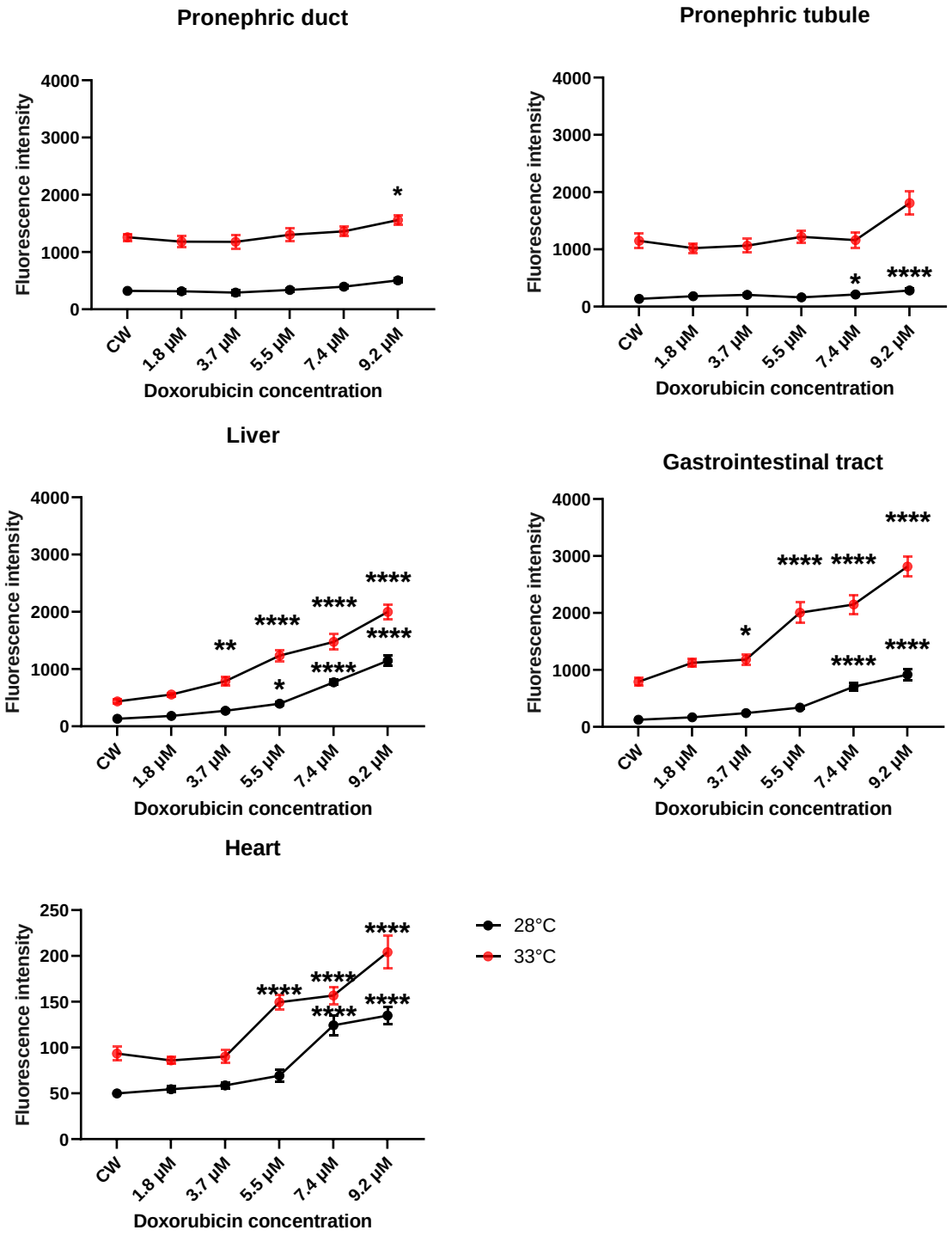


*Figure 6.5* ***Effect of temperature on Dox-induced OS****. Embryos were exposed from 6 hpf to 3 dpf to a range of Dox concentrations and raised at 28 or 33°C. Data shows mean values (+/- SEM, N= 14) for the mean pixel intensity within the organs of 3 dpf larvae Data were normally distributed qith equal variance and so were analysed using 2-way ANOVA followed by Dunnett's, except PT which was tested using Kruskal-Wallis followed by Dunn's. Asterisks show significant difference to the control of the same temperature group * = P< 0.05, **= P< 0.005, **= P<0.0005, ****= P< 0.0001.*

### 6.3.4 Interaction of temperature and pharmaceutical-induced oxidative stress: across different temperatures

A significant difference in APAP-induced OS was observed across the different temperatures tested (Fig. 6.4). Embryo-larvae raised at 24°C showed a reduced background level of OS and reduced drug-induced OS compared to those raised at 28°C. Culturing embryos at only 2°C higher than the control temperature (30°C compared to 28°C) enhanced the OS response in the pronephros but not the liver. The PT appeared particularly responsive, showing the greatest level of OS induction by APAP exposure for all temperatures.

However, temperature did not appear to have a linear relationship with APAP-induced OS, as the difference in mCherry fluorescence intensity between SC and APAP-treated larvae was smaller at higher temperatures than in larvae raised at 28°C. At 28°C, APAP induced a 3-fold higher fluorescence in the liver compared to the SC, but this difference was only 1-fold at 30°C and 33°C.

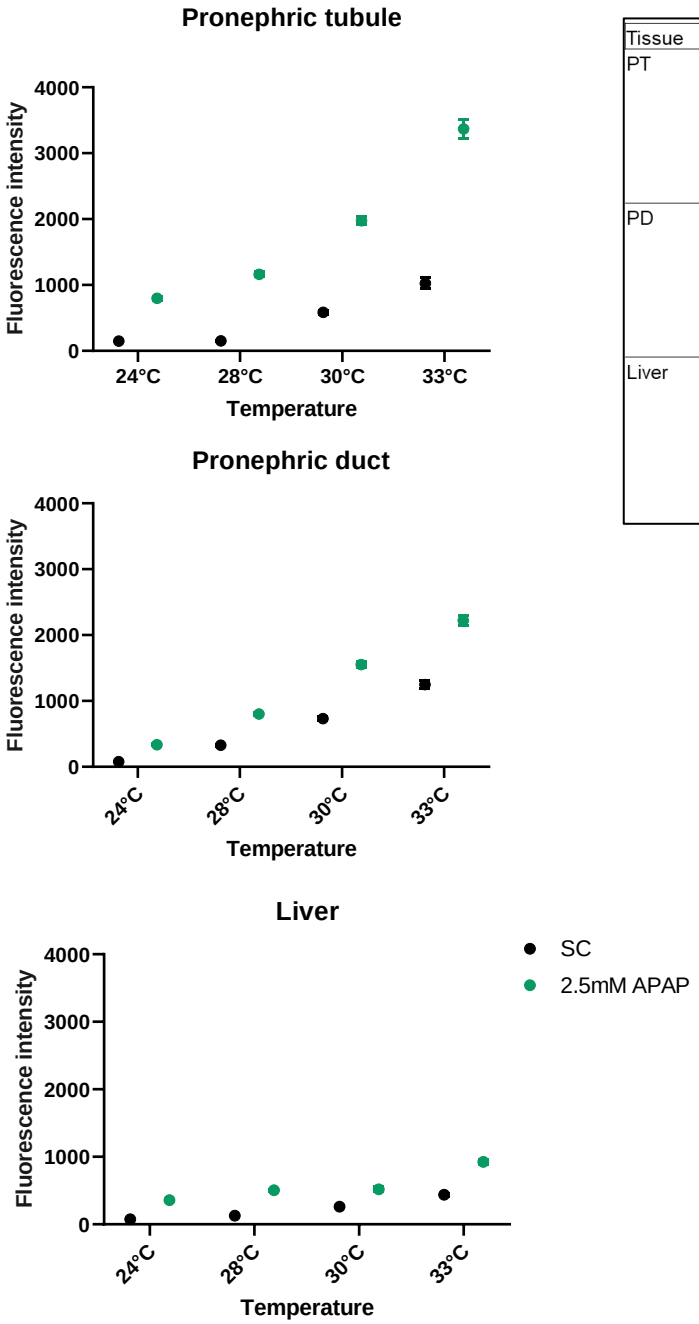


| Tissue | Treatment group A | Treatment group B | Significance? |
|---|---|---|---|
| PT | 24 °C SC | 28 °C SC | ns |
| | 24 °C APAP | 28 °C APAP | **** |
| | 28 °C SC | 30 °C SC | **** |
| | 28 °C APAP | 30 °C APAP | **** |
| | 30 °C SC | 33 °C SC | **** |
| | 30 °C APAP | 33 °C APAP | **** |
| PD | 24 °C SC | 28 °C SC | **** |
| | 24 °C APAP | 28 °C APAP | **** |
| | 28 °C SC | 30 °C SC | **** |
| | 28 °C APAP | 30 °C APAP | **** |
| | 30 °C SC | 33 °C SC | **** |
| | 30 °C APAP | 33 °C APAP | **** |
| Liver | 24 °C SC | 28 °C SC | ns |
| | 24 °C APAP | 28 °C APAP | **** |
| | 28 °C SC | 30 °C SC | **** |
| | 28 °C APAP | 30 °C APAP | ns |
| | 30 °C SC | 33 °C SC | **** |
| | 30 °C APAP | 33 °C APAP | **** |

*Figure 6.6* ***APAP-induced OS across the temperature range assessed****. Embryos were exposed to 2.5 mM APAP or a SC from 6 hpf and raised at a range of different temperatures in separate experiments. Control groups showed no statistical difference and so were pooled together, therefore, each data point represents an N of 18, performed in triplicate. Data shows mean values (+/- SEM, N= 12) for the mean pixel intensity within the organs of 3 dpf larvae. Data were normally distributed and had equal variance, and so were analysed using and ANOVA followed by Bonferroni's to confirm exposure to 2.5 mM APAP induced significantly higher fluorescence than the SC at each temperature tested (P<0.0001). [Inset] Pairwise comparisons between temperature groups. Following an ANOVA, Tukey's test was used to compare effect of temperature on SC and APAP separately. * = P< 0.05, **= P< 0.005, ***= P<0.0005, ****= P< 0.0001.*

### 6.3.5 Interaction of temperature and pharmaceutical-induced oxidative stress: across time and different temperatures

Figures 6.7 and 6.8 show how EpRE:mCherry embryo-larvae responded to a single concentration of drug when raised at a range of different temperatures, with the fluorescent intensity measured at 2, 3 and 4 dpf. For both APAP and DCF, 33°C had the greatest impact on drug-induced OS compared with the other temperatures tested. The difference is particularly pronounced in embryo-larvae treated with DCF, where all three target organs showed significant DCF-induced OS at 2 dpf when cultured at 33°C ($P<0.0005$) but not at 28°C (Table 6.3). The lower temperature of 24°C appeared to result in a reduced drug-induced OS response. This is again particularly prominent in embryo-larvae treated with DCF shown to cause significant DCF-induced OS at 3 dpf when cultured at 28°C ($P<0.0005$), but no OS was observed when embryos were raised at 24°C (Table 6.3).

The most responsive organs were, again, drug related, with the liver most responsive to DCF at 30°C and 33°C (reaching a maximum fluorescence intensity in the 33°C regimen of around 20000 arbitrary units, compared to around 6000 in the PT or 4000 in the PD), whereas the PT was most responsive to APAP exposure at higher temperatures (reaching a maximum of approximately 7000 arbitrary units compared to 2000 in the liver or 5000 in the PD). The difference in OS in the PT between exposed embryos raised at 28°C versus 30°C appeared greater at 4 dpf than 3 dpf.

**2.5 mM APAP**

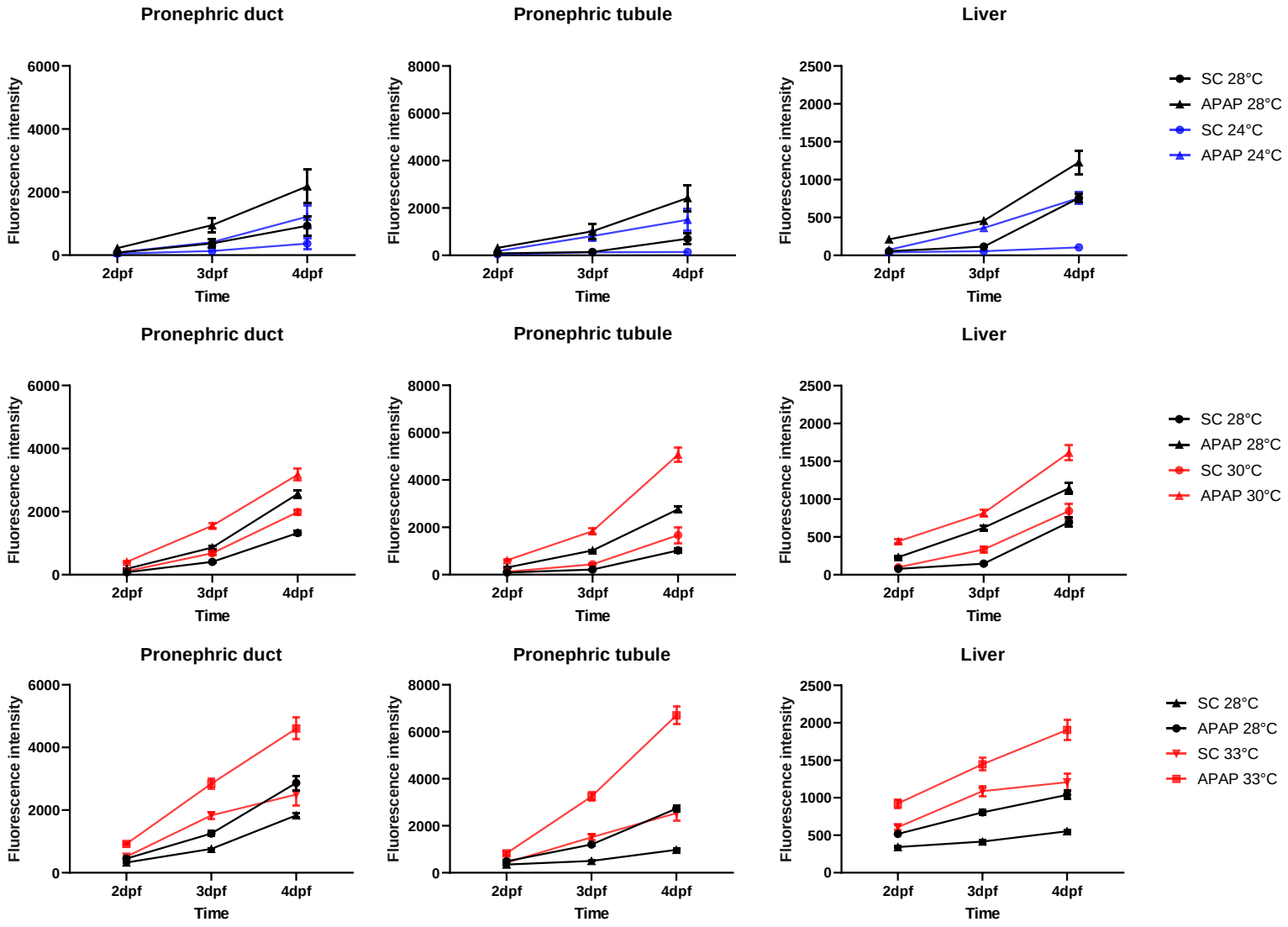


*Fig. 6.7* ***Embryos exposed to 2.5 mM APAP from 6 hpf and raised at different temperatures, where mCherry fluorescence intensity was measured over time.*** Data shows mean values (+/- SEM, N= 24) for the mean pixel intensity within the organs

| Comparisons between drug treatments **(within temperature groups)** | | | | |
|---|---|---|---|---|
| | | Significance of difference between **SC and APAP exposure** | | |
| | | **2 dpf** | **3 dpf** | **4 dpf** |
| PD | **28°C** | ns | **** ↑ | **** ↑ |
| | 24°C | ns | ** ↑ | **** ↑ |
| PT | **28°C** | * ↑ | **** ↑ | **** ↑ |
| | 24°C | ns | **** ↑ | **** ↑ |
| liver | **28°C** | ns | *** ↑ | **** ↑ |
| | 24°C | ns | ** ↑ | **** ↑ |
| PD | **28°C** | ns | *** ↑ | **** ↑ |
| | 30°C | * ↑ | **** ↑ | **** ↑ |
| PT | **28°C** | ns | **** ↑ | **** ↑ |
| | 30°C | * ↑ | **** ↑ | **** ↑ |
| liver | **28°C** | ns | **** ↑ | **** ↑ |
| | 30°C | **** ↑ | **** ↑ | **** ↑ |
| PD | **28°C** | ns | ns | *** ↑ |
| | 33°C | ns | *** ↑ | **** ↑ |
| PT | **28°C** | ns | * ↑ | **** ↑ |
| | 33°C | ns | **** ↑ | **** ↑ |
| liver | **28°C** | ns | *** ↑ | **** ↑ |
| | 33°C | ** ↑ | *** ↑ | **** ↑ |

| Comparisons **between temperatures** (within drug treatment) | | | | | |
|---|---|---|---|---|---|
| | | | Significance of difference between **control (28°C) and experimental temperature** | | |
| | | | **2 dpf** | **3 dpf** | **4 dpf** |
| 24°C | PD | **SC** | ns | * ↓ | **** ↓ |
| | | **APAP** | ns | **** ↓ | **** ↓ |
| | PT | **SC** | ns | ns | **** ↓ |
| | | **APAP** | ns | ns | **** ↓ |
| | liver | **SC** | ns | ns | **** ↓ |
| | | **APAP** | ns | ns | **** ↓ |
| 30°C | PD | **SC** | ns | ns | **** ↑ |
| | | **APAP** | ns | **** ↑ | **** ↑ |
| | PT | **SC** | ns | ns | ** ↑ |
| | | **APAP** | ns | **** ↑ | **** ↑ |
| | liver | **SC** | ns | * ↑ | ns |
| | | **APAP** | * ↑ | * ↑ | **** ↑ |
| 33°C | PD | **SC** | ns | **** ↑ | * ↑ |
| | | **APAP** | ns | **** ↑ | **** ↑ |
| | PT | **SC** | ns | *** ↑ | **** ↑ |
| | | **APAP** | ns | **** ↑ | **** ↑ |
| | liver | **SC** | * ↑ | **** ↑ | **** ↑ |
| | | **APAP** | *** ↑ | **** ↑ | **** ↑ |

*Table 6.2* ***Results of statistical analyses for data outlined in Fig. 6.7.*** *Both panels show the same experiments, [left] compared within temperature groups and [right] compared within drug treatment. Data were normally distributed and had equal variance and so were analysed using a 2-way ANOVA followed by Tukey's multiple comparison test. An interaction effect was found between temperature and APAP exposure (P<0.00001). Asterisks represent multiplicity adjusted P values: * = P< 0.05, **= P< 0.005, **= P<0.0005, ****= P< 0.0001.*

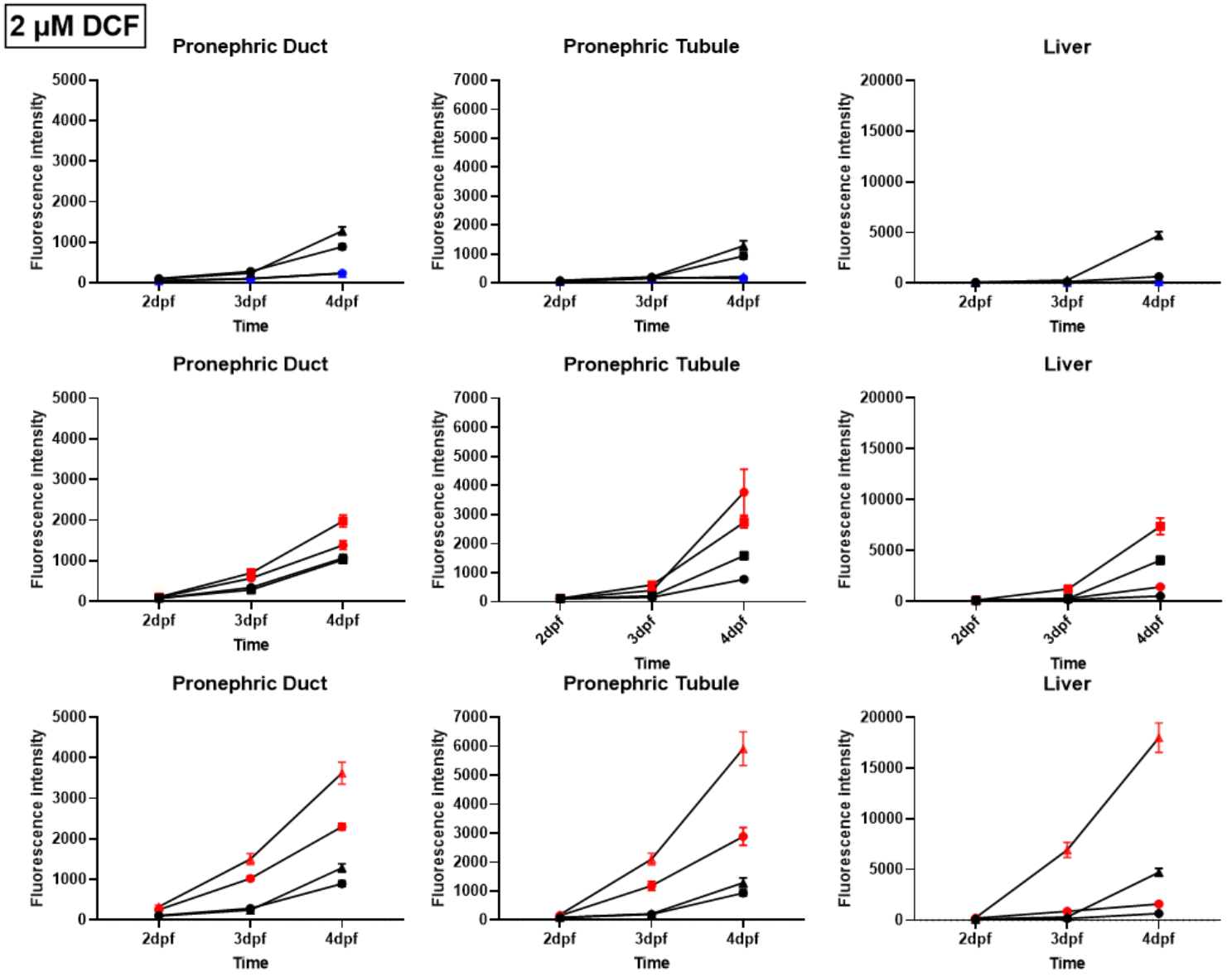


*Figure 6.8* ***Embryos exposed to 2 µM DCF from 6 hpf and raised at different temperatures, where mCherry fluorescence intensity was measured across time.*** *Data shows mean values (+/- SEM, N= 24) for the mean pixel intensity within the organs.*

| Comparisons between drug treatments **(within temperature groups)** | | | | |
|---|---|---|---|---|
| | | Significance of difference between **CW and DCF exposure** | | |
| | | **2 dpf** | **3 dpf** | **4 dpf** |
| PD | **28°C** | ns | ns | **** ↑ |
| | 24°C | ns | ns | ns |
| PT | **28°C** | ns | ns | *** ↑ |
| | 24°C | ns | ns | ns |
| liver | **28°C** | ns | ns | **** ↑ |
| | 24°C | ns | ns | ns |
| PD | **28°C** | ns | ns | ns |
| | 30°C | ns | ns | ** ↑ |
| PT | **28°C** | ns | ns | ns |
| | 30°C | ns | ns | * ↑ |
| liver | **28°C** | ns | ns | **** ↑ |
| | 30°C | ns | * ↑ | **** ↑ |
| PD | **28°C** | ns | ns | ** ↑ |
| | 33°C | ns | *** ↑ | **** ↑ |
| PT | **28°C** | ns | ns | ns |
| | 33°C | ns | *** ↑ | **** ↑ |
| liver | **28°C** | ns | ns | **** ↑ |
| | 33°C | ns | **** ↑ | **** ↑ |

| Comparisons **between temperatures** (within drug treatment) | | | | | |
|---|---|---|---|---|---|
| | | | Significance of difference between **control (28°C) and experimental temperature** | | |
| | | | **2 dpf** | **3 dpf** | **4 dpf** |
| 24°C | PD | **CW** | ns | ** ↓ | **** ↓ |
| | | **DCF** | ns | ns | **** ↓ |
| | PT | **CW** | ns | ns | **** ↓ |
| | | **DCF** | ns | ns | **** ↓ |
| | liver | **CW** | ns | ns | ** ↓ |
| | | **DCF** | ns | ns | **** ↓ |
| 30°C | PD | **CW** | ns | ns | ** ↑ |
| | | **DCF** | ns | *** ↑ | ** ↑ |
| | PT | **CW** | ns | ns | ** ↑ |
| | | **DCF** | ns | ns | ** ↑ |
| | liver | **CW** | ns | ns | * ↑ |
| | | **DCF** | ns | * ↑ | **** ↑ |
| 33°C | PD | **CW** | ns | **** ↑ | **** ↑ |
| | | **DCF** | ns | **** ↑ | **** ↑ |
| | PT | **CW** | ns | *** ↑ | **** ↑ |
| | | **DCF** | ns | **** ↑ | **** ↑ |
| | liver | **CW** | ns | ns | ns |
| | | **DCF** | ns | **** ↑ | **** ↑ |

*Table 6.3* ***Results of statistical analyses for data outlined in Fig. 6.8****. Both panels show the same experiments, [left] compared within temperature groups and [right] compared within drug treatment. Data were normally distributed with equal variance and so were analysed using a 2-way ANOVA followed by Tukey's multiple comparison test. An interaction effect was found between temperature and DCF exposure (P<0.00001). * = P< 0.05, **= P< 0.005, **= P<0.0005, ****= P< 0.0001.*

### 6.3.6 Effect of temperature on drug uptake

Elevated temperature drove increased uptake of APAP (Figs. 6.9 and 6.10) in exposed WIK embryo-larvae. Significant differences in the amount of APAP detected in larvae raised at the two different temperatures (28 and 33°C) occurred within the first 24 hours of exposure and also at later time points, specifically 68 and 72 hours post dose (a pattern seen in every replicate).

APAP levels measured in WIK larvae were used to infer the uptake dynamics in the TG larvae imaged as there were no differences in internal APAP levels between WIK or EpRE:mCherry larvae measured at 48 or 96 hours post dose were found (Figs. 6.9 and 6.10).

A pilot study revealed a considerable drop in internal APAP concentration at 48 hours post dose in the 33°C group and a similar scenario was seen for the 28°C treatment group 24 hr later, at 72 hr post dose (see Appendix 2, Fig. 2) which was linked to differing hatching times. This was confirmed through manually dechorionating the larvae at 48 hours post dose, which nullified this difference between temperature groups (Figs. 6.9 and 6.10). This suggests a large portion (around 75%) of the APAP detected in embryos pre-dechorionation was within the chorion and/or perivitelline space.

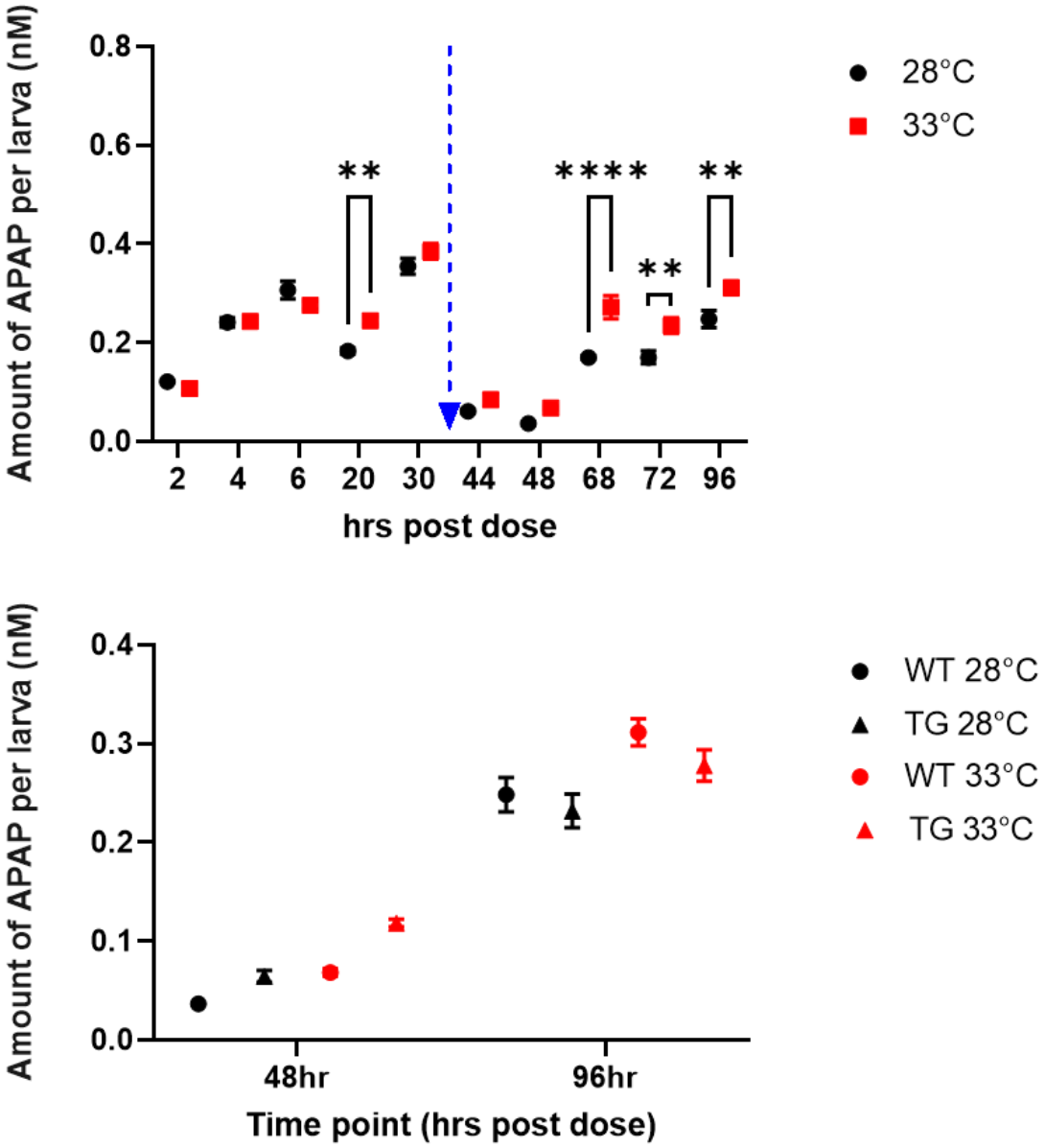


*Figure 6.9 [Top]* ***Effect of temperature on uptake dynamics of APAP in WIK embryos exposed to 2.5 mM APAP from 6hpf.*** *Data shown as mean concentration detected in the larval body (+/- SEM; N=6) using LC-MS/MS. Arrow indicates manual dechorionation at 42 hrs post dose. Data were normally distributed with equal variance and so were analysed using an ordinary one-way ANOVA followed by Bonferroni's test to compare different temperature groups at each time point. *= P<0.05, **=P<0.005, ***=P<0.0005, ****=P<0.0001. [Bottom]* ***Comparison of APAP uptake in EpRE:mCherry versus WT embryos*** *(N=6). Data shown as mean +/- SEM. Data were not normally distributed and so were tested using a Kruskal-Wallis followed by Dunn's test. No significant difference was found between TG and WT embryos.*

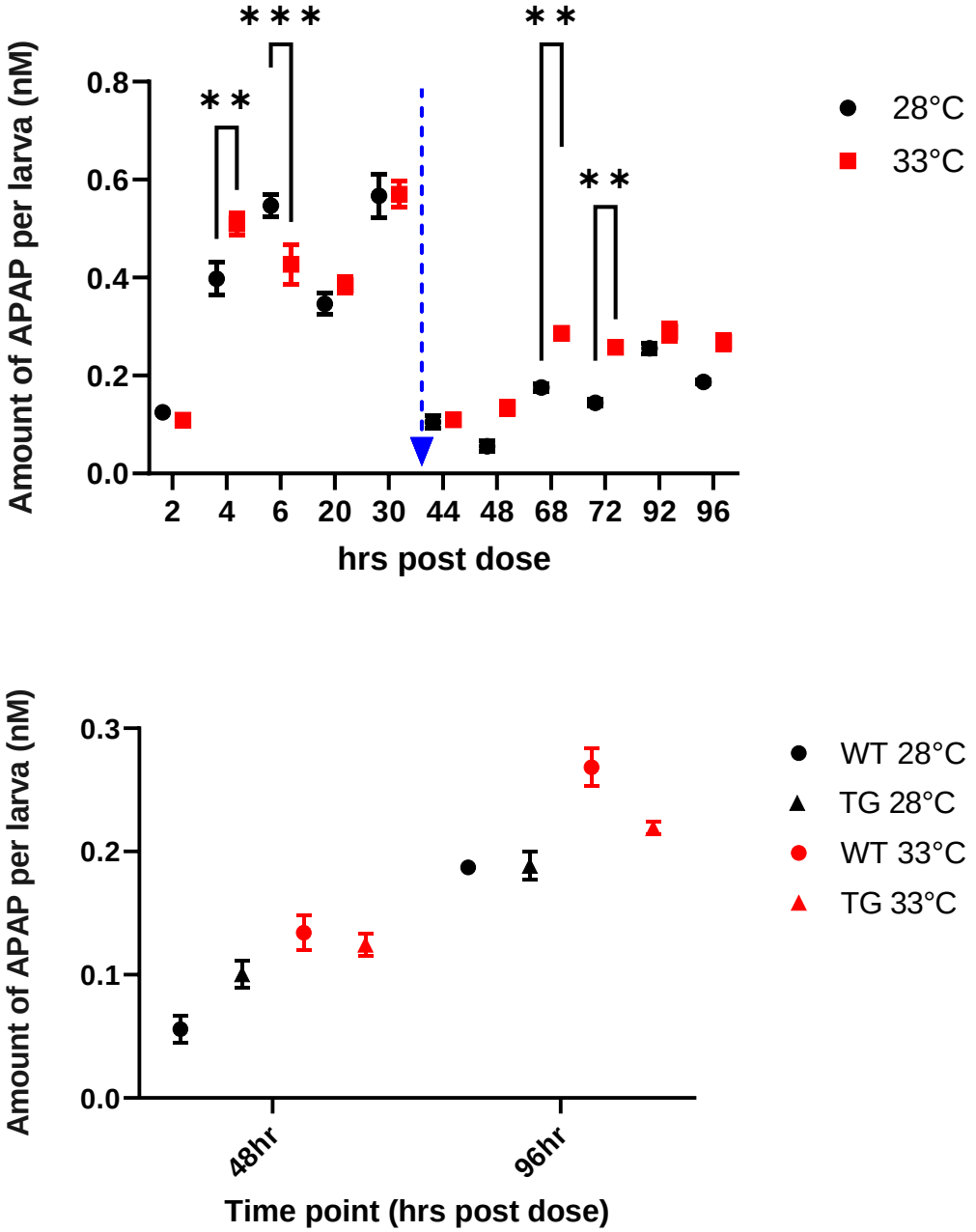


*Figure 6.10 Repeat of the above experiment. [Top]* ***Effect of temperature on uptake dynamics of APAP in WIK embryos exposed from 6 hpf****. Data shown as mean concentration detected in the larval body (+/- SEM; N=6) using LC-MS/MS. Arrow indicates manual dechorionation at 42 hrs post dose. Data were normally distributed with equal variance and so were analysed using an ordinary one-way ANOVA followed by Bonferroni's test to compare different temperature groups at each time point. *= P<0.05, **=P<0.005, ***=P<0.0005, ****=P<0.0001. [Bottom]* ***Comparison of APAP uptake in EpRE:mCherry versus WT embryos*** *(N=6). Data shown as Mean +/- SEM. Data were not normally distributed and so were tested using a Kruskal-wallis followed by Dunn's test. No significant difference was found between TG and WT embryos.*

## 6.4 Discussion

As expected, elevated temperature can exacerbate drug-induced OS, and this effect has been demonstrated here for three different pharmaceuticals, across a range of temperatures, concentrations, and time points. The LC-MS/MS data suggests this interaction is at least partly a result of increased uptake of the drug, although other mechanisms are also likely to be involved such as enhanced drug biotransformation or diminished antioxidant defences of thermally stressed larvae.

### 6.4.1 Effect of temperature on basal redox status

As Fig. 6.1 shows, temperature alone can affect OS. Increased OS in non-chemically treated EpRE:mCherry larvae raised at 33°C compared to 28°C (Fig. 6.1) aligns with what is known about the relationship between metabolism and temperature (Clarke & Fraser, 2004). Higher temperature results in a higher level of kinetic energy which drives faster enzymatic processes, which requires more ATP and so also drives increased respiration (Gillooly, 2001). Indeed, previous studies on zebrafish embryos have shown they consume a higher amount of oxygen when raised at 31°C compared to 28°C, and a lower oxygen consumption when raised at 25°C (Barrionuevo & Burggren, 1999). Hence, warmer conditions result in increased ROS production by the mitochondrial electron transport chain (Heise, 2003), which in the current study required buffering by antioxidants and resulted in upregulation of the EpRE.

### 6.4.2 Effect of temperature on drug-induced OS

Culturing larvae at 5°C above standard husbandry conditions was shown to exacerbate drug induced OS and resulted in a lower LOEC, as was shown for exposure to APAP (Fig. 6.3), Dox (Fig. 6.4) and DCF (Fig. 6.5). This could have been the result of an additive effect between the pro-oxidative action of the chemical and the increased basal OS caused by temperature. However, there is strong evidence in the literature for a direct interaction between temperature and drug toxicity. Elevated temperature has been shown to increase APAP toxicity in *D. magna* (Kim et al., 2010) and medaka (Kataoka *et al.*, 2019). Both studies proposed an increase in rates of drug uptake and drug metabolism to be the main drivers behind this interaction, although neither included any analytical chemistry data to support their postulations.

The interaction between DCF and temperature has been found to be more complex and species-dependent. DCF-induced OS was exacerbated in juvenile seabass (*Dicenthrachus labrax*) cultured at 5°C above the control, likely through the enhanced inhibition of antioxidant enzyme activity, such as for CAT and SOD (Maulvault et al., 2018a). Mussels (*Mytilus galloprovincialis)* showed a reduction in their metabolic activity at elevated temperatures to preserve antioxidant defences, although this was not sufficient to prevent DCF-induced OS (Freitas *et al.*, 2019). In contrast, in the clams *Ruditapes philippinarum* and *Ruditapes decussatus,* increased temperature drove an increase in respiration and metabolism which reduced the bioaccumulation of DCF and in turn reduced OS (Costa *et al.*, 2020), in direct contrast with the results presented in Figs. 6.5 and 6.8.

The enhancement of Dox-induced OS at warmer rearing conditions is a novel finding. Depending on the species, Dox is currently assumed to present a medium-low risk in the environment due to its potential for genotoxic effects but low concentrations detected in surface waters (Martín et al., 2014). There are, however, no ecotoxicological data available in the literature regarding the interaction of Dox with temperature. The data in this thesis shows that increasing environmental temperatures have the potential to increase the risk associated with exposure to this pharmaceutical due to induction of OS at lower concentrations of the drug (Fig. 6.4).

As was seen in Chapter 4, the PT was particularly resistant to OS induction by Dox. Consequently, there was minimal OS in this tissue for the elevated temperature to exacerbate. Despite the increased background OS measured in larvae raised at 33°C compared to 28°C, and the OS induced by 7.4 or 9.2 µM Dox at the normal temperature, the two stressors combined did not increase the OS in the PT beyond background levels for the 33°C treatment group (Fig. 6.4).

In contrast with Dox-exposed larvae, the PT of APAP-exposed larvae showed one of the greatest increases in OS when raised at warmer temperatures compared with other tissues (Fig. 6.4). This is likely to relate to the innate sensitivity of the PT as a result of its lower levels of endogenous antioxidants (Chevalier, 2016). However, the liver exhibited the earliest induction of OS by APAP when raised at 33°C (at 2 dpf compared to 3 dpf for the PT or PD; Table 6.2), perhaps due to its faster development compared with the pronephros, which

doesn't fully mature until 4 dpf (although leaky glomerular filtration does begin at 2 dpf) while the liver becomes functional at 3 dpf (Drummond & Davidson, 2010). Indeed, a significant difference in basal OS (i.e., as measured in SC larvae) between larvae raised at 28°C and 33°C is first detectable in the liver at 2 dpf, compared with 3 dpf for the PT and PD (Table 6.2).

To further understand the relationship between temperature and drug-induced OS, embryo-larvae were exposed to APAP under one of several temperature regimens with varying severity. The data presented in Fig. 6.6 shows that any increase in incubation temperature caused an absolute increase in OS induction by APAP; exacerbation of APAP-induced OS was observed at an extreme temperature (33°C) and at a small increase in temperature (2°C), particularly in the PT. However, the larvae's OS response to APAP appears to diminish at higher incubation temperatures compared with the response to increased temperature alone; the difference in OS between chemically treated and non-treated larvae was smaller at 33°C compared with 28°C incubation (Fig. 6.6). However, only two temperatures above normal conditions were tested, so further study testing a greater range of temperatures is needed to confirm if the difference in OS between exposed and non-exposed larvae continues to decrease at higher incubation temperatures (i.e., if this relationship is non-linear). The thermal stress caused by higher incubation temperatures likely overburdened the antioxidant defences, impeding the larvae's ability to respond to the additive effect of the chemical stressor.

The current data, generated using the EpRE:mCherry model, can only indicate activation of the EpRE (and therefore upregulation of antioxidant defences). However, if the larvae's defences are at their limit, further increases in OS and damage would not be reflected in mCherry expression. Therefore, although the EpRE response to APAP exposure is proportionally smaller at higher temperatures, the oxidative damage caused by the chemical may not be. A future study could benefit from measuring biomarkers of oxidative damage such as MDA (a product of lipid peroxidation) or DNA breakage. The quantification of direct consequences of OS caused by a chemical at higher temperature would show if the relative effect of APAP compared to temperature is reduced at 33°C, or if only the animal's ability to respond to APAP-induced OS is reduced.

The data presented in this chapter also suggests that APAP-induced OS was lower when the embryo-larvae were raised at 24°C compared to 28°C (Figs. 6.6 and 6.7). As mentioned previously, incubation at the lower temperature resulted in a retardation of embryonic development, resulting in smaller sized larvae at every time point (Fig. 6.2). Therefore, it was difficult to establish whether the lower relative fluorescence intensity represents a suppression of the OS response due to the direct effect of temperature, or reduction in cell numbers to emit fluorescence as a result of underdeveloped organs. A lower level of OS induction by APAP would align with what is known about the relationship between temperature and contaminant uptake/metabolism (discussed below). Alternatively, the reduced fluorescence could be indicative of suppression of the antioxidant defence system due to reduced metabolic activity, ultimately resulting in higher level of OS, as has previously been reported in juvenile pacu (*Piaractus mesopotamicus)* (Pinto *et al.*, 2019). However, this seems unlikely in the present study as reduced metabolic activity would also impede biotransformation of APAP, reducing its toxicity.

### 6.4.3 Effect of temperature on drug pharmacokinetics

Incubation of the embryo-larvae at 33°C resulted in higher levels of APAP in the body of exposed larvae compared to those raised at the standard temperature (Figs. 6.9 and 6.10). The present pharmacokinetic study used only APAP to investigate the effect of temperature on uptake dynamics, but the uptake of DCF and Dox are assumed to show a similar response as they also followed a similar trend in temperature enhanced OS. Indeed, higher temperature has been shown to increase the amount of DCF bound to a zebrafish embryo, possibly as a result of increased metabolic activity and increased flow rate (Chen et al., 2015).

It is unknown if the more rapid uptake observed would eventually result in a higher steady state concentration within the larva, or if the steady state would be reached sooner in larvae incubated at 33°C, as internal concentrations did not reach equilibrium during the exposure period. Interestingly, one of the replicates (Fig. 6.10), would suggest that increased temperature drove the APAP toxicokinetics to reach steady state at a faster rate, as the internal APAP levels in the 33°C treatment group plateaued from 68 hours post dose, whilst this did not occur until 92 hours post does in the 28°C group. Furthermore, final internal concentrations did not appear to be affected as there was no statistical difference

in APAP levels between the temperature groups at 92 and 96 hours post dose. However, this pattern was not seen in the first replicate (Fig. 6.9). A follow up experiment with a longer exposure period to allow steady state to be reached within the larvae is needed to confirm this.

There are several possible mechanisms by which elevated temperature could have driven increased APAP uptake. Increased ventilation rate (Heugens *et al.*, 2003) (as proposed in the Introduction) is not a possible factor at this developmental stage as larvae do not require gills for ventilation until approximately 14 dpf (oxygen can be absorbed directly through the skin in embryo-larvae) (Rombough, 2002).

Higher temperatures appear to have driven increased uptake via accelerated larval development, as embryo-larvae raised at 33°C were shown to achieve longer body lengths at 2 dpf (Fig. 6.2), hatch up to 24 hours earlier and develop more inflated swim bladders by 4 dpf compared to control zebrafish. In unhatched embryos, this could have resulted in increased chorion permeability, a factor which has been shown to increase with age (Adams et al., 2005; Ali et al., 2017; Hagedorn et al., 1997), and therefore allowed more drug to reach the embryo (even when all larvae were manually dechorionated at the same time).

In hatched larvae, accelerated development could have resulted in earlier opening of the mouth, providing a new absorption route (i.e., via the gut) in addition to diffusion across the skin and gills. Indeed, previous studies into the ADME of APAP in zebrafish have shown a sharp increase in APAP absorption rate in zebrafish larvae between 3 and 4 dpf (Kantae *et al.*, 2016; Van Wijk *et al.*, 2018) which was postulated to be related to the opening of the mouth at 3 dpf (Van Wijk *et al.*, 2018) (also see Fig. 3.3 in Chapter 3). This aligns with the pattern observed in the present study, in which APAP levels in both temperature treatment groups suddenly increased at 3 dpf (between 48- and 68-hours post dose) (Figs. 6.9 and 6.10). After manual dechorionation at 42 hours post dose, APAP levels were not significantly different between the two temperature groups until 68 hours post dose, at which point the amount of APAP detected in larvae raised at 33°C was significantly higher than in larvae raised at 28°C. The mouths of larvae raised at 33°C are likely to have opened sooner compared to those at 28°C (between 48- and 68-hours post dose), allowing higher levels of APAP absorption. In further support of this hypothesis, higher incubation temperatures

resulted in greatest increase in drug-induced OS in the GI tract compared with the other body tissues measured, as demonstrated for every drug tested (Figs. 6.3, 6.4, 6.5).

The drop in internal APAP volume at 20 hours post dose compared to the previous time point was seen in every experiment replicate (including the pilot study, shown in Appendix 2), for all temperature treatments. This does not seem to have been previously reported in the literature but could likely be explained by the ontogenetic expression of active drug transporters in the body of the larvae. ATP-binding cassette (ABC) transporters are a superfamily of membrane proteins; ABCB4 has been shown to expel xenobiotics and protect zebrafish embryos from their toxic effects (Fischer *et al.*, 2013). Fischer *et al.* showed that, while transcript levels of *abcb4* were highest at 1 hpf due to maternally transferred mRNA, levels progressively declined until 12 hpf, then began to rise again at 24 hpf, peaking at 48 hpf. The timing of the rise in *abcb4* expression coordinates with the reduced APAP volume detected in the embryos at 20 hours post dose/26 hpf in the present study. Indeed, Fischer *et al.* showed that inhibition of this transporter resulted in higher levels of contaminants entering the body from the exposure media. Previous studies have also shown ABCB transporters protect freshwater species from environmental pollutants (Ferreira et al., 2014; Luckenbach & Epel, 2008). Interestingly, in one of the replicated experiments (Fig. 6.10), the volume of APAP detected in embryos in the 33°C group was significantly lower than in the 28°C group at 6 hours post dose, the only time point at which the higher temperature resulted in a lower internal dose of the drug. This could potentially reflect the accelerated development of embryos incubated at 33°C which resulted in an earlier onset of *abcb4* expression and hence expulsion of the drug.

Mammalian data indicates that APAP is highly bioavailable and uptake can occur passively, while its metabolites require active transporters such as solute carrier transporters and ABC transporters (Mazaleuskaya *et al.*, 2015). Therefore, although active drug transport may have expelled some APAP at 26 hpf, the overall increased uptake at higher temperatures was probably linked to enhanced diffusion of APAP across membranes, driven by an increase in kinetic energy (Pinheiro *et al.*, 2021).

However, increased drug uptake does not appear to be the only mechanism driving increased OS in exposed larvae incubated at higher temperatures as the difference in APAP uptake between larvae raised at 28 and 33°C was not as sizable as the differences in OS measured at these time points. Furthermore, in one of the replicates (Fig. 6.9) there was no difference in APAP levels between the temperature treatment groups by the end of the exposure period.

### 6.4.4 Alternative mechanisms driving enhanced APAP-induced OS

Environmental factors, including temperature, are known to influence all elements of ADME of a pharmaceutical, as well as the interactions between the drug and target molecules (Hooper *et al.*, 2013). Higher temperatures have been shown to drive chemical biotransformation via increased enzymatic activity (Buckman *et al.*, 2007), which can increase production of toxic metabolites, as has been proposed to drive increased APAP toxicity in *D. magna* cultured at higher temperatures (Kim et al., 2010). However, Kim *et al.* 's study lacked chemical analysis to support this hypothesis.

Juvenile European perch (*Perca fluviatilis*) exposed to the anxiolytic drug temazepam in warmer conditions showed increased metabolism and uptake, resulting in increased accumulation of its metabolites. However, this was not in dragonfly (*Sympetrum* sp.) larvae, indicating a species-specific effect (Cerveny *et al.*, 2021). Medaka larvae reared at higher temperatures have also been reported to show increased metabolism of APAP as a result of accelerated liver development (indicated by decreasing ATP levels and larger liver/increased yolk absorption, respectively) (Kataoka *et al.*, 2019). Kataoka *et al.* proposed enhanced CYP activity as the mechanism responsible, and indeed, hepatic CYP1A has previously shown temperature- enhanced translational activity in killifish (*Fundulus heteroclitus)* (Kloepper-Sams & Stegeman, 1992). However, no changes were detected in CYP1a activity in adult zebrafish raised at 30°C compared to 27°C (Cardoso et al., 2019), suggesting the influence of stressors on CYP activity is species dependent. The capacity of zebrafish larvae for CYP metabolism at the 3 to 4 dpf stages are explored in Chapter 4 (section 4.3.5). It is possible that, when raised at 33°C, CYP metabolism in the zebrafish larvae was enhanced and resulted in increased production of toxic metabolites such as NAPQI for the APAP exposure. NAPQI is highly reactive, but levels of its conjugates could be measured to indicate the effect of temperature on

metabolism rate. This was attempted in my thesis work using MSI (see chapter 4) but was unsuccessful. With more time, other methods for quantifying APAP metabolites could have been explored.

Whilst in the present study the effect of different incubation temperatures on drug excretion was not tested, increased biotransformation at higher temperatures has previously been linked to increased elimination. However, conflicting data in the literature indicates species-dependent effects. Northern leopard frog (*Lithobates pipiens*) tadpoles showed increase elimination rates of polychlorinated biphenyls (PCBs) under warmer conditions, but this was balanced by more rapid uptake, resulting in unchanged steady state tissue levels of the compounds (Brown et al., 2021). In contrast, higher temperatures have been shown to impair the ability of the liver in various juvenile fish species to detoxify pharmaceuticals and other pollutants (Maulvault et al., 2016, 2018b). A depuration study testing the effects of different temperature regimens would be required to fully understand the effect of temperature on the dynamics of APAP elimination in zebrafish larvae.

The temperature sensitivity of metabolism in juvenile zebrafish has been shown to be lower at later life stages, suggesting larvae develop the capacity to regulate oxygen consumption from around 20 dpf (Barrionuevo & Burggren, 1999). This suggests that, while the larvae in the present study showed high sensitivity to temperature alone and in combination with a drug, this interaction may not occur/be lessened in older fish. It would be interesting to follow up with a longitudinal study using similar exposure conditions but for adult zebrafish (see Pinheiro *et al.* 2021 for a review on the influence of developmental stage on responsiveness to temperature). Additionally, previous studies have shown that the husbandry temperature for early development can have lasting effects on the physiology of zebrafish persisting into adulthood, including affecting how they respond to stressors later in life (Dimitriadi et al., 2018; Zhang et al., 2018) or how they can acclimate to changing conditions (Scott & Johnston, 2012). Building on the increased OS detected in the EpRE:mCherry model here, a valuable future study might investigate how extreme temperature conditions in early life affect the ability of an adult zebrafish to buffer against pharmaceutical-induced OS. An acute exposure study would also be valuable to test if elevated temperature and drug exposure have to coincide for the two stressors to interact, or if pre-exposure to one influences the animal's response to the other.

The natural habitat of zebrafish can range from 6°C in winter to 38°C in summer across the geographical range of zebrafish (Spence et al., 2008), and between 29 and 33°C across sites in the dry season (Spence et al., 2006). Zebrafish are therefore generally fairly tolerant of temperature changes, but this plasticity is laid down by developmental conditions (de Alba et al., 2021). There are scant studies on how rapidly larvae can acclimate to different temperatures, but data shows that rearing at a constant temperature of 26°C compared with a daily thermocycler of 28°C – 24°C from 0 hpf could affect how a 4 dpf larvae responds to heat stress (de Alba *et al.*, 2021), indicating that even this short time period is sufficient to confer thermal tolerance. Hence, even within the acute exposure period of the present study, it is possible that the larvae began to acclimate to the elevated temperature which could reduce the effect of temperature on basal or drug-induced OS. Further study is needed to find if, following a longer exposure period, the difference in OS detected between control and higher temperature larvae declines over time. Although the temperatures tested in this study are within the thermal tolerance range of zebrafish, it could also be interesting to monitor changes in expression of heat shock proteins (HSPs) as a further indicator of how larvae respond to elevated temperature both in the absence and presence of drug exposure.

## 6.5 Conclusions

As global temperatures continue to increase and extreme weather events become more frequent, there is a clear need for better understanding of how abiotic factors may influence the toxicity of environmental pollutants. Despite this, TG zebrafish models are surprisingly underutilised for such studies. This chapter demonstrates the application of EpRE:mCherry model to quantify OS induced by temperature change, and the exacerbation of pharmaceutical-induced OS by extreme temperatures.

Environmentally relevant elevated temperatures have been shown to exacerbate drug-induced OS in an incremental-dependent manner. This has been demonstrated for three different drugs from two different classes and with varying potencies, target organs and mechanisms of toxicity, indicating that the effect of temperature is not a drug-specific interaction. When larvae were raised at 5°C above normal conditions, the LOEC of a drug was reduced, and culturing larvae at just 2°C above normal conditions resulted in earlier induction of OS compared

to when larvae were cultured at 28°C. The augmentation effect of temperature also appeared to increase over time with the exposure period.

This interaction was found to be at least partly due to increased uptake of the drug, a mechanism which has been proposed by many previous studies into the interaction of temperature and drug toxicity, but surprisingly few of them used analytical chemistry to support their postulations. However, the differences in drug uptake between the different temperature groups do not appear to be as drastic as difference in OS detected, indicating the role of another mechanism. The most likely candidate appears to be enhanced metabolism of the drug, but further study is required. The chemistry data presented in this chapter emphasises the importance of these analyses for understanding the mechanism for the responses seen; such analytical chemistry is often lacking in the literature for studies of this nature.

The finding that elevated temperatures can result in a lower LOEC of drug-induced OS is particularly relevant, as it implies that changing temperature conditions have the potential to lower the response thresholds of environmental pharmaceuticals. Depending on the level of this effect, this finding might suggest that compounds currently classified as low risk due to their low environmental concentrations could become more damaging to wildlife at elevated water temperatures. Use of the EpRE:mCherry model has therefore demonstrated the risk of physical-chemical interactions and the present data highlights the need for environmental risk assessments to consider the influence of temperature.

# Chapter 7- General Discussion

## 7.1 Application of imaging tools and transgenic zebrafish in ecotoxicology

TG zebrafish models have advanced our knowledge in the field of developmental biology and are now increasingly being brought more into ecotoxicology. They allow for the detection of compounds interacting in the body with greater sensitivity than many conventional methods, enable identification of novel target organs, and have can be used for HTS for specific toxic actions. TG models have considerable potential for supporting AOPs for environmental toxins by linking cellular interactions to whole body reactions, and for studies into the interactive effect of chemicals for mixture effects.

In this thesis, the combination of the Acquifer imaging platform and TG EpRE:mCherry model were shown to provide effective high throughput assays, well suited for rapid assessment of chemical and temperature effects whilst indicating areas of further study.

The semi-automation of the Acquifer allows rapid assessments of several chemicals in a single plate, which is in stark contrast with confocal microscopy which can take up to 15 mins to embed and image one sample. However, the Acquifer cannot always detect more sensitive changes in fluorescence expression, such as the assessment of neuromasts in Chapter 3. The Acquifer therefore represents a trade-off between sensitivity and throughput (as many imaging platforms do, discussed in Chapter 1). Likewise, the EpRE:mCherry provides a more efficient and meaningful assessment of the regulatory response to OS through visualisation of EpRE activation, which indicates the activity of numerous downstream genes involved in antioxidant defences, each of which would otherwise require separate analysis and tissue samples. However, the EpRE:mCherry model also appears limited in its ability to detect environmentally relevant concentrations of pharmaceuticals.

### 7.1.2 Potential limitations of the EpRE:mCherry model and the study

The EpRE:mCherry model has provided insight into the mechanism of toxicity for a range of drugs and interactions and can help identify potential risks and/or vulnerable organs that merit further study. The model could only respond to

pharmaceuticals at concentrations exceeding environmental concentrations, but this is not necessarily a limitation. The use of higher concentrations for acute exposure assays is a popular technique for predicting potential chronic low-concentration exposure effects (Vestel *et al.*, 2016). However, the EpRE:mCherry model would not be suitable as a biosensor for environmental samples as it could not detect environmental concentrations of the pharmaceuticals screened; other models for other target genes would allow for more sensitive detection (see Table 7.1).

Further study is required to assess how inhibition of downstream antioxidants feedback to activation of the EpRE, and how levels of EpRE activation corresponds quantitively to ROS generation. This includes, for example, identification of the minimum ROS threshold required for EpRE activation. A future study could use methods such as fluorescent molecular dye which can provide a non-invasive method for quantifying ROS or GSH levels in zebrafish larvae (Lackmann *et al.*, 2018). If this protocol was used in an EpRE:mCherry larvae, a clear link could be drawn between ROS generation and EpRE activation.

A potential limitation of the study on the effect of temperature in general is that there may be some overlap of the molecular pathways for OS defence and temperature responses. The current experimental design does not allow for this distinction and so further study is required to identify genes common between the two pathways, and molecular techniques could quantify the changes in expression of these genes under various temperature regimens. Given the data presented in this thesis, this could start with focussing on expression in the pronephros and how this changes over time with elevated temperature compared to standard husbandry temperatures.

Additionally, chemical exposures in this thesis began at 6 hpf. This developmental stage was deliberately chosen in order to select embryos that are showing normal development and ensure all embryos were at the same stage at the start of the exposure period. However, this is not representative of environmental conditions, where fish are exposed to pollutants from the moment of spawning (and potentially even prior to this in the case of maternal exposure). Very early life stages show distinct vulnerability to chemicals and the change in exposure from 1 hpf to 6 hpf has the potential to affect the OS response measured later in life. In order to avoid this potential limitation, future studies using the EpRE:mCherry

TG model, along with any other zebrafish models, should aim to begin exposure periods within the first two hours of fertilisation.

Future studies using the EpRE:mCherry may also wish to consider alternative exposure routes which were not investigated in the present study, such as ingestion. The mouth opens in zebrafish larvae at around 3 dpf, and so absorption of pollutants across the GI may occur at this stage, and indeed an increase in OS was observed in the GI of the EpRE:mCherry model at 3-4 dpf. However, at the early life stage used in the current project and other FET assays, larvae are not capable of independent feeding and so aqueous exposure via the media is the primary exposure route. Other routes may become more important at later life stages, but at older ages the efficacy of a TG zebrafish model is reduced due to the opacity of tissue and so would not be suitable for such studies.

### 7.1.3 3Rs

The EpRE:mCherry model is a sensitive biomarker in that it can detect OS at compound concentrations below those needed to induce overt toxicity (i.e., observed as pericardial oedemas; as shown in Chapter 4). This facilitates conformance to the 3Rs by allowing the use of less severe endpoints, a common aim in the application of TG models. It can also minimise the need for older, protected animals in longer term experiments by visualising OS induction in an acute exposure before the drug can go on to cause tissue damage. Additionally, use of the EpRE:mCherry model can help to reduce the total number of animals needed for any given experiment by providing more in-depth information on the chemical effect compared with assessment of malformations. The Acquifer could also reduce the total number of animals needed for certain assays by allowing a larva to be recovered after imaging so the same individual can be imaged at multiple time points.

*Table 7.1* ***Revised table from General introduction, showing the sensitivities of popular TG models****. Highlighted in green is the greatest sensitivity achieved using the EpRE:mCherry model in the pharmaceutical screen from chapter 5.*

| TG model | Biomarker | Sensitivity (nM) | Test Compound | Exposure time (from 0dpf unless otherwise stated) | Imaging method | Reference |
|---|---|---|---|---|---|---|
| cyp1a:GFP (zebrafish model, medaka promoter) | Cytochrome P450 | 0.001 | TCDD | 1 day (from 4 dpf) | Fluorescent stereomicroscope | Xu *et al.* 2015 |
| ERE:GFP | Oestrogen | 0.00337 | EE2 | 4 days | Inverted confocal microscope | Lee *et al.* 2012a |
| casper ERE:GFP | Oestrogen | 0.00337 | EE2 | 5 days | ArrayScan | Green *et al.* 2016 |
| ERE-kaede-casper | Oestrogen | 0.00337 | EE2 | 5 days | Inverted compound microscope | Green *et al.* 2018 |
| ere-zvtg1: gfp | Oestrogen (via vitellogenin) | 0.00337 | EE2 | 5 days | Fluorescence microscope | Chen *et al.* 2010 |
| vtg1:mCherry | Oestrogen (via vitellogenin) | 0.00337 | EE2 | 5 days | Fluorescent stereomicroscope | Bakos *et al.* 2019 |
| cyp1a:GFP (medaka model) | Cytochrome P450 | 0.005 | TCDD | 1day | Inverted fluorescence microscope | Ng and Gong 2013 |
| cyp1a:nls-eGFP (zebrafish model, zebrafish promotor) | Cytochrome P450 | 0.01 | TCDD | 3 days | Fluorescent stereomicroscope and confocal (for fixed embryos) | Kim *et al.* 2013 |
| Cyp19a1b-GFP | Oestrogen (via Brain aromatase) | 0.05 | EE2 | 5 days | Fluorescent microscope and confocal (for fixed embryos) | Brion *et al.* 2012 |
| ERE-Luc (not in vivo visualisation) | Oestrogen | 0.1 | EE2 | 4 days | Luciferase activity assayed using a luminometer following homogenisation | Legler *et al.* 2000 |
| 5xERE:GFP | Oestrogen | 1.6869 | EE2 | 3 days | Fluorescent stereomicroscope | Gorelick and Halpern 2011 |
| Vtg1:EGFP | Oestrogen (via vitellogenin) | 5 | E2 | 3 days | Fluorescent stereomicroscope | Abdelmoneim, Clark and Mukai 2020 |
| 3EpRE:hsp70:mCherry | Oxidative stress | 17.31 | copper | 2 days (from 2dpf) | Fluorescence microscope and Confocal microscope | Mourabit *et al.* 2019 |
| cyp19a1a-EGFP | Oestrogen (via Gondal aromatase) | 45.66 | EE2 | 21 days (adults) | IVIS Lumina II fluorescence imaging system | De Oliveira *et al.* 2020 |
| EPRE-LUC-GFP | Oxidative stress | 200 | HgCl2 | 1 day | Inverted fluorescence microscope (visualisation of GFP) and luciferase assay (quantification) | Kusik, Carvan and Udvadia 2008 |
| hsp70:GFP | Heat shock proteins | 200 | cadmium | 3 hours (from 3dpf) | Epifluorecent microscope | Blechinger *et al.* 2002 |
| 3EpRE:hsp70:mCherry | Oxidative stress | 367.97 | Doxorubicin | 4 days | Acquifer | Chapter 4 |
| fabp10a:DsRed;elaA:eGFP | Liver and Pancreas (LiPan) | 810.714 | phenylbutazone | 5 days | Fluorescent microscope | Zhang, Li, Gong 2014 |
| fli1:eGFP | Vasculature | N/A | N/A | N/A | Inverted fluorescence microscope | Delov *et al.* 2014 |
| LysC:EGFP and LysC::DsRED2 | Myelomonocytic cells | N/A | N/A | N/A | Fluorescent stereomicroscope | Hall *et al.* 2007 |
| Fms:nfsB.mCherry | Macrophage | N/A | N/A | N/A | | |
| Mpeg1.1:eGFP | Neutrophils | N/A | N/A | N/A | | |
| mpeg1.1:mCherry | Neutrophils | N/A | N/A | N/A | | |

### 7.1.4 Potential future applications of the EpRE:mCherry model

The EpRE:mCherry model could be paired with other TG models to build AOPs, although not achieved in this project due to time constraints. To build on the identification by EpRE:mCherry of the pronephros as a target organ of drug-induced OS, a new experiment could use more tissue-targeted TG zebrafish models to visualise the consequences of OS in this organ. These could include enpep:GFP to visualise the development of the PD and PT (Seiler & Pack, 2011) or wt1b:GFP to visualise the PT and glomerulus (Lo *et al.*, 2014), furthering our understanding of how OS in these tissues may lead to functional or structural changes. Furthermore, this could elucidate the difference in drug-induced OS response observed between the PCT and glomerulus, suggesting that the PCT had a higher baseline of OS, but the glomerulus may be more vulnerable to APAP-induced OS (Chapter 3).

In the wider field of ecotoxicology, the EpRE:mCherry model could also be applied in the investigation of other interactive factors in the environment. For instance, as OS can play a role in pathogenesis (Russo et al., 2012) and injury and wound healing (Cano Sanchez et al., 2018), it could also be used to understand the effects of viruses or bacteria in the water, as well as how this interacts with chemical exposure, as well as the animals' response to injury.

The EpRE:mCherry model can also be translated between species. The Nrf2/Keap1 pathway and its tissue-specific induction are highly conserved among vertebrates and all vertebrate GST genes contain an EpRE-like sequence in the regulatory region (Suzuki *et al.*, 2005; Tsujita *et al.*, 2011). However, the drug screen also alluded to some species-specific effects such as for IBF which has been linked to OS in some teleost species but has limited evidence for OS induction in zebrafish (Bartoskova *et al.*, 2013; Gutiérrez-Noya *et al.*, 2020) and did not cause a response in the model.

The EpRE:mCherry model could also have application in biomedical research (Mourabit *et al.*, 2019), as zebrafish are a popular non-mammalian model for human health because approximately 70% of human genes have at least 1 zebrafish ortholog (Bradford *et al.* 2017; Howe *et al.* 2013). Additionally, the Nrf2/Keap1 is involved in cancer progression (Song et al., 2021).

The interaction between temperature and drug toxicity as indicated by the EpRE:mCherry model could also be relevant to human biology and drug safety. This could indicate the potential for APAP to carry increased risk in patients with an already compromised redox status, particularly as APAP is popular for treating fever and inflammation. However, a study using mice suggests APAP overdose can induce hypothermia (Vaquero et al., 2006), and evidence derived from clinical trials indicate this reduction in body temperature can be beneficial for acute stroke victims (Fang et al., 2017). *Vice versa*, *in vitro* data has indicated that hypothermic conditions can protect against APAP-induced liver injury by conserving mitochondrial function and repressing JNK activation, along with other antioxidant effects such as increased GSH recycling (Tan & Ho, 2020). The EpRE:mCherry could be a valuable *in vivo* tool for the development of hypothermia as a clinical therapy for drug-induced liver injury.

As mentioned in Chapter 1, AOPs are an increasingly popular framework for the assessment of the environmental risk of chemicals. The EpRE:mCherry model may be applied in future ERAs to connect the induction of EpRE with adverse outcomes.

While the EpRE:mCherry did not necessarily have sufficient sensitivity for the detection of OS caused by environmental concentrations of pharmaceuticals, it could be used as a springboard to prioritise and refine subsequent studies using later developmental stages. For instance, through its identification of the liver and pronephros as particularly vulnerable organs, future studies can use more sensitive or targeted measures of OS to further investigate, such as antioxidant enzyme activity assays. Chapters 3 and 4 demonstrate that this TG model can be used for different purposes with different imaging platforms; while the Acquifer allowed rapid screening of the TG embryos to identify pharmaceuticals with potential pro-oxidative action in the pronpehros, the confocal microscope allowed in-depth analysis of the effect of APAP on this tissue by distinguishing the glomerulus from the pronephric convoluted tubule.

### 7.1.5 Future of transgenic models

Recent advances in zebrafish transgenics for developmental biology present opportunities for ecotoxicology; for example, multispectral cell labelling for identifying and tracking individual cells in real-time *in vivo.* The random combination of fluorophores, generated by Cre/*lox* recombination, allows

distinction of adjacent cells facilitating visualisation of cell dynamics and interactions. This has facilitated tracking cell fate in the development of individual neurons, in the case of 'brainbow' fish (Albert Pan *et al.*, 2013), and the movement of superficial epithelial cells in the 'skinbow' fish (Chen et al., 2016). These models could be used to further our understanding of mechanisms behind contaminant-induced developmental toxicity. The skinbow fish, for example, could be used to help understand the OS observed in ionocytes of the EpRE:mCherry larvae resulting from embryo decontamination.

The emergence and now widespread adoption of CRISPR/Cas9 as a gene-editing tool will likely accelerate the development of the TG models. Compared with more traditional TG methods, CRISPR/Cas9 is relatively cheap, convenient, and has higher success rates, particularly for the generation of models with multiple transgenes (Liu et al., 2019). This will allow the development of more complex models which can be used to understand cross-talk between different chemical-effect pathways, build detailed AOPs and investigate interactive effects of pollutants and physico-chemical stressors. The potential utility of mixed TG models was highlighted in Chapter 5 by the EpRE:mCherry:ERE:GFP line, which could have helped elucidate the link between ERE activation and the antioxidant response, but unfortunately was limited by the heterozygous breeding stock.

## 7.2 Role of endogenous defences in embryo toxicity

The EpRE:mCherry model has allowed the discovery of potential new defences in zebrafish embryos through the induction of mCherry fluorescence following inhibition of endogenous oestrogen during pro-oxidant exposure. As discussed in Chapter 5, oestrogen has previously been linked to antioxidant mechanisms in *in vitro* and *in vivo* studies, but this is the first time that its inhibition has been shown to exacerbate drug-induced OS in a whole-body fish model. Interestingly, while Duong *et al.* 2020 also showed that inhibition of sex steroids exacerbated OS in certain cell types, they proposed that oestrogen was not protective when the cells are undergoing OS, as supplementation of oestrogen following hydrogen peroxide exposure exacerbated the damage. This aligns to some degree with the data presented in Chapter 5 which shows EE2 treatment did not buffer APAP-induced OS. However, my data implies oestrogen only becomes a critical factor when the larvae are experiencing OS, as suppression of oestrogen in the absence of APAP had no effect on the animal's redox status, whereas some

exacerbation was observed when larvae were also exposed to the pro-oxidant. This suggests that supplementation of oestrogen is not anti-oxidative (concurring with Duong *et al.*), but endogenous oestrogen does play a protective role under OS. To confirm this, the experiments could be repeated using supplementation of natural oestrogen instead of the synthetic EE2. Additionally, as discussed in Chapter 5, repeats of the experiments using ICI were not consistently significant, adding uncertainty to the findings.

There is a clear need to better understand the role of endogenous defences when assessing chemical effects as my data imply they may be more complex than has been indicated through the use of *in vitro* systems. Indeed, the involvement of additional biological variation in the larvae, potentially sex-related, has been indicated by the variable response of APAP-exposed larvae to oestrogen inhibition (Chapter 5).

Expulsion of APAP from the larvae at 26 hpf (or 20 hours post dose), postulated to occur at the onset of *abcb5* transcription, was another unexpected innate defence observed. This work further shows the importance of including analytical chemistry to support bioassays, as this response would have been far more difficult to interpret from the measurement of the fluorescence signals alone. This is because a) tissue-specific fluorescence could not be accurately measured in embryos of this age using the Acquifer and b) data in Chapter 4 relating depuration of APAP to degradation of the mCherry fluorescence signal shows that mCherry fluorescence intensity would not respond to sudden, short-term changes in internal drug concentration as the fluorophore persists for hours after expulsion of the drug from the larval body.

Understanding efflux transporter activity can be valuable for understanding the pharmacokinetics of exposure compounds. A standardised protocol has recently been developed which uses the fluorescent dye rhodamine B and the VAST system to assess the effect of compounds on inhibition of Abcb5 in intact zebrafish larvae in medium throughput (Bieczynski et al., 2021). The authors only assessed a single time point (72 hpf), but application of the EpRE:mCherry model in this system across multiple time points could allow real-time visualisation of efflux activity which could be directly linked to the development of the OS response in the same individual. This could further our understanding of how

toxicokinetics links to the timing of toxic responses, and potentially link the activity of two endogenous defences: xenobiotic elimination and antioxidant activity.

The work in this thesis has also shown how defence mechanisms can be self-defeating when efforts to detoxify a compound result in more damaging products. Data in chapter 5 showed that co-exposure to the synthetic antioxidant LGR and the pharmaceutical APAP simultaneously resulted in overt toxicity, while introduction of LGR following removal of APAP allowed the larvae to recover from the OS more rapidly. Data in chapter 4 showed that, by 24 hours in clean water, all APAP had been removed so while there may have been some APAP and LGR in the first 24 hours of LGR exposure, for the second day the animal is only exposed to LGR. APAP-GSH conjugates have previously been shown to be nephrotoxic (Stern *et al.*, 2005) but this is the first time that LGR supplementation has been reported to result in a toxic effect.

There are numerous examples from toxicology wherein biotransformation of a xenobiotic, in an attempt at detoxification, can produce a more toxic compound. Indeed, in the case of pro-drugs such as CP and Cloz, this is a deliberate design of the pharmaceutical to improve the physicochemical, pharmaceutical or pharmokinetic properties of the drug (Rautio *et al.*, 2008). However, this can have adverse consequences in the environment. For example, the biotransformation of DCF by aquatic invertebrates (*Gammarus pulex* and *Hyalella Azteca*) can result in the production of a methylated metabolite more toxic and with greater bioaccumulation potential than the parent compound due to increased hydrophobicity (Fu *et al.*, 2020). Therefore, there is a need to better understand how metabolic activation can influence the toxicity of a drug in the environment.

TG zebrafish models could be a valuable tool in answering questions on metabolic activation. However, there is conflicting evidence in the literature on the metabolic capacity of early life-stage zebrafish larvae. The data presented in Chapter 4 shows that the larvae were able to metabolise Cloz and CP (although this did not appear to influence the pro-oxidative action of either drug). In particular, LC-MS/MS and DESI data strongly indicate the 4 dpf larvae were able to produce the active metabolites of Cloz. Evidence of drug bioactivation allows more confidence in the model as a pharmaceutical screening tool. However, a wider range of pro-drugs should be tested as the present study only demonstrated this for two compounds.

The studies in Chapter 4 also demonstrate the application of MSI to visualise and quantify the distribution of pharmaceutical compounds and their metabolites in the body of a zebrafish embryo. This system could be developed in the future to co-localise the distribution of metabolites (and other biomarkers such as GSH/GSSG) with the fluorescence pattern observed in the EpRE:mCherry model, further expanding the application of the TG model as a highly integrated tool by indicating drug uptake, metabolism, and chemical effects all in a single animal.

## 7.3 Developmental stage is a critical factor in chemical effects assessments

A recurring theme throughout this thesis highlights the influence of developmental stage on fish embryo bioassays, both in terms of practicality for assessments, and interpretation of the data produced. The Acquifer in particular is best suited to the assessment of embryo-larvae between 2 and 4 dpf, as embryos below this age could not be positioned using the agarose grooves (described in Chapter 3) for optimum imaging of specific tissues. Conversely, larvae at 5 dpf or older are challenging to mount using this tool as the inflated swim bladder causes them to float out of position. There is a clear need for future imaging platforms to consider how developmental stage may affect sample orientation for consistent imaging as it is a common challenge for users of zebrafish (Bieczynski *et al.*, 2021; Lackmann *et al.*, 2018). The orientation tool used in the current thesis (Wittbrodt *et al.*, 2014) helps with this challenge, but is not suitable for <2 dpf or >5 dpf larvae. There seems to be more success with the use of algorithms to automatically position larvae, e.g. in (Zhang et al., 2021b), in the use of microfluidics for automated zebrafish embryo culturing and imaging, a rapidly expanding field. However, these tools are also only used for larvae <5 dpf and haven't generally been tested on older larvae.

The confocal microscope allowed the EpRE:mCherry model to be imaged up to at least 10 dpf, indicating the mCherry fluorescence in this model may still be visualised into the juvenile stage. For a complete assessment of the EpRE:mCherry model, a future study could assess the fluorescence daily to find at which age the larvae becomes too optically dense or too pigmented for the fluorescence to be detected.

There is a clear need to consider the zebrafish embryo-larvae as a developing, dynamic system, even within the short period of an acute chemical assay, as this can create a challenge in the interpretation of results. Indeed, this was seen in Chapter 4 (Fig. 4.36 and 4.27) where increase in background OS over time as a result of the growing larvae needed to be controlled for in order to facilitate quantification of the changes in OS resulting from the APAP exposure conditions.

The timing of exposure (both in terms of the age of the fish and length of exposure) can also result in misleading interpretation of drug-screening data. This is most clearly typified in the results of the Cis exposure assays, where exposure from 0-4 dpf resulted in no observable OS induction in the EpRE:mCherry model, whereas exposure from 2-4 dpf did. The morphological data from these assays revealed that the lack of observable OS in larvae exposed from 0 dpf was due to tissue damage caused by the earlier exposure to Cis. This highlights the importance of considering the vulnerability of specific life stages when conducting chemical exposure assays. Although, the reduced toxicity of Cis may have been a result of the later developmental stage or the shorter overall exposure period (2 days compared with 4 days)

The results of the Cis screen also support the observation made earlier in this thesis, that the EpRE:mCherry seems to have a very narrow concentration range in which it is useful. The model cannot detect chemicals at environmental levels, but also cannot be used to reliably quantify OS induction by particularly potent compounds, or at high concentrations or prolonged exposure. However, this is by no means a problem exclusive to the EpRE:mCherry model and reaffirms the application of TG models as sensitive biomarkers, designed for the assessment of chemical effects without the need for overt toxicity.

## 7.4 Changes in temperature have the potential to increase the risk of pharmaceuticals in the environment

There is a need for better understanding of the effect of temperature on OS, and of compound toxicity as a whole, demonstrated in this thesis by exacerbation of pharmaceutical-induced OS by elevated temperature as visualised in the EpRE:mCherry model. Global temperatures are increasing and predicted to rise by at least 1.0-1.8 °C by 2100 compared to the 1850-1900 average, or by as much as 5.7 °C in the high CO2 emissions scenario (IPCC, 2021). Extreme weather events are also predicted to become more frequent, particularly extreme

temperatures (IPCC, 2021). There is an obvious potential for a changing climate to exacerbate the toxicity of pollutants in surface waters with numerous recent studies to support this (Balbus et al., 2013; Benateau et al., 2019; Bunke et al., 2019). However, the present study is one of the first to use a TG fish model to illustrate exacerbation of OS as a mechanism of this interaction.

As discussed in Chapter 1, TG zebrafish are currently underused in the study of abiotic stressors, but the work in this thesis has shown that, while the EpRE:mCherry model could not detect the present pharmaceuticals at environmentally relevant concentrations, it did prove sensitive to small and environmentally relevant differences in temperatures (as little as 2°C).

However, this thesis represents just one model of one species at one life stage. A longer-term study is required to confirm how this interaction manifests in adult zebrafish, or how the response varies with chronic exposures. Further, the effect of temperature on drug-induced OS reported here may not be translatable to all other species. Indeed, ectotherms are particularly vulnerable to changes in ROS generation caused by rising temperatures due to their limited capacity to maintain their body temperature (Burraco et al., 2020), whilst endothermic species may be more resilient. The susceptibility of an animal to thermal stress can also depend on their status as a thermal generalist or specialist, and their capacity to acclimatise (Huey *et al.*, 2012), and so this also has the potential to influence their susceptibility to temperature -enhanced drug toxicity.

The present study used embryos spawned from fish that are accustomed to stable temperatures and other husbandry conditions. Fish in the environment naturally would experience more variable conditions and so may be more tolerant of changing temperatures, potentially experiencing reduced exacerbation of chemical toxicity compared to that observed in laboratory fish. To further this study and improve its environmental relevance, future studies might repeat some of these studies using fish from the wild to assess their sensitivity to elevated temperatures and how this affects their OS response to chemical exposure.

There is also a growing interest in the potential for other physical stressors to exacerbate the toxic effects of environmental pollutants. These include factors such as pH and dissolved organic matter, as touched on in the General

Introduction and reviewed by (Pinheiro *et al.*, 2021), but were outside the scope of this thesis.

The finding that a small temperature difference can alter the outcome of a chemical exposure assay also holds implications for current ERAs, which are typically based on chemical exposure assays conducted in laboratories under strictly controlled parameters. This thesis has demonstrated that the actual LOEC or PNEC for a compound in the environment may differ depending on the local conditions, potentially presenting a greater risk than previously predicted. Future ERAs therefore need to consider the influence of current abiotic conditions, as well as that of future climate change.

# Appendix 1 – Supplementary information for Chapter 5

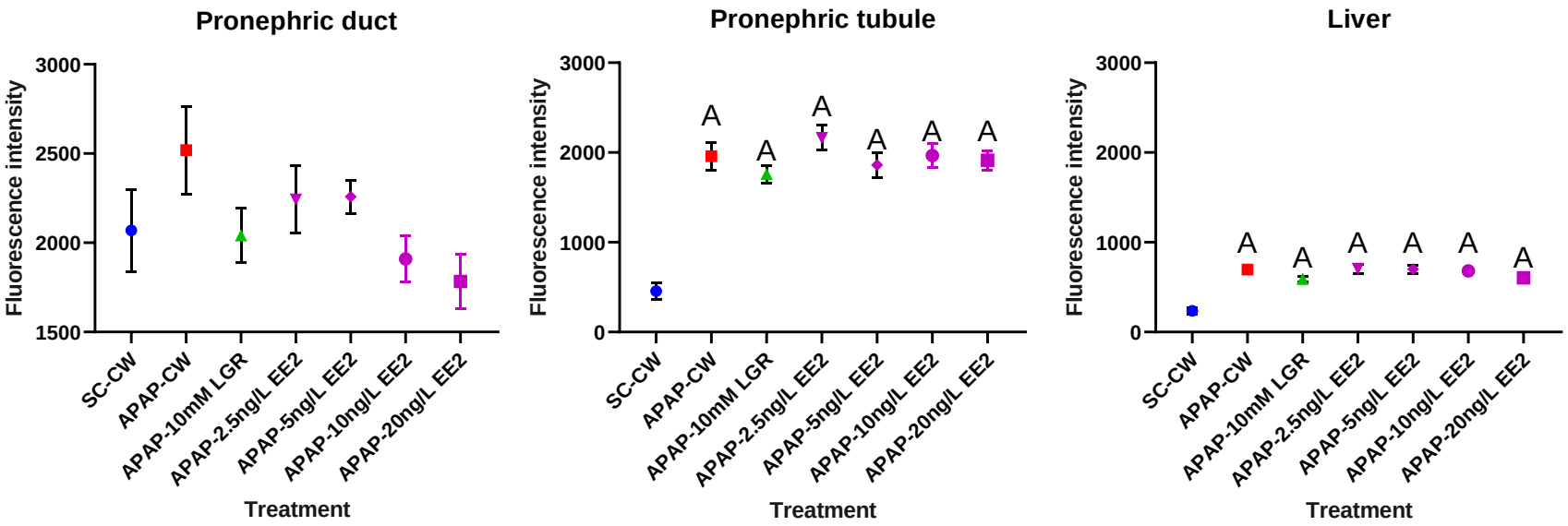


*Figure.1* ***Rescue at 2 dpf repeat****. Data points show mean +/- SEM, N=2-. Data were not normally distributed so tested using Kruskal-Wallis followed by Dunn's multiple comparison test. A= significant difference from solvent control to clean water (SC-CW) treatment group. No treatment groups were significantly different from APAP to clean water (APAP-CW) treatment group.*

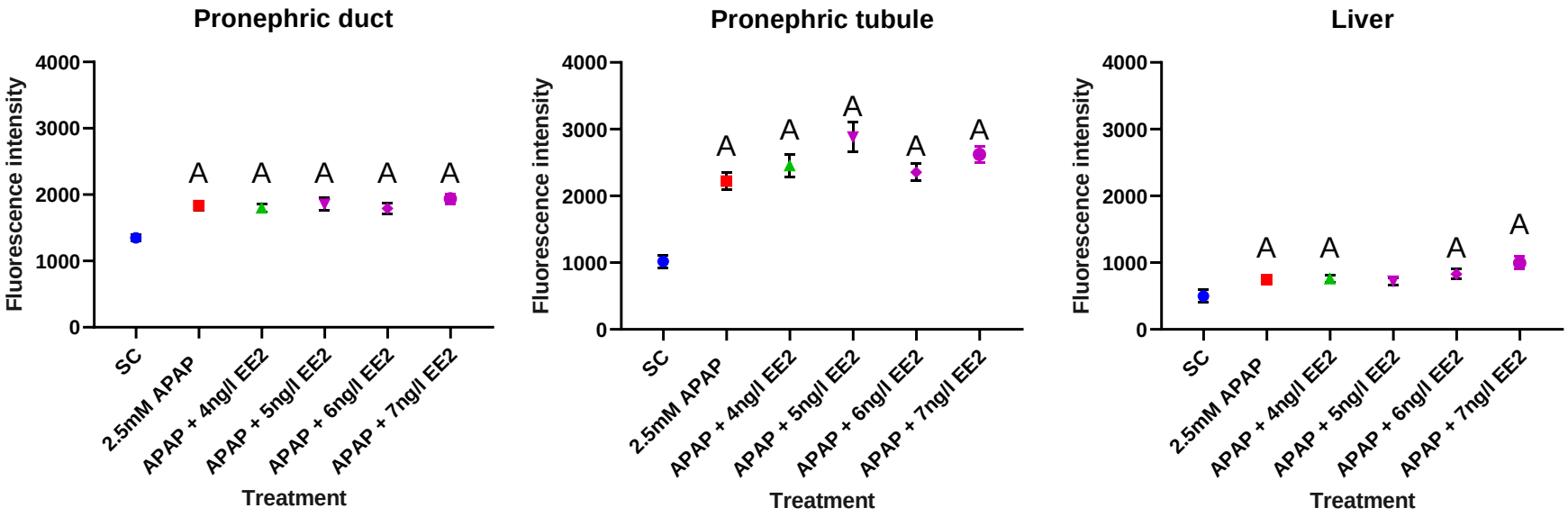


*Figure 2* ***Simultaneous dose 0-4 dpf.*** *Data points show mean +/- SEM, N=24. Data from the PD were normally distributed so were analysed using a one-way ANOVA followed by Tukey's multiple comparison test. The PT and liver were analysed using Kruskal-Wallis followed by Dunn's . A= significant difference from the solvent control (SC). No treatment groups were significantly different from 2.5mM APAP treatment group.*

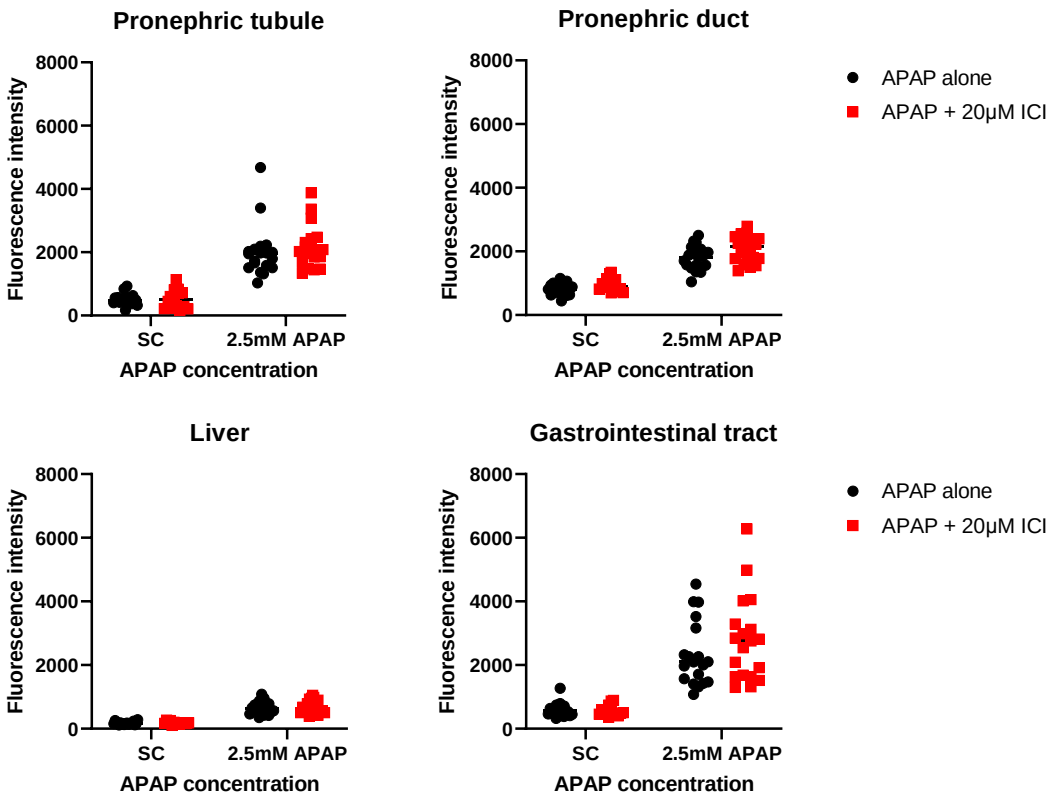


*Figure 3* ***APAP vs ICI.2: repeat of assay to test effect of oestrogen blocker ICI on APAP-induced OS,*** *N=20. Data from the PD were normally distributed so were analysed using a one-way ANOVA followed by Tukey's multiple comparison test. The PT, liver and GI were analysed using Kruskal-Wallis followed by Dunn's. ICI had no significant effect.*

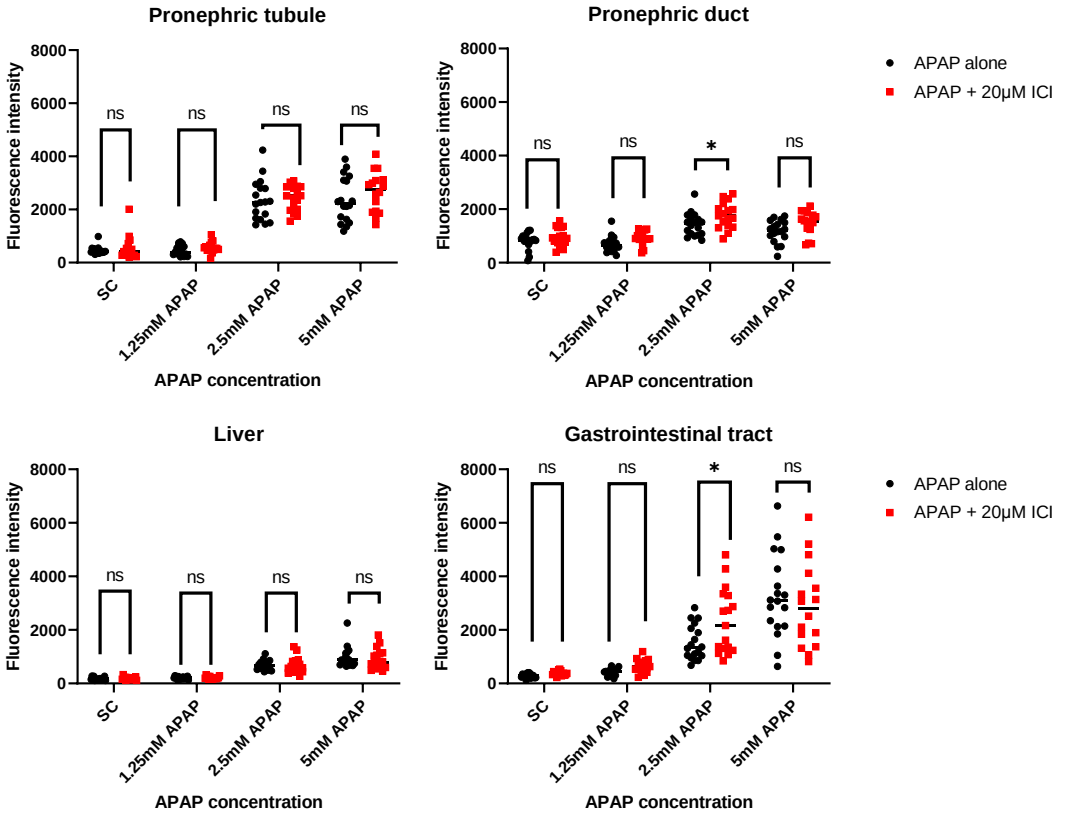


*Figure 4* ***APAP vs ICI.3: repeat of assay to test effect of oestrogen blocker ICI on APAP-induced OS, tested across a range of APAP concentrations,*** *N=18. PT data were not normally distributed, so were compared using multiple Mann-Whitney tests. PD, liver and GI were normally distributed, so analysed using two-way ANOVAs followed by Bonferroni multiple comparison test. * = P< 0.05, **= P< 0.005, **= P<0.0005, ****= P< 0.0001.*

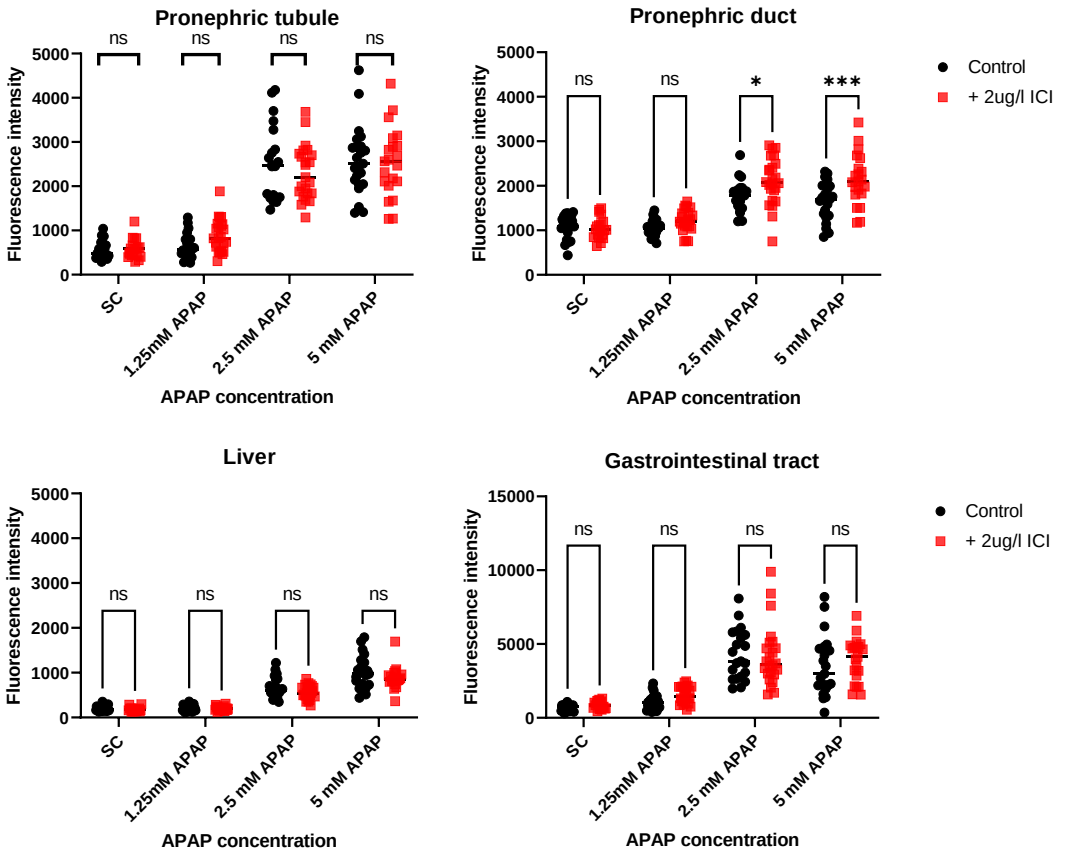


*Figure.5* ***APAP vs ICI.5: repeat of assay to test effect of oestrogen blocker ICI on APAP-induced OS, tested across a range of APAP concentrations,*** *N=24. PD and PT data were not normally distributed, so were compared using multiple Mann-Whitney tests. Liver and GI were normally distributed, so analysed using two-way ANOVAs followed by Bonferroni multiple comparison test. * = P< 0.05, **= P< 0.005, **= P<0.0005, ****= P< 0.0001.*

# Appendix 2- Supplementary information for Chapter 6

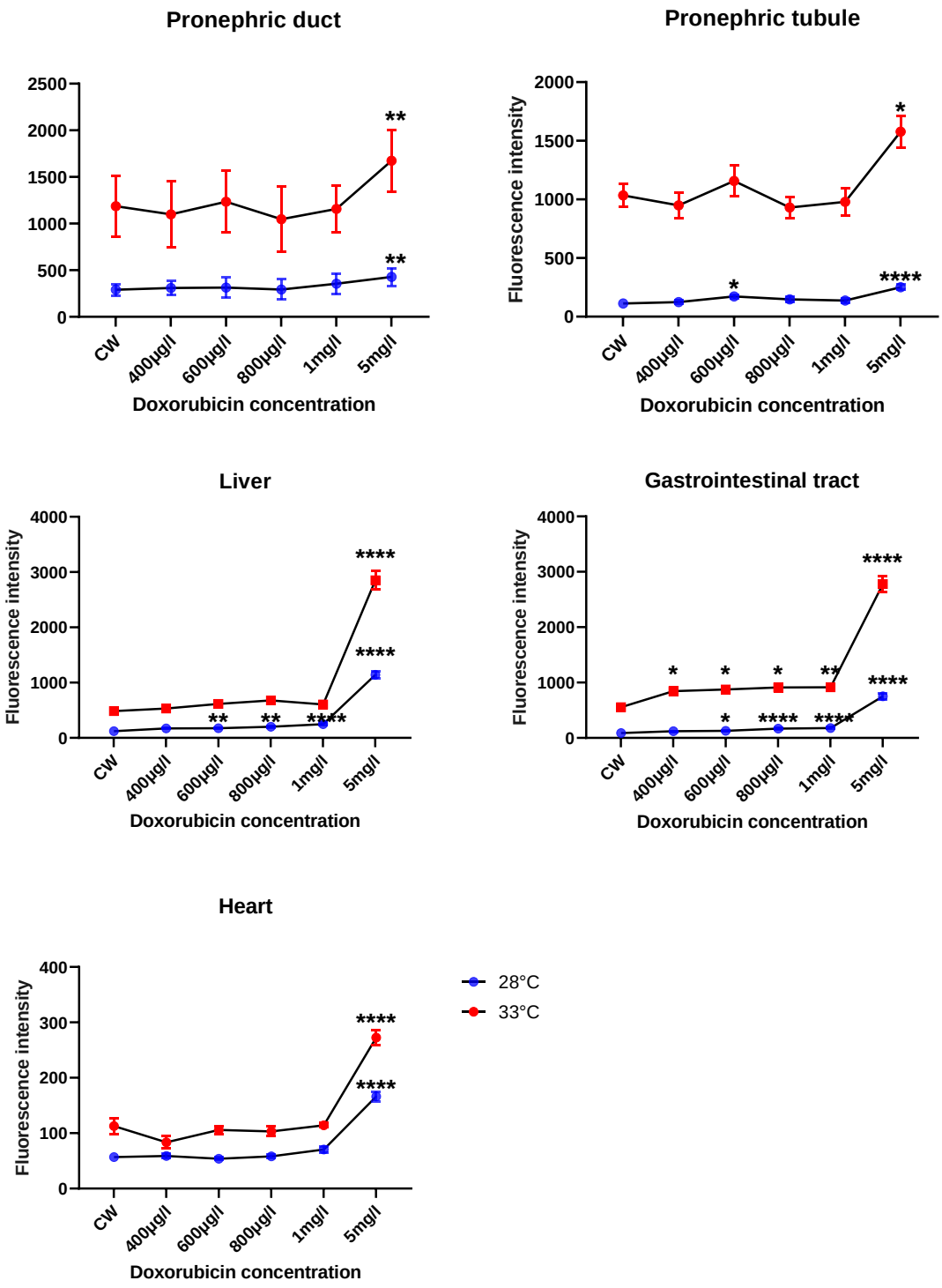


*Figure.1* ***Pilot study for effect of temperature on doxorubicin-induced OS in 3 dpf EpRE:mCherry larvae****. N=16, graphs show mean +/- SEM. Data was not normally distributed so analysed using Kruskal-Wallis followed by Dunn's multiple comparisons test. Asterisks show significant difference to the control (CW) of the same temperature group (multiplicity adjusted P-values): * = P< 0.05, **= P< 0.005, **= P<0.0005, ****= P< 0.0001. Mann-whitney test confirmed that the temperature groups are significantly different from one another at every drug concentration, including CW.*

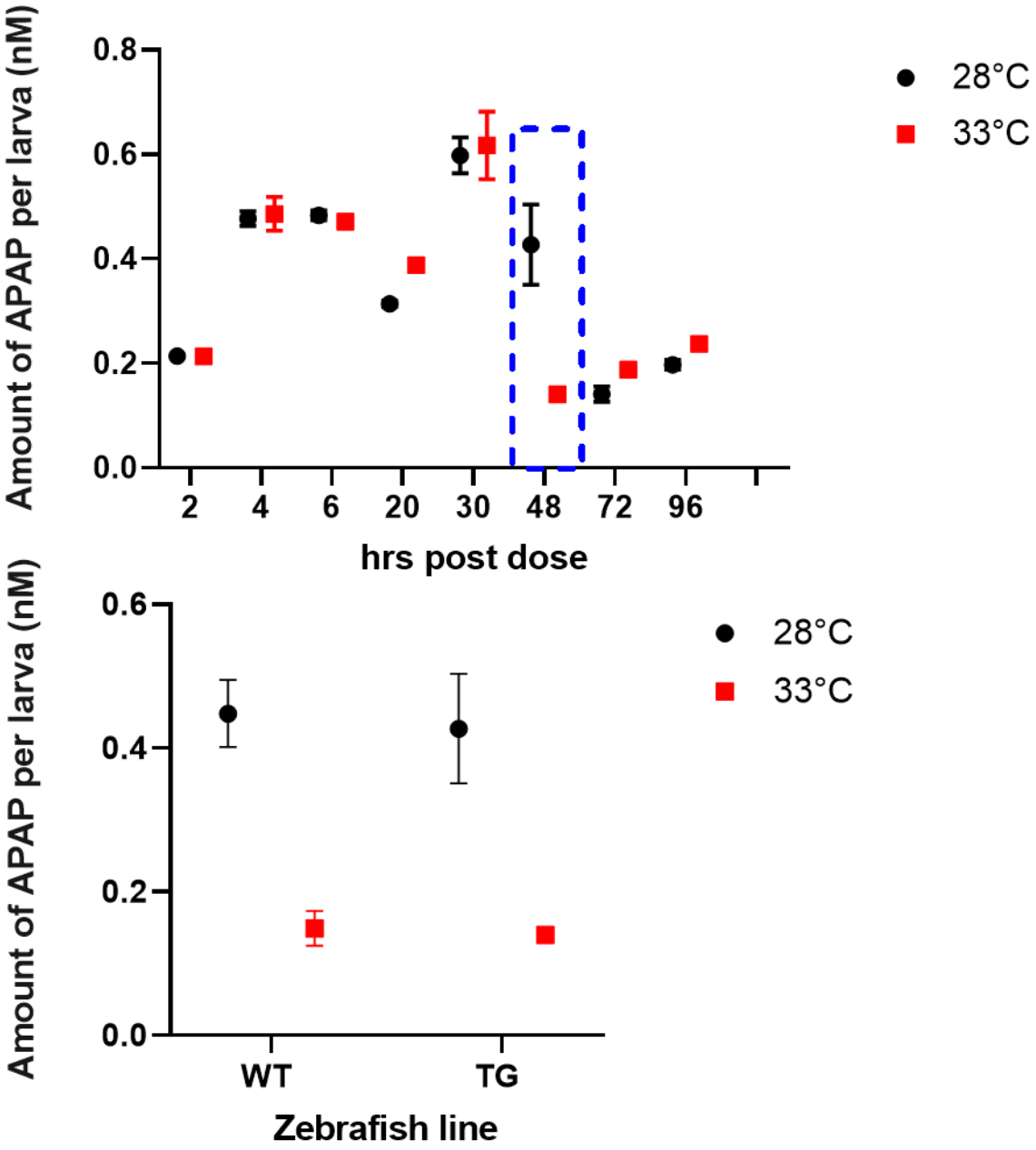


*Figure.2* ***Pilot study for effect of temperature on APAP uptake dynamics.*** *[Top] Amount of APAP detected in wild type (WT) zebrafish embryos raised at 28°C or 33°C. Blue dashed box shows where larvae in higher temperature group hatched up to 24 hours earlier, indicating need for manual dechorionation. [Bottom] Amount of APAP detected at 48 hours post dose in WT and TG(EpRE:mCherry) larvae raised at 28°C or 33°C. Raw data is unavailable so statistical analysis could not be performed.*

# Bibliography

Abdel-Wahab, B. A., & Metwally, M. E. (2015). Clozapine-induced cardiotoxicity: role of oxidative stress, tumour necrosis factor alpha and NF-κβ. *Cardiovascular Toxicology*, *15*(4), 355–365. https://doi.org/10.1007/s12012-014-9304-9

Abdelmoneim, A., Clark, C. L., & Mukai, M. (2020). Fluorescent reporter zebrafish line for estrogenic compound screening generated using a crispr/cas9-mediated knock-in system. *Toxicological Sciences*, *173*(2), 336–346. https://doi.org/10.1093/toxsci/kfz224

Abdul Hamid, Z., Budin, S. B., Wen Jie, N., Hamid, A., Husain, K., & Mohamed, J. (2012). Nephroprotective effects of Zingiber zerumbet Smith ethyl acetate extract against paracetamol-induced nephrotoxicity and oxidative stress in rats. *Journal of Zhejiang University SCIENCE B*, *13*(3), 176–185. https://doi.org/10.1631/jzus.B1100133

Abràmoff, M. D., Magalhães, P. J., & Ram, S. J. (2004). Image processing with imageJ. *Biophotonics International*, *11*(7), 36–41. https://doi.org/10.1201/9781420005615.ax4

Adams, S. L., Zhang, T., & Rawson, D. M. (2005). The effect of external medium composition on membrane water permeability of zebrafish (*Danio rerio*) embryos. *Theriogenology*, *64*(7), 1591–1602. https://doi.org/10.1016/j.theriogenology.2005.03.018

Adeel, M., Song, X., Wang, Y., Francis, D., & Yang, Y. (2017). Environmental impact of estrogens on human, animal and plant life: A critical review. *Environment International*, *99*, 107–119. https://doi.org/10.1016/j.envint.2016.12.010

Aderemi, A., Hunter, C., Pahl, O., Roberts, J., & Shu, X. (2020). Developmental anomalies and oxidative stress responses in zebrafish (*Danio rerio*) following embryonic exposure to human pharmaceuticals. *Journal of Toxicology and Environmental Health*, *5*(1), 109-125.

Aharon, D., & Marlow, F. L. (2022). Sexual determination in zebrafish. *Cellular and Molecular Life Sciences*, *79*(1), 8. https://doi.org/10.1007/s00018-021-04066-4

Ahmad, I., Hamid, T., Fatima, M., Chand, H. S., Jain, S. K., Athar, M., & Raisuddin, S. (2000). Induction of hepatic antioxidants in freshwater catfish (*Channa punctatus Bloch*) is a biomarker of paper mill effluent exposure. *Biochimica et Biophysica Acta - General Subjects*, *1523*(1), 37–48. https://doi.org/10.1016/S0304-4165(00)00098-2

Aït-Aïssa, S., Porcher, J. M., Arrigo, A. P., & Lambré, C. (2000). Activation of the hsp70 promoter by environmental inorganic and organic chemicals: Relationships with cytotoxicity and lipophilicity. *Toxicology*, *145*(2–3), 147–157. https://doi.org/10.1016/S0300-483X(00)00145-1

Akagi, J., Khoshmanesh, K., Evans, B., Hall, C. J., Crosier, K. E., Cooper, J. M., Crosier, P. S., & Wlodkowic, D. (2012). Miniaturized embryo array for automated trapping, immobilization and microperfusion of zebrafish embryos. *PLoS ONE*, *7*(5), 12–15. https://doi.org/10.1371/journal.pone.0036630

Albert Pan, Y., Freundlich, T., Weissman, T. A., Schoppik, D., Cindy Wang, X., Zimmerman, S., Ciruna, B., Sanes, J. R., Lichtman, J. W., & Schier, A. F. (2013). Zebrabow: Multispectral cell labeling for cell tracing and lineage analysis in zebrafish. *Development (Cambridge)*, *140*(13), 2835–2846. https://doi.org/10.1242/dev.094631

Ali, J. M., Palandri, M. T., Kallenbach, A. T., Chavez, E., Ramirez, J., Onanong, S., Snow, D. D., & Kolok, A. S. (2018). Estrogenic effects following larval exposure to the putative anti-estrogen, fulvestrant, in the fathead minnow (*Pimephales promelas*). *Comparative Biochemistry and Physiology Part - C: Toxicology and Pharmacology*, *204*(November 2017), 26–35. https://doi.org/10.1016/j.cbpc.2017.10.013

Ali, M. K., Saber, S. P., Taite, D. R., Emadi, S., & Irving, R. (2017). The protective layer of zebrafish embryo changes continuously with Advancing Age of Embryo Development (AGED). *Journal of Toxicology and Pharmacology*, *1*(2), 009. http://www.scientificoajournals.org/pdf/jtp.1009.pdf

Alidadi Soleimani, T., Sattari, A., Kheirandish, R., & Sharifpour, I. (2017). Safety evaluation of chloramine-T on ornamental zebra fish (*Danio rerio*) using

LC50 calculation and organ pathology. *Iranian Journal of Fisheries Sciences*, *16*(1), 26–37.

Almeida, Â., Calisto, V., Esteves, V. I., Schneider, R. J., Figueira, E., Soares, A. M. V. M., & Freitas, R. (2021). Can ocean warming alter sub-lethal effects of antiepileptic and antihistaminic pharmaceuticals in marine bivalves? *Aquatic Toxicology*, *230*(October 2020). https://doi.org/10.1016/j.aquatox.2020.105673

Anders, M. W. (2004). Glutathione- dependent bioactivation of haloalkanes and haloalkenes. *Drug Metabolism Reviews*, *36*(3–4), 583–594. https://doi.org/10.1081/DMR-200033451

Ando, R., Hama, H., Yamamoto-Hino, M., Mizuno, H., & Miyawaki, A. (2002). An optical marker based on the UV-induced green-to-red photoconversion of a fluorescent protein. *Proceedings of the National Academy of Sciences*, *99*(20), 12651–12656. https://doi.org/10.1073/pnas.202320599

Ankley, G. T., Bennett, R. S., Erickson, R. J., Hoff, D. J., Hornung, M. W., Johnson, R. D., Mount, D. R., Nichols, J. W., Russom, C. L., Schmieder, P. K., Serrrano, J. A., Tietge, J. E., & Villeneuve, D. L. (2010). Adverse outcome pathways: A conceptual framework to support ecotoxicology research and risk assessment. *Environmental Toxicology and Chemistry*, *29*(3), 730–741. https://doi.org/10.1002/etc.34

Atakisi, O., Erdogan, H. M., Atakisi, E., Citil, M., Kanici, A., Merhan, O., & Uzun, M. (2010). Effects of reduced glutathione on nitric oxide level, total antioxidant and oxidant capacity and adenosine deaminase activity. *European Review for Medical and Pharmacological Sciences*, *14*(1), 19–23. http://www.ncbi.nlm.nih.gov/pubmed/20184085

Ates, B., Abraham, L., & Ercal, N. (2008). Antioxidant and free radical scavenging properties of N-acetylcysteine amide (NACA) and comparison with N-acetylcysteine (NAC). *Free Radical Research*, *42*(4), 372–377. https://doi.org/10.1080/10715760801998638

Backhaus, T. (2014). Medicines, shaken and stirred: a critical review on the ecotoxicology of pharmaceutical mixtures. *Philosophical Transactions of the Royal Society B: Biological Sciences*, *369*(1656), 20130585.

https://doi.org/10.1098/rstb.2013.0585

Backhaus, T. (2016). Environmental risk assessment of pharmaceutical mixtures: demands, gaps, and possible bridges. *The AAPS Journal*, *18*(4), 804–813. https://doi.org/10.1208/s12248-016-9907-0

Bäckström, E., Hamm, G., Nilsson, A., Fihn, B. M., Strittmatter, N., Andrén, P., Goodwin, R. J. A., & Fridén, M. (2018). Uncovering the regional localization of inhaled salmeterol retention in the lung. *Drug Delivery*, *25*(1), 838–845. https://doi.org/10.1080/10717544.2018.1455762

Badamasi, I., Odong, R., & Masembe, C. (2020). Threats posed by xenoestrogenic chemicals to the aquatic ecosystem, fish reproduction and humans: a review. *African Journal of Aquatic Science*, *45*(3), 243–258. https://doi.org/10.2989/16085914.2020.1746233

Bakos, K., Kovacs, R., Balogh, E., Sipos, D. K., Reining, M., Gyomorei-Neuberger, O., Balazs, A., Kriszt, B., Bencsik, D., Csepeli, A., Gazsi, G., Hadzhiev, Y., Urbanyi, B., Mueller, F., Kovacs, B., & Csenki, Z. (2019). Estrogen sensitive liver transgenic zebrafish (*Danio rerio*) line (Tg(vtg1:mCherry)) suitable for the direct detection of estrogenicity in environmental samples. *Aquatic Toxicology*, *208*(January), 157–167. https://doi.org/10.1016/j.aquatox.2019.01.008

Balbus, J. M., Boxall, A. B. A., Fenske, R. A., McKone, T. E., & Zeise, L. (2013). Implications of global climate change for the assessment and management of human health risks of chemicals in the natural environment. *Environmental Toxicology and Chemistry*, *32*(1), 62–78. https://doi.org/10.1002/etc.2046

Bardet, P., Horard, B., Robinson-Rechavi, M., Laudet, V., & Vanacker, J. (2002). Characterization of oestrogen receptors in zebrafish (*Danio rerio*). *Journal of Molecular Endocrinology*, *28*(3), 153–163. https://doi.org/10.1677/jme.0.0280153

Barrionuevo, W. R., & Burggren, W. W. (1999). O2 consumption and heart rate in developing zebrafish (*Danio rerio*): Influence of temperature and ambient O2. *American Journal of Physiology - Regulatory Integrative and Comparative Physiology*, *276*(2 45-2), 505–513.

https://doi.org/10.1152/ajpregu.1999.276.2.r505

Bartoskova, M., Dobsikova, R., Stancova, V., Zivna, D., Blahova, J., Marsalek, P., Zelníckova, L., Bartos, M., di Tocco, F. C., & Faggio, C. (2013). Evaluation of ibuprofen toxicity for zebrafish (*Danio rerio*) targeting on selected biomarkers of oxidative stress. *Neuro Endocrinology Letters*, *34 Suppl 2*, 102–108. http://www.ncbi.nlm.nih.gov/pubmed/24362101

Basile, D. P., Anderson, M. D., & Sutton, T. A. (2012). Pathophysiology of Acute Kidney Injury. In *Comprehensive Physiology* (Vol. 2, Issue 2, pp. 1303–1353). Wiley. https://doi.org/10.1002/cphy.c110041

Baumann, M., Weiss, K., Maletzki, D., Schüssler, W., Schudoma, D., Kopf, W., & Kühnen, U. (2015). Aquatic toxicity of the macrolide antibiotic clarithromycin and its metabolites. *Chemosphere*, *120*, 192–198. https://doi.org/10.1016/j.chemosphere.2014.05.089

Bello, S. M., Heideman, W., & Peterson, R. E. (2004). 2,3,7,8-Tetrachlorodibenzo-P-Dioxin inhibits regression of the common cardinal vein in developing zebrafish. *Toxicological Sciences*, *78*(2), 258–266. https://doi.org/10.1093/toxsci/kfh065

Benateau, S., Gaudard, A., Stamm, C., & Altermatt, F. (2019). Climate change and freshwater ecosystems: Impacts on water quality and ecological status. *Hydro-CH2018 Project*, *April*, 110. https://doi.org/10.5167/uzh-169641

Bieczynski, F., Burkhardt- Medicke, K., Luquet, C. M., Scholz, S., & Luckenbach, T. (2021). Chemical effects on dye efflux activity in live zebrafish embryos and on zebrafish Abcb4 ATPase activity. *FEBS Letters*, *595*(6), 828–843. https://doi.org/10.1002/1873-3468.14015

Bio, S., & Nunes, B. (2020). Acute effects of diclofenac on zebrafish: Indications of oxidative effects and damages at environmentally realistic levels of exposure. *Environmental Toxicology and Pharmacology*, *78*(October 2019), 103394. https://doi.org/10.1016/j.etap.2020.103394

Birnie-Gauvin, K., Costantini, D., Cooke, S. J., & Willmore, W. G. (2017). A comparative and evolutionary approach to oxidative stress in fish: A review. *Fish and Fisheries*, *18*(5), 928–942. https://doi.org/10.1111/faf.12215

Bittner, L., Teixido, E., Seiwert, B., Escher, B. I., & Klüver, N. (2018). Influence of pH on the uptake and toxicity of B-blockers in embryos of zebrafish, *Danio rerio*. *Aquatic Toxicology*, *201*(May), 129–137. https://doi.org/10.1016/j.aquatox.2018.05.020

Blechinger, S. R., Warren, J. T., Kuwada, J. Y., & Krone, P. H. (2002). Developmental toxicology of cadmium in living embryos of a stable transgenic zebrafish line. *Environmental Health Perspectives*, *110*(10), 1041–1046. https://doi.org/10.1289/ehp.021101041

Bolte, S., & Cordelières, F. P. (2006). A guided tour into subcellular colocalization analysis in light microscopy. *Journal of Microscopy*, *224*(3), 213–232. https://doi.org/10.1111/j.1365-2818.2006.01706.x

Bolton, J. L., Trush, M. A., Penning, T. M., Dryhurst, G., & Monks, T. J. (2000). Role of quinones in toxicology. *Chemical Research in Toxicology*, *13*(3), 135–160. https://doi.org/10.1021/tx9902082

Bondesson, M., Hao, R., Lin, C.-Y., Williams, C., & Gustafsson, J.-Å. (2015). Estrogen receptor signaling during vertebrate development. *Biochimica et Biophysica Acta*, *1849*(2), 142–151. https://doi.org/10.1016/j.bbagrm.2014.06.005

Borrás, C., Gambini, J., López-Grueso, R., Pallardó, F. V., & Viña, J. (2010). Direct antioxidant and protective effect of estradiol on isolated mitochondria. *Biochimica et Biophysica Acta - Molecular Basis of Disease*, *1802*(1), 205–211. https://doi.org/10.1016/j.bbadis.2009.09.007

Bound, J. P., & Voulvoulis, N. (2005). Household disposal of pharmaceuticals as a pathway for aquatic contamination in the United Kingdom. *Environmental Health Perspectives*, *113*(12), 1705–1711. https://doi.org/10.1289/ehp.8315

Braeckman, B., Smagghe, G., Brutsaert, N., Cornelis, R., & Raes, H. (1999). Cadmium uptake and defense mechanism in insect cells. *Environmental Research*, *80*(3), 231–243. https://doi.org/10.1006/enrs.1998.3897

Brion, F., Le Page, Y., Piccini, B., Cardoso, O., Tong, S.-K., Chung, B., & Kah, O. (2012). Screening estrogenic activities of chemicals or mixtures in vivo using transgenic (cyp19a1b-GFP) zebrafish embryos. *PLoS ONE*, *7*(5),

e36069. https://doi.org/10.1371/journal.pone.0036069

Brown, A. R., Green, J. M., Moreman, J., Gunnarsson, L. M., Mourabit, S., Ball, J., Winter, M. J., Trznadel, M., Correia, A., Hacker, C., Perry, A., Wood, M. E., Hetheridge, M. J., Currie, R. A., & Tyler, C. R. (2019). Cardiovascular effects and molecular mechanisms of bisphenol A and its metabolite MBP in zebrafish. *Environmental Science & Technology*, *53*(1), 463–474. https://doi.org/10.1021/acs.est.8b04281

Brown, A. R., Gunnarsson, L., Kristiansson, E., & Tyler, C. R. (2014). Assessing variation in the potential susceptibility of fish to pharmaceuticals, considering evolutionary differences in their physiology and ecology. *Philosophical Transactions of the Royal Society B: Biological Sciences*, *369*(1656), 20130576. https://doi.org/10.1098/rstb.2013.0576

Brown, A. R., Owen, S. F., Peters, J., Zhang, Y., Soffker, M., Paull, G. C., Hosken, D. J., Wahab, M. A., & Tyler, C. R. (2015). Climate change and pollution speed declines in zebrafish populations. *Proceedings of the National Academy of Sciences*, *112*(11), E1237–E1246. https://doi.org/10.1073/pnas.1416269112

Brown, C. T., Yahn, J. M., & Karasov, W. H. (2021). Warmer temperature increases toxicokinetic elimination of PCBs and PBDEs in Northern leopard frog larvae (*Lithobates pipiens*). *Aquatic Toxicology*, *234*(September 2020), 105806. https://doi.org/10.1016/j.aquatox.2021.105806

Brown, J. N., Paxéus, N., Förlin, L., & Larsson, D. G. J. (2007). Variations in bioconcentration of human pharmaceuticals from sewage effluents into fish blood plasma. *Environmental Toxicology and Pharmacology*, *24*(3), 267–274. https://doi.org/10.1016/j.etap.2007.06.005

Buck, L. M. J., Winter, M. J., Redfern, W. S., & Whitfield, T. T. (2012). Ototoxin-induced cellular damage in neuromasts disrupts lateral line function in larval zebrafish. *Hearing Research*, *284*(1–2), 67–81. https://doi.org/10.1016/j.heares.2011.12.001

Buckman, A. H., Brown, S. B., Small, J., Muir, D. C. G., Parrott, J., Solomon, K. R., & Fisk, A. T. (2007). Role of temperature and enzyme induction in the biotransformation of polychlorinated biphenyls and bioformation of

hydroxylated polychlorinated biphenyls by rainbow trout (*Oncorhynchus mykiss*). *Environmental Science and Technology*, *41*(11), 3856–3863. https://doi.org/10.1021/es062437y

Bunke, D., Moritz, S., Brack, W., Herráez, D. L., Posthuma, L., & Nuss, M. (2019). Developments in society and implications for emerging pollutants in the aquatic environment. *Environmental Sciences Europe*, *31*(1), 32. https://doi.org/10.1186/s12302-019-0213-1

Burraco, P., Orizaola, G., Monaghan, P., & Metcalfe, N. B. (2020). Climate change and ageing in ectotherms. *Global Change Biology*, *26*(10), 5371–5381. https://doi.org/10.1111/gcb.15305

Busquet, F., Nagel, R., Von Landenberg, F., Mueller, S. O., Huebler, N., & Broschard, T. H. (2008). Development of a new screening assay to identify proteratogenic substances using zebrafish *Danio rerio* embryo combined with an exogenous mammalian metabolic activation system (mDarT). *Toxicological Sciences*, *104*(1), 177–188. https://doi.org/10.1093/toxsci/kfn065

Canayakin, D., Bayir, Y., Kilic Baygutalp, N., Sezen Karaoglan, E., Atmaca, H. T., Kocak Ozgeris, F. B., Keles, M. S., & Halici, Z. (2016). Paracetamol-induced nephrotoxicity and oxidative stress in rats: the protective role of Nigella sativa. *Pharmaceutical Biology*, *54*(10), 2082–2091. https://doi.org/10.3109/13880209.2016.1145701

Cano Sanchez, M., Lancel, S., Boulanger, E., & Neviere, R. (2018). Targeting oxidative stress and mitochondrial dysfunction in the treatment of impaired wound healing: a systematic review. *Antioxidants*, *7*(8), 98. https://doi.org/10.3390/antiox7080098

Cappetta, D., De Angelis, A., Sapio, L., Prezioso, L., Illiano, M., Quaini, F., Rossi, F., Berrino, L., Naviglio, S., & Urbanek, K. (2017). Oxidative stress and cellular response to doxorubicin: a common factor in the complex milieu of anthracycline cardiotoxicity. *Oxidative Medicine and Cellular Longevity*, *2017*, 1–13. https://doi.org/10.1155/2017/1521020

Cardoso, P. G., Resende-de-Oliveira, R., & Rocha, E. (2019). Combined effects of increased temperature and levonorgestrel exposure on zebrafish female

liver, using stereology and immunohistochemistry against catalase, CYP1A, HSP90 and vitellogenin. *Environmental Pollution*, *252*, 1059–1067. https://doi.org/10.1016/j.envpol.2019.06.058

Carvan, M. J., Sonntag, D. M., Cmar, C. B., Cook, R. S., Curran, M. A., & Miller, G. L. (2001). Oxidative stress in zebrafish cells: Potential utility of transgenic zebrafish as a deployable sentinel for site hazard ranking. *Science of the Total Environment*, *274*(1–3), 183–196. https://doi.org/10.1016/S0048-9697(01)00742-2

Cauci, S., Xodo, S., Buligan, C., Colaninno, C., Barbina, M., Barbina, G., & Francescato, M. P. (2021). Oxidative stress is increased in combined oral contraceptives users and is positively associated with high-sensitivity C-reactive protein. *Molecules*, *26*(4), 1070. https://doi.org/10.3390/molecules26041070

Cerveny, D., Fick, J., Klaminder, J., McCallum, E. S., Bertram, M. G., Castillo, N. A., & Brodin, T. (2021). Water temperature affects the biotransformation and accumulation of a psychoactive pharmaceutical and its metabolite in aquatic organisms. *Environment International*, *155*(June), 106705. https://doi.org/10.1016/j.envint.2021.106705

Chakraborty, C., Sharma, A. R., Sharma, G., & Lee, S. S. (2016). Zebrafish: A complete animal model to enumerate the nanoparticle toxicity. *Journal of Nanobiotechnology*, *14*(1), 1–13. https://doi.org/10.1186/s12951-016-0217-6

Chang, T. Y., Pardo-Martin, C., Allalou, A., Wählby, C., & Yanik, M. F. (2012). Fully automated cellular-resolution vertebrate screening platform with parallel animal processing. *Lab on a Chip*, *12*(4), 711–716. https://doi.org/10.1039/c1lc20849g

Charlier, C., Kintz, P., Dubois, N., & Plomteux, G. (2004). Fatal overdosage with cisplatin. *Journal of Analytical Technology, 28*(4), 1–3.

Chaturantabut, S., Shwartz, A., Garnaas, M. K., LaBella, K., Li, C.-C., Carroll, K. J., Cutting, C. C., Budrow, N., Palaria, A., Gorelick, D. A., Tremblay, K. D., North, T. E., & Goessling, W. (2020). Estrogen acts via estrogen receptor 2b to regulate hepatobiliary fate during vertebrate development.

*Hepatology*. https://doi.org/10.1002/hep.31184

Chen, B., Legant, W. R., Wang, K., Shao, L., Milkie, D. E., Davidson, M. W., Janetopoulos, C., Wu, X. S., Hammer, J. A., Liu, Z., English, B. P., Mimori-Kiyosue, Y., Romero, D. P., Ritter, A. T., Lippincott-Schwartz, J., Fritz-Laylin, L., Mullins, R. D., Mitchell, D. M., Bembenek, J. N., … Betzig, E. (2014). Lattice light-sheet microscopy: Imaging molecules to embryos at high spatiotemporal resolution. *Science*, *346*(6208), 1257998. https://doi.org/10.1126/science.1257998

Chen, C. H., Puliafito, A., Cox, B. D., Primo, L., Fang, Y., Di Talia, S., & Poss, K. D. (2016). Multicolor cell barcoding technology for long-term surveillance of epithelial regeneration in zebrafish. *Developmental Cell*, *36*(6), 668–680. https://doi.org/10.1016/j.devcel.2016.02.017

Chen, H., Hu, J., Yang, J., Wang, Y., Xu, H., Jiang, Q., Gong, Y., Gu, Y., & Song, H. (2010). Generation of a fluorescent transgenic zebrafish for detection of environmental estrogens. *Aquatic Toxicology*, *96*(1), 53–61. https://doi.org/10.1016/j.aquatox.2009.09.015

Chen, H., Sheng, L., Gong, Z., Ru, S., & Bian, H. (2018). Investigation of the molecular mechanisms of hepatic injury upon naphthalene exposure in zebrafish (*Danio rerio*). *Ecotoxicology*, *27*(6), 650–660. https://doi.org/10.1007/s10646-018-1943-3

Chen, J.-B., Gao, H.-W., Zhang, Y.-L., Zhang, Y., Zhou, X.-F., Li, C.-Q., & Gao, H.-P. (2015). Developmental toxicity of diclofenac and elucidation of gene regulation in zebrafish (*Danio rerio*). *Scientific Reports*, *4*(1), 4841. https://doi.org/10.1038/srep04841

Chen, J., Xia, L., Bruchas, M. R., & Solnica-Krezel, L. (2017). Imaging early embryonic calcium activity with GCaMP6s transgenic zebrafish. *Developmental Biology*, *430*(2), 385–396. https://doi.org/10.1016/j.ydbio.2017.03.010

Chevalier, R. L. (2016). The proximal tubule is the primary target of injury and progression of kidney disease: role of the glomerulotubular junction. *American Journal of Physiology-Renal Physiology*, *311*(1), F145–F161. https://doi.org/10.1152/ajprenal.00164.2016

Choi, E., Alsop, D., & Wilson, J. Y. (2018). The effects of chronic acetaminophen exposure on the kidney, gill and liver in rainbow trout (*Oncorhynchus mykiss*). *Aquatic Toxicology*, *198*(February), 20–29. https://doi.org/10.1016/j.aquatox.2018.02.007

Choi, J., Im, G. J., Chang, J., Chae, S. W., Lee, S. H., Kwon, S. Y., Chung, A. Y., Park, H. C., & Jung, H. H. (2013). Protective effects of apocynin on cisplatin-induced ototoxicity in an auditory cell line and in zebrafish. *Journal of Applied Toxicology*, *33*(2), 125–133. https://doi.org/10.1002/jat.1729

Clarke, A., & Fraser, K. P. P. (2004). Why does metabolism scale with temperature? *Functional Ecology*, *18*(2), 243–251. https://doi.org/10.1111/j.0269-8463.2004.00841.x

Cooper, R., David, A., Kudoh, T., & Tyler, C. R. (2021a). Seasonal variation in oestrogenic potency and biological effects of wastewater treatment works effluents assessed using ERE-GFP transgenic zebrafish embryo-larvae. *Aquatic Toxicology*, *237*(May), 105864. https://doi.org/10.1016/j.aquatox.2021.105864

Cooper, R., David, A., Lange, A., & Tyler, C. R. (2021b). Health effects and life stage sensitivities in zebrafish exposed to an estrogenic wastewater treatment works effluent. *Frontiers in Endocrinology*, *12*(April), 1–16. https://doi.org/10.3389/fendo.2021.666656

Corcoran, G. B., & Wong, B. K. (1986). Role of glutathione in prevention of acetaminophen-induced hepatotoxicity by N-acetyl-L-cysteine in vivo: studies with N-acetyl-D-cysteine in mice. *Journal of Pharmacology and Experimental Therapeutics*, *238*(1), 54 LP – 61. http://jpet.aspetjournals.org/content/238/1/54.abstract

Corcoran, J., Winter, M. J., & Tyler, C. R. (2010). Pharmaceuticals in the aquatic environment: A critical review of the evidence for health effects in fish. *Critical Reviews in Toxicology*, *40*(4), 287–304. https://doi.org/10.3109/10408440903373590

Cosnefroy, A., Brion, F., Maillot-Maréchal, E., Porcher, J.-M., Pakdel, F., Balaguer, P., & Aït-Aïssa, S. (2012). Selective activation of zebrafish estrogen receptor subtypes by chemicals by using stable reporter gene

assay developed in a zebrafish liver cell line. *Toxicological Sciences*, *125*(2), 439–449. https://doi.org/10.1093/toxsci/kfr297

Costa, S., Coppola, F., Pretti, C., Intorre, L., Meucci, V., Soares, A. M. V. M., Freitas, R., & Solé, M. (2020). The influence of climate change related factors on the response of two clam species to diclofenac. *Ecotoxicology and Environmental Safety*, *189*(October 2019), 109899. https://doi.org/10.1016/j.ecoenv.2019.109899

D'Agati, G., Beltre, R., Sessa, A., Burger, A., Zhou, Y., Mosimann, C., & White, R. M. (2017). A defect in the mitochondrial protein Mpv17 underlies the transparent casper zebrafish. *Developmental Biology*, *430*(1), 11–17. https://doi.org/10.1016/j.ydbio.2017.07.017

Dallak, M., Dawood, A. F., Haidara, M. A., Abdel Kader, D. H., Eid, R. A., Kamar, S. S., Shams Eldeen, A. M., & Al-Ani, B. (2020). Suppression of glomerular damage and apoptosis and biomarkers of acute kidney injury induced by acetaminophen toxicity using a combination of resveratrol and quercetin. *Drug and Chemical Toxicology*, *0*(0), 1–7. https://doi.org/10.1080/01480545.2020.1722156

David, A., & Pancharatna, K. (2009). Effects of acetaminophen (paracetamol) in the embryonic development of zebrafish, *Danio rerio*. *Journal of Applied Toxicology*, *29*(7), 597–602. https://doi.org/10.1002/jat.1446

de Alba, G., López-Olmeda, J. F., & Sánchez-Vázquez, F. J. (2021). Rearing temperature conditions (constant vs. thermocycle) affect daily rhythms of thermal tolerance and sensing in zebrafish. *Journal of Thermal Biology*, *97*(February), 102880. https://doi.org/10.1016/j.jtherbio.2021.102880

de Alvarenga, K. A. F., Sacramento, E. K., Rosa, D. V., Souza, B. R., de Rezende, V. B., & Romano-Silva, M. A. (2017). Effects of antipsychotics on intestinal motility in zebrafish larvae. *Neurogastroenterology and Motility*, *29*(5), 1–7. https://doi.org/10.1111/nmo.13006

De Oliveira, J., Chadili, E., Piccini, B., Turies, C., Maillot-Maréchal, E., Palluel, O., Pardon, P., Budzinski, H., Cousin, X., Brion, F., & Hinfray, N. (2020). Refinement of an OECD test guideline for evaluating the effects of endocrine disrupting chemicals on aromatase gene expression and

reproduction using novel transgenic cyp19a1a-eGFP zebrafish. *Aquatic Toxicology*, *220*(December 2019), 105403. https://doi.org/10.1016/j.aquatox.2020.105403

de Souza Anselmo, C., Sardela, V. F., de Sousa, V. P., & Pereira, H. M. G. (2018). Zebrafish ( Danio rerio ): A valuable tool for predicting the metabolism of xenobiotics in humans? *Comparative Biochemistry and Physiology Part C: Toxicology & Pharmacology*, *212*(June), 34–46. https://doi.org/10.1016/j.cbpc.2018.06.005

Deavall, D. G., Martin, E. A., Horner, J. M., & Roberts, R. (2012). Drug-induced oxidative stress and toxicity. *Journal of Toxicology*, *2012*, 1–13. https://doi.org/10.1155/2012/645460

Delov, V., Muth-Köhne, E., Schäfers, C., & Fenske, M. (2014). Transgenic fluorescent zebrafish Tg(fli1:EGFP)y1 for the identification of vasotoxicity within the zFET. *Aquatic Toxicology*, *150*, 189–200. https://doi.org/10.1016/j.aquatox.2014.03.010

Derouiche, L., Keller, M., Duittoz, A. H., & Pillon, D. (2015). Developmental exposure to ethinylestradiol affects transgenerationally sexual behavior and neuroendocrine networks in male mice. *Scientific Reports*, *5*(October), 1–12. https://doi.org/10.1038/srep17457

Dimitriadi, A., Beis, D., Arvanitidis, C., Adriaens, D., & Koumoundouros, G. (2018). Developmental temperature has persistent, sexually dimorphic effects on zebrafish cardiac anatomy. *Scientific Reports*, *8*(1), 1–10. https://doi.org/10.1038/s41598-018-25991-8

Diniz, M. S., Salgado, R., Pereira, V. J., Carvalho, G., Oehmen, A., Reis, M. A. M., & Noronha, J. P. (2015). Ecotoxicity of ketoprofen, diclofenac, atenolol and their photolysis byproducts in zebrafish (*Danio rerio*). *Science of the Total Environment*, *505*, 282–289. https://doi.org/10.1016/j.scitotenv.2014.09.103

Doerr-MacEwen, N. A., & Haight, M. E. (2006). Expert stakeholders' views on the management of human pharmaceuticals in the environment. *Environmental Management*, *38*(5), 853–866. https://doi.org/10.1007/s00267-005-0306-z

Doerr, A. (2012). (Protein) timing is everything. *Nature Methods*, *9*(8), 783–783. https://doi.org/10.1038/nmeth.2120

Drummond, I. A., & Davidson, A. J. (2010). Zebrafish kidney development. In *Methods in Cell Biology* (Third Edit, Vol. 100, Issue C). Elsevier Inc. https://doi.org/10.1016/B978-0-12-384892-5.00009-8

Duan, J., Hu, H., Li, Q., Jiang, L., Zou, Y., Wang, Y., & Sun, Z. (2016). Combined toxicity of silica nanoparticles and methylmercury on cardiovascular system in zebrafish (*Danio rerio*) embryos. *Environmental Toxicology and Pharmacology*, *44*, 120–127. https://doi.org/10.1016/j.etap.2016.05.004

Duffy, J. B. (2002). GAL4 system in Drosophila: A fly geneticist's Swiss army knife. *Genesis*, *34*(1–2), 1–15. https://doi.org/10.1002/gene.10150

Dunaway, S., Odin, R., Zhou, L., Ji, L., Zhang, Y., & Kadekaro, A. L. (2018). Natural antioxidants: multiple mechanisms to protect skin from solar radiation. *Frontiers in Pharmacology*, *9*(APR). https://doi.org/10.3389/fphar.2018.00392

Duong, P., Tenkorang, M. A. A., Trieu, J., McCuiston, C., Rybalchenko, N., & Cunningham, R. L. (2020). Neuroprotective and neurotoxic outcomes of androgens and estrogens in an oxidative stress environment. *Biology of Sex Differences*, *11*(1), 12. https://doi.org/10.1186/s13293-020-0283-1

Ellett, F., & Lieschke, G. J. (2010). Zebrafish as a model for vertebrate hematopoiesis. *Current Opinion in Pharmacology*, *10*(5), 563–570. https://doi.org/10.1016/j.coph.2010.05.004

Escudero, J., Muñoz, J. L., Morera-Herreras, T., Hernandez, R., Medrano, J., Domingo-Echaburu, S., Barceló, D., Orive, G., & Lertxundi, U. (2021). Antipsychotics as environmental pollutants: An underrated threat? *Science of the Total Environment*, *769*, 144634. https://doi.org/10.1016/j.scitotenv.2020.144634

Fang, J., Chen, C., Cheng, H., Wang, R., & Ma, L. (2017). Effect of paracetamol (acetaminophen) on body temperature in acute stroke: A meta-analysis. *The American Journal of Emergency Medicine*, *35*(10), 1530–1535. https://doi.org/10.1016/j.ajem.2017.03.039

Ferreira, M., Costa, J., & Reis-Henriques, M. A. (2014). ABC transporters in fish species: a review. *Frontiers in Physiology*, *5*(July), 1–12. https://doi.org/10.3389/fphys.2014.00266

Ferrero, G., Gomez, E., lyer, S., Rovira, M., Miserocchi, M., Langenau, D. M., Bertrand, J. Y., & Wittamer, V. (2020). The macrophage-expressed gene (mpeg) 1 identifies a subpopulation of B cells in the adult zebrafish. *Journal of Leukocyte Biology*, *107*(3), 431–443. https://doi.org/10.1002/JLB.1A1119-223R

Filby, A. L., & Tyler, C. R. (2005). Molecular characterization of estrogen receptors 1, 2a, and 2b and their tissue and ontogenic expression profiles in fathead minnow (*Pimephales promelas*)1. *Biology of Reproduction*, *73*(4), 648–662. https://doi.org/10.1095/biolreprod.105.039701

Filipowicz, W., & Paszkowski, J. (2013). Gene silencing. In *Brenner's Encyclopedia of Genetics* (pp. 221–222). Elsevier. https://doi.org/10.1016/B978-0-12-374984-0.00603-3

Fischer, S., Klüver, N., Burkhardt-Medicke, K., Pietsch, M., Schmidt, A. M., Wellner, P., Schirmer, K., & Luckenbach, T. (2013). Abcb4 acts as multixenobiotic transporter and active barrier against chemical uptake in zebrafish (*Danio rerio*) embryos. *BMC Biology*, *11*. https://doi.org/10.1186/1741-7007-11-69

Fitzsimmons, P. N., Fernandez, J. D., Hoffman, A. D., Butterworth, B. C., & Nichols, J. W. (2001). Branchial elimination of superhydrophobic organic compounds by rainbow trout (*Oncorhynchus mykiss*). *Aquatic Toxicology*, *55*(1–2), 23–34. https://doi.org/10.1016/S0166-445X(01)00174-6

Flouriot, G., Vaillant, C., Salbert, G., Pelissero, C., Guiraud, J. M., & Valotaire, Y. (1993). Monolayer and aggregate cultures of rainbow trout hepatocytes: Long-term and stable liver-specific expression in aggregates. *Journal of Cell Science*, *105*(2), 407–416.

Fonseca, T. G., Auguste, M., Ribeiro, F., Cardoso, C., Mestre, N. C., Abessa, D. M. S., & Bebianno, M. J. (2018). Environmental relevant levels of the cytotoxic drug cyclophosphamide produce harmful effects in the polychaete *Nereis diversicolor*. *Science of The Total Environment*, *636*, 798–809.

https://doi.org/10.1016/j.scitotenv.2018.04.318

Franquet-Griell, H., Gómez-Canela, C., Ventura, F., & Lacorte, S. (2015). Predicting concentrations of cytostatic drugs in sewage effluents and surface waters of Catalonia (NE Spain). *Environmental Research*, *138*, 161–172. https://doi.org/10.1016/j.envres.2015.02.015

Freitas, R., Coppola, F., Costa, S., Pretti, C., Intorre, L., Meucci, V., Soares, A. M. V. M., & Solé, M. (2019). The influence of temperature on the effects induced by Triclosan and Diclofenac in mussels. *Science of the Total Environment*, *663*, 992–999. https://doi.org/10.1016/j.scitotenv.2019.01.189

Froehlicher, M., Liedtke, A., Groh, K. J., Neuhauss, S. C. F., Segner, H., & Eggen, R. I. L. (2009). Zebrafish (*Danio rerio*) neuromast: Promising biological endpoint linking developmental and toxicological studies. *Aquatic Toxicology*, *95*(4), 307–319. https://doi.org/10.1016/j.aquatox.2009.04.007

Fu, Q., Fedrizzi, D., Kosfeld, V., Schlechtriem, C., Ganz, V., Derrer, S., Rentsch, D., & Hollender, J. (2020). Biotransformation changes bioaccumulation and toxicity of diclofenac in aquatic organisms. *Environmental Science and Technology*, *54*(7), 4400–4408. https://doi.org/10.1021/acs.est.9b07127

Furutani-Seiki, M., & Wittbrodt, J. (2004). Medaka and zebrafish, an evolutionary twin study. *Mechanisms of Development*, *121*(7–8), 629–637. https://doi.org/10.1016/j.mod.2004.05.010

Ganai, A. A., & Farooqi, H. (2015). Bioactivity of genistein: A review of *in vitro* and *in vivo* studies. *Biomedicine & Pharmacotherapy*, *76*, 30–38. https://doi.org/10.1016/j.biopha.2015.10.026

Gasperi, J., Garnaud, S., Rocherc, V., & Moillerona, R. (2008). Priority pollutants in wastewater and combined sewer overflow. *Science of The Total Environment*, *407*(1), 263–272. https://doi.org/10.1016/j.scitotenv.2008.08.015

Ghysen, A., & Dambly-Chaudière, C. (2004). Development of the zebrafish lateral line. *Current Opinion in Neurobiology*, *14*(1), 67–73. https://doi.org/10.1016/j.conb.2004.01.012

Gillooly, J. F. (2001). Effects of Size and Temperature on Metabolic Rate. *Science*, *293*(5538), 2248–2251. https://doi.org/10.1126/science.1061967

Godoy, A. A., de Oliveira, Á. C., Silva, J. G. M., Azevedo, C. C. de J., Domingues, I., Nogueira, A. J. A., & Kummrow, F. (2019). Single and mixture toxicity of four pharmaceuticals of environmental concern to aquatic organisms, including a behavioral assessment. *Chemosphere*, *235*, 373–382. https://doi.org/10.1016/j.chemosphere.2019.06.200

Goldstone, J. V., McArthur, A. G., Kubota, A., Zanette, J., Parente, T., Jönsson, M. E., Nelson, D. R., & Stegeman, J. J. (2010). Identification and developmental expression of the full complement of Cytochrome P450 genes in zebrafish. *BMC Genomics*, *11*(1), 643. https://doi.org/10.1186/1471-2164-11-643

Goll, M. G., Anderson, R., Stainier, D. Y. R., Spradling, A. C., & Halpern, M. E. (2009). Transcriptional silencing and reactivation in transgenic zebrafish. *Genetics*, *182*(3), 747–755. https://doi.org/10.1534/genetics.109.102079

Gómez-Oliván, L. M., Galar-Martínez, M., García-Medina, S., Valdés-Alanís, A., Islas-Flores, H., & Neri-Cruz, N. (2014a). Genotoxic response and oxidative stress induced by diclofenac, ibuprofen and naproxen in *Daphnia magna*. *Drug and Chemical Toxicology*, *37*(4), 391–399. https://doi.org/10.3109/01480545.2013.870191

Gómez-Oliván, L. M., Neri-Cruz, N., Galar-Martínez, M., Islas-Flores, H., & García-Medina, S. (2014b). Binary mixtures of diclofenac with paracetamol, ibuprofen, naproxen, and acetylsalicylic acid and these pharmaceuticals in isolated form induce oxidative stress on *Hyalella azteca*. *Environmental Monitoring and Assessment*, *186*(11), 7259–7271. https://doi.org/10.1007/s10661-014-3925-0

Gómez-Oliván, L. M., Neri-Cruz, N., Galar-Martínez, M., Vieyra-Reyes, P., García-Medina, S., Razo-Estrada, C., Dublán-García, O., & Corral-Avitia, A. Y. (2012). Assessing the oxidative stress induced by paracetamol spiked in artificial sediment on *Hyalella azteca*. *Water, Air, and Soil Pollution*, *223*(8), 5097–5104. https://doi.org/10.1007/s11270-012-1261-y

Gong, Z., Wu, Y. L., Mudumana, S. P., & Lin, S. (2004). *Transgenic Fish for*

*Developmental Biology Studies* (pp. 476–516). https://doi.org/10.1142/9789812565761_0014

Gorelick, D. A., & Halpern, M. E. (2011). Visualization of estrogen receptor transcriptional activation in zebrafish. *Endocrinology*, *152*(7), 2690–2703. https://doi.org/10.1210/en.2010-1257

Gorelick, D. A., Iwanowicz, L. R., Hung, A. L., Blazer, V. S., & Halpern, M. E. (2014). Transgenic zebrafish reveal tissue-specific differences in estrogen signaling in response to environmental water samples. *Environmental Health Perspectives*, *122*(4), 356–362. https://doi.org/10.1289/ehp.1307329

Gorrini, C., Gang, B. P., Bassi, C., Wakeham, A., Baniasadi, S. P., Hao, Z., Li, W. Y., Cescon, D. W., Li, Y.-T., Molyneux, S., Penrod, N., Lupien, M., Schmidt, E. E., Stambolic, V., Gauthier, M. L., & Mak, T. W. (2014). Estrogen controls the survival of BRCA1-deficient cells via a PI3K-NRF2-regulated pathway. *Proceedings of the National Academy of Sciences*, *111*(12), 4472–4477. https://doi.org/10.1073/pnas.1324136111

Gravel, A., & Vijayan, M. M. (2007). Non-steroidal anti-inflammatory drugs disrupt the heat shock response in rainbow trout. *Aquatic Toxicology*, *81*(2), 197–206. https://doi.org/10.1016/j.aquatox.2006.12.001

Gray, C., Loynes, C. A., Whyte, M. K. B., Crossman, D. C., Renshaw, S. A., & Chico, T. J. A. (2011). Simultaneous intravital imaging of macrophage and neutrophil behaviour during inflammation using a novel transgenic zebrafish. *Thrombosis and Haemostasis*, *105*(5), 811–819. https://doi.org/10.1160/TH10-08-0525

Great Britain, & Home Office. (2019). *Annual statistics of scientific procedures on living animals: Great Britain 2018*. https://www.gov.uk/government/uploads/system/uploads/attachment_data/file/327854/spanimals13.pdf

Green, J. M., Lange, A., Scott, A., Trznadel, M., Wai, H. A., Takesono, A., Brown, A. R., Owen, S. F., Kudoh, T., & Tyler, C. R. (2018). Early life exposure to ethinylestradiol enhances subsequent responses to environmental estrogens measured in a novel transgenic zebrafish. *Scientific Reports*, *8*(1), 2699. https://doi.org/10.1038/s41598-018-20922-z

Green, J. M., Metz, J., Lee, O., Trznadel, M., Takesono, A., Brown, A. R., Owen, S. F., Kudoh, T., & Tyler, C. R. (2016). High-content and semi-automated quantification of responses to estrogenic chemicals using a novel translucent transgenic zebrafish. *Environmental Science and Technology*, *50*(12), 6536–6545. https://doi.org/10.1021/acs.est.6b01243

Griskevicius, L., Yasar, Ü., Sandberg, M., Hidestrand, M., Eliasson, E., Tybring, G., Hassan, M., & Dahl, M.-L. (2003). Bioactivation of cyclophosphamide: the role of polymorphic CYP2C enzymes. *European Journal of Clinical Pharmacology*, *59*(2), 103–109. https://doi.org/10.1007/s00228-003-0590-6

Guiloski, I. C., Ribas, J. L. C., Piancini, L. D. S., Dagostim, A. C., Cirio, S. M., Fávaro, L. F., Boschen, S. L., Cestari, M. M., da Cunha, C., & Silva de Assis, H. C. (2017). Paracetamol causes endocrine disruption and hepatotoxicity in male fish *Rhamdia quelen* after subchronic exposure. *Environmental Toxicology and Pharmacology*, *53*(May), 111–120. https://doi.org/10.1016/j.etap.2017.05.005

Gunnarsson, L., Snape, J. R., Verbruggen, B., Owen, S. F., Kristiansson, E., Margiotta-Casaluci, L., Österlund, T., Hutchinson, K., Leverett, D., Marks, B., & Tyler, C. R. (2019). Pharmacology beyond the patient – The environmental risks of human drugs. *Environment International*, *129*(March), 320–332. https://doi.org/10.1016/j.envint.2019.04.075

Guo, J., Peng, J., Lei, Y., Kanerva, M., Li, Q., Song, J., Guo, J., & Sun, H. (2020). Comparison of oxidative stress induced by clarithromycin in two freshwater microalgae *Raphidocelis subcapitata* and *Chlorella vulgaris*. *Aquatic Toxicology*, *219*(September 2019). https://doi.org/10.1016/j.aquatox.2019.105376

Guo, Y., Veneman, W. J., Spaink, H. P., & Verbeek, F. J. (2017). Three-dimensional reconstruction and measurements of zebrafish larvae from high-throughput axial-view in vivo imaging. *Biomedical Optics Express*, *8*(5), 2611. https://doi.org/10.1364/BOE.8.002611

Gutiérrez-Noya, V. M., Gómez-Oliván, L. M., Ramírez-Montero, M. del C., Islas-Flores, H., Galar-Martínez, M., Dublán-García, O., & Romero, R. (2020). Ibuprofen at environmentally relevant concentrations alters embryonic

development, induces teratogenesis and oxidative stress in *Cyprinus carpio*. *Science of the Total Environment*, *710*, 136327. https://doi.org/10.1016/j.scitotenv.2019.136327

Hagedorn, M., Kleinhans, F. W., Freitas, R., Liu, J., Hsu, E. W., Wildt, D. E., & Rall, W. F. (1997). Water distribution and permeability of zebrafish embryos, *Brachydanio rerio*. *The Journal of Experimental Zoology*, *278*(6), 356–371. https://doi.org/10.1002/(SICI)1097-010X(19970815)278:6<356::AID-JEZ3>3.0.CO;2-N

Hahn, M. E., McArthur, A. G., Karchner, S. I., Franks, D. G., Jenny, M. J., Timme-Laragy, A. R., Stegeman, J. J., Woodin, B. R., Cipriano, M. J., & Linney, E. (2014). The transcriptional response to oxidative stress during vertebrate development: Effects of tert-butylhydroquinone and 2,3,7,8-tetrachlorodibenzo-p-dioxin. *PLoS ONE*, *9*(11). https://doi.org/10.1371/journal.pone.0113158

Hall, C., Flores, M., Storm, T., Crosier, K., & Crosier, P. (2007). The zebrafish lysozyme C promoter drives myeloid-specific expression in transgenic fish. *BMC Developmental Biology*, *7*, 1–17. https://doi.org/10.1186/1471-213X-7-42

Halloran, M. C., Sato-Maeda, M., Warren, J. T., Su, F., Lele, Z., Krone, P. H., Kuwada, J. Y., & Shoji, W. (2000). Laser-induced gene expression in specific cells of transgenic zebrafish. *Development*, *127*(9), 1953–1960.

Hamilton, P. B., Lange, A., Nicol, E., Bickley, L. K., De-Bastos, E. S. R., Jobling, S., & Tyler, C. R. (2015). Effects of exposure to WWTW effluents over two generations on sexual development and breeding in roach *Rutilus rutilus*. *Environmental Science and Technology*, *49*(21), 12994–13002. https://doi.org/10.1021/acs.est.5b03777

Hao, R., Bondesson, M., Singh, A. V., Riu, A., McCollum, C. W., Knudsen, T. B., Gorelick, D. A., & Gustafsson, J. Å. (2013). Identification of estrogen target genes during zebrafish embryonic development through transcriptomic analysis. *PLoS ONE*, *8*(11), 1–18. https://doi.org/10.1371/journal.pone.0079020

Hartley, K. O., Nutt, S. L., & Amaya, E. (2002). Targeted gene expression in

transgenic Xenopus using the binary Gal4-UAS system. *Proceedings of the National Academy of Sciences of the United States of America*, *99*(3), 1377–1382. https://doi.org/10.1073/pnas.022646899

Hatta, K., Tsujii, H., & Omura, T. (2006). Cell tracking using a photoconvertible fluorescent protein. *Nature Protocols*, *1*(2), 960–967. https://doi.org/10.1038/nprot.2006.96

Hayat, M., Joyce, C. P., Townes, T. M., Chen, T. T., Powers, D. A., & Dunham, R. A. (1991). Survival and integration rate of channel catfish and common carp embryos microinjected with DNA at various developmental stages. *Aquaculture*, *99*(3–4), 249–255. https://doi.org/10.1016/0044-8486(91)90245-3

Hayes, J. D., Flanagan, J. U., & Jowsey, I. R. (2005). Glutathione Transferases. *Annual Review of Pharmacology and Toxicology*, *45*(1), 51–88. https://doi.org/10.1146/annurev.pharmtox.45.120403.095857

He, J. H., Guo, S. Y., Zhu, F., Zhu, J. J., Chen, Y. X., Huang, C. J., Gao, J. M., Dong, Q. X., Xuan, Y. X., & Li, C. Q. (2013). A zebrafish phenotypic assay for assessing drug-induced hepatotoxicity. *Journal of Pharmacological and Toxicological Methods*, *67*(1), 25–32. https://doi.org/10.1016/j.vascn.2012.10.003

Hebisch, E., Knebel, J., Landsberg, J., Frey, E., & Leisner, M. (2013). High variation of fluorescence protein maturation times in closely related *Escherichia coli* strains. *PLoS ONE*, *8*(10), e75991. https://doi.org/10.1371/journal.pone.0075991

Heise, K. (2003). Production of reactive oxygen species by isolated mitochondria of the Antarctic bivalve *Laternula elliptica* (King and Broderip) under heat stress. *Comparative Biochemistry and Physiology Part C: Toxicology & Pharmacology*, *134*(1), 79–90. https://doi.org/10.1016/S1532-0456(02)00212-0

Hendouei, N., Farnia, S., Mohseni, F., Salehi, A., Bagheri, M., Shadfar, F., Barzegar, F., Hoseini, S. D., Charati, J. Y., & Shaki, F. (2018). Alterations in oxidative stress markers and its correlation with clinical findings in schizophrenic patients consuming perphenazine, clozapine and

risperidone. *Biomedicine & Pharmacotherapy*, *103*(April), 965–972. https://doi.org/10.1016/j.biopha.2018.04.109

Hentschel, D. M., Kwon, M. P., Cilenti, L., Zervos, A. S., Drummond, I., & Bonventre, J. V. (2005). Acute renal failure in zebrafish: A novel system to study a complex disease. *American Journal of Physiology - Renal Physiology*, *288*(5 57-5), 923–929. https://doi.org/10.1152/ajprenal.00386.2004

Heppert, J. K., Dickinson, D. J., Pani, A. M., Higgins, C. D., Steward, A., Ahringer, J., Kuhn, J. R., & Goldstein, B. (2016). Comparative assessment of fluorescent proteins for in vivo imaging in an animal model system. *Molecular Biology of the Cell*, *27*(22), 3385–3394. https://doi.org/10.1091/mbc.E16-01-0063

Heugens, E. H. W., Jager, T., Creyghton, R., Kraak, M. H. S., Hendriks, A. J., Van Straalen, N. M., & Admiraal, W. (2003). Temperature-dependent effects of cadmium on *Daphnia magna* : accumulation versus sensitivity. *Environmental Science & Technology*, *37*(10), 2145–2151. https://doi.org/10.1021/es0264347

Hinfray, N., Tebby, C., Piccini, B., Bourgine, G., Aït-Aïssa, S., Porcher, J.-M., Pakdel, F., & Brion, F. (2018). Mixture concentration-response modeling reveals antagonistic effects of estradiol and genistein in combination on brain aromatase gene (cyp19a1b) in zebrafish. *International Journal of Molecular Sciences*, *19*(1047). https://doi.org/10.3390/ijms19041047

Holmstrup, M., Bindesbøl, A.-M., Oostingh, G. J., Duschl, A., Scheil, V., Köhler, H.-R., Loureiro, S., Soares, A. M. V. M., Ferreira, A. L. G., Kienle, C., Gerhardt, A., Laskowski, R., Kramarz, P. E., Bayley, M., Svendsen, C., & Spurgeon, D. J. (2010). Interactions between effects of environmental chemicals and natural stressors: A review. *Science of The Total Environment*, *408*(18), 3746–3762. https://doi.org/10.1016/j.scitotenv.2009.10.067

Hooper, M. J., Ankley, G. T., Cristol, D. A., Maryoung, L. A., Noyes, P. D., & Pinkerton, K. E. (2013). Interactions between chemical and climate stressors: A role for mechanistic toxicology in assessing climate change

risks. *Environmental Toxicology and Chemistry*, *32*(1), 32–48. https://doi.org/10.1002/etc.2043

Huang, W.-C., Hsieh, Y.-S., Chen, I.-H., Wang, C.-H., Chang, H.-W., Yang, C.-C., Ku, T.-H., Yeh, S.-R., & Chuang, Y.-J. (2010). Combined use of MS-222 (tricaine) and isoflurane extends anesthesia time and minimizes cardiac rhythm side effects in adult zebrafish. *Zebrafish*, *7*(3), 297–304. https://doi.org/10.1089/zeb.2010.0653

Huey, R. B., Kearney, M. R., Krockenberger, A., Holtum, J. A. M., Jess, M., & Williams, S. E. (2012). Predicting organismal vulnerability to climate warming: roles of behaviour, physiology and adaptation. *Philosophical Transactions of the Royal Society B: Biological Sciences*, *367*(1596), 1665–1679. https://doi.org/10.1098/rstb.2012.0005

Huggett, D. B., Cook, J. C., Ericson, J. F., & Williams, R. T. (2003). A theoretical model for utilizing mammalian pharmacology and safety data to prioritize potential impacts of human pharmaceuticals to fish. *Human and Ecological Risk Assessment: An International Journal*, *9*(7), 1789–1799. https://doi.org/10.1080/714044797

Huggett, D. B., Ericson, J. F., Cook, J. C., & Williams, R. T. (2004). Plasma concentrations of human pharmaceuticals as predictors of pharmacological responses in fish. In K. Kümmerer (Ed.), *Pharmaceuticals in the Environment* (pp. 373–386). Springer Berlin Heidelberg. https://doi.org/10.1007/978-3-662-09259-0_27

Hung, G.-Y., Wu, C.-L., Chou, Y.-L., Chien, C.-T., Horng, J.-L., & Lin, L.-Y. (2019). Cisplatin exposure impairs ionocytes and hair cells in the skin of zebrafish embryos. *Aquatic Toxicology*, *209*(February), 168–177. https://doi.org/10.1016/j.aquatox.2019.02.006

Icha, J., Schmied, C., Sidhaye, J., Tomancak, P., Preibisch, S., & Norden, C. (2016). Using light sheet fluorescence microscopy to image zebrafish eye development. *Journal of Visualized Experiments*, *110*, 1–21. https://doi.org/10.3791/53966

Islas-Flores, H., Gómez-Oliván, L. M., Galar-Martínez, M., Colín-Cruz, A., Neri-Cruz, N., & García-Medina, S. (2013). Diclofenac-induced oxidative stress

in brain, liver, gill and blood of common carp (*Cyprinus carpio*). *Ecotoxicology and Environmental Safety*, *92*, 32–38. https://doi.org/10.1016/j.ecoenv.2013.01.025

Islas-Flores, H., Gómez-Oliván, L. M., Galar-Martínez, M., García-Medina, S., Neri-Cruz, N., & Dublán-García, O. (2014). Effect of ibuprofen exposure on blood, gill, liver, and brain on common carp (*Cyprinus carpio*) using oxidative stress biomarkers. *Environmental Science and Pollution Research*, *21*(7), 5157–5166. https://doi.org/10.1007/s11356-013-2477-0

Iwayama, K., Kimura, J., Mishima, A., Kusakabe, A., Ohtaki, K., Tampo, Y., & Hayase, N. (2018). Low concentrations of clarithromycin upregulate cellular antioxidant enzymes and phosphorylation of extracellular signal-regulated kinase in human small airway epithelial cells. *Journal of Pharmaceutical Health Care and Sciences*, *4*(1), 1–14. https://doi.org/10.1186/s40780-018-0120-4

Iwayama, K., Kusakabe, A., Ohtsu, K., Nawano, T., Tatsunami, R., Ohtaki, K. ichi, Tampo, Y., & Hayase, N. (2017). Long-term treatment of clarithromycin at a low concentration improves hydrogen peroxide-induced oxidant/antioxidant imbalance in human small airway epithelial cells by increasing Nrf2 mRNA expression. *BMC Pharmacology and Toxicology*, *18*(1), 1–15. https://doi.org/10.1186/s40360-017-0119-8

Izumi, H., Sato, K., Kojima, K., Saito, T., Saido, T. C., & Fukunaga, K. (2020). Oral glutathione administration inhibits the oxidative stress and the inflammatory responses in AppNL−G-F/NL−G-F knock-in mice. *Neuropharmacology*, *168*(February), 108026. https://doi.org/10.1016/j.neuropharm.2020.108026

Jackson, L. M., Felgenhauer, B. E., & Klerks, P. L. (2019). Feminization, altered gonadal development, and liver damage in least killifish (*Heterandria formosa*) exposed to sublethal concentrations of 17α-ethinylestradiol. *Ecotoxicology and Environmental Safety*, *170*(December 2018), 331–337. https://doi.org/10.1016/j.ecoenv.2018.11.094

Jaeschke, H., McGill, M. R., & Ramachandran, A. (2012). Oxidant stress, mitochondria, and cell death mechanisms in drug-induced liver injury:

Lessons learned from acetaminophen hepatotoxicity. *Drug Metabolism Reviews*, *44*(1), 88–106. https://doi.org/10.3109/03602532.2011.602688

Jain, M. K., & Das, A. (2017). Impact of mine waste leachates on aquatic environment: a review. *Current Pollution Reports*, *3*(1), 31–37. https://doi.org/10.1007/s40726-017-0050-z

Jarque, S., Fetter, E., Veneman, W. J., Spaink, H. P., Peravali, R., Strahle, U., & Scholz, S. (2018). A fully automated screening method for detecting compounds with goitrogenic activity using transgenic zebrafish embryos. *PLoS ONE*, *13*(8). https://doi.org/https://doi.org/10.1016/j.reprotox.2016.06.064

Jemielita, M., Taormina, M. J., Delaurier, A., Kimmel, C. B., & Parthasarathy, R. (2013). Comparing phototoxicity during the development of a zebrafish craniofacial bone using confocal and light sheet fluorescence microscopy techniques. *Journal of Biophotonics*, *6*(11–12), 920–928. https://doi.org/10.1002/jbio.201200144

Jergensen, T., Cusmano, D., & Roy, N. M. (2019). Di-butyl phthalate (DBP) induces craniofacial defects during embryonic development in zebrafish. *Ecotoxicology*, *28*(8), 995–1002. https://doi.org/10.1007/s10646-019-02100-7

Ji, K., Seo, J., Kho, Y., & Choi, K. (2019). Co-exposure to ketoconazole alters effects of bisphenol A in *Danio rerio* and H295R cells. *Chemosphere*, *237*, 124414. https://doi.org/10.1016/j.chemosphere.2019.124414

Jiang, D., Huang, Y., Han, N., Xu, M., Xu, L., Zhou, L., Wang, S., & Fan, W. (2014). Fulvestrant, a selective estrogen receptor down-regulator, sensitizes estrogen receptor negative breast tumors to chemotherapy. *Cancer Letters*, *346*(2), 292–299. https://doi.org/10.1016/j.canlet.2014.01.008

Jin, M., Ji, X., Zhang, B., Sheng, W., Wang, R., & Liu, K. (2019). Synergistic effects of Pb and repeated heat pulse on developmental neurotoxicity in zebrafish. *Ecotoxicology and Environmental Safety*, *172*(January), 460–470. https://doi.org/10.1016/j.ecoenv.2019.01.104

Jin, Y., Zheng, S., Pu, Y., Shu, L., Sun, L., Liu, W., & Fu, Z. (2011).

Cypermethrin has the potential to induce hepatic oxidative stress, DNA damage and apoptosis in adult zebrafish (*Danio rerio*). *Chemosphere*, *82*(3), 398–404. https://doi.org/10.1016/j.chemosphere.2010.09.072

Jobling, S., Beresford, N., Nolan, M., Rodgers-Gray, T., Brighty, G. C., Sumpter, J. P., & Tyler, C. R. (2002). Altered sexual maturation and gamete production in wild roach (*Rutilus rutilus*) living in rivers that receive treated sewage effluents. *Biology of Reproduction*, *66*(2), 272–281. https://doi.org/10.1095/biolreprod66.2.272

Jones, H. S., Trollope, H. T., Hutchinson, T. H., Panter, G. H., & Chipman, J. K. (2012). Metabolism of ibuprofen in zebrafish larvae. *Xenobiotica*, *42*(11), 1069–1075. https://doi.org/10.3109/00498254.2012.684410

Jonkman, J., Brown, C. M., Wright, G. D., Anderson, K. I., & North, A. J. (2020). Tutorial: guidance for quantitative confocal microscopy. *Nature Protocols*, *15*(5), 1585–1611. https://doi.org/10.1038/s41596-020-0313-9

Kaczmarek, A., Brinkman, B. M., Heyndrickx, L., Vandenabeele, P., & Krysko, D. V. (2012). Severity of doxorubicin-induced small intestinal mucositis is regulated by the TLR-2 and TLR-9 pathways. *The Journal of Pathology*, *226*(4), 598–608. https://doi.org/10.1002/path.3009

Kander, M. C., Cui, Y., & Liu, Z. (2017). Gender difference in oxidative stress: a new look at the mechanisms for cardiovascular diseases. *Journal of Cellular and Molecular Medicine*, *21*(5), 1024–1032. https://doi.org/10.1111/jcmm.13038

Kantae, V., Krekels, E. H. J., Ordas, A., González, O., Van Wijk, R. C., Harms, A. C., Racz, P. I., Van Der Graaf, P. H., Spaink, H. P., & Hankemeier, T. (2016). Pharmacokinetic modeling of paracetamol uptake and clearance in zebrafish larvae: Expanding the allometric scale in vertebrates with five orders of magnitude. *Zebrafish*, *13*(6), 504–510. https://doi.org/10.1089/zeb.2016.1313

Kasprzyk-Hordern, B., Dinsdale, R. M., & Guwy, A. J. (2009). The removal of pharmaceuticals, personal care products, endocrine disruptors and illicit drugs during wastewater treatment and its impact on the quality of receiving waters. *Water Research*, *43*(2), 363–380.

https://doi.org/10.1016/j.watres.2008.10.047

Kataoka, C., Sugiyama, T., Kitagawa, H., Takeshima, A., Kagami, Y., Tatsuta, H., & Kashiwada, S. (2019). Temperature-dependent toxicity of acetaminophen in Japanese medaka larvae. *Environmental Pollution*, *254*, 113092. https://doi.org/10.1016/j.envpol.2019.113092

Kaufmann, A., Mickoleit, M., Weber, M., & Huisken, J. (2012). Multilayer mounting enables long-term imaging of zebrafish development in a light sheet microscope. *Development (Cambridge)*, *139*(17), 3242–3247. https://doi.org/10.1242/dev.082586

Keller, P. J., Schmidt, A. D., Wittbrodt, J., & Stelzer, E. H. K. (2008). Reconstruction of zebrafish early embryonic development by scanned light sheet microscopy. *Science*, *322*(5904), 1065–1069. https://doi.org/10.1126/science.1162493

Kent, M. L., Buchner, C., Barton, C., & Tanguay, R. L. (2014). Toxicity of chlorine to zebrafish embryos. *Diseases of Aquatic Organisms*, *107*(3), 235–240. https://doi.org/10.3354/dao02683

Khayyat, A., Tobwala, S., Hart, M., & Ercal, N. (2016). N-acetylcysteine amide, a promising antidote for acetaminophen toxicity. *Toxicology Letters*, *241*, 133–142. https://doi.org/10.1016/j.toxlet.2015.11.008

Kidd, K. A., Blanchfield, P. J., Mills, K. H., Palace, V. P., Evans, R. E., Lazorchak, J. M., & Flick, R. W. (2007). Collapse of a fish population after exposure to a synthetic estrogen. *Proceedings of the National Academy of Sciences of the United States of America*, *104*(21), 8897–8901. https://doi.org/10.1073/pnas.0609568104

Kim, J., Park, J., Kim, P. G., Lee, C., Choi, K., & Choi, K. (2010). Implication of global environmental changes on chemical toxicity-effect of water temperature, pH, and ultraviolet B irradiation on acute toxicity of several pharmaceuticals in *Daphnia magna*. *Ecotoxicology*, *19*(4), 662–669. https://doi.org/10.1007/s10646-009-0440-0

Kim, K. H., Park, H. J., Kim, J. H., Kim, S., Williams, D. R., Kim, M. K., Jung, Y. Do, Teraoka, H., Park, H. C., Choy, H. E., Shin, B. A., & Choi, S. Y. (2013a). Cyp1a reporter zebrafish reveals target tissues for dioxin. *Aquatic*

*Toxicology*, *134–135*, 57–65. https://doi.org/10.1016/j.aquatox.2013.03.010

Kim, R. O., Kim, B. M., Hwang, D. S., Au, D. W. T., Jung, J. H., Shim, W. J., Leung, K. M. Y., Wu, R. S. S., Rhee, J. S., & Lee, J. S. (2013b). Evaluation of biomarker potential of cytochrome P450 1A (CYP1A) gene in the marine medaka, *Oryzias melastigma* exposed to water-accommodated fractions (WAFs) of Iranian crude oil. *Comparative Biochemistry and Physiology - C Toxicology and Pharmacology*, *157*(2), 172–182. https://doi.org/10.1016/j.cbpc.2012.11.003

Kimmel, C. B., Ballard, W. W., Kimmel, S. R., Ullmann, B., & Schilling, T. F. (1995). Stages of embryonic development of the zebrafish. *Dev Dyn*, *203*(3), 253–310. https://doi.org/10.1002/aja.1002030302

Kimura, Y., Hisano, Y., Kawahara, A., & Higashijima, S. I. (2014). Efficient generation of knock-in transgenic zebrafish carrying reporter/driver genes by CRISPR/Cas9-mediated genome engineering. *Scientific Reports*, *4*, 1–7. https://doi.org/10.1038/srep06545

Kithcart, A., & MacRae, C. A. (2017). Using zebrafish for high-throughput screening of novel cardiovascular drugs. *JACC: Basic to Translational Science*, *2*(1), 1–12. https://doi.org/10.1016/j.jacbts.2017.01.004

Kloepper-Sams, P. J., & Stegeman, J. J. (1992). Effects of temperature acclimation on the expression of hepatic cytochrome P4501A mRNA and protein in the fish *Fundulus heteroclitus*. *Archives of Biochemistry and Biophysics*, *299*(1), 38–46. https://doi.org/10.1016/0003-9861(92)90241-N

Korzh, S., Pan, X., Garcia-Lecea, M., Winata, C. L., Pan, X., Wohland, T., Korzh, V., & Gong, Z. (2008). Requirement of vasculogenesis and blood circulation in late stages of liver growth in zebrafish. *BMC Developmental Biology*, *8*, 1–15. https://doi.org/10.1186/1471-213X-8-84

Kossack, M. E., & Draper, B. W. (2019). Genetic regulation of sex determination and maintenance in zebrafish (*Danio rerio*). In *Physiology & behavior* (Vol. 176, Issue 1, pp. 119–149). https://doi.org/10.1016/bs.ctdb.2019.02.004

Kostich, M. S., Batt, A. L., & Lazorchak, J. M. (2014). Concentrations of prioritized pharmaceuticals in effluents from 50 large wastewater treatment plants in the US and implications for risk estimation. *Environmental*

*Pollution*, *184*, 354–359. https://doi.org/10.1016/j.envpol.2013.09.013

Kruidering, M., Van De Water, B., De Heer, E., Mulder, G. J., & Nagelkerke, J. F. (1997). Cisplatin-induced nephrotoxicity in porcine proximal tubular cells: Mitochondrial dysfunction by inhibition of complexes I to iv of the respiratory chain. *Journal of Pharmacology and Experimental Therapeutics*, *280*(2), 638–649.

Kteeba, S. M., El-Ghobashy, A. E., El-Adawi, H. I., El-Rayis, O. A., Sreevidya, V. S., Guo, L., & Svoboda, K. R. (2018). Exposure to ZnO nanoparticles alters neuronal and vascular development in zebrafish: Acute and transgenerational effects mitigated with dissolved organic matter. *Environmental Pollution*, *242*, 433–448. https://doi.org/10.1016/j.envpol.2018.06.030

Kurdyukov, S., & Bullock, M. (2016). DNA methylation analysis: choosing the right method. *Biology*, *5*(1), 3. https://doi.org/10.3390/biology5010003

Kusik, B. W., Carvan, M. J., & Udvadia, A. J. (2008). Detection of mercury in aquatic environments using EPRE reporter zebrafish. *Marine Biotechnology*, *10*(6), 750–757. https://doi.org/10.1007/s10126-008-9113-x

Küster, A., Alder, A. C., Escher, B. I., Duis, K., Fenner, K., Garric, J., Hutchinson, T. H., Lapen, D. R., Péry, A., Römbke, J., Snape, J., Ternes, T., Topp, E., Wehrhan, A., & Knackerk, T. (2010). Environmental risk assessment of human pharmaceuticals in the European union: A case study with the β-blocker atenolol. *Integrated Environmental Assessment and Management*, *6*(SUPPL. 1), 514–523. https://doi.org/10.1897/IEAM-2009-050.1

Lackmann, C., Santos, M. M. M., Rainieri, S., Barranco, A., Hollert, H., Spirhanzlova, P., Velki, M., & Seiler, T.-B. B. (2018). Novel procedures for whole organism detection and quantification of fluorescence as a measurement for oxidative stress in zebrafish (*Danio rerio*) larvae. *Chemosphere*, *197*, 200–209. https://doi.org/10.1016/j.chemosphere.2018.01.045

Lam, P., Kutchukian, P., Anand, R., Imbriglio, J., Andrews, C., Padilla, H., Vohra, A., Lane, S., Parker, D. L., Cornella Taracido, I., Johns, D. G.,

Beerens, M., MacRae, C. A., Caldwell, J. P., Sorota, S., Asnani, A., & Peterson, R. T. (2020). Cyp1 inhibition prevents doxorubicin-induced cardiomyopathy in a zebrafish heart-failure model. *ChemBioChem*, *21*(13), 1905–1910. https://doi.org/10.1002/cbic.201900741

Lange, A., & Paull, G. (2009). Sexual reprogramming and estrogenic sensitization in wild fish exposed to ethinylestradiol. *Environ. Sci. Technol.* , *43*(4), 1219–1225. https://doi.org/10.1021/es802661p

Lantz-Mcpeak, S., Guo, X., Cuevas, E., Dumas, M., Newport, G. D., Ali, S. F., Paule, M. G., & Kanungo, J. (2015). Developmental toxicity assay using high content screening of zebrafish embryos. *Journal of Applied Toxicology*, *35*(3), 261–272. https://doi.org/10.1002/jat.3029

Lassiter, C. S., Kelley, B., & Linney, E. (2002). Genomic structure and embryonic expression of estrogen receptor beta a (ERβa) in zebrafish (*Danio rerio*). *Gene*, *299*(1–2), 141–151. https://doi.org/10.1016/S0378-1119(02)01050-8

Laurenson, J. P., Bloom, R. A., Page, S., & Sadrieh, N. (2014). Ethinyl estradiol and other human pharmaceutical estrogens in the aquatic environment: a review of recent risk assessment data. *The AAPS Journal*, *16*(2), 299–310. https://doi.org/10.1208/s12248-014-9561-3

Lauterburg, B. H., Corcoran, G. B., & Mitchell, J. R. (1983). Mechanism of action of N-acetylcysteine in the protection against the hepatotoxicity of acetaminophen in rats *in vivo*. *Journal of Clinical Investigation*, *71*(4), 980–991. https://doi.org/10.1172/JCI110853

Lawson, N. D., & Weinstein, B. M. (2002). In vivo imaging of embryonic vascular development using transgenic zebrafish. *Developmental Biology*, *248*(2), 307–318. https://doi.org/10.1006/dbio.2002.0711

Lee, J. E., Nakagawa, T., Kim, T. S., Endo, T., Shiga, A., Iguchi, F., Lee, S. H., & Ito, J. (2004). Role of reactive radicals in degeneration of the auditory system of mice following cisplatin treatment. *Acta Oto-Laryngologica*, *124*(10), 1131–1135. https://doi.org/10.1080/00016480410017521

Lee, O., Green, J. M., & Tyler, C. R. (2015). Transgenic fish systems and their application in ecotoxicology. In *Critical Reviews in Toxicology* (Vol. 45,

Issue 2, pp. 124–141). https://doi.org/10.3109/10408444.2014.965805

Lee, O., Takesono, A., Tada, M., Tyler, C. R., & Kudoh, T. (2012a). Biosensor zebrafish provide new insights into potential health effects of environmental estrogens. *Environ Health Perspect*, *120*(7), 990–996. https://doi.org/10.1289/ehp.1104433

Lee, O., Tyler, C. R., & Kudoh, T. (2012b). Development of a transient expression assay for detecting environmental oestrogens in zebrafish and medaka embryos. *BMC Biotechnology*, *12*. https://doi.org/10.1186/1472-6750-12-32

Lee, S. H., Kim, H. R., Han, R. X., Oqani, R. K., & Jin, D. Il. (2013). Cardiovascular risk assessment of atypical antipsychotic drugs in a zebrafish model. *Journal of Applied Toxicology*, *33*(6), 466–470. https://doi.org/10.1002/jat.1768

Lee, S., & Hu, L. (2020). Nrf2 activation through the inhibition of Keap1–Nrf2 protein–protein interaction. *Medicinal Chemistry Research*, *29*(5), 846–867. https://doi.org/10.1007/s00044-020-02539-y

Lee, S. R., Kwon, S. W., Lee, Y. H., Kaya, P., Kim, J. M., Ahn, C., Jung, E.-M., Lee, G.-S., An, B.-S., Jeung, E.-B., Park, B., & Hong, E.-J. (2019). Dietary intake of genistein suppresses hepatocellular carcinoma through AMPK-mediated apoptosis and anti-inflammation. *BMC Cancer*, *19*(1), 6. https://doi.org/10.1186/s12885-018-5222-8

Legler, J., Broekhof, J. L. M., Brouwer, A., Lanser, P. H., Murk, A. J., Van Der Saag, P. T., Dick Vethaak, A., Wester, P., Zivkovic, D., & Van Der Burg, B. (2000). A novel in vivo bioassay for (xeno-)estrogens using transgenic zebrafish. *Environmental Science and Technology*, *34*(20), 4439–4444. https://doi.org/10.1021/es0000605

Liska, D. A. J. (1998). The detoxification enzyme systems. *Alternative Medicine Review*, *3*(3), 187–198.

Liu, H., Gooneratne, R., Huang, X., Lai, R., Wei, J., & Wang, W. (2015). A rapid in vivo zebrafish model to elucidate oxidative stress-mediated PCB126-induced apoptosis and developmental toxicity. *Free Radical Biology and Medicine*, *84*, 91–102. https://doi.org/10.1016/j.freeradbiomed.2015.03.002

Liu, K., Petree, C., Requena, T., Varshney, P., & Varshney, G. K. (2019). Expanding the CRISPR toolbox in zebrafish for studying development and disease. *Frontiers in Cell and Developmental Biology*, *7*(MAR), 1–15. https://doi.org/10.3389/fcell.2019.00013

Liu, L., Yan, Y., Wang, J., Wu, W., & Xu, L. (2016). Generation of mt:egfp transgenic zebrafish biosensor for the detection of aquatic zinc and cadmium. *Environmental Toxicology and Chemistry*, *35*(8), 2066–2073. https://doi.org/10.1002/etc.3362

Lo, K. C., Sun, C. Y., Ding, Y. J., Tsai, J. N., Chang, K. P., Wen, Y. E., Chang, W. L., Chang, S. C., Chang, M. F., Wang, Y. H., & Chen, Y. H. (2014). Nephrotoxicity assessments of benzo(a)pyrene during zebrafish embryogenesis. *Research on Chemical Intermediates*, *40*(6), 2177–2185. https://doi.org/10.1007/s11164-014-1595-8

Logan, S. L., Dudley, C., Baker, R. P., Taormina, M. J., Hay, E. A., & Parthasarathy, R. (2018). Automated high-throughput light-sheet fluorescence microscopy of larval zebrafish. *BioRxiv*, 1–14. https://doi.org/10.1101/330639

Luckenbach, T., & Epel, D. (2008). ABCB- and ABCC-type transporters confer multixenobiotic resistance and form an environment-tissue barrier in bivalve gills. *American Journal of Physiology-Regulatory, Integrative and Comparative Physiology*, *294*(6), R1919–R1929. https://doi.org/10.1152/ajpregu.00563.2007

Lushchak, V. I. (2011). Environmentally induced oxidative stress in aquatic animals. *Aquatic Toxicology*, *101*(1), 13–30. https://doi.org/10.1016/j.aquatox.2010.10.006

Lushchak, V. I. (2016). Contaminant-induced oxidative stress in fish: a mechanistic approach. *Fish Physiology and Biochemistry*, *42*(2), 711–747. https://doi.org/10.1007/s10695-015-0171-5

Maier, T., Güell, M., & Serrano, L. (2009). Correlation of mRNA and protein in complex biological samples. *FEBS Letters*, *583*(24), 3966–3973. https://doi.org/10.1016/j.febslet.2009.10.036

Malaj, E., Von Der Ohe, P. C., Grote, M., Kühne, R., Mondy, C. P., Usseglio-

Polatera, P., Brack, W., & Schäfer, R. B. (2014). Organic chemicals jeopardize the health of freshwater ecosystems on the continental scale. *Proceedings of the National Academy of Sciences of the United States of America*, *111*(26), 9549–9554. https://doi.org/10.1073/pnas.1321082111

Manley, H. R., Potter, D. L., Heddleston, J. M., Chew, T. L., Keightley, M. C., & Lieschke, G. J. (2020). Frontline Science: Dynamic cellular and subcellular features of migrating leukocytes revealed by in vivo lattice lightsheet microscopy. *Journal of Leukocyte Biology*, *108*(2), 455–468. https://doi.org/10.1002/JLB.3HI0120-589R

Martín, J., Camacho-Muñoz, D., Santos, J. L., Aparicio, I., & Alonso, E. (2014). Occurrence and ecotoxicological risk assessment of 14 cytostatic drugs in wastewater. *Water, Air, & Soil Pollution*, *225*(3), 1896. https://doi.org/10.1007/s11270-014-1896-y

Mathieu-Denoncourt, J., Wallace, S. J., de Solla, S. R., & Langlois, V. S. (2015). Plasticizer endocrine disruption: Highlighting developmental and reproductive effects in mammals and non-mammalian aquatic species. *General and Comparative Endocrinology*, *219*, 74–88. https://doi.org/10.1016/j.ygcen.2014.11.003

Matsui, H., Gavinio, R., & Takahashi, R. (2012). Medaka fish parkinson's disease model. *Experimental Neurobiology*, *21*(3), 94. https://doi.org/10.5607/en.2012.21.3.94

Matthiessen, P., Wheeler, J. R., & Weltje, L. (2018). A review of the evidence for endocrine disrupting effects of current-use chemicals on wildlife populations. *Critical Reviews in Toxicology*, *48*(3), 195–216. https://doi.org/10.1080/10408444.2017.1397099

Mattingly, C. J., McLachlan, J. a, & Toscano, W. a. (2001). Green fluorescent protein (GFP) as a marker of aryl hydrocarbon receptor (AhR) function in developing zebrafish (*Danio rerio*). *Environmental Health Perspectives*, *109*(8), 845–849. https://doi.org/10.2307/3454829

Maulvault, A. L., Barbosa, V., Alves, R., Anacleto, P., Camacho, C., Cunha, S., Fernandes, J. O., Ferreira, P. P., Rosa, R., Marques, A., & Diniz, M. (2018a). Integrated multi-biomarker responses of juvenile seabass to

diclofenac, warming and acidification co-exposure. *Aquatic Toxicology*, *202*(May), 65–79. https://doi.org/10.1016/j.aquatox.2018.06.016

Maulvault, A. L., Custódio, A., Anacleto, P., Repolho, T., Pousão, P., Nunes, M. L., Diniz, M., Rosa, R., & Marques, A. (2016). Bioaccumulation and elimination of mercury in juvenile seabass (*Dicentrarchus labrax*) in a warmer environment. *Environmental Research*, *149*, 77–85. https://doi.org/10.1016/j.envres.2016.04.035

Maulvault, A. L., Santos, L. H. M. L. M., Camacho, C., Anacleto, P., Barbosa, V., Alves, R., Pousão Ferreira, P., Serra-Compte, A., Barceló, D., Rodriguez-Mozaz, S., Rosa, R., Diniz, M., & Marques, A. (2018b). Antidepressants in a changing ocean: Venlafaxine uptake and elimination in juvenile fish (*Argyrosomus regius*) exposed to warming and acidification conditions. *Chemosphere*, *209*, 286–297. https://doi.org/10.1016/j.chemosphere.2018.06.004

Mazaleuskaya, L. L., Sangkuhl, K., Thorn, C. F., FitzGerald, G. A., Altman, R. B., & Klein, T. E. (2015). PharmGKB summary: Pathways of acetaminophen metabolism at the therapeutic versus toxic doses. *Pharmacogenetics and Genomics*, *25*(8), 416–426. https://doi.org/10.1097/FPC.0000000000000150

Mazer, M., & Perrone, J. (2008). Acetaminophen-induced nephrotoxicity: Pathophysiology, clinical manifestations, and management. *Journal of Medical Toxicology*, *4*(1), 2–6. https://doi.org/10.1007/BF03160941

McKee, R. A., & Wingert, R. A. (2015). Zebrafish renal pathology: emerging models of acute kidney injury. *Current Pathobiology Reports*, *3*(2), 171–181. https://doi.org/10.1007/s40139-015-0082-2

McRae, N. K., Glover, C. N., Burket, S. R., Brooks, B. W., & Gaw, S. (2018). Acute exposure to an environmentally relevant concentration of diclofenac elicits oxidative stress in the culturally important galaxiid fish *Galaxias maculatus*. *Environmental Toxicology and Chemistry*, *37*(1), 224–235. https://doi.org/10.1002/etc.3948

Mehdi, H., Bragg, L. M., Servos, M. R., & Craig, P. M. (2019). Multiple stressors in the environment: the effects of exposure to an antidepressant

(venlafaxine) and increased temperature on zebrafish metabolism. *Frontiers in Physiology*, *10*(November), 1–10. https://doi.org/10.3389/fphys.2019.01431

Menuet, A., Le Page, Y., Torres, O., Kern, L., Kah, O., & Pakdel, F. (2004). Analysis of the estrogen regulation of the zebrafish estrogen receptor (ER) reveals distinct effects of ERalpha, ERbeta1 and ERbeta2. *Journal of Molecular Endocrinology*, *32*(3), 975–986. https://doi.org/10.1677/jme.0.0320975

Metcalfe, W. K., Kimmel, C. B., & Schabtach, E. (1985). Anatomy of the posterior lateral line system in young larvae of the zebrafish. *The Journal of Comparative Neurology*, *233*(3), 377–389. https://doi.org/10.1002/cne.902330307

Miyanishi, H., Inokuchi, M., Nobata, S., & Kaneko, T. (2016). Past seawater experience enhances seawater adaptability in medaka, *Oryzias latipes*. *Zoological Letters*, *2*(1), 1–10. https://doi.org/10.1186/s40851-016-0047-2

Mo, N., Zhang, M., Wang, R., Xia, S., Meng, F., Qian, Y., & Li, M. (2019). Effects of α-ethinyl estradiol (EE2) and diethylhexyl phthalate (DEHP) on growth performance, antioxidant status and immune response of juvenile yellow catfish Pelteobagrus fulvidraco. *Comparative Biochemistry and Physiology Part - C: Toxicology and Pharmacology*, *226*(July), 108615. https://doi.org/10.1016/j.cbpc.2019.108615

Moon, W.-K. K., Atique, U., & An, K.-G. G. (2020). Ecological risk assessments and eco-toxicity analyses using chemical, biological, physiological responses, DNA damages and gene-level biomarkers in Zebrafish (*Danio rerio*) in an urban stream. *Chemosphere*, *239*, 124754. https://doi.org/10.1016/j.chemosphere.2019.124754

Moreman, J., Lee, O., Trznadel, M., David, A., Kudoh, T., & Tyler, C. R. (2017). Acute toxicity, teratogenic, and estrogenic effects of bisphenol A and its alternative replacements bisphenol S, bisphenol F, and bisphenol AF in zebrafish embryo-larvae. *Environmental Science and Technology*, *51*(21), 12796–12805. https://doi.org/10.1021/acs.est.7b03283

Moreman, J., Takesono, A., Trznadel, M., Winter, M. J., Perry, A., Wood, M. E.,

Rogers, N. J., Kudoh, T., & Tyler, C. R. (2018). Estrogenic mechanisms and cardiac responses following early life exposure to bisphenol A (BPA) and its metabolite 4-methyl-2,4-bis(p -hydroxyphenyl)pent-1-ene (MBP) in zebrafish. *Environmental Science and Technology*, *52*(11), 6656–6665. https://doi.org/10.1021/acs.est.8b01095

Morthorst, J. E., Holbech, H., & Bjerregaard, P. (2010). Trenbolone causes irreversible masculinization of zebrafish at environmentally relevant concentrations. *Aquatic Toxicology*, *98*(4), 336–343. https://doi.org/10.1016/j.aquatox.2010.03.008

Mourabit, S., Fitzgerald, J. A., Ellis, R. P., Takesono, A., Porteus, C. S., Trznadel, M., Metz, J., Winter, M. J., Kudoh, T., & Tyler, C. R. (2019). New insights into organ-specific oxidative stress mechanisms using a novel biosensor zebrafish. *Environment International*, *133*(May), 105138. https://doi.org/10.1016/j.envint.2019.105138

Nakajima, H., Nakajima-Takagi, Y., Tsujita, T., Akiyama, S.-I., Wakasa, T., Mukaigasa, K., Kaneko, H., Tamaru, Y., Yamamoto, M., & Kobayashi, M. (2011). Tissue-restricted expression of Nrf2 and its target genes in zebrafish with gene-specific variations in the induction profiles. *PLoS ONE*, *6*(10), e26884. https://doi.org/10.1371/journal.pone.0026884

Nallani, G. C., Edziyie, R. E., Paulos, P. M., Venables, B. J., Constantine, L. A., & Huggett, D. B. (2016). Bioconcentration of two basic pharmaceuticals, verapamil and clozapine, in fish. *Environmental Toxicology and Chemistry*, *35*(3), 593–603. https://doi.org/10.1002/etc.3244

Nallani, G. C., Paulos, P. M., Constantine, L. A., Venables, B. J., & Huggett, D. B. (2011). Bioconcentration of ibuprofen in fathead minnow (*Pimephales promelas*) and channel catfish (*Ictalurus punctatus*). *Chemosphere*, *84*(10), 1371–1377. https://doi.org/10.1016/j.chemosphere.2011.05.008

National Center for Biotechnology Information. (n.d.). *PubChem Compound Summary for CID 104741, Fulvestrant*. Retrieved February 24, 2022, from https://pubchem.ncbi.nlm.nih.gov/compound/Fulvestrant

Newman, T. A. C., Carleton, C. R., Leeke, B., Hampton, M. B., & Horsfield, J. A. (2015). Embryonic oxidative stress results in reproductive impairment for

adult zebrafish. *Redox Biology*, *6*, 648–655. https://doi.org/10.1016/j.redox.2015.10.010

Nieto, E., Hampel, M., González-Ortegón, E., Drake, P., & Blasco, J. (2016). Influence of temperature on toxicity of single pharmaceuticals and mixtures, in the crustacean *A. desmarestii*. *Journal of Hazardous Materials*, *313*, 159–169. https://doi.org/10.1016/j.jhazmat.2016.03.061

Nogueira, A. F., & Nunes, B. (2021). Effects of paracetamol on the polychaete *Hediste diversicolor*: occurrence of oxidative stress, cyclooxygenase inhibition and behavioural alterations. *Environmental Science and Pollution Research*, *28*(21), 26772–26783. https://doi.org/10.1007/s11356-020-12046-7

Notch, E. G., & Mayer, G. D. (2011). Efficacy of pharmacological estrogen receptor antagonists in blocking activation of zebrafish estrogen receptors. *General and Comparative Endocrinology*, *173*(1), 183–189. https://doi.org/10.1016/j.ygcen.2011.05.008

Noyes, P. D., McElwee, M. K., Miller, H. D., Clark, B. W., Van Tiem, L. A., Walcott, K. C., Erwin, K. N., & Levin, E. D. (2009). The toxicology of climate change: Environmental contaminants in a warming world. *Environment International*, *35*(6), 971–986. https://doi.org/10.1016/j.envint.2009.02.006

Nuñez, V. A., Sarrazin, A. F., Cubedo, N., Allende, M. L., Dambly-Chaudière, C., & Ghysen, A. (2009). Postembryonic development of the posterior lateral line in the zebrafish. *Evolution and Development*, *11*(4), 391–404. https://doi.org/10.1111/j.1525-142X.2009.00346.x

Nwaneshiudu, A., Kuschal, C., Sakamoto, F. H., Rox Anderson, R., Schwarzenberger, K., & Young, R. C. (2012). Introduction to Confocal Microscopy. *Journal of Investigative Dermatology*, *132*(12), 1–5. https://doi.org/10.1038/jid.2012.429

Octavia, Y., Tocchetti, C. G., Gabrielson, K. L., Janssens, S., Crijns, H. J., & Moens, A. L. (2012). Doxorubicin-induced cardiomyopathy: From molecular mechanisms to therapeutic strategies. *Journal of Molecular and Cellular Cardiology*, *52*(6), 1213–1225. https://doi.org/10.1016/j.yjmcc.2012.03.006

Ogungbemi, A., Leuthold, D., Scholz, S., & Küster, E. (2019). Hypo- or

hyperactivity of zebrafish embryos provoked by neuroactive substances: a review on how experimental parameters impact the predictability of behavior changes. *Environmental Sciences Europe*, *31*(1), 88. https://doi.org/10.1186/s12302-019-0270-5

Oliveira, L. L. D., Antunes, S. C., Gonçalves, F., Rocha, O., & Nunes, B. (2015). Evaluation of ecotoxicological effects of drugs on *Daphnia magna* using different enzymatic biomarkers. *Ecotoxicology and Environmental Safety*, *119*, 123–131. https://doi.org/10.1016/j.ecoenv.2015.04.028

Op de Beeck, L., Verheyen, J., Olsen, K., & Stoks, R. (2017). Negative effects of pesticides under global warming can be counteracted by a higher degradation rate and thermal adaptation. *Journal of Applied Ecology*, *54*(6), 1847–1855. https://doi.org/10.1111/1365-2664.12919

Ormandy, E. H., Dale, J., & Griffin, G. (2011). Animal Welfare Bien-être des animaux Genetic engineering of animals : Ethical issues , including welfare concerns. *Canadian Veterinary Journal*, *52*(5), 544–550.

Osborne, C. K., Wakeling, A., & Nicholson, R. I. (2004). Fulvestrant: an oestrogen receptor antagonist with a novel mechanism of action. *British Journal of Cancer*, *90*(S1), S2–S6. https://doi.org/10.1038/sj.bjc.6601629

Osburn, W., & Kensler, T. (2008). Nrf2 signaling: An adaptive response pathway for protection against environmental toxic insults. *Mutation Research/Reviews in Mutation Research*, *659*(1–2), 31–39. https://doi.org/10.1016/j.mrrev.2007.11.006

Otte, J. C., Schmidt, A. D., Hollert, H., & Braunbeck, T. (2010). Spatio-temporal development of CYP1 activity in early life-stages of zebrafish (*Danio rerio*). *Aquatic Toxicology*, *100*(1), 38–50. https://doi.org/10.1016/j.aquatox.2010.07.006

Ou, H. C., Raible, D. W., & Rubel, E. W. (2007). Cisplatin-induced hair cell loss in zebrafish (*Danio rerio*) lateral line. *Hearing Research*, *233*(1–2), 46–53. https://doi.org/10.1016/j.heares.2007.07.003

Overturf, M. D., Overturf, C. L., Baxter, D., Hala, D. N., Constantine, L., Venables, B., & Huggett, D. B. (2012). Early life-stage toxicity of eight pharmaceuticals to the fathead minnow, *pimephales promelas*. *Archives of*

*Environmental Contamination and Toxicology*, *62*(3), 455–464. https://doi.org/10.1007/s00244-011-9723-6

Oviedo-Gómez, D. G. C., Galar-Martínez, M., García-Medina, S., Razo-Estrada, C., & Gómez-Oliván, L. M. (2010). Diclofenac-enriched artificial sediment induces oxidative stress in *Hyalella azteca*. *Environmental Toxicology and Pharmacology*, *29*(1), 39–43. https://doi.org/10.1016/j.etap.2009.09.004

Owens, K. N., Coffin, A. B., Hong, L. S., Bennett, K. O., Rubel, E. W., & Raible, D. W. (2009). Response of mechanosensory hair cells of the zebrafish lateral line to aminoglycosides reveals distinct cell death pathways. *Hearing Research*, *253*(1–2), 32–41. https://doi.org/10.1016/j.heares.2009.03.001

Özdemir, Ö. M. A., Ergin, H., Yenisey, Ç., Türk, N. Ş., & Şimşek, N. G. (2010). Protective effects of clarithromycin in rats with hypoxia/reoxygenation-induced intestinal injury. *Journal of Pediatric Surgery*, *45*(11), 2169–2174. https://doi.org/10.1016/j.jpedsurg.2010.06.024

Pal, A., Gin, K. Y.-H., Lin, A. Y.-C., & Reinhard, M. (2010). Impacts of emerging organic contaminants on freshwater resources: Review of recent occurrences, sources, fate and effects. *Science of The Total Environment*, *408*(24), 6062–6069. https://doi.org/10.1016/j.scitotenv.2010.09.026

Pardo-Martin, C., Allalou, A., Medina, J., Eimon, P. M., Wahlby, C., & Yanik, M. F. (2013). High-throughput hyperdimensional vertebrate phenotyping. *Nature Communications*, *4*. https://doi.org/10.1038/ncomms2475

Pardo-Martin, C., Chang, T. Y., Koo, B. K., Gilleland, C. L., Wasserman, S. C., & Yanik, M. F. (2010). High-throughput in vivo vertebrate screening. *Nature Methods*, *7*(8), 634–636. https://doi.org/10.1038/nmeth.1481

Parichy, D. M., Elizondo, M. R., Mills, M. G., Gordon, T. N., & Engeszer, R. E. (2009). Normal table of postembryonic zebrafish development: Staging by externally visible anatomy of the living fish. *Developmental Dynamics*, *238*(12), 2975–3015. https://doi.org/10.1002/dvdy.22113

Park, H., Lee, J. Y., Park, S., Song, G., & Lim, W. (2020). Developmental toxicity of fipronil in early development of zebrafish (*Danio rerio*) larvae: Disrupted vascular formation with angiogenic failure and inhibited neurogenesis. *Journal of Hazardous Materials*, *385*(August 2019), 121531.

https://doi.org/10.1016/j.jhazmat.2019.121531

Patel, A., Panter, G. H., Trollope, H. T., Glennon, Y. C., Owen, S. F., Sumpter, J. P., & Rand-Weaver, M. (2016). Testing the “read-across hypothesis” by investigating the effects of ibuprofen on fish. *Chemosphere*, *163*, 592–600. https://doi.org/10.1016/j.chemosphere.2016.08.041

Peng, H.-C., Wang, Y.-H., Wen, C.-C., Wang, W.-H., Cheng, C.-C., & Chen, Y.-H. (2010). Nephrotoxicity assessments of acetaminophen during zebrafish embryogenesis. *Comparative Biochemistry and Physiology Part C: Toxicology & Pharmacology*, *151*(4), 480–486. https://doi.org/10.1016/j.cbpc.2010.02.004

Pensado-López, A., Fernández-Rey, J., Reimunde, P., Crecente-Campo, J., Sánchez, L., & Torres Andón, F. (2021). Zebrafish models for the safety and therapeutic testing of nanoparticles with a focus on macrophages. *Nanomaterials*, *11*(7), 1784. https://doi.org/10.3390/nano11071784

Peravali, R., Gehrig, J., Giselbrecht, S., Lütjohann, D. S., Hadzhiev, Y., Müller, F., & Liebel, U. (2011). Automated feature detection and imaging for high-resolution screening of zebrafish embryos. *BioTechniques*, *50*(5), 319–324. https://doi.org/10.2144/000113669

Pereira, A., & Dean, B. (2006). Clozapine bioactivation induces dose-dependent, drug-specific toxicity of human bone marrow stromal cells: A potential *in vitro* system for the study of agranulocytosis. *Biochemical Pharmacology*, *72*(6), 783–793. https://doi.org/10.1016/j.bcp.2006.06.006

Perez, C. J., Tata, A., de Campos, M. L., Peng, C., & Ifa, D. R. (2017). Monitoring toxic ionic liquids in zebrafish (*Danio rerio*) with desorption electrospray ionization mass spectrometry imaging (DESI-MSI). *Journal of the American Society for Mass Spectrometry*, *28*(6), 1136–1148. https://doi.org/10.1007/s13361-016-1515-9

Petersen, K., Fetter, E., Kah, O., Brion, F., Scholz, S., & Tollefsen, K. E. (2013). Transgenic (cyp19a1b-GFP) zebrafish embryos as a tool for assessing combined effects of oestrogenic chemicals. *Aquatic Toxicology*, *138–139*, 88–97. https://doi.org/10.1016/j.aquatox.2013.05.001

Petersen, K., & Tollefsen, K. E. (2011). Assessing combined toxicity of estrogen

receptor agonists in a primary culture of rainbow trout (*Oncorhynchus mykiss*) hepatocytes. *Aquatic Toxicology*, *101*(1), 186–195. https://doi.org/10.1016/j.aquatox.2010.09.018

Phaniendra, A., Jestadi, D. B., & Periyasamy, L. (2015). Free radicals: properties, sources, targets, and their implication in various diseases. *Indian Journal of Clinical Biochemistry*, *30*(1), 11–26. https://doi.org/10.1007/s12291-014-0446-0

Pinheiro, J. P. S., Windsor, F. M., Wilson, R. W., & Tyler, C. R. (2021). Global variation in freshwater physico-chemistry and its influence on chemical toxicity in aquatic wildlife. *Biological Reviews*, *96*(4), 1528–1546. https://doi.org/10.1111/brv.12711

Pinto, D., Pellegrin, L., Nitz, L. F., da Costa, S. T., Monserrat, J. M., & Garcia, L. (2019). Haematological and oxidative stress responses in *Piaractus mesopotamicus* under temperature variations in water. *Aquaculture Research*, *50*(10), 3017–3027. https://doi.org/10.1111/are.14260

Pirmohamed, M., Williams, D., Madden, S., Templeton, E., & Park, B. K. (1995). Metabolism and bioactivation of clozapine by human liver in vitro. *Journal of Pharmacology and Experimental Therapeutics*, *272*(3), 984–990. https://doi.org/272 (3) 984-990

Pirro, V., Guffey, S. C., Sepúlveda, M. S., Mahapatra, C. T., Ferreira, C. R., Jarmusch, A. K., & Cooks, R. G. (2016). Lipid dynamics in zebrafish embryonic development observed by DESI-MS imaging and nanoelectrospray-MS. *Molecular BioSystems*, *12*(7), 2069–2079. https://doi.org/10.1039/C6MB00168H

Polson, J., & Lee, W. M. (2005). AASLD position paper: The management of acute liver failure. *Hepatology*, *41*(5), 1179–1197. https://doi.org/10.1002/hep.20703

Poon, K. L., Wang, X., Lee, S. G. P., Ng, A. S., Goh, W. H., Zhao, Z., Al-Haddawi, M., Wang, H., Mathavan, S., Ingham, P. W., McGinnis, C., & Carney, T. J. (2017). Transgenic zebrafish reporter lines as alternative *in vivo* organ toxicity models. *Toxicological Sciences*, *156*(1), 133–148. https://doi.org/10.1093/toxsci/kfw250

Porseryd, T., Larsson, J., Kellner, M., Bollner, T., Dinnétz, P., & Porsch Hällström, I. (2019). Altered non-reproductive behavior and feminization caused by developmental exposure to 17α-ethinylestradiol persist to adulthood in three-spined stickleback (*Gasterosteus aculeatus*). *Aquatic Toxicology*, *207*(October 2018), 142–152. https://doi.org/10.1016/j.aquatox.2018.11.024

Praskova, E., Plhalova, L., Chromcova, L., Stepanova, S., Bedanova, I., Blahova, J., Hostovsky, M., Skoric, M., Maršálek, P., Voslarova, E., & Svobodova, Z. (2014). Effects of subchronic exposure of diclofenac on growth, histopathological changes, and oxidative stress in zebrafish (*Danio rerio*). *The Scientific World Journal*, *2014*, 1–5. https://doi.org/10.1155/2014/645737

Prideaux, B., & Stoeckli, M. (2012). Mass spectrometry imaging for drug distribution studies. *Journal of Proteomics*, *75*(16), 4999–5013. https://doi.org/10.1016/j.jprot.2012.07.028

Priyadarshini, M., Orosco, L. A., & Panula, P. J. (2013). Oxidative stress and regulation of pink1 in zebrafish (*Danio rerio*). *PLoS ONE*, *8*(11), 1–11. https://doi.org/10.1371/journal.pone.0081851

Proia, L., Osorio, V., Soley, S., Köck-Schulmeyer, M., Pérez, S., Barceló, D., Romaní, A. M., & Sabater, S. (2013). Effects of pesticides and pharmaceuticals on biofilms in a highly impacted river. *Environmental Pollution*, *178*, 220–228. https://doi.org/10.1016/j.envpol.2013.02.022

Qiu, W., Fang, M., Magnuson, J. T., Greer, J. B., Chen, Q., Zheng, Y., Xiong, Y., Luo, S., Zheng, C., & Schlenk, D. (2020). Maternal exposure to environmental antibiotic mixture during gravid period predicts gastrointestinal effects in zebrafish offspring. *Journal of Hazardous Materials*, *399*(March), 123009. https://doi.org/10.1016/j.jhazmat.2020.123009

Queirós, V., Azeiteiro, U. M., Soares, A. M. V. M., & Freitas, R. (2021). The antineoplastic drugs cyclophosphamide and cisplatin in the aquatic environment – Review. *Journal of Hazardous Materials*, *412*(December 2020). https://doi.org/10.1016/j.jhazmat.2020.125028

Ramírez-Montero, M. del C., Gómez-Oliván, L. M., Gutiérrez-Noya, V. M., Orozco-Hernández, J. M., Islas-Flores, H., Elizalde-Velázquez, G. A., SanJuan-Reyes, N., & Galar-Martínez, M. (2022). Acute exposure to 17-α-ethinylestradiol disrupt the embryonic development and oxidative status of *Danio rerio*. *Comparative Biochemistry and Physiology Part C: Toxicology & Pharmacology*, *251*(July 2021), 109199. https://doi.org/10.1016/j.cbpc.2021.109199

Raschi, E., Vasina, V., Ursino, M. G., Boriani, G., Martoni, A., & De Ponti, F. (2010). Anticancer drugs and cardiotoxicity: Insights and perspectives in the era of targeted therapy. *Pharmacology & Therapeutics*, *125*(2), 196–218. https://doi.org/10.1016/j.pharmthera.2009.10.002

Rautio, J., Kumpulainen, H., Heimbach, T., Oliyai, R., Oh, D., Järvinen, T., & Savolainen, J. (2008). Prodrugs: design and clinical applications. *Nature Reviews. Drug Discovery*, *7*(3), 255–270. https://doi.org/10.1038/nrd2468

Regoli, F., Pellegrini, D., Winston, G. W., Gorbi, S., Giuliani, S., Virno-Lamberti, C., & Bompadre, S. (2002). Application of biomarkers for assessing the biological impact of dredged materials in the Mediterranean: The relationship between antioxidant responses and susceptibility to oxidative stress in the red mullet (*Mullus barbatus*). *Marine Pollution Bulletin*, *44*(9), 912–922. https://doi.org/10.1016/S0025-326X(02)00120-0

Reinke, A., Martins, M. R., Lima, M. S., Moreira, J. C., Dal-Pizzol, F., & Quevedo, J. (2004). Haloperidol and clozapine, but not olanzapine, induces oxidative stress in rat brain. *Neuroscience Letters*, *372*(1–2), 157–160. https://doi.org/10.1016/j.neulet.2004.09.032

Reis, E. O., Santos, L. V. S., & Lange, L. C. (2021). Prioritization and environmental risk assessment of pharmaceuticals mixtures from Brazilian surface waters. *Environmental Pollution*, *288*(July), 117803. https://doi.org/10.1016/j.envpol.2021.117803

Renshaw, S. A., Loynes, C. A., Trushell, D. M. I., Elworthy, S., Ingham, P. W., & Whyte, M. K. B. (2006). A transgenic zebrafish model of neutrophilic inflammation. *Blood*, *108*(13), 3976–3978. https://doi.org/10.1182/blood-2006-05-024075

Richardson, R., Metzger, M., Knyphausen, P., Ramezani, T., Slanchev, K., Kraus, C., Schmelzer, E., & Hammerschmidt, M. (2016). Re-epithelialization of cutaneous wounds in adult zebrafish combines mechanisms of wound closure in embryonic and adult mammals. *Development (Cambridge)*, *143*(12), 2077–2088. https://doi.org/10.1242/dev.130492

Roberts, P. H., & Thomas, K. V. (2006). The occurrence of selected pharmaceuticals in wastewater effluent and surface waters of the lower Tyne catchment. *Science of the Total Environment*, *356*(1–3), 143–153. https://doi.org/10.1016/j.scitotenv.2005.04.031

Rodvold, K. A. (1999). Clinical pharmacokinetics of clarithromycin. *Clinical Pharmacokinetics*, *37*(5), 385–398. https://doi.org/10.2165/00003088-199937050-00003

Romano, S. N., Edwards, H. E., Souder, J. P., Ryan, K. J., Cui, X., & Gorelick, D. A. (2017). G protein-coupled estrogen receptor regulates embryonic heart rate in zebrafish. *PLoS Genetics*, *13*(10), 1–26. https://doi.org/10.1371/journal.pgen.1007069

Rombough, P. (2002). Gills are needed for ionoregulation before they are needed for O2 uptake in developing zebrafish, *Danio rerio*. *Journal of Experimental Biology*, *205*(12), 1787–1794. https://doi.org/10.1242/jeb.205.12.1787

Rotundo, L., & Pyrsopoulos, N. (2020). Liver injury induced by paracetamol and challenges associated with intentional and unintentional use. *World Journal of Hepatology*, *12*(4), 125–136. https://doi.org/10.4254/wjh.v12.i4.125

Russo, G., Curcio, F., Bulli, G., Aran, L., Della-morte, D., Testa, G., Cacciatore, F., Bonaduce, D., & Abete, P. (2012). Oxidative stress and diseases. In V. Lushchak (Ed.), *Oxidative Stress and Diseases*. InTech. https://doi.org/10.5772/2535

Ruzicka, L., Howe, D. G., Ramachandran, S., Toro, S., Van Slyke, C. E., Bradford, Y. M., Eagle, A., Fashena, D., Frazer, K., Kalita, P., Mani, P., Martin, R., Moxon, S. T., Paddock, H., Pich, C., Schaper, K., Shao, X., Singer, A., & Westerfield, M. (2019). The Zebrafish Information Network:

new support for non-coding genes, richer Gene Ontology annotations and the Alliance of Genome Resources. *Nucleic Acids Research*, *47*(D1), D867–D873. https://doi.org/10.1093/nar/gky1090

Saaristo, M., Lagesson, A., Bertram, M. G., Fick, J., Klaminder, J., Johnstone, C. P., Wong, B. B. M., & Brodin, T. (2019). Behavioural effects of psychoactive pharmaceutical exposure on European perch (*Perca fluviatilis*) in a multi-stressor environment. *Science of the Total Environment*, *655*, 1311–1320. https://doi.org/10.1016/j.scitotenv.2018.11.228

Sager, J. J., Bai, Q., & Burton, E. A. (2010). Transgenic zebrafish models of neurodegenerative diseases. *Brain Structure and Function*, *214*(2–3), 285–302. https://doi.org/10.1007/s00429-009-0237-1

Saito, C., Zwingmann, C., & Jaeschke, H. (2010). Novel mechanisms of protection against acetaminophen hepatotoxicity in mice by glutathione and N-acetylcysteine. *Hepatology*, *51*(1), 246–254. https://doi.org/10.1002/hep.23267

Saliner, A. G., Netzeva, T. I., & Worth, A. P. (2006). Prediction of estrogenicity: Validation of a classification model. *SAR and QSAR in Environmental Research*, *17*(2), 195–223. https://doi.org/10.1080/10659360600636022

Salla, R. F., Gamero, F. U., Rissoli, R. Z., Dal-Medico, S. E., Castanho, L. M., Carvalho, C. dos S., Silva-Zacarin, E. C. M., Kalinin, A. L., Abdalla, F. C., & Costa, M. J. (2016). Impact of an environmental relevant concentration of 17α-ethinylestradiol on the cardiac function of bullfrog tadpoles. *Chemosphere*, *144*(November), 1862–1868. https://doi.org/10.1016/j.chemosphere.2015.10.042

Salminen, W. F., Voellmy, R., & Roberts, S. M. (1996). Induction of hsp 70 in HepG2 cells in response to hepatotoxicants. *Toxicology and Applied Pharmacology*, *141*(1), 117–123. https://doi.org/10.1006/taap.1996.0267

Sander, V., Patke, S., Sahu, S., Teoh, C. L., Peng, Z., Chang, Y. T., & Davidson, A. J. (2015). The small molecule probe PT-Yellow labels the renal proximal tubules in zebrafish. *Chemical Communications*, *51*(2), 395–398. https://doi.org/10.1039/c4cc08075k

Santos, L. H. M. L. M., Paíga, P., Araújo, A. N., Pena, A., Delerue-Matos, C., & Montenegro, M. C. B. S. M. (2013). Development of a simple analytical method for the simultaneous determination of paracetamol, paracetamol-glucuronide and p-aminophenol in river water. *Journal of Chromatography B: Analytical Technologies in the Biomedical and Life Sciences*, *930*, 75–81. https://doi.org/10.1016/j.jchromb.2013.04.032

Sanz, A. B., Santamaría, B., Ruiz-Ortega, M., Egido, J., & Ortiz, A. (2008). Mechanisms of renal apoptosis in health and disease. *Journal of the American Society of Nephrology*, *19*(9), 1634–1642. https://doi.org/10.1681/ASN.2007121336

Sarrazin, A. F., Nuñez, V. A., Sapède, D., Tassin, V., Dambly-Chaudière, C., & Ghysen, A. (2010). Origin and early development of the posterior lateral line system of zebrafish. *Journal of Neuroscience*, *30*(24), 8234–8244. https://doi.org/10.1523/JNEUROSCI.5137-09.2010

Sato, T., Takahoko, M., & Okamoto, H. (2006). HuC:Kaede, a useful tool to label neural morphologies in networks in vivo. *Genesis*, *44*(3), 136–142. https://doi.org/10.1002/gene.20196

Sawyer, D. B., Peng, X., Chen, B., Pentassuglia, L., & Lim, C. C. (2010). Mechanisms of anthracycline cardiac injury: can we identify strategies for cardioprotection? *Progress in Cardiovascular Diseases*, *53*(2), 105–113. https://doi.org/10.1016/j.pcad.2010.06.007

Schmid, S., Willi, R. A., Salgueiro-González, N., & Fent, K. (2020). Effects of new generation progestins, including as mixtures and in combination with other classes of steroid hormones, on zebrafish early life stages. *Science of the Total Environment*, *709*, 136262. https://doi.org/10.1016/j.scitotenv.2019.136262

Schmieder, P. K., Ankley, G., Mekenyan, O., Walker, J. D., & Bradbury, S. (2003). Quantitative structure-activity relationship models for prediction of estrogen receptor binding affinity of structurally diverse chemicals. *Environmental Toxicology and Chemistry*, *22*(8), 1844–1854. https://doi.org/10.1897/01-345

Schulz, M., Iwersen-Bergmann, S., Andresen, H., & Schmoldt, A. (2012).

Therapeutic and toxic blood concentrations of nearly 1,000 drugs and other xenobiotics. *Critical Care*, *16*(4), R136. https://doi.org/10.1186/cc11441

Scott, G. R., & Johnston, I. A. (2012). Temperature during embryonic development has persistent effects on thermal acclimation capacity in zebrafish. *Proceedings of the National Academy of Sciences*, *109*(35), 14247–14252. https://doi.org/10.1073/pnas.1205012109

Sebastine, I. M., & Wakeman, R. J. (2003). Consumption and environmental hazards of pharmaceutical substances in the UK. *Process Safety and Environmental Protection: Transactions of the Institution of Chemical Engineers, Part B*, *81*(4), 229–235. https://doi.org/10.1205/095758203322299743

Seeland, A., Albrand, J., Oehlmann, J., & Müller, R. (2013). Life stage-specific effects of the fungicide pyrimethanil and temperature on the snail *Physella acuta* (Draparnaud, 1805) disclose the pitfalls for the aquatic risk assessment under global climate change. *Environmental Pollution*, *174*, 1–9. https://doi.org/10.1016/j.envpol.2012.10.020

Seiler, C., & Pack, M. (2011). Transgenic labeling of the zebrafish pronephric duct and tubules using a promoter from the enpep gene. *Gene Expression Patterns*, *11*(1–2), 118–121. https://doi.org/10.1016/j.gep.2010.10.002

Serra, H., Scholze, M., Altenburger, R., Busch, W., Budzinski, H., Brion, F., & Aït-Aïssa, S. (2019). Combined effects of environmental xeno-estrogens within multi-component mixtures: Comparison of in vitro human- and zebrafish-based estrogenicity bioassays. *Chemosphere*, *227*, 334–344. https://doi.org/10.1016/j.chemosphere.2019.04.060

Shahab, M., Rosati, R., Meyers, D., Sheilds, J., Crofts, E., Baker, T. R., & Jamesdaniel, S. (2021). Cisplatin-induced hair cell loss in zebrafish neuromasts is accompanied by protein nitration and Lmo4 degradation. *Toxicology and Applied Pharmacology*, *410*(November 2020), 115342. https://doi.org/10.1016/j.taap.2020.115342

Shahid, M., Takamiya, M., Stegmaier, J., Middel, V., Gradl, M., Kluver, N., Mikut, R., Dickmeis, T., Scholz, S., Rastegar, S., Yang, L., & Strahle, U. (2016). Zebrafish biosensor for toxicant induced muscle hyperactivity.

*Scientific Reports*, *6*(March), 1–14. https://doi.org/10.1038/srep23768

Shaner, N. C., Steinbach, P. A., & Tsien, R. Y. (2005). A guide to choosing fluorescent proteins. *Nature Methods*, *2*(12), 905–909. https://doi.org/10.1038/nmeth819

Skillman, A. D., Nagler, J. J., Hook, S. E., Small, J. A., & Schultz, I. R. (2006). Dynamics of 17α-ethynylestradiol exposure in rainbow trout (*Oncorhynchus mykiss*): absorption, tissue distribution, and hepatic gene expression pattern. *Environmental Toxicology and Chemistry*, *25*(11), 2997. https://doi.org/10.1897/05-565R.1

Son, Y., Cheong, Y.-K., Kim, N.-H., Chung, H.-T., Kang, D. G., & Pae, H.-O. (2011). Mitogen-activated protein kinases and reactive oxygen species: How can ROS activate MAPK pathways? *Journal of Signal Transduction*, *2011*, 1–6. https://doi.org/10.1155/2011/792639

Song, C.-H., Kim, N., Kim, D.-H., Lee, H.-N., & Surh, Y.-J. (2019). 17-β estradiol exerts anti-inflammatory effects through activation of Nrf2 in mouse embryonic fibroblasts. *PLOS ONE*, *14*(8), e0221650. https://doi.org/10.1371/journal.pone.0221650

Song, M.-Y., Lee, D.-Y., Chun, K.-S., & Kim, E.-H. (2021). The role of NRF2/KEAP1 signaling pathway in cancer metabolism. *International Journal of Molecular Sciences*, *22*(9), 4376. https://doi.org/10.3390/ijms22094376

Songbo, M., Lang, H., Xinyong, C., Bin, X., Ping, Z., & Liang, S. (2019). Oxidative stress injury in doxorubicin-induced cardiotoxicity. *Toxicology Letters*, *307*(February), 41–48. https://doi.org/10.1016/j.toxlet.2019.02.013

Sousa Borges, R., César Matias Pereira, A., Custodio de Souza, G., & Carlos Tavares Carvalho, J. (2020). Histopathology of zebrafish (*Danio rerio*) in nonclinical toxicological studies of new drugs . *Zebrafish in Biomedical Research*. https://doi.org/10.5772/intechopen.88639

Spence, R., Fatema, M. K., Reichard, M., Huq, K. A., Wahab, M. A., Ahmed, Z. F., & Smith, C. (2006). The distribution and habitat preferences of the zebrafish in Bangladesh. *Journal of Fish Biology*, *69*(5), 1435–1448. https://doi.org/10.1111/j.1095-8649.2006.01206.x

Spence, R., Gerlach, G., Lawrence, C., & Smith, C. (2008). The behaviour and ecology of the zebrafish, *Danio rerio*. *Biological Reviews*, *83*(1), 13–34. https://doi.org/10.1111/j.1469-185X.2007.00030.x

Spinu, N., Cronin, M. T. D., Enoch, S. J., Madden, J. C., & Worth, A. P. (2020). Quantitative adverse outcome pathway (qAOP) models for toxicity prediction. *Archives of Toxicology*, *94*(5), 1497–1510. https://doi.org/10.1007/s00204-020-02774-7

Stern, S. T., Bruno, M. K., Hennig, G. E., Horton, R. A., Roberts, J. C., & Cohen, S. D. (2005). Contribution of acetaminophen-cysteine to acetaminophen nephrotoxicity in CD-1 mice: I. Enhancement of acetaminophen nephrotoxicity by acetaminophen-cysteine. *Toxicology and Applied Pharmacology*, *202*(2), 151–159. https://doi.org/10.1016/j.taap.2004.06.030

Subedi, A., Macurak, M., Gee, S. T., Monge, E., Goll, M. G., Potter, C. J., Parsons, M. J., & Halpern, M. E. (2014). Adoption of the Q transcriptional regulatory system for zebrafish transgenesis. *Methods*, *66*(3), 433–440. https://doi.org/10.1016/j.ymeth.2013.06.012

Suli, A., Guler, A. D., Raible, D. W., & Kimelman, D. (2014). A targeted gene expression system using the tryptophan repressor in zebrafish shows no silencing in subsequent generations. *Development*, *141*(5), 1167–1174. https://doi.org/10.1242/dev.100057

Sun, L., Gu, L., Tan, H., Liu, P., Gao, G., Tian, L., Chen, H., Lu, T., Qian, H., Fu, Z., & Pan, X. (2018). Effects of 17α‐ethinylestradiol on caudal fin regeneration in zebrafish larvae. *Science of The Total Environment*, #pagerange#. https://doi.org/10.1016/j.scitotenv.2018.10.275

Suzuki, T., Takagi, Y., Osanai, H., Li, L. I., Takeuchi, M., Katoh, Y., Kobayashi, M., & Yamamoto, M. (2005). Pi class glutathione S-transferase genes are regulated by Nrf2 through an evolutionarily conserved regulatory element in zebrafish. *Biochemical Journal*, *388*(1), 65–73. https://doi.org/10.1042/BJ20041860

Swales, J. G., Hamm, G., Clench, M. R., & Goodwin, R. J. A. (2019). Mass spectrometry imaging and its application in pharmaceutical research and

development: A concise review. *International Journal of Mass Spectrometry*, *437*, 99–112. https://doi.org/10.1016/j.ijms.2018.02.007

Takesono, A., Schirrmacher, P., Scott, A., Green, J. M., Lee, O., Winter, M. J., Kudoh, T., & Tyler, C. R. (2022). Estrogens regulate early embryonic development of the olfactory sensory system via estrogen-responsive glia. *Development*, *149*(1). https://doi.org/10.1242/dev.199860

Tan, Y. L., & Ho, H. K. (2020). Hypothermia advocates functional mitochondria and alleviates oxidative stress to combat acetaminophen-induced hepatotoxicity. *Cells*, *9*(11), 2354. https://doi.org/10.3390/cells9112354

Tao, T., & Peng, J. (2009). Liver development in zebrafish (*Danio rerio*). *Journal of Genetics and Genomics*, *36*(6), 325–334. https://doi.org/10.1016/S1673-8527(08)60121-6

Ternes, T. A. (1998). Occurrence of drugs in German sewage treatment plants and rivers. *Water Research*, *32*(11), 3245–3260. https://doi.org/10.1016/S0043-1354(98)00099-2

*Test No. 229: Fish Short Term Reproduction Assay*. (2012). OECD. https://doi.org/10.1787/9789264185265-en

*Test No. 250: EASZY assay - Detection of Endocrine Active Substances, acting through estrogen receptors, using transgenic tg(cyp19a1b:GFP) Zebrafish embrYos*. (2021). OECD. https://doi.org/10.1787/0a39b48b-en

Thilagam, H., Gopalakrishnan, S., Qu, H. D., Bo, J., & Wang, K. J. (2010). 17β estradiol induced ROS generation, DNA damage and enzymatic responses in the hepatic tissue of Japanese sea bass. *Ecotoxicology*, *19*(7), 1258–1267. https://doi.org/10.1007/s10646-010-0510-3

Thorn, C. F., Müller, D. J., Altman, R. B., & Klein, T. E. (2018). PharmGKB summary: Clozapine pathway, pharmacokinetics. *Pharmacogenetics and Genomics*, *28*(9), 214–222. https://doi.org/10.1097/FPC.0000000000000347

Thummel, R., Burket, C. T., & Hyde, D. R. (2006). Two different transgenes to study gene silencing and re-expression during zebrafish caudal fin and retinal regeneration. *TheScientificWorldJournal*, *6*(SUPPL.1), 65–81.

https://doi.org/10.1100/tsw.2006.328

Tiedeken, J. A., & Ramsdell, J. S. (2007). Embryonic exposure to domoic acid increases the susceptibility of zebrafish larvae to the chemical convulsant pentylenetetrazole. *Environmental Health Perspectives*, *115*(11), 1547–1552. https://doi.org/10.1289/ehp.10344

Tsujita, T., Li, L., Nakajima, H., Iwamoto, N., Nakajima-Takagi, Y., Ohashi, K., Kawakami, K., Kumagai, Y., Freeman, B. A., Yamamoto, M., & Kobayashi, M. (2011). Nitro-fatty acids and cyclopentenone prostaglandins share strategies to activate the Keap1-Nrf2 system: A study using green fluorescent protein transgenic zebrafish. *Genes to Cells*, *16*(1), 46–57. https://doi.org/10.1111/j.1365-2443.2010.01466.x

Tully, D. B., Collins, B. J., Overstreet, J. D., Smith, C. S., Dinse, G. E., Mumtaz, M. M., & Chapin, R. E. (2000). Effects of arsenic, cadmium, chromium, and lead on gene expression regulated by a battery of 13 different promoters in recombinant HepG2 cells. *Toxicology and Applied Pharmacology*, *168*(2), 79–90. https://doi.org/10.1006/taap.2000.9014

Tyler, C. R., & Jobling, S. (2008). Roach, Sex, and Gender-Bending Chemicals: The feminization of wild fish in english rivers. *BioScience*, *58*(11), 1051–1059. https://doi.org/10.1641/B581108

Tyler, C. R., Jobling, S., & Sumpter, J. P. (1998). Endocrine disruption in wildlife: A critical review of the evidence. *Critical Reviews in Toxicology*, *28*(4), 319–361. https://doi.org/10.1080/10408449891344236

Ucheya, R. ., & Igweh, J. . (2010). Histological changes in kidney structure following a long – term administration of paracetamol (acetaminophen) in pregnant sprague dawley rats. *Nigerian Journal of Physiological Sciences*, *21*(1–2), 77–81. https://doi.org/10.4314/njps.v21i1-2.53973

Uddin, M. S., Rahman, M. M., Jakaria, M., Rahman, M. S., Hossain, M. S., Islam, A., Ahmed, M., Mathew, B., Omar, U. M., Barreto, G. E., & Ashraf, G. M. (2020). Estrogen signaling in Alzheimer's disease: molecular insights and therapeutic targets for Alzheimer's dementia. In *Molecular Neurobiology* (Vol. 57, Issue 6, pp. 2654–2670). Molecular Neurobiology. https://doi.org/10.1007/s12035-020-01911-8

Uno, T., Ishizuka, M., & Itakura, T. (2012). Cytochrome P450 (CYP) in fish. *Environmental Toxicology and Pharmacology*, *34*(1), 1–13. https://doi.org/10.1016/j.etap.2012.02.004

Van den Belt, K., Verheyen, R., & Witters, H. (2001). Reproductive effects of ethynylestradiol and 4t-octylphenol on the zebrafish (*Danio rerio*). *Archives of Environmental Contamination and Toxicology*, *41*(4), 458–467. https://doi.org/10.1007/s002440010272

Van Wijk, R., Krekels, E., Kantae, V., Harms, A., Hankemeier, T., Van der Graaf, P., & Spaink, H. (2018). Impact of post-hatching maturation on the pharmacokinetics of exogenous compounds in zebrafish larvae. *Scientific Reports (Submitted)*, *December 2018*, 1–9. https://doi.org/10.1038/s41598-019-38530-w

Vaquero, J., Belanger, M., Blei, A. T., & Butterworth, R. F. (2006). Lack of assessment of body temperature in mice with acetaminophen toxicity. *Hepatology*, *44*(1), 279–280. https://doi.org/10.1002/hep.21251

Verbueken, E., Alsop, D., Saad, M., Pype, C., Van Peer, E., Casteleyn, C., Van Ginneken, C., Wilson, J., & Van Cruchten, S. (2017). In vitro biotransformation of two human CYP3A probe substrates and their inhibition during early zebrafish development. *International Journal of Molecular Sciences*, *18*(1), 217. https://doi.org/10.3390/ijms18010217

Verbueken, E., Bars, C., Ball, J. S., Periz-Stanacev, J., Marei, W. F. A., Tochwin, A., Gabriëls, I. J., Michiels, E. D. G., Stinckens, E., Vergauwen, L., Knapen, D., Van Ginneken, C. J., & Van Cruchten, S. J. (2018). From mRNA expression of drug disposition genes to in vivo assessment of CYP-mediated biotransformation during zebrafish embryonic and larval development. *International Journal of Molecular Sciences*, *19*(12), 3976. https://doi.org/10.3390/ijms19123976

Verderame, M., Limatola, E., & Scudiero, R. (2016). Estrogenic contamination by manure fertilizer in organic farming: a case study with the lizard Podarcis sicula. *Ecotoxicology*, *25*(1), 105–114. https://doi.org/10.1007/s10646-015-1571-0

Vestel, J., Caldwell, D. J., Constantine, L., D'Aco, V. J., Davidson, T., Dolan, D.

G., Millard, S. P., Murray-Smith, R., Parke, N. J., Ryan, J. J., Straub, J. O., & Wilson, P. (2016). Use of acute and chronic ecotoxicity data in environmental risk assessment of pharmaceuticals. *Environmental Toxicology and Chemistry*, *35*(5), 1201–1212. https://doi.org/10.1002/etc.3260

Vieira, H. C., Bordalo, M. D., Rodrigues, A. C. M., Pires, S. F. S., Rocha, R. J. M., Soares, A. M. V. M., Rendón-von Osten, J., Abreu, S. N., & Morgado, F. (2021). Water temperature modulates mercury accumulation and oxidative stress status of common goby (*Pomatoschistus microps*). *Environmental Research*, *193*(December 2020), 1–9. https://doi.org/10.1016/j.envres.2020.110585

Villeneuve, D. L., Crump, D., Garcia-Reyero, N., Hecker, M., Hutchinson, T. H., LaLone, C. A., Landesmann, B., Lettieri, T., Munn, S., Nepelska, M., Ottinger, M. A., Vergauwen, L., & Whelan, M. (2014). Adverse outcome pathway (AOP) development I: Strategies and principles. *Toxicological Sciences*, *142*(2), 312–320. https://doi.org/10.1093/toxsci/kfu199

Vliegenthart, A. D. B., Tucker, C. S., Del Pozo, J., & Dear, J. W. (2014). Zebrafish as model organisms for studying drug-induced liver injury. *British Journal of Clinical Pharmacology*, *78*(6), 1217–1227. https://doi.org/10.1111/bcp.12408

von Hofsten, J., & Olsson, P. E. (2005). Zebrafish sex determination and differentiation: Involvement of FTZ-F1 genes. *Reproductive Biology and Endocrinology*, *3*, 1–11. https://doi.org/10.1186/1477-7827-3-63

Vredenburg, G., Vassell, K. P. T., Commandeur, J. N. M., Vermeulen, N. P. E., & Vos, J. C. (2013). Reconstitution of the interplay between cytochrome P450 and human glutathione S-transferases in clozapine metabolism in yeast. *Toxicology Letters*, *222*(3), 247–256. https://doi.org/10.1016/j.toxlet.2013.07.023

Wahli, W., Dawid, I., Ryffel, G., & Weber, R. (1981). Vitellogenesis and the vitellogenin gene family. *Science*, *212*(4492), 298–304. https://doi.org/10.1126/science.7209528

Wang, L., Li, A., Liu, Y., Zhan, S., Zhong, L., Du, Y., Xu, D., Wang, W., &

Huang, W. (2020a). Genistein protects against acetaminophen-induced liver toxicity through augmentation of SIRT1 with induction of Nrf2 signalling. *Biochemical and Biophysical Research Communications*, *527*(1), 90–97. https://doi.org/10.1016/j.bbrc.2020.04.100

Wang, Q., Tan, X., Jiao, S., You, F., & Zhang, P. J. (2014). Analyzing cold tolerance mechanism in transgenic zebrafish (*Danio rerio*). *PLoS ONE*, *9*(7), 1–12. https://doi.org/10.1371/journal.pone.0102492

Wang, X., Hui, R., Chen, Y., Wang, W., Chen, Y., Gong, X., & Jin, J. (2019). Discovery of Novel Doxorubicin Metabolites in MCF7 doxorubicin-resistant cells. *Frontiers in Pharmacology*, *10*(December), 1–7. https://doi.org/10.3389/fphar.2019.01434

Wang, X., Wu, Q., Liu, A., Anadón, A., Rodríguez, J.-L., Martínez-Larrañaga, M.-R., Yuan, Z., & Martínez, M.-A. (2017). Paracetamol: overdose-induced oxidative stress toxicity, metabolism, and protective effects of various compounds in vivo and in vitro. *Drug Metabolism Reviews*, *49*(4), 395–437. https://doi.org/10.1080/03602532.2017.1354014

Wang, Z., Walker, G. W., Muir, D. C. G., & Nagatani-Yoshida, K. (2020b). Toward a global understanding of chemical pollution: a first comprehensive analysis of national and regional chemical inventories. *Environmental Science and Technology*, *54*(5), 2575–2584. https://doi.org/10.1021/acs.est.9b06379

Weigt, S., Huebler, N., Braunbeck, T., von Landenberg, F., & Broschard, T. H. (2010). Zebrafish teratogenicity test with metabolic activation (mDarT): Effects of phase I activation of acetaminophen on zebrafish *Danio rerio* embryos. *Toxicology*, *275*(1–3), 36–49. https://doi.org/10.1016/j.tox.2010.05.012

Weigt, S., Huebler, N., Strecker, R., Braunbeck, T., & Broschard, T. H. (2011). Zebrafish (*Danio rerio*) embryos as a model for testing proteratogens. *Toxicology*, *281*(1–3), 25–36. https://doi.org/10.1016/j.tox.2011.01.004

Wendel, A., Jaeschke, H., & Gloger, M. (1982). Drug-induced lipid peroxidation in mice—II. *Biochemical Pharmacology*, *31*(22), 3601–3605. https://doi.org/10.1016/0006-2952(82)90582-2

Westhoff, J. H., Steenbergen, P. J., Thomas, L. S. V., Heigwer, J., Bruckner, T., Cooper, L., Tönshoff, B., Hoffmann, G. F., & Gehrig, J. (2020). In vivo high-content screening in zebrafish for developmental nephrotoxicity of approved drugs. *Frontiers in Cell and Developmental Biology*, *8*(April), 1–13. https://doi.org/10.3389/fcell.2020.00583

Wheeler, J. R., Gimeno, S., Crane, M., Lopez-Juez, E., & Morritt, D. (2005). Vitellogenin: A review of analytical methods to detect (anti) estrogenic activity in fish. *Toxicology Mechanisms and Methods*, *15*(4), 293–306. https://doi.org/10.1080/15376520590968789

Williams, R. T., & Cook, J. C. (2007). Exposure to pharmaceuticals present in the environment. *Drug Information Journal*, *41*(2), 133–141. https://doi.org/10.1177/009286150704100202

Wingert, R. A., & Davidson, A. J. (2008). The zebrafish pronephros: A model to study nephron segmentation. *Kidney International*, *73*(10), 1120–1127. https://doi.org/10.1038/ki.2008.37

Winter, M. J., Lillicrap, A. D., Caunter, J. E., Schaffner, C., Alder, A. C., Ramil, M., Ternes, T. A., Giltrow, E., Sumpter, J. P., & Hutchinson, T. H. (2008). Defining the chronic impacts of atenolol on embryo-larval development and reproduction in the fathead minnow (*Pimephales promelas*). *Aquatic Toxicology*, *86*(3), 361–369. https://doi.org/10.1016/j.aquatox.2007.11.017

Winter, M. J., Pinion, J., Tochwin, A., Takesono, A., Ball, J. S., Grabowski, P., Metz, J., Trznadel, M., Tse, K., Redfern, W. S., Hetheridge, M. J., Goodfellow, M., Randall, A. D., & Tyler, C. R. (2021). Functional brain imaging in larval zebrafish for characterising the effects of seizurogenic compounds acting via a range of pharmacological mechanisms. *British Journal of Pharmacology*, *178*(13), 2671–2689. https://doi.org/10.1111/bph.15458

Winter, M. J., Windell, D., Metz, J., Matthews, P., Pinion, J., Brown, J. T., Hetheridge, M. J., Ball, J. S., Owen, S. F., Redfern, W. S., Moger, J., Randall, A. D., & Tyler, C. R. (2017). 4-dimensional functional profiling in the convulsant-treated larval zebrafish brain. *Scientific Reports*, *7*(1), 6581. https://doi.org/10.1038/s41598-017-06646-6

Wittbrodt, J. N., Liebel, U., & Gehrig, J. (2014). Generation of orientation tools for automated zebrafish screening assays using desktop 3D printing. *BMC Biotechnology*, *14*(1), 36. https://doi.org/10.1186/1472-6750-14-36

Wu, J., Williams, D., Walter, G. A., Thompson, W. E., & Sidell, N. (2014). Estrogen increases Nrf2 activity through activation of the PI3K pathway in MCF-7 breast cancer cells. *Experimental Cell Research*, *328*(2), 351–360. https://doi.org/10.1016/j.yexcr.2014.08.030

Wu, M., Xu, H., Shen, Y., Qiu, W., & Yang, M. (2011). Oxidative stress in zebrafish embryos induced by short-term exposure to bisphenol A, nonylphenol, and their mixture. *Environmental Toxicology and Chemistry*, *30*(10), 2335–2341. https://doi.org/10.1002/etc.634

Xu, H., Li, C., Li, Y., Ng, G. H. B., Liu, C., Zhang, X., & Gong, Z. (2015). Generation of Tg(cyp1a:gfp) transgenic zebrafish for development of a convenient and sensitive in vivo assay for aryl hydrocarbon receptor activity. *Marine Biotechnology*, *17*(6), 831–840. https://doi.org/10.1007/s10126-015-9669-1

Xu, H., Li, C., Suklai, P., Zeng, Q., Chong, R., & Gong, Z. (2018). Differential sensitivities to dioxin-like compounds PCB 126 and PeCDF between Tg(cyp1a:gfp) transgenic medaka and zebrafish larvae. *Chemosphere*, *192*, 24–30. https://doi.org/10.1016/j.chemosphere.2017.10.130

Xu, H., Yang, J., Wang, Y., Jiang, Q., Chen, H., & Song, H. (2008). Exposure to 17α-ethynylestradiol impairs reproductive functions of both male and female zebrafish (Danio rerio). *Aquatic Toxicology*, *88*(1), 1–8. https://doi.org/10.1016/j.aquatox.2008.01.020

Xu, H., Yang, M., Qiu, W., Pan, C., & Wu, M. (2013). The impact of endocrine-disrupting chemicals on oxidative stress and innate immune response in zebrafish embryos. *Environmental Toxicology and Chemistry*, *32*(8), 1793–1799. https://doi.org/10.1002/etc.2245

Yan, Z., Huang, X., Xie, Y., Song, M., Zhu, K., & Ding, S. (2019). Macrolides induce severe cardiotoxicity and developmental toxicity in zebrafish embryos. *Science of the Total Environment*, *649*, 1414–1421. https://doi.org/10.1016/j.scitotenv.2018.07.432

Yang, F., Gao, C., Wang, P., Zhang, G. J., & Chen, Z. (2016). Fish-on-a-chip: Microfluidics for zebrafish research. In *Lab on a Chip* (Vol. 16, Issue 7, pp. 1106–1125). https://doi.org/10.1039/c6lc00044d

Yoon, E., Babar, A., Choudhary, M., Kutner, M., & Pyrsopoulos, N. (2016). Acetaminophen-induced hepatotoxicity: a comprehensive update. *Journal of Clinical and Translational Hepatology*, *4*(2), 131–142. https://doi.org/10.14218/JCTH.2015.00052

Zbikowska, H. M. (2003). Fish can be first - Advances in fish transgenesis for commercial applications. *Transgenic Research*, *12*(4), 379–389. https://doi.org/10.1023/A:1024267416522

Zhang, F., Han, L., Wang, J., Shu, M., Liu, K., Zhang, Y., Hsiao, C., Tian, Q., & He, Q. (2021a). Clozapine induced developmental and cardiac toxicity on zebrafish embryos by elevating oxidative stress. *Cardiovascular Toxicology*, *21*(5), 399–409. https://doi.org/10.1007/s12012-021-09632-7

Zhang, G., Yu, X., Huang, G., Lei, D., & Tong, M. (2021b). An improved automated zebrafish larva high-throughput imaging system. *Computers in Biology and Medicine*, *136*(July), 104702. https://doi.org/10.1016/j.compbiomed.2021.104702

Zhang, Q., Kopp, M., Babiak, I., & Fernandes, J. M. O. (2018). Low incubation temperature during early development negatively affects survival and related innate immune processes in zebrafish larvae exposed to lipopolysaccharide. *Scientific Reports*, *8*(1), 1–14. https://doi.org/10.1038/s41598-018-22288-8

Zhang, W., Sun, X., Chen, L., Lin, K. F., Dong, Q. X., Huang, C. J., Fu, R. B., & Zhu, J. (2012). Toxicological effect of joint cadmium selenium quantum dots and copper ion exposure on zebrafish. *Environmental Toxicology and Chemistry*, *31*(9), 2117–2123. https://doi.org/10.1002/etc.1918

Zhang, X., Li, C., & Gong, Z. (2014). Development of a convenient in vivo hepatotoxin assay using a transgenic zebrafish line with liver-specific dsred expression. *PLoS ONE*, *9*(3). https://doi.org/10.1371/journal.pone.0091874

Zhou, H., George, S., Li, C., Gurusamy, S., Sun, X., Gong, Z., & Qian, H. (2017). Combined toxicity of prevalent mycotoxins studied in fish cell line

and zebrafish larvae revealed that type of interactions is dose-dependent. *Aquatic Toxicology*, *193*, 60–71. https://doi.org/10.1016/j.aquatox.2017.09.030

Zhou, L. Z. H., Johnson, A. P., & Rando, T. A. (2001). NFκB and AP-1 mediate transcriptional responses to oxidative stress in skeletal muscle cells. *Free Radical Biology and Medicine*, *31*(11), 1405–1416. https://doi.org/10.1016/S0891-5849(01)00719-5

Zhou, W., Boucher, R. C., Bollig, F., Englert, C., & Hildebrandt, F. (2010). Characterization of mesonephric development and regeneration using transgenic zebrafish. *American Journal of Physiology - Renal Physiology*, *299*(5), 1040–1047. https://doi.org/10.1152/ajprenal.00394.2010

Zhou, X., Li, Y., Li, H., Yang, Z., & Zuo, C. (2019). Responses in the crucian carp (*Carassius auratus*) exposed to environmentally relevant concentration of 17α-Ethinylestradiol based on metabolomics. *Ecotoxicology and Environmental Safety*, *183*(June), 109501. https://doi.org/10.1016/j.ecoenv.2019.109501

Zhu, Z., Geng, Y., Yuan, Z., Ren, S., Liu, M., Meng, Z., & Pan, D. (2019). A bubble-free microfluidic device for easy-to-operate immobilization, culturing and monitoring of zebrafish embryos. *Micromachines*, *10*(3), 168. https://doi.org/10.3390/mi10030168